

---

Electronic Theses and Dissertations, 2004-2019

---

2015

## ZrB<sub>2</sub>-SiC Based Ultra High Temperature Ceramic Composites: Mechanical Performance and Measurement and Design of Thermal Residual Stresses for Hypersonic Vehicle Applications

Richard Stadelmann  
*University of Central Florida*



Part of the [Mechanical Engineering Commons](#)

Find similar works at: <https://stars.library.ucf.edu/etd>

University of Central Florida Libraries <http://library.ucf.edu>

This Doctoral Dissertation (Open Access) is brought to you for free and open access by STARS. It has been accepted for inclusion in Electronic Theses and Dissertations, 2004-2019 by an authorized administrator of STARS. For more information, please contact [STARS@ucf.edu](mailto:STARS@ucf.edu).

---

### STARS Citation

Stadelmann, Richard, "ZrB<sub>2</sub>-SiC Based Ultra High Temperature Ceramic Composites: Mechanical Performance and Measurement and Design of Thermal Residual Stresses for Hypersonic Vehicle Applications" (2015). *Electronic Theses and Dissertations, 2004-2019*. 1407.

<https://stars.library.ucf.edu/etd/1407>



ZrB<sub>2</sub>-SiC BASED ULTRA HIGH TEMPERATURE CERAMIC COMPOSITES:  
MECHANICAL PERFORMANCE AND MEASUREMENT AND DESIGN OF  
THERMAL RESIDUAL STRESSES FOR HYPERSONIC VEHICLE  
APPLICATIONS

by

RICHARD PHILIP STADELMANN

B.S. University of Central Florida, 2011

M.S. University of Central Florida, 2013

A dissertation submitted in partial fulfillment of the requirements  
for the degree of Doctor of Philosophy  
in the Department of Mechanical & Aerospace Engineering  
in the College of Engineering & Computer Science  
at the University of Central Florida  
Orlando, Florida

Fall Term  
2015

Major Professor: Nina Orlovskaya

© 2015 Richard P. Stadelmann

## ABSTRACT

Ultra-high temperature ceramics (UHTCs), such as ZrB<sub>2</sub>-based ceramic composites, have been identified as next generation candidate materials for leading edges and nose cones in hypersonic air breathing vehicles. Mechanical performance of ceramic composites play an important role in the ultra-high temperature applications, therefore SiC is added to ZrB<sub>2</sub> as a strengthening phase to enhance its mechanical performance. The high melting temperatures of both ZrB<sub>2</sub> and SiC, as well as the ability of SiC to form SiO<sub>2</sub> refractory oxide layers upon oxidation make ZrB<sub>2</sub>-SiC ceramics very suitable for aerospace applications.

Thermal residual stresses appearing during processing are unavoidable in sintered ZrB<sub>2</sub>-SiC ceramic composites. Residual microstresses appear at the microstructural level (intergranular microstresses) or at the crystal structure level (intragranular microstresses). These microstresses are of enormous importance for the failure mechanisms in ZrB<sub>2</sub>-SiC ceramics, such as ratio of the trans- and intergranular fracture; crack branching or bridging, microcracking, subcritical crack growth and others, as they govern crack propagation-induced energy dissipation and affect the toughness and strength of the ceramic material. Therefore, understanding the evolution of residual stress state in processed ZrB<sub>2</sub>-SiC ceramic composites and accurate measurements of these stresses are of high priority.

In the present research the ZrB<sub>2</sub>-17vol%SiC, ZrB<sub>2</sub>-32vol%SiC, and ZrB<sub>2</sub>-45vol%SiC ultra-high temperature particulate ceramic composites were sintered using both Hot Pressing (HP) and Spark Plasma Sintering (SPS) techniques. The mechanical performance of the ZrB<sub>2</sub>-SiC composites was investigated using 3- and 4-point bending techniques for measurements of

instantaneous fracture strength and fracture toughness. Resonant Ultrasound Spectroscopy was used for measurement of Young's, shear, and bulk moduli as well as Poisson's ratio of the composites. The distribution of thermal residual stresses and the effect of the applied external load on their re-distribution was studied using micro-Raman spectroscopy. Piezospectroscopic coefficients were determined for all compositions of  $ZrB_2$ -SiC ceramic under study and their experimentally obtained values were compared with the piezospectroscopic coefficients both published in the literature and calculated using theoretical approach. Finally, the novel  $ZrB_2$ - $IrB_2$ -SiC ceramic composites were also produced using Spark Plasma Sintering (SPS), where  $IrB_2$  powder was synthesized using mechanochemical route. It is expected that the  $IrB_2$  additive phase might contribute to the improved overall oxidation resistance of  $ZrB_2$  based ultra-high temperature ceramic composites.

*This dissertation is dedicated to my wife, Paulette Stadelmann, for giving all her love and support throughout the preparation of my thesis and my graduate academic career. Also to my parents and sister for all of their love and support throughout my entire life.*

## ACKNOWLEDGMENTS

This dissertation is a result of the guidance, patience, and support I have received from my advisor, Dr. Nina Orlovskaya.

I would like to give a special thanks to Billy Hughes for assisting me in my research and the I<sup>3</sup>: UCF Embraces a Knowledge Based Economy-0963146 grant for funding Billy's research.

I am very grateful for Cassandra Carpenter, who laid down the foundation of the research conducted in this dissertation. Likewise, I am grateful for Dr. Sglavo, Dr. Radovic, and Dr. Reece for their contributions to this work.

I would like to thank Dr. Ranganathan Kumar, Dr. Stephen Kuebler, and Dr. Seetha Raghavan for being on my committee.

Finally, I would like to thank all of my friends and family for the added support in my life to accomplish anything I want.

I would like to thank the DoD SMART Scholarship for funding my PhD study.

This research was supported by NSF projects DMR-0748364 and CMMI-0968911.

## TABLE OF CONTENTS

|                                                                                                           |     |
|-----------------------------------------------------------------------------------------------------------|-----|
| LIST OF FIGURES .....                                                                                     | 10  |
| LIST OF TABLES .....                                                                                      | 23  |
| CHAPTER 1: INTRODUCTION .....                                                                             | 1   |
| 1.1: Hypersonic Flow .....                                                                                | 3   |
| 1.1.1: Hypersonic Shock and Expansion Waves .....                                                         | 7   |
| 1.1.2: Hypersonic Shockwaves of Chemically Reacting Flow in Equilibrium .....                             | 10  |
| 1.1.3: Hypersonic Shockwaves of Chemically Reacting Flow in Non-equilibrium .....                         | 20  |
| 1.1.4: Hypersonic Flow Navier-Stokes Equations .....                                                      | 26  |
| 1.1.5: Summary of Hypersonic Flow Fields .....                                                            | 30  |
| 1.2: Material Requirements for Hypersonic Vehicles Applications .....                                     | 33  |
| 1.3: Proposed Material Candidate Properties .....                                                         | 34  |
| 1.3.1: Crystal Structure and Phase Diagram of $ZrB_2$ , $IrB_2$ , and SiC .....                           | 34  |
| 1.3.2: Mechanochemical Synthesis .....                                                                    | 41  |
| 1.3.3: Sintering Processes of $ZrB_2$ -SiC, $ZrB_2$ - $IrB_2$ -SiC, and pure SiC Ceramic Composites ..... | 44  |
| 1.3.4: Mechanical Properties of $ZrB_2$ , SiC, and $ZrB_2$ -SiC .....                                     | 46  |
| 1.3.5: Fatigue and Oxidation of $ZrB_2$ -SiC .....                                                        | 55  |
| 1.3.6: Thermal Properties and Thermal Shock of $ZrB_2$ -SiC .....                                         | 57  |
| 1.3.7: Ablation and Arc Jet (Arc Heater) Testing of $ZrB_2$ -SiC .....                                    | 63  |
| 1.4: Raman Spectroscopy .....                                                                             | 73  |
| 1.4.1: Phonon Dispersion Curve for 6H-SiC .....                                                           | 73  |
| 1.4.2: Strong and Weak Modes and Anisotropy of 6H-SiC Raman Modes .....                                   | 75  |
| 1.4.3: 6H-SiC Raman Modes Notation and Selection Rules .....                                              | 78  |
| 1.4.4: Raman Spectra of 6H-SiC .....                                                                      | 80  |
| 1.5: Thermal Residual Stresses in $ZrB_2$ -SiC Ceramic Composites .....                                   | 86  |
| 1.6: Raman Piezo-Spectroscopy .....                                                                       | 91  |
| 1.6.1: The Origin of Raman Piezo-Spectroscopy .....                                                       | 92  |
| 1.6.2: Laser Penetration Depth .....                                                                      | 97  |
| 1.6.3: Piezo-Spectroscopy Found in Publications .....                                                     | 101 |



|                                                                                                                                                                                  |     |
|----------------------------------------------------------------------------------------------------------------------------------------------------------------------------------|-----|
| 1.7: Effect of Residual Stress on Mechanical Properties in Ceramic Composites.....                                                                                               | 107 |
| CHAPTER 2: EXPERIMENTAL PROCEDURE.....                                                                                                                                           | 113 |
| 2.1: Processing the ZrB <sub>2</sub> -SiC Ceramic Composites Samples .....                                                                                                       | 113 |
| 2.2.: Fracturography analysis and microstructure determination .....                                                                                                             | 114 |
| 2.3: Calibration of Piezo-Spectroscopy Coefficient via 3-Point Bending .....                                                                                                     | 114 |
| 2.3.1: <i>In-Situ</i> 3-Point Bending Device: Design and Calibration .....                                                                                                       | 114 |
| 2.3.2: Determination of Laser Penetration Depth.....                                                                                                                             | 120 |
| 2.4: Raman Spectra Collection, Raman Map Collection and the 2D Mapping of Thermal Residual Stress of ZrB <sub>2</sub> -SiC Ceramic Composites .....                              | 123 |
| 2.4.1: Collection of Raman Spectra and the Optimization of Parameters for Collecting 2D Raman Maps of ZrB <sub>2</sub> -SiC .....                                                | 123 |
| 2.4.2: Collection of 2D Raman Maps of ZrB <sub>2</sub> -SiC Ceramic Composites .....                                                                                             | 127 |
| 2.5: Determining the Mechanical Properties of the Produced ZrB <sub>2</sub> -SiC Ceramic Composites .....                                                                        | 128 |
| 2.6: Processing and Preparing the ZrB <sub>2</sub> -IrB <sub>2</sub> -SiC Ceramic Composites.....                                                                                | 130 |
| 2.6.1: Synthesis of IrB <sub>2</sub> Powders.....                                                                                                                                | 130 |
| 2.6.2: Preparing the ZrB <sub>2</sub> -IrB <sub>2</sub> -SiC Powder .....                                                                                                        | 132 |
| 2.6.3: XRD and XRD Refinement of ZrB <sub>2</sub> -IrB <sub>2</sub> -SiC .....                                                                                                   | 132 |
| CHAPTER 3: RESULTS.....                                                                                                                                                          | 134 |
| 3.1: Sintering and Microstructure of ZrB <sub>2</sub> -SiC Ceramic Composites Samples by SPS .....                                                                               | 134 |
| 3.1.1: Sintering of ZrB <sub>2</sub> -SiC Ceramic Composites Samples by SPS .....                                                                                                | 134 |
| 3.1.2: Microstructure of ZrB <sub>2</sub> -SiC Ceramic Composites Samples by SPS .....                                                                                           | 136 |
| 3.2: Calibration of Piezo-Spectroscopy Coefficient via 3-Point Bending .....                                                                                                     | 139 |
| 3.3: Raman Line and 2D mapping of Thermal Residual Stress of ZrB <sub>2</sub> -SiC Ceramic Composites .....                                                                      | 140 |
| 3.3.1: Optimization of Parameters for Collecting 2D Raman Maps of ZrB <sub>2</sub> -SiC.....                                                                                     | 141 |
| 3.3.2: Raman Mapping Methodology of Selection of Proper Data Points (Band) Filtering                                                                                             | 150 |
| 3.3.3: 2D Raman Maps: Peak Intensity, Peak Width, and Peak Position.....                                                                                                         | 153 |
| 3.3.4: Calculation of Thermal Residual Stresses in SiC Grains of ZrB <sub>2</sub> -SiC Ceramic Composites Based on Previously Published SiC Piezospectroscopy Coefficients ..... | 155 |

|                                                                                                                                                                       |     |
|-----------------------------------------------------------------------------------------------------------------------------------------------------------------------|-----|
| 3.3.5: Determination of the Distribution of Thermal Residual Stresses and Resulting 2D Thermal Residual Stress Maps of ZrB <sub>2</sub> -SiC Ceramic Composites ..... | 160 |
| 3.4: Statistical Distribution of Thermal Residual Stress in SiC Grains Under Applied Load in ZrB <sub>2</sub> -SiC Ceramic Composites .....                           | 165 |
| 3.5: Mechanical Properties of the Produced SPS ZrB <sub>2</sub> -SiC Ceramic Composites .....                                                                         | 167 |
| 3.6: Sintering and Preliminary XRD Results of ZrB <sub>2</sub> -IrB <sub>2</sub> -SiC Ceramic Composites .....                                                        | 175 |
| 3.6.1: Spark Plasma Sintering of the ZrB <sub>2</sub> -IrB <sub>2</sub> -SiC Ceramic Composites.....                                                                  | 175 |
| 3.6.2: XRD Patterns of the ZrB <sub>2</sub> -IrB <sub>2</sub> -SiC Ceramic Composites.....                                                                            | 182 |
| CHAPTER 4: CONCLUSIONS .....                                                                                                                                          | 185 |
| APPENDIX: COPYRIGHT PERMISSION LETTERS.....                                                                                                                           | 190 |
| LIST OF REFERENCES.....                                                                                                                                               | 224 |

## LIST OF FIGURES

|                                                                                                                                                                                                                                                                                                                   |    |
|-------------------------------------------------------------------------------------------------------------------------------------------------------------------------------------------------------------------------------------------------------------------------------------------------------------------|----|
| Figure 1: Re-entry to Earth's atmosphere [2] .....                                                                                                                                                                                                                                                                | 2  |
| Figure 2: Temperature behind a normal shock at high velocities. Reprinted from Hypersonic and High Temperature Gas Dynamics 2 <sup>nd</sup> Ed., Copyright (2006), with permission from John D. Anderson, Jr. [1] ..                                                                                              | 4  |
| Figure 3: Thin hypersonic shock layer. Reprinted from Hypersonic and High Temperature Gas Dynamics 2 <sup>nd</sup> Ed., Copyright (2006), with permission from John D. Anderson, Jr. [1] .....                                                                                                                    | 5  |
| Figure 4: Viscous interaction effects. Reprinted from Hypersonic and High Temperature Gas Dynamics 2 <sup>nd</sup> Ed., Copyright (2006), with permission from John D. Anderson, Jr. [1] .....                                                                                                                    | 5  |
| Figure 5: Entropy Layer. Reprinted from Hypersonic and High Temperature Gas Dynamics 2 <sup>nd</sup> Ed., Copyright (2006), with permission from John D. Anderson, Jr. [1] .....                                                                                                                                  | 6  |
| Figure 6: Recap of the phenomena experienced in hypersonic regime. Reprinted from Hypersonic and High Temperature Gas Dynamics 2 <sup>nd</sup> Ed., Copyright (2006), with permission from John D. Anderson, Jr. [1] ..                                                                                           | 7  |
| Figure 7: Oblique shock-wave geometry. Reprinted from Hypersonic and High Temperature Gas Dynamics 2 <sup>nd</sup> Ed., Copyright (2006), with permission from John D. Anderson, Jr. [1] .....                                                                                                                    | 8  |
| Figure 8: Expansion-wave geometry. Reprinted from Hypersonic and High Temperature Gas Dynamics 2 <sup>nd</sup> Ed., Copyright (2006), with permission from John D. Anderson, Jr. [1] .....                                                                                                                        | 9  |
| Figure 9: Ratio of specific heat. Reprinted from Hypersonic and High Temperature Gas Dynamics 2 <sup>nd</sup> Ed., Copyright (2006), with permission from John D. Anderson, Jr. [1] .....                                                                                                                         | 11 |
| Figure 10: Influence of pressure on the normal shockwave temperature in equilibrium air. Reprinted from Hypersonic and High Temperature Gas Dynamics 2 <sup>nd</sup> Ed., Copyright (2006), with permission from John D. Anderson, Jr. [1]. .....                                                                 | 16 |
| Figure 11: Variation of normal shock density with velocity and altitude; velocity range below (A) and near & above (B) orbital velocity (From Huber [7]). Reprinted from Hypersonic and High Temperature Gas Dynamics 2 <sup>nd</sup> Ed., Copyright (2006), with permission from John D. Anderson, Jr. [1] ..... | 16 |

Figure 12: Relative locations of blunt-body bow shockwaves (A), and oblique shockwaves (B) for calorically perfect and chemically reacting gases. Reprinted from Hypersonic and High Temperature Gas Dynamics 2<sup>nd</sup> Ed., Copyright (2006), with permission from John D. Anderson, Jr. [1]..... 17

Figure 13: Oblique shockwave geometry. Reprinted from Hypersonic and High Temperature Gas Dynamics 2<sup>nd</sup> Ed., Copyright (2006), with permission from John D. Anderson, Jr. [1]..... 18

Figure 14: Deflection angle-wave angle-velocity diagram for oblique shocks on high-temperature air at 10,000 ft altitude (From Moeckel [8]). Reprinted from Hypersonic and High Temperature Gas Dynamics 2<sup>nd</sup> Ed., Copyright (2006), with permission from John D. Anderson, Jr. [1]..... 19

Figure 15: Equilibrium chemical species variations behind normal shock (A) and behind 30-deg oblique shock (B) for two different trajectories (From [9]). Reprinted from Hypersonic and High Temperature Gas Dynamics 2<sup>nd</sup> Ed., Copyright (2006), with permission from John D. Anderson, Jr. [1]..... 20

Figure 16: Distributions of the chemical species for the nonequilibrium flow through a normal shock wave in air:  $M_\infty=12.28$ ,  $\rho_\infty=1.0\text{mm Hg}$ , and  $T_\infty=300\text{K}$  (From Marrone [10]). Reprinted from Hypersonic and High Temperature Gas Dynamics 2<sup>nd</sup> Ed., Copyright (2006), with permission from John D. Anderson, Jr. [1].23

Figure 17: Geometry for non-equilibrium flow behind a straight oblique shockwave (A), and the schematic of non-equilibrium flow over a compression corner (B). Reprinted from Hypersonic and High Temperature Gas Dynamics 2<sup>nd</sup> Ed., Copyright (2006), with permission from John D. Anderson, Jr. [1]..... 24

Figure 18: Different Regions in high-temperature blunt-body flowfield. Reprinted from Hypersonic and High Temperature Gas Dynamics 2<sup>nd</sup> Ed., Copyright (2006), with permission from John D. Anderson, Jr. [1]..... 31

Figure 19: Different flow regimes. Reprinted from Hypersonic and High Temperature Gas Dynamics 2<sup>nd</sup> Ed., Copyright (2006), with permission from John D. Anderson, Jr. [1]..... 32

Figure 20: ZrB<sub>2</sub> crystal structure, where the green balls are Zr atoms and the blue balls are B atoms. ZrB<sub>2</sub> unit cell view from the a or b-plane (A), c-plane (B), 111 plane (C), and a 3D view showing the alternating layers of B and Zr (D)..... 35

Figure 21: 6-hexagonal SiC crystal structure looking at the a or b-plane (A), c-plane (B), 111 plane (C), and finally a 3D view of the crystal structure (D) [15]..... 36

Figure 22: ReB<sub>2</sub>-type IrB<sub>2</sub> crystal structure looking at the a or b-plane (A), c-plane (B), 111 plane (C) and a 3D view of the structure (D) (from Xie [27])..... 37

Figure 23: Phase diagram Zr-B system without labels(a), and with labels of the phases(b)[29, 30]..... 38

Figure 24: Si-C binary system Phase Diagram. Reprinted from Journal of the European Ceramic Society, vol. 32, G. Honstein, C. Chatillon, and F. Baillet, "Thermodynamic approach to the vaporization and growth phenomena of SiC ceramics. I. SiC and SiC–SiO<sub>2</sub> mixtures under neutral conditions," pp. 1117-1135, Copyright (2012), with permission from Elsevier. [32]..... 39

Figure 25: ZrB<sub>2</sub>-SiC phase diagram. Reprinted from Journal of the European Ceramic Society, vol. 32, Q. Lonné, N. Glandut, and P. Lefort, "Surface densification of porous ZrB<sub>2</sub>–39mol.% SiC ceramic composites by a laser process," pp. 955-963, Copyright (2012), with permission from Elsevier. [33]..... 40

Figure 26: Ir-B phase diagram. Reprinted from *Journal of the Less Common Metals*, vol. 82, H. Ipser and P. Rogl, "Constitution diagrams of the binary systems Pd-B and Ir-B," pp. 363, Copyright (1981), with permission from Elsevier. [34, 35]..... 41

Figure 27: Mechanisms of ball milling. Reprinted from "Rhenium, osmium and iridium diborides by mechanochemistry : synthesis, structure, thermal stability and mechanical properties", Z. Xie, Copyright (2014), with permission from Zhilin Xie. [36] ..... 43

Figure 28: Hot pressure schematic. Reprinted from *Diamond and Related Materials*, vol. 21, Z. Yuan, Z. Jin, R. Kang, and Q. Wen, "Tribochemical polishing CVD diamond film with FeNiCr alloy polishing plate prepared by MA-HPS technique," pp. 50-57, Copyright (2012), with permission from Elsevier. [60] ..... 44

Figure 29: Spark plasma sintering schematic. Reprinted from *Materials Chemistry and Physics*, vol. 112, X. Dong, F. Lü, L. Yang, Y. Zhang, and X. Wang, "Influence of spark plasma sintering temperature on electrochemical performance of  $\text{La}_{0.80}\text{Mg}_{0.20}\text{Ni}_{3.75}$  alloy," pp. 596-602, Copyright (2008), with permission from Elsevier. [61]..... 45

Figure 30: Elastic modulus vs. temperature for  $\text{ZrB}_2$ . Reprinted from *Journal of the American Ceramic Society*, vol. 96, E. W. Neuman, G. E. Hilmas, and W. G. Fahrenholtz, "Strength of Zirconium Diboride to 2300°C," pp. 47-50, Copyright (2012), with permission from John Wiley and Sons. [104]..... 49

Figure 31: Flexure strength vs. temperature for  $\text{ZrB}_2$ . Reprinted from *Journal of the American Ceramic Society*, vol. 96, E. W. Neuman, G. E. Hilmas, and W. G. Fahrenholtz, "Strength of Zirconium Diboride to 2300°C," pp. 47-50, Copyright (2012), with permission from John Wiley and Sons. [104]..... 50

Figure 32: Summary of trends of the mechanical properties of  $\text{ZrB}_2$ -30vol%SiC (A) Young's Modulus [106], (B) Fracture toughness [106], (C) Flexure strength [106], and for completeness the oxide layer thicknesses. Reprinted from *Journal of the European Ceramic Society*, vol. 33, E. W. Neuman, G. E. Hilmas, and W. G. Fahrenholtz, "Mechanical behavior of zirconium diboride–silicon carbide ceramics at elevated temperature in air," pp. 2889-2899, Copyright (2013), with permission from Elsevier. [106] .... 51

Figure 33: Compressive strength for different  $\text{ZrB}_2$ -SiC composition as a function of temperature. Reprinted from *Journal of the European Ceramic Society*, vol. 31, J. Ramírez-Rico, M. A. Bautista, J. Martínez-Fernández, and M. Singh, "Compressive strength degradation in  $\text{ZrB}_2$ -based ultra-high temperature ceramic composites," pp. 1345-1352, Copyright (2011), with permission from Elsevier. [109]..... 52

Figure 34:  $\text{ZrB}_2$ -SiC Flexure strength after exposure. Reprinted from *Journal of the European Ceramic Society*, vol. 32, M. Patel, J. J. Reddy, V. V. Bhanu Prasad, and V. Jayaram, "Strength of hot pressed  $\text{ZrB}_2$ -SiC composite after exposure to high temperatures (1000–1700°C)," pp. 4455-4467, Copyright (2012), with permission from Elsevier. [107]..... 53

Figure 35: Thermal conductivity and diffusivity as a function of temperature. Reprinted from *Journal of the American Ceramic Society*, vol. 94, L. Zhang, D. A. Pejaković, J. Marschall, and M. Gasch, "Thermal and Electrical Transport Properties of Spark Plasma-Sintered HfB<sub>2</sub> and ZrB<sub>2</sub> Ceramics," pp. 2562-2570, Copyright (2011), with permission from John Wiley and Sons. [136] ..... 58

Figure 36: CTE bar chart of results obtained for the different composite investigated. Reprinted from *Journal of the European Ceramic Society*, vol. 32, M. Mallik, A. J. Kailath, K. K. Ray, and R. Mitra, "Electrical and thermophysical properties of ZrB<sub>2</sub> and HfB<sub>2</sub> based composites," pp. 2545-2555, Copyright (2013), with permission from Elsevier. [138] ..... 60

Figure 37: Specific heat capacity(A), thermal diffusivity (B), and thermal conduction (C) as a function of temperature. Reprinted from *Journal of the European Ceramic Society*, vol. 33, M. Patel, V. V. B. Prasad, and V. Jayaram, "Heat conduction mechanisms in hot pressed ZrB<sub>2</sub> and ZrB<sub>2</sub>SiC composites," pp. 1615-1624, Copyright (2013), with permission from Elsevier. [139] ..... 61

Figure 38: Thermal shock cycles effect on flexural strength. Reprinted from *International Journal of Refractory Metals and Hard Materials*, vol. 29, S. Meng, F. Qi, H. Chen, Z. Wang, and G. Bai, "The repeated thermal shock behaviors of a ZrB<sub>2</sub>-SiC composite heated by electric resistance method," pp. 44-48, Copyright (2011), with permission from Elsevier. [122] ..... 62

Figure 39: Thermal shock temperature difference effect on flexure strength. Reprinted from *Materials Chemistry and Physics*, vol. 113, Z. Wang, C. Hong, X. Zhang, X. Sun, and J. Han, "Microstructure and thermal shock behavior of ZrB<sub>2</sub>-SiC-graphite composite," pp. 338-341, Copyright (2009), with permission from Elsevier. [144] ..... 63

Figure 40: Mass ablation rate vs. ablation time. Reprinted from *Materials Science and Engineering: A*, vol. 465, S. Tang, J. Deng, S. Wang, W. Liu, and K. Yang, "Ablation behaviors of ultra-high temperature ceramic composites," pp. 1-7, Copyright (2007), with permission from Elsevier. [159]. ..... 65

Figure 41: Mass ablation rate vs. heat flux the sample experienced. Reprinted from *Materials Science and Engineering: A*, vol. 465, S. Tang, J. Deng, S. Wang, W. Liu, and K. Yang, "Ablation behaviors of ultra-high temperature ceramic composites," pp. 1-7, Copyright (2007), with permission from Elsevier [159].65

Figure 42: Sample before test of ZrB<sub>2</sub>-SiC (a), C/C (c), and after for ZrB<sub>2</sub>-SiC (b), and C/C (d). Reprinted from *Composites Science and Technology*, vol. 68, X. Zhang, P. Hu, J. Han, and S. Meng, "Ablation behavior of ZrB<sub>2</sub>-SiC ultra high temperature ceramics under simulated atmospheric re-entry conditions," pp. 1718-1726, Copyright (2008), with permission from Elsevier [166]. ..... 66

Figure 43: ZrB<sub>2</sub>-SiC sharp leading edge models with different nose radius. Reprinted from *Journal of Alloys and Compounds*, vol. 566, X. Jin, R. He, X. Zhang, and P. Hu, "Ablation behavior of ZrB<sub>2</sub>-SiC sharp leading edges," pp. 125-130, Copyright (2013), with permission from Elsevier [147]. ..... 67

Figure 44: ZrB<sub>2</sub>-SiC wedge sample on the left and the sample in the arc-jet on the right. Reprinted from *Journal of the American Ceramic Society*, vol. 95, F. Monteverde and R. Savino, "ZrB<sub>2</sub>-SiC Sharp Leading Edges in High Enthalpy Supersonic Flows," pp. 2282-2289, Copyright (2012), with permission from John Wiley and Sons [168]..... 68

Figure 45: the hemisphere and cone samples used in the 28kW test. Reprinted from *Aerospace Science and Technology*, vol. 14, R. Savino, M. De Stefano Fumo, D. Paterna, A. Di Maso, and F. Monteverde, "Arc-jet testing of ultra-high-temperature-ceramics," pp. 187, Copyright (2010), with permission from Elsevier Paris. [170]..... 69

Figure 46: the samples before (a and b) and after the test (c and d). Reprinted from *Journal of the European Ceramic Society*, vol. 30, F. Monteverde, R. Savino, M. D. S. Fumo, and A. Di Maso, "Plasma wind tunnel testing of ultra-high temperature ZrB<sub>2</sub>-SiC composites under hypersonic re-entry conditions," pp. 2313-2321, Copyright (2010), with permission from Elsevier [172]..... 70

Figure 47: Images of the samples surfaces after exposure to arc-jet for 5 minutes. Reprinted from *Journal of the European Ceramic Society*, vol. 30, M. Gasch and S. Johnson, "Physical characterization and arcjet



oxidation of hafnium-based ultra high temperature ceramics fabricated by hot pressing and field-assisted sintering," pp. 2337-2344, Copyright (2010), with permission from Elsevier [176]..... 72

Figure 48: 6H-SiC phonon dispersion curve. Reprinted from *Physical Review*, vol. 170, D. W. Feldman, J. H. Parker, W. J. Choyke, and L. Patrick, "Raman Scattering in 6H-SiC," pp. 698-704, Copyright (1968), with permission from American Physical Society [191]. ..... 74

Figure 49: Angular dependence of the strong  $A_1$  and  $E_1$  modes with that of weak modes of  $A_1$  and  $E_1$ . Reprinted from *Physical Review*, vol. 170, D. W. Feldman, J. H. Parker, W. J. Choyke, and L. Patrick, "Raman Scattering in 6H-SiC," pp. 698-704, Copyright (1968), with permission from American Physical Society [191]..... 77

Figure 50: Schematic showing all 15 lines, with rough classification into four degrees of relative intensity. Reprinted from *Physical Review*, vol. 170, D. W. Feldman, J. H. Parker, W. J. Choyke, and L. Patrick, "Raman Scattering in 6H-SiC," pp. 698-704, Copyright (1968), with permission from American Physical Society [191]..... 79

Figure 51: Experimental dispersion curve. Reprinted from *Physical Review*, vol. 170, D. W. Feldman, J. H. Parker, W. J. Choyke, and L. Patrick, "Raman Scattering in 6H-SiC," pp. 698-704, Copyright (1968), with permission from American Physical Society [191]. ..... 80

Figure 52: 6H-SiC experimental Raman spectra. Reprinted from *physica status solidi (a)*, vol. 162, S. Nakashima and H. Harima, "Raman Investigation of SiC Polytypes," pp. 39-64, Copyright (2001), with permission from John Wiley and Sons [190]..... 81

Figure 53: Raman spectra of a heavily disordered SiC crystal for FTA modes (A), and FTO modes (B). Reprinted from *physica status solidi (a)*, vol. 162, S. Nakashima and H. Harima, "Raman Investigation of SiC Polytypes," pp. 39-64, Copyright (2001), with permission from John Wiley and Sons [190] ..... 85

|                                                                                                                                                                                                                                                                                                                                                                                                    |     |
|----------------------------------------------------------------------------------------------------------------------------------------------------------------------------------------------------------------------------------------------------------------------------------------------------------------------------------------------------------------------------------------------------|-----|
| Figure 54: Effect of temperature on SiC Raman spectra. Reprinted from <i>physica status solidi (a)</i> , vol. 162, S. Nakashima and H. Harima, "Raman Investigation of SiC Polytypes," pp. 39-64, Copyright (2001), with permission from John Wiley and Sons [190].....                                                                                                                            | 86  |
| Figure 55: Effect of stress on virtual states [206] .....                                                                                                                                                                                                                                                                                                                                          | 92  |
| Figure 56: Strained and unstrained unit cell .....                                                                                                                                                                                                                                                                                                                                                 | 93  |
| Figure 57: Schematic of a composite with a fibrous inclusion .....                                                                                                                                                                                                                                                                                                                                 | 96  |
| Figure 58: Laser volume effect on Raman spectra. Reprinted from <i>Acta Materialia</i> , vol. 46, V. Sergo, G. Pezzotti, O. Sbaizero, and T. Nishida, "Grain size influence on residual stresses in alumina/zirconia composites," pp. 1701-1710, Copyright (1998), with permission from Elsevier [201].....                                                                                        | 98  |
| Figure 59: Raman spectra dependence on pressure (A) and the LO-TO splitting dependence on pressure (B). Reprinted from <i>Physical Review Letters</i> , vol. 72, J. Liu and Y. K. Vohra, "Raman Modes of 6H Polytype of Silicon Carbide to Ultrahigh Pressures: A Comparison with Silicon and Diamond," pp. 4105-4108, Copyright (1994), with permission from American Physical Society [219]..... | 102 |
| Figure 60: The Raman spectra of the X and Y propagation direction (Left) and the peak position shift dependence on pressure for the X and Y propagation direction (Right) [221] .....                                                                                                                                                                                                              | 103 |
| Figure 61: Stress dependence of Raman frequency with the slope representing the piezo-spectroscopic coefficients. Reprinted from <i>Journal of the American Ceramic Society</i> , vol. 90, A. M. Limarga and D. R. Clarke, "Piezo-Spectroscopic Coefficients of Tetragonal-Prime Yttria-Stabilized Zirconia," pp. 1272-1275, Copyright (2007), with permission from John Wiley and Sons [210]..... | 104 |
| Figure 62: peak splitting (A), peak intensity (B), and peak width (C) dependence on stress. Reprinted from <i>Journal of the American Ceramic Society</i> , vol. 90, A. M. Limarga and D. R. Clarke, "Piezo-Spectroscopic Coefficients of Tetragonal-Prime Yttria-Stabilized Zirconia," pp. 1272-1275, Copyright (2007), with permission from John Wiley and Sons [210].....                       | 105 |

Figure 63: Raman pattern for 6H SiC from a hot pressed ZrB<sub>2</sub>-SiC composite with unstressed peak positions identified with lines. Reprinted from *Journal of the European Ceramic Society*, vol. 30, J. Watts, G. Hilmas, W. G. Fahrenholtz, D. Brown, and B. Clausen, "Stress measurements in ZrB<sub>2</sub>-SiC composites using Raman spectroscopy and neutron diffraction," pp. 2165-2171, Copyright (2010), with permission from Elsevier [181]..... 106

Figure 64: Schematic of shielding of a microcrack with local (compressive) residual stresses. Reprinted from *Journal of the European Ceramic Society*, vol. 19, G. Pezzotti, V. Sergo, O. Sbaizero, N. Muraki, S. Meriani, and T. Nishida, "Strengthening contribution arising from residual stresses in Al<sub>2</sub>O<sub>3</sub>/ZrO<sub>2</sub> composites: a piezo-Spectroscopy investigation," pp. 247-253, Copyright (1999), with permission from Elsevier [249]..... 108

Figure 65: Comparison of experimental data of fracture strength to the theoretical predictions. Reprinted from *Journal of the European Ceramic Society*, vol. 19, G. Pezzotti, V. Sergo, O. Sbaizero, N. Muraki, S. Meriani, and T. Nishida, "Strengthening contribution arising from residual stresses in Al<sub>2</sub>O<sub>3</sub>/ZrO<sub>2</sub> composites: a piezo-Spectroscopy investigation," pp. 247-253, Copyright (1999), with permission from Elsevier [249]..... 110

Figure 66: Schematic of a thermal residual stresses in a particulate-reinforced ceramic composite (A) and semi-infinite crack advancing through a matrix compressive region toward articulate tensile region (B). Reprinted from *Journal of the American Ceramic Society*, vol. 73, M. Taya, S. Hayashi, A. S. Kobayashi, and H. S. Yoon, "Toughening of a Particulate-Reinforced Ceramic-Matrix Composite by Thermal Residual Stress," pp. 1382-1391, Copyright (2005), with permission from John Wiley and Sons. [240]..... 111

Figure 67: Comparison of crack growth resistance measured experimentally and calculated using models. Reprinted from *Journal of the American Ceramic Society*, vol. 73, M. Taya, S. Hayashi, A. S. Kobayashi, and H. S. Yoon, "Toughening of a Particulate-Reinforced Ceramic-Matrix Composite by Thermal Residual Stress," pp. 1382-1391, Copyright (2005), with permission from John Wiley and Sons. [240]..... 112

|                                                                                                                                                                                                                                                                                                                                                                                                                                       |     |
|---------------------------------------------------------------------------------------------------------------------------------------------------------------------------------------------------------------------------------------------------------------------------------------------------------------------------------------------------------------------------------------------------------------------------------------|-----|
| Figure 68: (a) Schematic of loading ceramic bar in three point bending for collection of <i>in-situ</i> scattered light. (b) A photograph of the <i>in-situ</i> loading device. (c) Loading device coupled with Leica optical microscope connected to InVia micro-Raman spectrometer. ....                                                                                                                                            | 116 |
| Figure 69: Force applied versus voltage output for calibration of the load cell.....                                                                                                                                                                                                                                                                                                                                                  | 117 |
| Figure 70: Strain measurement setup for the sample under investigation. ....                                                                                                                                                                                                                                                                                                                                                          | 118 |
| Figure 71: Stress-strain deformation curves obtained by loading (A) Al, (B) $\text{La}_{0.8}\text{Ca}_{0.2}\text{CoO}_3$ , (C) $\text{La}_{0.8}\text{Sr}_{0.2}\text{Ga}_{0.8}\text{Mg}_{0.2}\text{O}_3$ , and (D) $\text{B}_4\text{C}$ samples using the <i>in-situ</i> loading device. The Young's moduli of the samples obtained from the measurements showed a good coincidence with the published data on the same materials..... | 119 |
| Figure 72: Wedge sample schematic (A), anticipated penetration depth (B), optical micrographs of produced wedge samples for $\text{ZrB}_2$ -17vol%SiC (C), $\text{ZrB}_2$ -32vol%SiC (D), and $\text{ZrB}_2$ -45vol%SiC (E) ceramic composites                                                                                                                                                                                        |     |
| 2.3.3: Piezo-Spectroscopy Coefficient Determination Procedure and Collection of the Distribution of Thermal Residual Stresses.....                                                                                                                                                                                                                                                                                                    | 121 |
| Figure 73: Raman Spectrometer (A), Schematic of spectrometer with the laser power labelled throughout (B).....                                                                                                                                                                                                                                                                                                                        | 124 |
| Figure 74: Spex 8000 Mixer/Mill (A) and WC vial set (B): pictures taken by Zhilin Xie .....                                                                                                                                                                                                                                                                                                                                           | 131 |
| Figure 75: Rigaku MiniFlex6000 XRD machine.....                                                                                                                                                                                                                                                                                                                                                                                       | 132 |
| Figure 76: The pressure, temperature, and shrinkage plots showing the sintering parameters of three $\text{ZrB}_2$ -17, 32, and 45vol%SiC ceramic composites by SPS .....                                                                                                                                                                                                                                                             | 135 |
| Figure 77: SEM micrographs and Raman Spectra (100% laser power, 20s exposure, and 100-1050 $\text{cm}^{-1}$ Raman Shift Range): (A) SiC ; (B) $\text{ZrB}_2$ -17 vol%SiC; (C) $\text{ZrB}_2$ -32 vol%SiC; (D) $\text{ZrB}_2$ -45 vol%SiC....                                                                                                                                                                                          | 137 |
| Figure 78: SEM backscattered micrographs of $\text{ZrB}_2$ -17vol%SiC (A), $\text{ZrB}_2$ -32vol%SiC (B), and $\text{ZrB}_2$ -45vol%SiC (C) ceramic composites, respectively. Dark grains belong to SiC phase, and the light grains belong to $\text{ZrB}_2$ matrix phase .....                                                                                                                                                       | 138 |

|                                                                                                                                                                                                                                                                                                                                                                         |     |
|-------------------------------------------------------------------------------------------------------------------------------------------------------------------------------------------------------------------------------------------------------------------------------------------------------------------------------------------------------------------------|-----|
| Figure 79: 6H-SiC FLO peak position as a function of applied stress for pure SiC and ZrB <sub>2</sub> -17, 32, and 45vol%SiC ceramic composites.....                                                                                                                                                                                                                    | 139 |
| Figure 80: (A) Optical image of mapping area, (B) 791cm <sup>-1</sup> peak intensity map, (C) SEM backscattered image of ZrB <sub>2</sub> -17vol %SiC, the insert shows a laser spot size taken using 100x objective lens, (D) Typical Raman spectra for SiC phase, (E) Typical Raman spectra for ZrB <sub>2</sub> phase .....                                          | 142 |
| Figure 81: Raman maps of ZrB <sub>2</sub> -17vol%SiC with different step sizes: (A-C) optical micrograph corresponding to the maps in the same row, 791 cm <sup>-1</sup> peak intensity maps are shown with step sizes of 1 μm (D), 0.7 μm (E), 0.5 μm (F), and 791cm <sup>-1</sup> peak width maps are shown with step sizes of 1 μm (G), 0.7 μm (H), 0.5 μm (I) ..... | 144 |
| Figure 82: Raman maps of ZrB <sub>2</sub> -17vol%SiC created using static scan and 0.7μm resolution step size with different scan exposure times : (A,B) optical micrograph corresponding to the maps in the same row, 791cm <sup>-1</sup> peak intensity maps for 30 sec (C) and 60sec (D), and 791cm <sup>-1</sup> peak width maps for 30 sec (E) and 60 sec (F)..... | 146 |
| Figure 83: Raman maps of ZrB <sub>2</sub> -17vol%SiC created using different scanning parameters as shown in the first column with a resolution step size of 0.5 μm: (A-D) optical micrograph corresponding to the maps in the same row, 791cm <sup>-1</sup> peak intensity maps (E-H) .....                                                                            | 148 |
| Figure 84: Comparison step size on the Raman maps of SiC FTO 791cm <sup>-1</sup> Peak Intensity of ZrB <sub>2</sub> -17vol%SiC: (A,B) Optical micrographs that's correspond to the maps on the right in the same row, (C) 0.7μm resolution, (D) 0.5μm resolution.....                                                                                                   | 149 |
| Figure 85: ZrB <sub>2</sub> -17vol%SiC distribution of peak position based on filtering.....                                                                                                                                                                                                                                                                            | 151 |
| Figure 86: Comparison of pure SiC, and ZrB <sub>2</sub> -SiC composites: SiC (A) optical image, (B) Peak Intensity map, (C) Peak Width map, (D) Peak Position map, ZrB <sub>2</sub> -17vol%SiC (E) optical image, (F) Peak Intensity map, (G) Peak Width map, (H) Peak Position map; ZrB <sub>2</sub> -32vol%SiC (I) optical Image, (J) Peak Intensity                  |     |

|                                                                                                                                                                                                                                                                                                                                                                                                                                                   |     |
|---------------------------------------------------------------------------------------------------------------------------------------------------------------------------------------------------------------------------------------------------------------------------------------------------------------------------------------------------------------------------------------------------------------------------------------------------|-----|
| map, (K) Peak Width map (L) Peak Position map; ZrB <sub>2</sub> -45vol%SiC (M) optical Image, (N) Peak Intensity map, (O) Peak Width map, (P) Peak Position map .....                                                                                                                                                                                                                                                                             | 154 |
| Figure 87: Comparison of Raman peak position measured and calculated for different volume fractions of SiC (A) and thermal residual stresses of ZrB <sub>2</sub> -SiC ceramic composites calculated using experimental peak positions and the model [201] along with calculated thermal residual stress of ZrB <sub>2</sub> -30vol%SiC [181] (B), two piezospectroscopic coefficients were used [219, 220]. .....                                 | 157 |
| Figure 88: Comparison of average thermal residual stresses (A), and distribution of thermal residual stresses of ZrB <sub>2</sub> -17, 32, and 45vol%SiC at 0 MPa applied load (B).....                                                                                                                                                                                                                                                           | 163 |
| Figure 89: Optical micrographs of ZrB <sub>2</sub> -17vol%SiC (A), ZrB <sub>2</sub> -32vol%SiC (B), and ZrB <sub>2</sub> -45vol%SiC (C), the 2D maps of thermal residual stress in ZrB <sub>2</sub> -17vol%SiC (D), ZrB <sub>2</sub> -32vol%SiC (E), and ZrB <sub>2</sub> -45vol%SiC (F), and line maps along X-Y line of 2D maps for ZrB <sub>2</sub> -17vol%SiC (G), ZrB <sub>2</sub> -32vol%SiC (H), and ZrB <sub>2</sub> -45vol%SiC (I) ..... | 164 |
| Figure 90: Experimentally measured re-distribution of thermal residual stresses as a function of applied tensile stress for (A) ZrB <sub>2</sub> -17vol%SiC, (B) ZrB <sub>2</sub> -32vol%SiC, (C) ZrB <sub>2</sub> -45vol%SiC ceramic composites .....                                                                                                                                                                                            | 166 |
| Figure 91: Elastic properties: (A) Young's modulus and Poisson's ratio; (B) shear and bulk moduli of ZrB <sub>2</sub> -17, 32, and 45vol%SiC ceramic composites. ....                                                                                                                                                                                                                                                                             | 168 |
| Figure 92: 4-point bending strength (A) and fracture toughness (B) of ZrB <sub>2</sub> -17, 32, and 45vol%SiC ceramic composites. ● – measured values, ○ – estimated values accounting the effect of the thermal residual stresses in SiC grains, the dotted lines are the upper and lower bounds of uncertainty for the calculated values of fracture strength and fracture toughness. ....                                                      | 170 |
| Figure 93: Fractography of ZrB <sub>2</sub> -SiC ceramic composites. SEM micrographs of the whole fracture surfaces with areas indicated for locations of possible fracture origins (A, C, E) and the micrographs of the fracture                                                                                                                                                                                                                 |     |

|                                                                                                                                                                     |     |
|---------------------------------------------------------------------------------------------------------------------------------------------------------------------|-----|
| origins (B, D, F) of the ZrB <sub>2</sub> -17vol%SiC (A, B); ZrB <sub>2</sub> -32vol%SiC (C, D); ZrB <sub>2</sub> -45vol%SiC (E, F) tested in 4-point bending. .... | 171 |
| Figure 94: Shrinkage plot for 1950°C sintering temperature, 1 <sup>st</sup> cycle (A), and 2 <sup>nd</sup> cycle (B) .....                                          | 176 |
| Figure 95: Shrinkage plot for 1500°C sintering temperature.....                                                                                                     | 177 |
| Figure 96: Shrinkage plot for 1600°C sintering temperature.....                                                                                                     | 178 |
| Figure 97: Shrinkage plot for 1700°C sintering temperature.....                                                                                                     | 179 |
| Figure 98: Shrinkage plot for 1800°C sintering temperature.....                                                                                                     | 180 |
| Figure 99: Shrinkage plot for 1500°C sintering temperature with 10 minute dwell.....                                                                                | 181 |
| Figure 100: XRD results for the 1950°C samples with phase identification .....                                                                                      | 183 |
| Figure 101: XRD results for the 1500°C samples with phase identification .....                                                                                      | 184 |

## LIST OF TABLES

|                                                                                                                                                                                                             |     |
|-------------------------------------------------------------------------------------------------------------------------------------------------------------------------------------------------------------|-----|
| Table 1: Summary of lattice parameters of ZrB <sub>2</sub> , 6H-SiC, and ReB <sub>2</sub> -type IrB <sub>2</sub> .....                                                                                      | 37  |
| Table 2: Mechanical Properties of ZrB <sub>2</sub> and SiC .....                                                                                                                                            | 47  |
| Table 3: Summary of mechanical properties of pure ZrB <sub>2</sub> , pure 6H-SiC, and ZrB <sub>2</sub> -SiC ceramic composites at room temperature .....                                                    | 48  |
| Table 4: Mechanical properties of ZrB <sub>2</sub> -SiC with different weight percent of SiC [99] .....                                                                                                     | 49  |
| Table 5: 6H-SiC phonon symmetry modes [191] .....                                                                                                                                                           | 75  |
| Table 6: Identification of phonon symmetry and propagation directions and the significance of polarization and propagation symbols for their identification [191].....                                      | 78  |
| Table 7: Energies (cm <sup>-1</sup> ) of weak phonon modes with this presentations and assignments to the values of $x=q/q_{\max}$ : N.O. stands for not observed, and F. stands for forbidden [191] .....  | 79  |
| Table 8: Experimental Raman peak positions for multiple polytypes of SiC [190] .....                                                                                                                        | 81  |
| Table 9: The hexagonality and the reduced wave vector of the folded modes which show the strongest intensity of each branch (ref 12 in Nakashima)[190].....                                                 | 83  |
| Table 10: Various techniques and attributes for finding residual stresses [204] .....                                                                                                                       | 91  |
| Table 11: Laser power through spectrometer .....                                                                                                                                                            | 125 |
| Table 12: Density, porosity, and grain size of the SiC and ZrB <sub>2</sub> -SiC ceramics.....                                                                                                              | 136 |
| Table 13: Piezospectroscopy coefficients $\Pi$ of SiC phase measured in pure SiC and three ZrB <sub>2</sub> -SiC ceramic composites.....                                                                    | 140 |
| Table 14: Investigation of step size on Raman mapping parameters used.....                                                                                                                                  | 145 |
| Table 15: Investigation of scanning parameters on Raman mapping for 0.5, 0.7, and 1 $\mu$ m resolution....                                                                                                  | 147 |
| Table 16: Investigation of resolution between spectra on Raman mapping for larger area .....                                                                                                                | 149 |
| Table 17: Thermal Residual Stresses in SiC estimated from the shift in the FLO peak position of 6H-SiC using both theoretically calculated and experimentally measured piezospectroscopic coefficients..... | 156 |



|                                                                                                                                                                                                                       |     |
|-----------------------------------------------------------------------------------------------------------------------------------------------------------------------------------------------------------------------|-----|
| Table 18: Calculated values of thermal residual stresses in SiC grains of three ZrB <sub>2</sub> -SiC ceramic composites using piezospectroscopic coefficients $\Pi$ from Table 13 without external applied load..... | 162 |
| Table 19: Calculated thermal residual stresses in SiC grains of three ZrB <sub>2</sub> -SiC ceramic composites as a function of applied bending stress .....                                                          | 167 |
| Table 20: The summary of the parameters used for the calculation of $K_{1C}$ (Eqn. (88)) .....                                                                                                                        | 174 |
| Table 21: Density and porosity of ZrB <sub>2</sub> -5wt%IrB <sub>2</sub> -20wt%SiC ceramic composites sintered by SPS .....                                                                                           | 182 |

## **CHAPTER 1: INTRODUCTION**

From the beginning of time, mankind has sought ways to fly. In 1902, the Wright brothers made the dream of powered flight possible, allowing man to fly for extended periods of time. As the years grew on, advances in airplanes came about with the improvements of the understanding of aerodynamics. The development of planes had a great impact in war, especially during World War I, when the first dog fights occurred. From this war, both sides saw how important of a contribution an airplane would be to war; this caused the airplane to grow in design and development. With World War II (WWII), airplanes had a major role in combat. Not only did WWII give rise to an advent of new airplanes, it also led to the development of the new turbojet engine used in many military aircrafts to this day. After the wars were over, airplanes started to be used as a means of travel around the world. Airplanes had much shorter travel times compared to ships. When the Cold War set in, there were many secret government projects intended to develop the fastest and most technologically advanced airplanes in the world. Chuck Yeager broke the sound barrier using the Bell X-1 rocket, thus bringing man into the age of flying faster than the speed of sound. Chuck later broke this record by flying at a speed of Mach 2.44, or 2.44 times faster than the speed of sound. The “Space Race” during the Cold War brought about even more technological advances that gave way to a new era of rockets and airplanes.

With the research and development to make airplanes more efficient and fly faster than ever, we are constantly searching for the technology of the future, especially in hypersonic missiles, and re-entry aerial vehicles. This is creating high demand for more research and better materials. We have already been able to achieve sustained supersonic flight and short flights at hypersonic speed, speeds that are greater than 5 times the speed of sound or Mach  $>5$ . At sea level,

the speed of sound is around 342 m/s. So Mach >5 at sea level would be speeds higher than 1710 m/s. However, we have not been able to sustain flight at a hypersonic range for long periods of time, such as a couple of hours. This is mainly due to the fact that materials used today are not able to withstand the extreme environment of hypersonic flight for extended periods of time.

This hypersonic environment has many aspects that make it difficult to design aerospace vehicles that could withstand the conditions experienced, whether they are space crafts or aerial vehicles that stay in the Earth's atmosphere. When the Apollo 11 Lunar pod returned from the mission of landing on the moon it re-entered the Earth's atmosphere at Mach 36 and reach a maximum temperature of 11,000K [1]. This is almost two times hotter than the surface of the sun. This is the highest challenge for designing hypersonic aerial vehicles. Finding materials that can withstand these temperatures is difficult and there is no one right answer. Figure 1 below shows the flow and other aspects of re-entry to Earth's atmosphere.

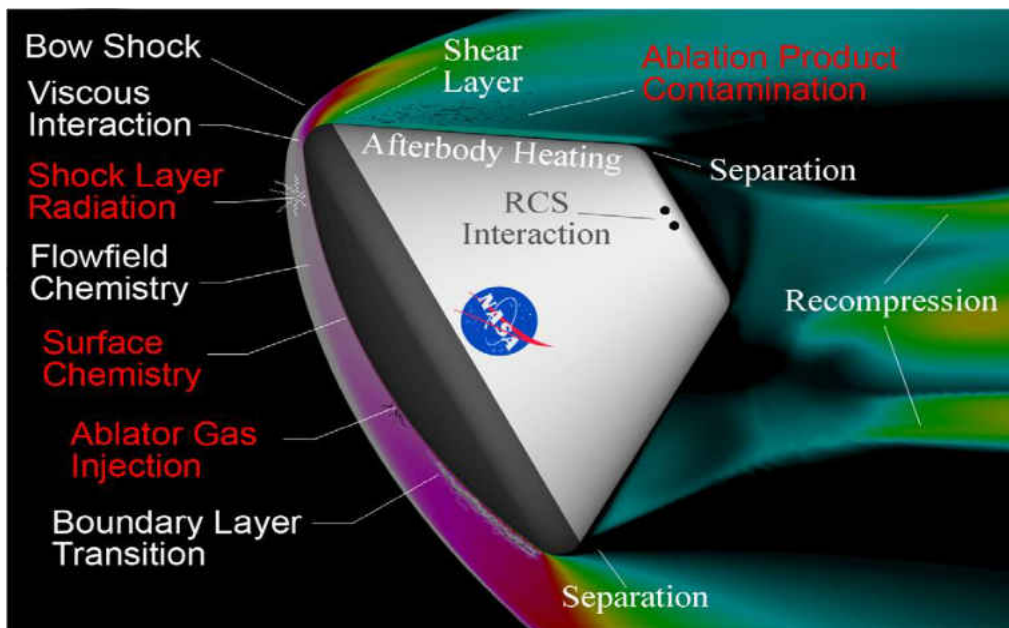
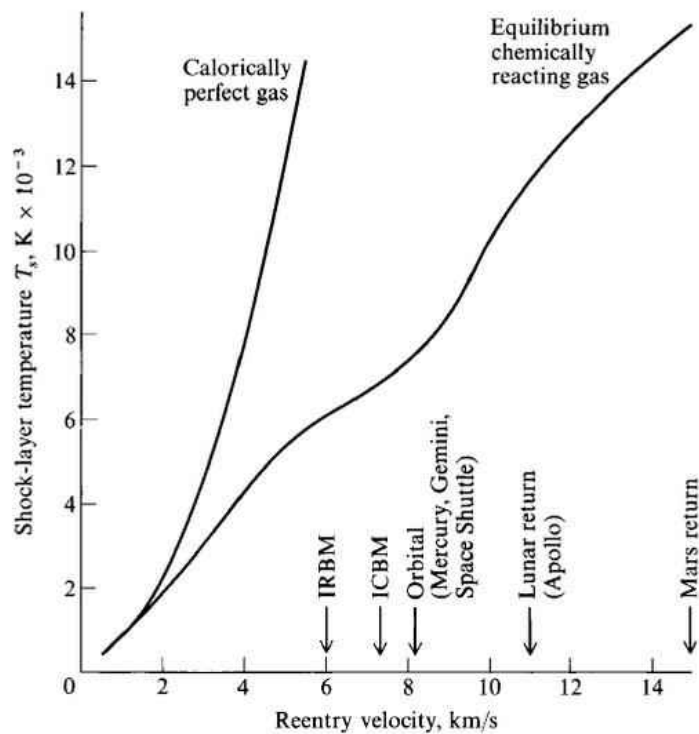


Figure 1: Re-entry to Earth's atmosphere [2]

## **1.1: Hypersonic Flow**

In this hypersonic flight regime there are many phenomena that occur. This includes strong separated bow shock, thin shock layer, viscous interaction, high-temperature flow, and entropy layer [1]. If one looks at the classic compressible flow theory, which assumes a calorically perfectly gas, and apply it to high Mach #s one finds that it over calculates the temperature behind the normal shock. This is mainly due to the fact that at high temperatures the specific heats are no longer constant. Thus kinetic theory and classical thermodynamics have to be used along with taking in to account chemically reacting flow to get an accurate representation of the true temperature behind the shock at high Mach #'s. This can be seen in below in Figure 2. This figure shows that for the case of the return of the lunar module it would greatly overestimate the temperature behind the shock. This is due to the fact that they do not take into consideration a chemically reacting flow.



**Figure 2: Temperature behind a normal shock at high velocities. Reprinted from Hypersonic and High Temperature Gas Dynamics 2<sup>nd</sup> Ed., Copyright (2006), with permission from John D. Anderson, Jr. [1]**

Now talking about each aspect of hypersonic flight mentioned in the paragraph above; first the thin shock layer. The shock layer is the flowfield between the shock wave and the body as shown in Figure 3 below [1]. As the Mach # is increased the shock layer becomes thinner and thinner, thus at high Mach #s this results in a considerably thin shock layer.

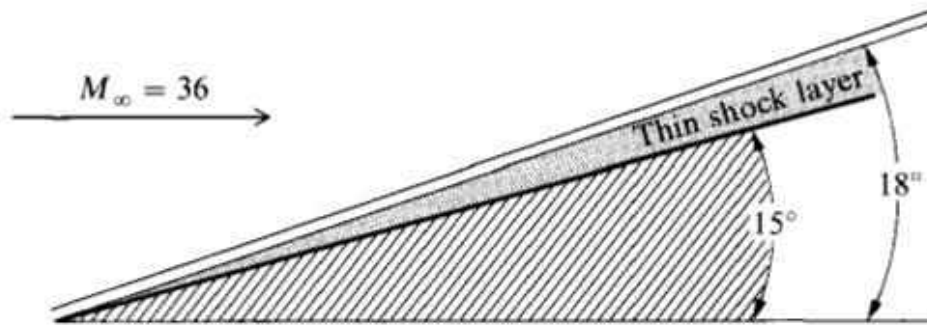


**Figure 3: Thin hypersonic shock layer.** Reprinted from *Hypersonic and High Temperature Gas Dynamics 2<sup>nd</sup> Ed.*, Copyright (2006), with permission from John D. Anderson, Jr. [1]

Next viscous interaction, shown below in Figure 4, is a major interaction between the boundary layer and the inviscid flow field. The main cause of this is viscous dissipation is when hypersonic flow is slowed down by viscous effects within the boundary layer. The loss of kinetic energy goes in part into the internal energy of the gas [1].

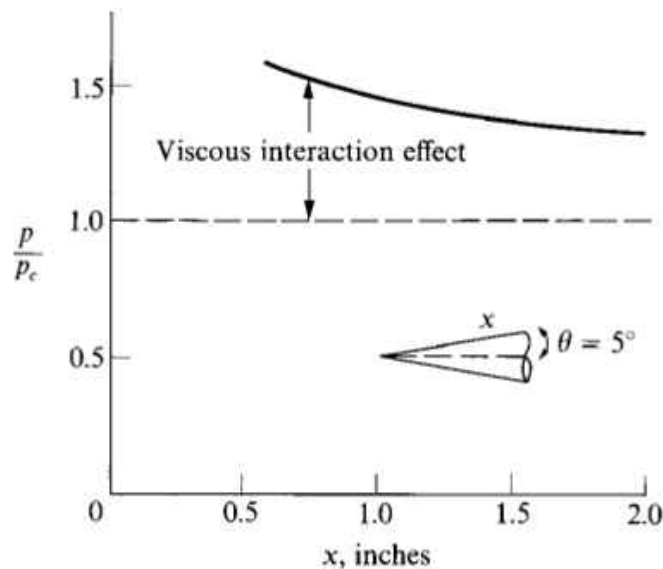


**Figure 4: Viscous interaction effects.** Reprinted from *Hypersonic and High Temperature Gas Dynamics 2<sup>nd</sup> Ed.*, Copyright (2006), with permission from John D. Anderson, Jr. [1]

As a result of a strong separated shock there is high temperature flow behind the shock. Because these temperatures are high enough to allow chemical reactions to occur, the temperature behind the shock actually decreases due to the fact that the chemical reactions occurring in the flow are dissociation reactions. These reactions are endothermic, which mean it requires heat and absorbs the heat; therefore, decreasing the overall temperature in the flow. This is one of the main reasons there is a big difference between the calorically perfect gas temperature behind the shock and chemically reacting flow gas temperature behind the shock. The entropy layer has the boundary layer growing inside it as shown below in Figure 5. The entropy layer is also a region of strong vorticity as related through the Crocco's theorem from classical compressible flow. This is also called vorticity interaction [1].

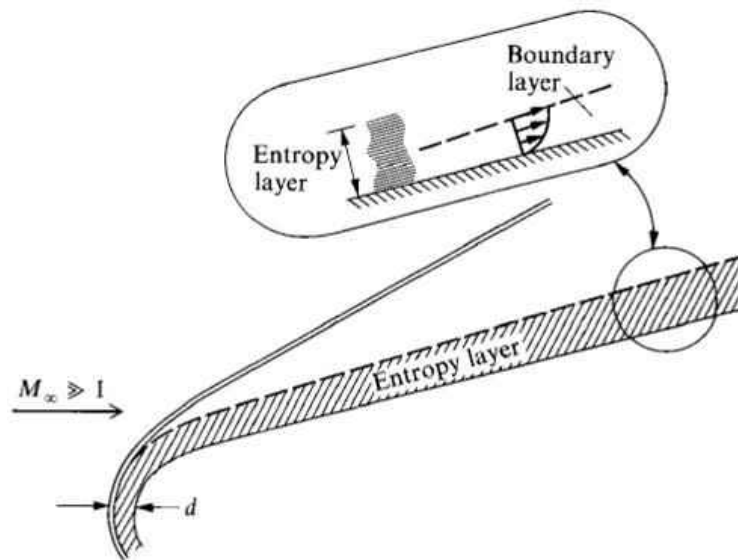


**Figure 5: Entropy Layer. Reprinted from Hypersonic and High Temperature Gas Dynamics 2<sup>nd</sup> Ed., Copyright (2006), with permission from John D. Anderson, Jr. [1]**

Figure 6 below show a picture summary of the phenomena of hypersonic flow described above.

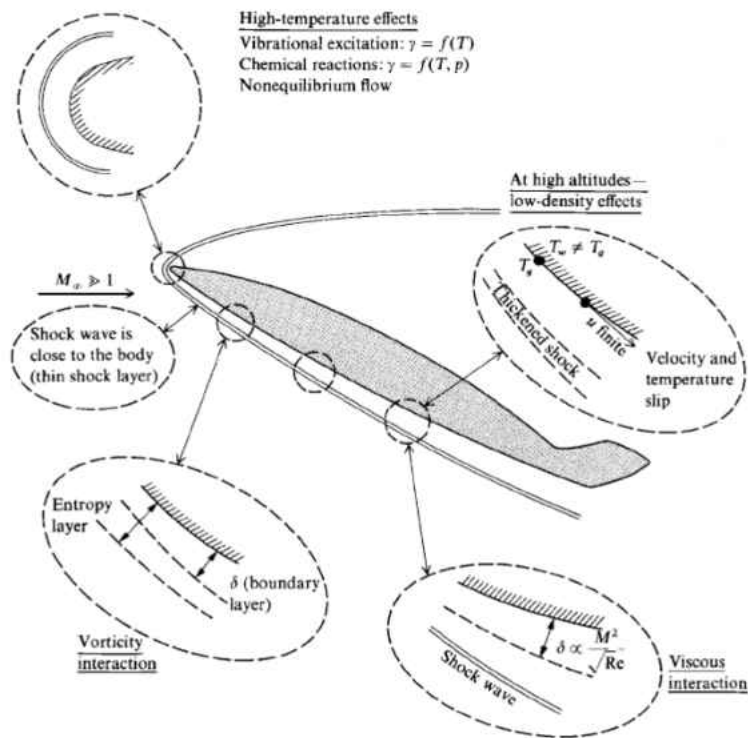


**Figure 6: Recap of the phenomena experienced in hypersonic regime. Reprinted from Hypersonic and High Temperature Gas Dynamics 2<sup>nd</sup> Ed., Copyright (2006), with permission from John D. Anderson, Jr. [1]**

### 1.1.1: Hypersonic Shock and Expansion Waves

In the beginning of hypersonic flow study the classical inviscid compressible flow shock theoretical relations were attempted to be applied to hypersonics. This was done by taking the limits of the compressible flow shock relations where  $M_1$  tends to  $\infty$  and assuming small deflecting angle,  $\theta$ . For an oblique shock one would get the relations shown in the following Figure 7.



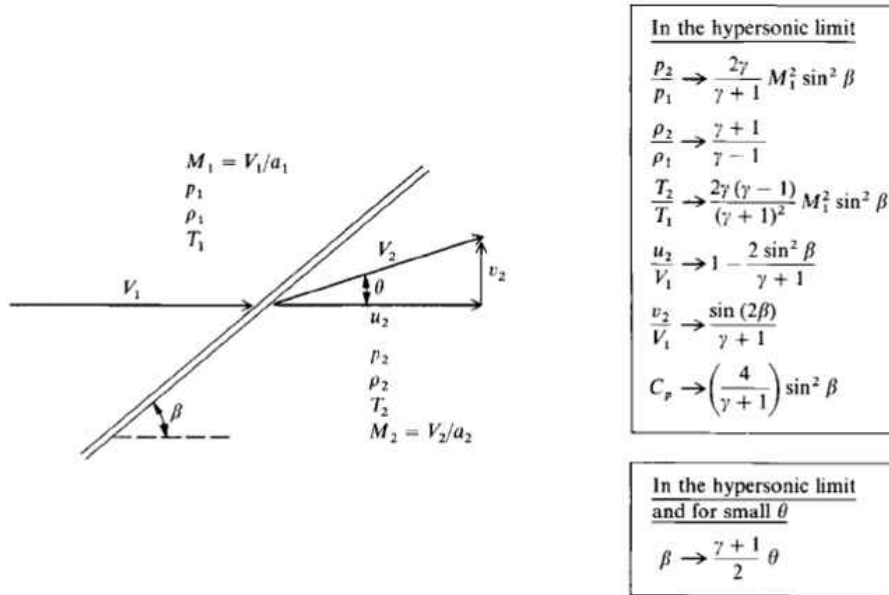


**Figure 7: Oblique shock-wave geometry. Reprinted from Hypersonic and High Temperature Gas Dynamics 2<sup>nd</sup> Ed., Copyright (2006), with permission from John D. Anderson, Jr. [1]**

For the rest of this dissertation any variable with a subscript 1 and 2 denote the properties of the flow before and after a shockwave respectively. It was found that in the hypersonic regime the Mach # and constant ratio of specific heats,  $\gamma$ , dependence break down and a new parameter is found. This new parameter is called for the hypersonic similarity parameter, K. The definition of the hypersonic similarity parameter is shown below as Equation (Eqn.) (1) [1]:

$$K = M_1 \theta \tag{1}$$

where  $M_1$  is the free stream Mach number and  $\theta$  is the deflection angle of the flow. With this parameter one can come up with the shock relations as a function mainly of K. These oblique shock relations are shown below as Eqns. (2)-(3) [1]; they are valid for hypersonic flow with large but finite Mach number and small angles of deflections:

$$\frac{P_2}{P_1} = 1 + \frac{\gamma(\gamma + 1)}{4} K^2 + \gamma K^2 \sqrt{\left(\frac{\gamma + 1}{4}\right)^2 + \frac{1}{K^2}} \quad (2)$$

$$C_p = 2\theta^2 \left[ \frac{\gamma + 1}{4} + \sqrt{\left(\frac{\gamma + 1}{4}\right)^2 + \frac{1}{K^2}} \right] \quad (3)$$

where  $P_2$  and  $P_1$  are the static pressure before and after the shock,  $K$  is the hypersonic similarity parameter, described in Eqn. (1),  $\gamma$  is the ratio of specific heat,  $\theta$  is the flow deflection angle, and finally  $C_p$  is the coefficient of pressure after the shock. Looking at Eqn. (3) one sees that  $\frac{C_p}{\theta^2} = fn(K, \gamma)$  and not a function of  $\gamma$  and  $M$  as found typically in supersonic flows.

Continuing our talk about the initial theory of taking supersonic relations and expanding them to hypersonic flow by taking  $M_1$  tends to  $\infty$  and assuming small deflecting angle,  $\theta$ . The next information wanted is the flow properties after an expansion or turning of the flow. This is done through the expansion-wave relations also known as Prandtl-Meyer flow. Figure 8 below shows the geometry of the hypersonic expansion-wave as well as the nomenclature before and after the turn.

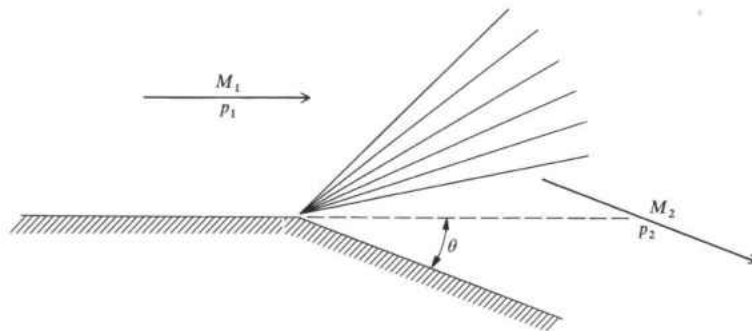


**Figure 8: Expansion-wave geometry. Reprinted from Hypersonic and High Temperature Gas Dynamics 2<sup>nd</sup> Ed., Copyright (2006), with permission from John D. Anderson, Jr. [1]**

This can give the pressure coefficient after the flow has turned such as on a nose cone downstream of the shock. Therefore one can estimate the lift and drag of the object with supersonic relations, with the assumptions that the Mach number is high but finite and that the deflection angle,  $\theta$ , is small. Also expressing the relations in terms of the hypersonic similarity parameter  $K$  one gets the following Eqns. (4)-(6) [1]:

$$\theta = \frac{2}{\gamma - 1} \left( \frac{1}{M_1} - \frac{1}{M_2} \right) \quad (4)$$

$$\frac{P_1}{P_2} = \left( 1 - \frac{\gamma - 1}{2} K \right)^{\frac{2\gamma}{\gamma - 1}} \quad (5)$$

$$C_p = \frac{2\theta^2}{\gamma K^2} \left[ \left( 1 - \frac{\gamma - 1}{2} K \right)^{\frac{2\gamma}{\gamma - 1}} - 1 \right] \quad (6)$$

where  $C_p$  is the coefficient of pressure after the expansion fan,  $\theta$  is the angle of the deflection as shown in Figure 8,  $K$  is the hypersonic similarity parameter as described in Eqn. (1) above,  $\gamma$  is the ratio of specific heats,  $P$  is the pressure, and the subscripts 1 and 2 designate the properties of the flow before and after the expansion fan, respectively.

Theses relations just give the basic results of the fluid before and after the shock and the flow turning about an angle. Surprisingly these relationships are perfect to give initial guesses for hypersonic Computational Fluid Dynamics (CFD) and actually estimate the properties immediately before and after the shock wave and expansion wave pretty closely [1].

### **1.1.2: Hypersonic Shockwaves of Chemically Reacting Flow in Equilibrium**

At high temperature experience in hypersonic flow, the ratio of specific heats,  $\gamma$ , is not long a constant and thus  $\gamma = \text{fn}(T)$  [3]. This is shown in Figure 9 below.

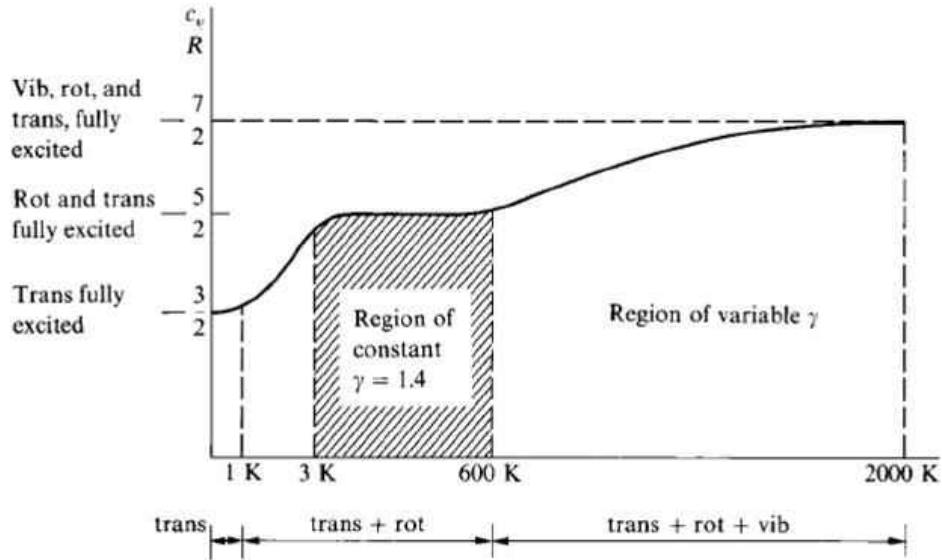


**Figure 9: Ratio of specific heat. Reprinted from Hypersonic and High Temperature Gas Dynamics 2<sup>nd</sup> Ed., Copyright (2006), with permission from John D. Anderson, Jr. [1]**

Now that one knows that there are chemical reactions occurring hypersonic flow and that the ratio of specific heat is no longer constant in hypersonic flow, the typical compressible flow theory shock relations, found in most fluids textbooks, are no longer valid [3-5]. These relations are shown below as Eqns. (7)-(11) for normal shocks:

$$M_2^2 = \frac{M_1^2 + \frac{2}{\gamma - 1}}{\frac{2\gamma}{\gamma - 1} M_1^2 - 1} \quad (7)$$

$$\frac{T_2}{T_1} = \frac{\left(1 + \frac{\gamma - 1}{2} M_1^2\right) \left(\frac{2\gamma}{\gamma - 1} M_1^2 - 1\right)}{\left[\frac{(\gamma - 1)^2}{2(\gamma - 1)}\right] M_1^2} \quad (8)$$

$$\frac{p_2}{p_1} = \frac{2\gamma M_1^2}{\gamma + 1} - \frac{\gamma - 1}{\gamma + 1} \quad (9)$$

$$\frac{\rho_2}{\rho_1} = \frac{(\gamma + 1)M_1^2}{(\gamma - 1)M_1^2 + 2} \quad (10)$$

$$\frac{p_{o2}}{p_{o1}} = \left[ \frac{\frac{\gamma + 1}{2} M_1^2}{1 + \frac{\gamma - 1}{2} M_1^2} \right]^{\frac{\gamma}{\gamma - 1}} \left[ \frac{1}{\frac{2\gamma}{\gamma + 1} M_1^2 - \frac{\gamma - 1}{\gamma + 1}} \right]^{\frac{1}{\gamma - 1}} \quad (11)$$

where  $M$  is the Mach number,  $\gamma$  is the ratio of specific heats,  $\rho$  is the density,  $p$  is the pressure,  $u$  is x-direction component of velocity,  $h$  is the enthalpy. The subscripts 1, and 2 stand for the static properties of the flow before and after the shockwave, respectively. The subscripts o1, and o2 stand for the stagnation properties of the flow before and after the shockwave, respectively. Again the reason for the typical compressible flow theory shock relations not being valid is because the ratio of specific heat is no longer constant (the main assumption made when deriving the compressible flow theory shock relations) as well as the chemical reactions occurring in the flow affect the properties after the shock wave. Therefore, one would like to investigate the governing equations for shockwaves in hypersonic flow with equilibrium and non-equilibrium chemical reactions occurring in the flow. The shock relations shown as Eqns. (4)-(6) are valid only for very high Mach #'s and for very small deflection angles, but this is not always the case, since most hypersonic nose cones, leading edges, etc., are blunt bodies due to the aerodynamic heating that occurs at high Mach #'s. If a wedge used in typical supersonic flow is used in hypersonic flow the wedge would simply melt away and would ultimately fail. Thus a deeper understanding of shockwaves is not only beneficial, it's necessary for determining if the materials under consideration are candidates for hypersonic aerial vehicles. The use of the most suitable materials could also help improve the performance of the vehicles by being used in leading edges or nose cones for hypersonic aerial vehicles.

To derive the appropriate governing equations, start first by looking at normal shocks in equilibrium flows, where the equilibrium conditions hold behind the shock. An equilibrium flow is defined as flow that is in local thermodynamic and chemical equilibrium [1]. Starting with the derivation of the normal shock equation for equilibrium flows with the conservations of mass (continuity), momentum, and energy shown below as Eqns. (12)-(14), respectively[1]:

$$\rho_1 u_1 = \rho_2 u_2 \quad (12)$$

$$p_1 + \rho_1 u_1^2 = p_2 + \rho_2 u_2^2 \quad (13)$$

$$h_1 + \frac{u_1^2}{2} = h_2 + \frac{u_2^2}{2} \quad (14)$$

where  $\rho$  is the density,  $p$  is the pressure,  $u$  is x-direction component of velocity,  $h$  is the enthalpy, while the subscripts 1 and 2 stand for the properties of the flow before and after the shockwave respectively. Then with some rearrangement one gets the following expression for the pressure behind the shock, shown below as Eqn. (15), and the enthalpy behind the shock, as shown below as Eqn. (16) [1]:

$$p_2 = p_1 + \rho_1 u_1^2 \left[1 - \frac{\rho_1}{\rho_2}\right] \quad (15)$$

$$h_2 = h_1 + \frac{u_1^2}{2} \left[1 - \left(\frac{\rho_1}{\rho_2}\right)^2\right] \quad (16)$$

where  $\rho$  is the density,  $p$  is the pressure,  $u$  is x-direction component of velocity,  $h$  is the enthalpy, while the subscripts 1 and 2 stand for the properties of the flow before and after the shockwave respectively. The properties behind the shocks are then calculated by using the Eqs. (15) and (16) above, and the following iterative numerical solution method found in the book written by

Anderson [1]. The iterative numerical solution to hypersonic normal shockwave in equilibrium flow is as follows:

1. Assume a value of  $\rho_1/\rho_2$  (an initial value of 0.1 is usually a good first guess).
2. Calculate  $P_2$  using the Eqn. (15) above and  $h_2$  from Eqn. (16) above.
3. With the values of  $P_2$  and  $h_2$  just obtained, calculate  $\rho_2$  from any equilibrium thermodynamic properties table, graph, or equations
4. Form a new value of  $\rho_1/\rho_2$  using the value of  $\rho_2$  obtained from step 3
5. Use this new value of  $\rho_1/\rho_2$  to calculate new values of  $P_2$  and  $h_2$  using the same equations as in step 2. Repeats steps 1-5 until convergence has been reached, i.e. the change in  $\rho_1/\rho_2$  from one iteration to the next is negligible.
6. Now we have the correct values of  $P_2$ ,  $h_2$ , and  $\rho_2$ . Now obtain the correct value of  $T_2$  from any equilibrium thermodynamic properties table, graph, or equations
7. Next obtain the correct value of  $u_2$  from equations

Completing steps 1-7 above one can find all the properties behind a normal shock in hypersonic equilibrium flow based on the flow properties before the shockwave. Upon review of the results for normal shockwaves, one finds that the ratio of density, pressure, and enthalpy is a function of three freestream (flow properties before the shockwave) of velocity, pressure and temperature; instead of being just a function of the freestream Mach # as found in calorically perfect gas normal shock relations [3-6]. In addition to the flow properties behind the shock, the equilibrium composition behind the front depends on the values of  $P_2$  and  $T_2$ , with these two values being dependent on the freestream properties of  $P_1$  and  $T_1$ . From the equations and the above statement

one can determine that chemically reacting gas is mainly governed by the following variables of velocity, temperature, and pressure. In equilibrium flow the definition of the Mach # is the same as defined for a calorically perfect gas. However, when non-equilibrium flow is being considered, the definition of Mach # becomes less obvious and further loses its importance [1]. Temperature is the parameter that is the most sensitive variable when chemical reactions are occurring. On the contrary, chemical reactions have almost no effect on pressure. This is because pressure is mainly governed by fluid mechanics instead of thermodynamics. One will also notice that in an equilibrium gas, with dissociating and ionizing reactions, increasing the pressure at a constant temperature tends to decrease the atom and ion mass fractions. Thus increasing the pressure at a constant temperature prevents the ionization and dissociating reactions. This is shown below in the following Figure 10, where the temperature ratio across the shock is plotted vs. upstream velocity [1]. Looking at Figure 10, one can see that at higher pressures there is less dissociation and ionization reactions occurring, thus resulting in a higher  $T_2/T_1$  ratio across the shockwave.



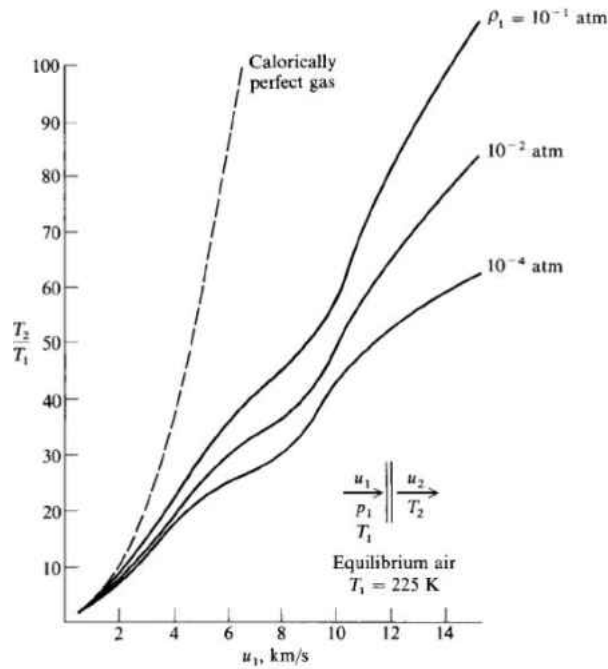


Figure 10: Influence of pressure on the normal shockwave temperature in equilibrium air. Reprinted from Hypersonic and High Temperature Gas Dynamics 2<sup>nd</sup> Ed., Copyright (2006), with permission from John D. Anderson, Jr. [1].

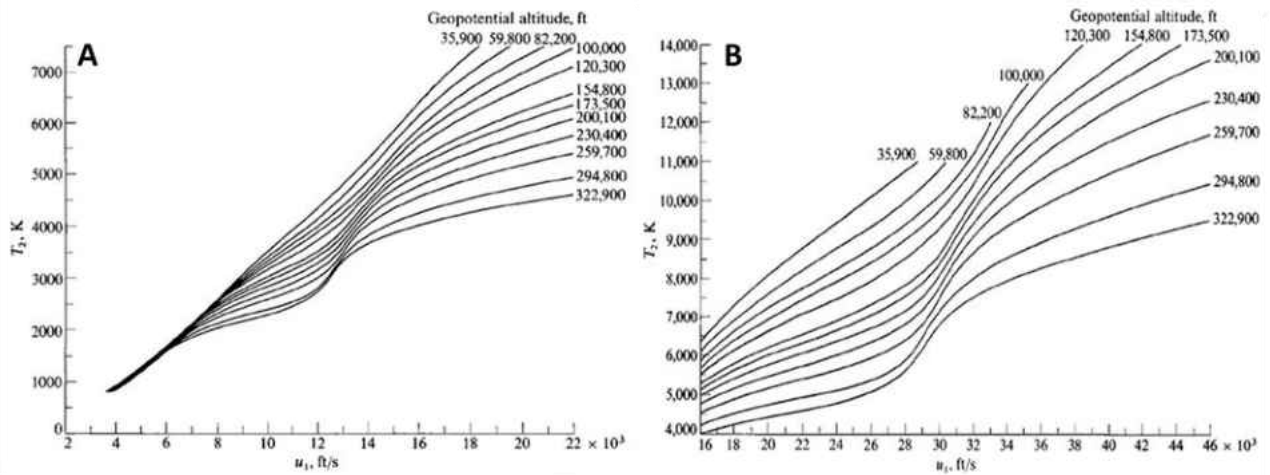
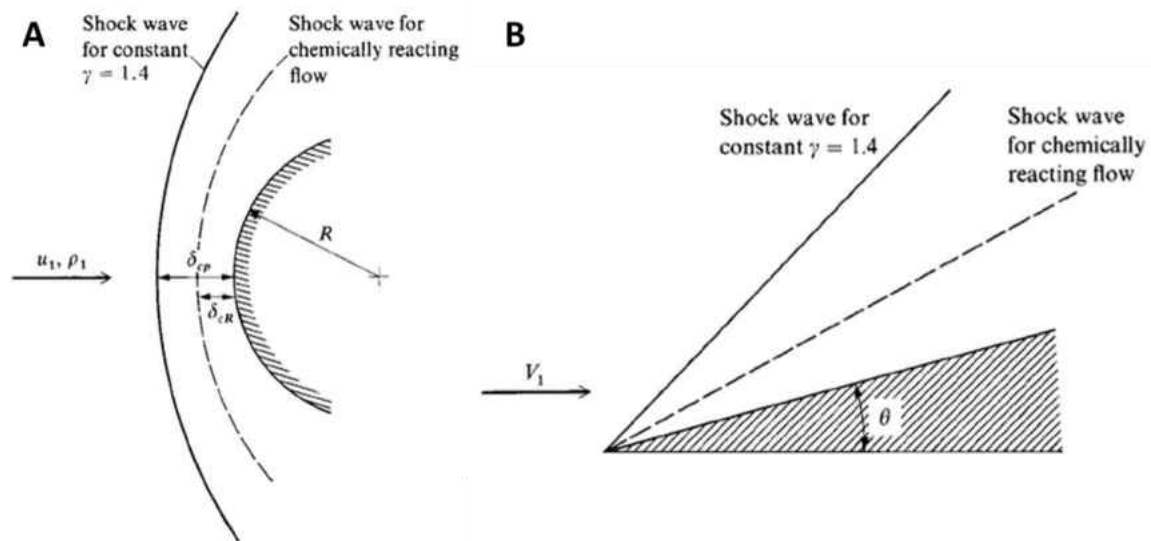


Figure 11: Variation of normal shock density with velocity and altitude; velocity range below (A) and near & above (B) orbital velocity (From Huber [7]). Reprinted from Hypersonic and High Temperature Gas Dynamics 2<sup>nd</sup> Ed., Copyright (2006), with permission from John D. Anderson, Jr. [1]

The ratio of densities  $\rho_2/\rho_1$  has a very important effect on the normal shock detachment distance. This is expressed as the following approximation shown below in Eqn. (17) [1]:

$$\frac{\delta}{R} \approx \frac{\rho_1}{\rho_2} = \frac{1}{\frac{\rho_2}{\rho_1}} \quad (17)$$

where  $\delta$  is the shock detachment distance,  $R$  is the radius of the blunt-body,  $\rho_1$  is the density of the flow before the shockwave, and  $\rho_2$  is the density of the flow behind the shockwave. This equation above is valid only at high velocities. The shock detachment distance is greatly affected by chemical reactions. When chemical reactions occur it results in higher density ratios across the shockwave and thus decreases the shock detachment distance as shown graphically as Figure 12 below (A for normal shock and B for oblique shockwave) [1]:



**Figure 12: Relative locations of blunt-body bow shockwaves (A), and oblique shockwaves (B) for calorically perfect and chemically reacting gases. Reprinted from Hypersonic and High Temperature Gas Dynamics 2<sup>nd</sup> Ed., Copyright (2006), with permission from John D. Anderson, Jr. [1].**

The oblique shockwave equations are derived by looking at the following geometry shown below as Figure 13.

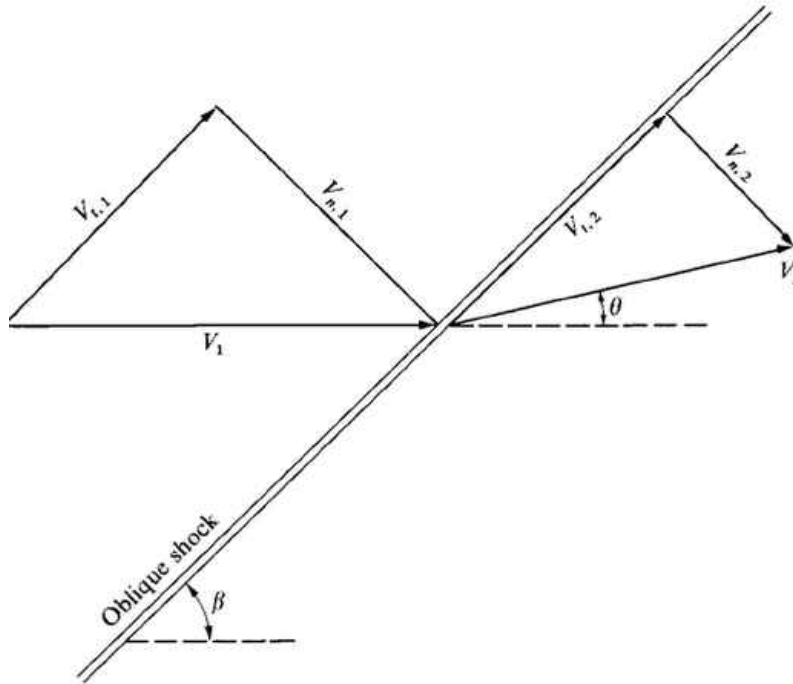


**Figure 13: Oblique shockwave geometry. Reprinted from Hypersonic and High Temperature Gas Dynamics 2<sup>nd</sup> Ed., Copyright (2006), with permission from John D. Anderson, Jr. [1]**

Based on the geometry shown in the figure above, one can derive Eqn. (18) shown below for the ratio of the normal and tangential component of the velocity vector behind the shock wave:

$$\tan(\beta - \theta) = \frac{V_{n,2}}{V_{t,1}} = \frac{V_{n,2}}{V_{n,1}} \frac{V_{n,1}}{V_{t,1}} \quad (18)$$

where the angles  $\beta, \theta$  are defined in Figure 13. The velocities component before,  $V_{n,1}$  and  $V_{t,1}$ , and after,  $V_{n,2}$  and  $V_{t,2}$ , the shockwave are also defined in Figure 13. The  $n$  and  $t$  subscripts stand for the normal and tangential components of velocity, respectively. While the subscripts 1 and 2

stand for the properties of the flow before and after the shockwave, respectively. Now substituting in the fact that the tangential component of the velocity vector is the same across the shockwave, i.e.  $V_{t1}=V_{t2}$ , thus one gets the following Eqn. (19) shown below:

$$\tan(\beta - \theta) = \frac{V_{n,2}}{V_{n,1}} \tan(\beta) \quad (19)$$

where the variables  $\beta$ ,  $\theta$ ,  $V_{n,2}$ ,  $V_{n,1}$  all have the same mean as in Eqn. (18) and Figure 13. The Eqn. (19) above is for the equilibrium high-temperature case, which relates the wave angle,  $\beta$ , the deflection angle  $\theta$ , and the upstream velocity  $V_1$ . Combining this equation with the normal shock Eqns. (12)-(16) one can create the following  $\theta$ - $\beta$ - $V$  Figure 14 shown below for equilibrium flows across oblique shocks [1].

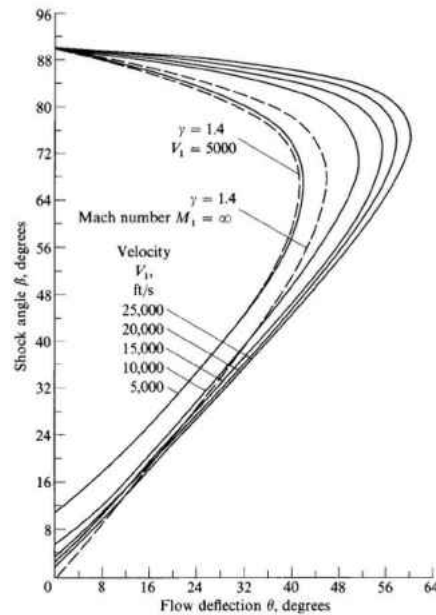


**Figure 14: Deflection angle-wave angle-velocity diagram for oblique shocks on high-temperature air at 10,000 ft altitude (From Moeckel [8]). Reprinted from Hypersonic and High Temperature Gas Dynamics 2<sup>nd</sup> Ed., Copyright (2006), with permission from John D. Anderson, Jr. [1].**

Now that one has defined all of the normal and oblique shock relations one would like to look at the overall results. Therefore, using the velocity-altitude map by Bussing and Eberhardt [9], one can construct the equilibrium chemical species behind the shockwave for a normal shock Figure 15A, and oblique shock Figure 15B shown below[1].

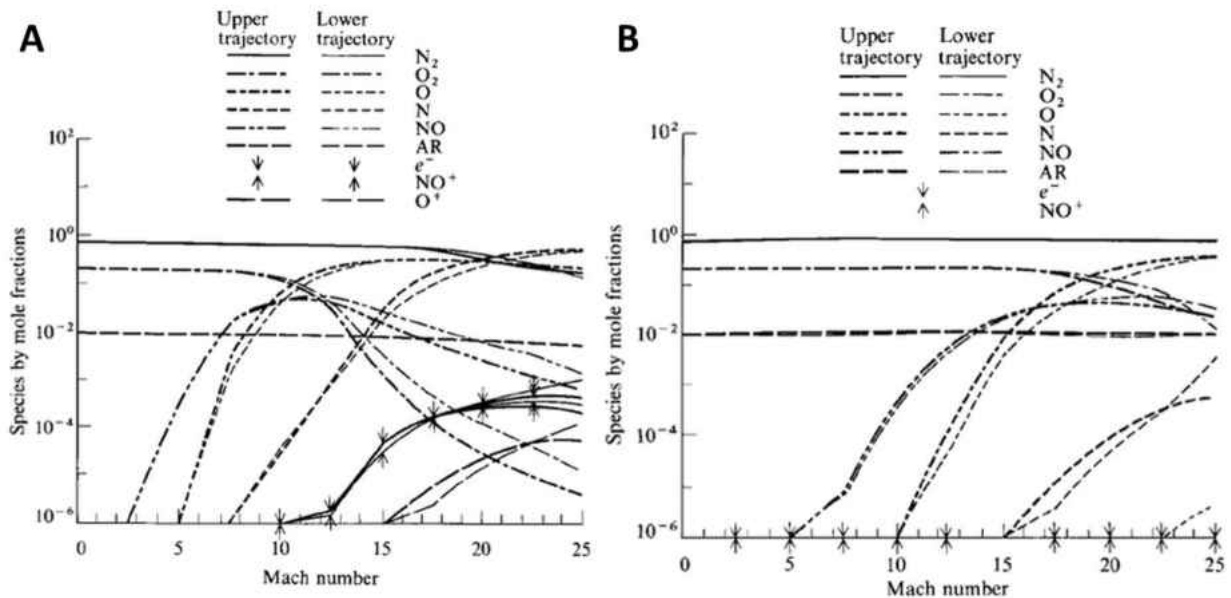


**Figure 15: Equilibrium chemical species variations behind normal shock (A) and behind 30-deg oblique shock (B) for two different trajectories (From [9]). Reprinted from Hypersonic and High Temperature Gas Dynamics 2<sup>nd</sup> Ed., Copyright (2006), with permission from John D. Anderson, Jr. [1].**

### 1.1.3: Hypersonic Shockwaves of Chemically Reacting Flow in Non-equilibrium

Before one can start talking about shockwave in a non-equilibrium flow one must first define the meaning of a *shock front*. The shock front is defined as the thin region where large gradients in temperature, pressure, and velocity occur, and where the transport phenomena of viscosity and thermal conduction are important [1]. Due to the fact that in chemical equilibrium and calorically perfect gas, the gradients in the flow take place almost discontinuously within a

thin region, which is the shockwave itself. In this case the shockwave was the shock front. But in chemical non-equilibrium flow the reactions take place at a finite rate, thus the shockwave now consists of the shock front and the non-equilibrium region behind the front. Because the shock front is only a few mean paths thick, therefore the flow properties immediately behind the shock front are frozen properties and then downstream the finite-rate reactions take place and the properties of the flow relax to their equilibrium values [1].

Now let's look at the derivation of the equations that define shockwaves in chemical non-equilibrium flows, specifically normal and oblique shock. Starting with the normal shockwave, and looking at the shock front region one obtains the properties immediately behind the shock front. This is done by taking the flow properties of a frozen flow, that is the typically calorically perfect gas, i.e.  $\gamma$  is constant and equal to 1.4 for air, shown above as Eqns.(7)-(11). From this one obtains the values of  $T_{\text{frozen}}$  and  $\rho_{\text{frozen}}$ .

Due to the fact that dissociating and ionizing reactions are endothermic in nature, the static temperature behind the shock front decreases and therefore the density increases, with the chemical species reaching equilibrium values downstream. This can be found by performing a numerical calculation of the non-equilibrium region behind the shock front. Assuming the flow behind the shock front is 1-D steady state one gets the following Eqns. (20)-(23) for continuity, momentum, energy, and species continuity respectively [1]:

$$\rho du + u dp = 0 \quad (20)$$

$$dp = -\rho u du \quad (21)$$

$$dh_0 = 0 \quad (22)$$

$$u dc_i = \frac{\dot{w}_i}{\rho} dx \quad (23)$$

where  $\rho$  is the density,  $p$  is the pressure,  $u$  is x-direction component of velocity,  $h$  is the enthalpy,  $c$  is the species concentration,  $x$  is the distance measured from the shock front, extending downstream,  $\dot{w}_i$  is the finite-rate chemical reaction term, and  $i$  is the  $i$ th species being considered in the numerical calculations. Solving these Eqns. (20)-(23) will give you the solution of the flowfield between the shock front and the hypersonic aerial vehicle body. One must use a numerical integrating technique for solving these ordinary differential equations. The very well-known Runge-Kutta technique is an excellent technique to integrate the mentioned flow field starting at the shock front to flow downstream in steps of  $\Delta x$ . The initial conditions used to start the calculations is by assuming the frozen flow across the shock front and obtaining the properties immediately behind the shock front using the typically compressible flow normal shock relations. This initial condition is assuming that the chemical composition across the shock front does not change. One should note that carrying out this calculation, if the finite-rate reactions are very fast, ie  $\dot{w}_i$  is very large in the above Eqn. (23), then a  $\Delta x$  must be chosen to be very small even with using a high order method. Such fast finite reactions results in a stiff species continuity equations lead to instabilities in the solution. Typical results of this numerical calculations, described above, is shown below as Figure 16 [1].

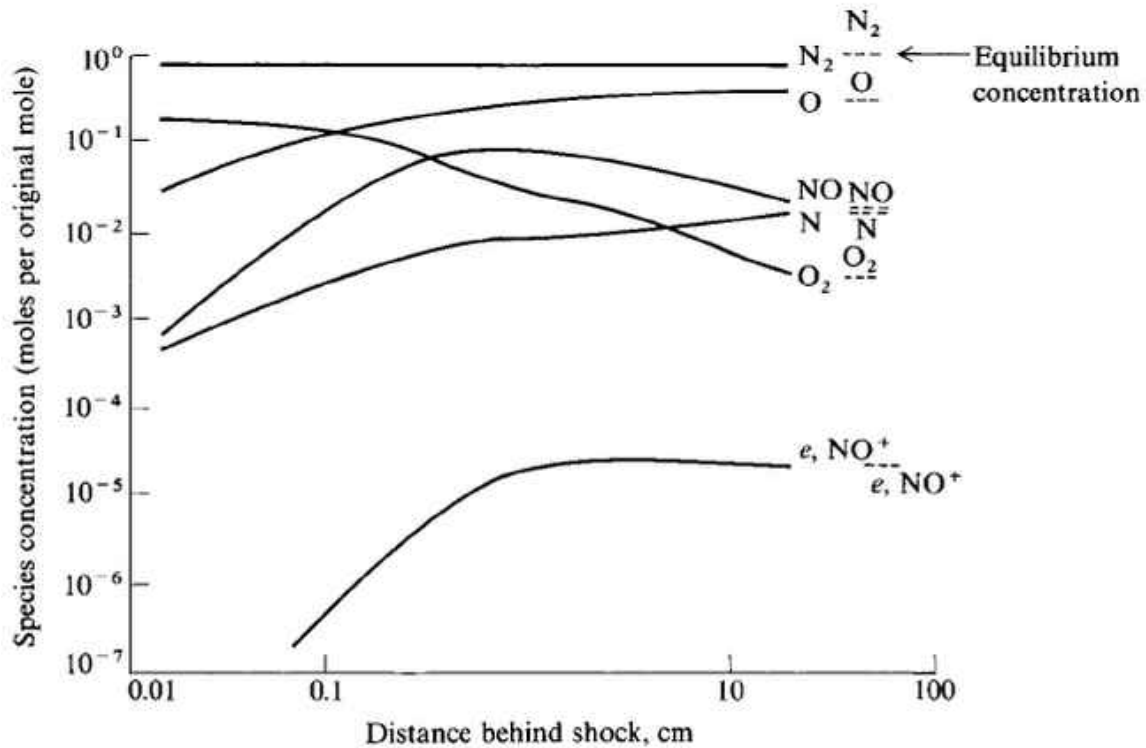


**Figure 16: Distributions of the chemical species for the nonequilibrium flow through a normal shock wave in air:  $M_\infty=12.28$ ,  $\rho_\infty=1.0\text{mm Hg}$ , and  $T_\infty=300\text{K}$  (From Marrone [10]). Reprinted from Hypersonic and High Temperature Gas Dynamics 2<sup>nd</sup> Ed., Copyright (2006), with permission from John D. Anderson, Jr. [1].**

Now, let's investigate the oblique shock waves in chemical non-equilibrium flow. One must first define the geometry of the oblique shockwave, one gets two cases: the first is the straight oblique shock shown in Figure 17A below, and the second is the compression corner shown below as Figure 17B.



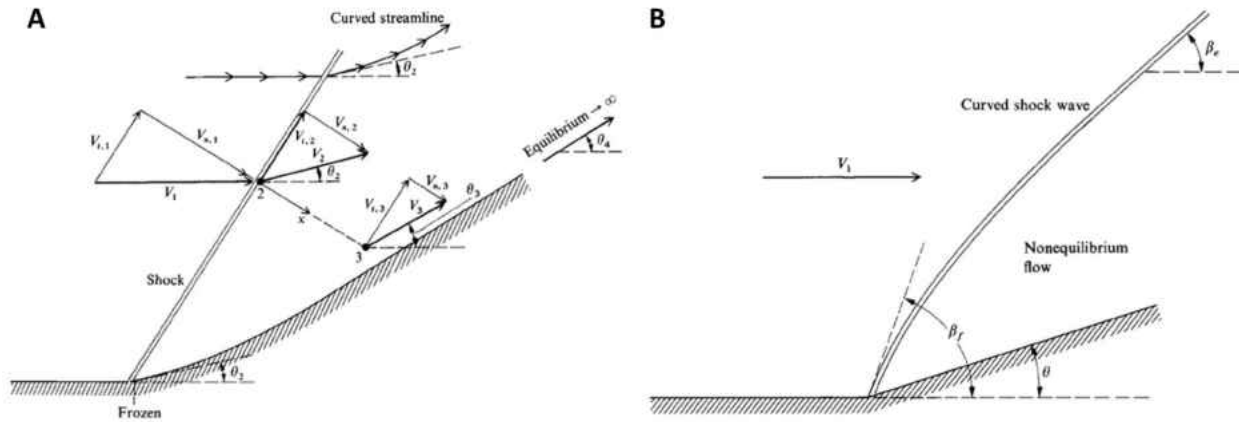


**Figure 17: Geometry for non-equilibrium flow behind a straight oblique shockwave (A), and the schematic of non-equilibrium flow over a compression corner (B). Reprinted from Hypersonic and High Temperature Gas Dynamics 2<sup>nd</sup> Ed., Copyright (2006), with permission from John D. Anderson, Jr. [1].**

From the oblique shockwave in chemical equilibrium flows one knows that the tangential component of velocity is constant, ie  $V_{t1}=V_{t2}=V_{ti}$ . This is still true in chemical non-equilibrium flow, thus the Eqns. (20)-(23) above for normal shock apply to oblique shocks. The same numerical solution used above with normal shocks in chemical non-equilibrium flow can be applied to oblique shockwaves in chemical non-equilibrium flows. Now since the tangential component of velocity is constant the normal component of velocity,  $V_n$ , varies with distance  $x$ , from the shock front. Since  $\rho V_n$  is constant across a normal shockwave, then since the density across a normal shock increases the normal component of velocity must decrease across the normal shockwave. Now that one knows that the velocity decreases with increases of distance,  $x$ , from the shock front, one can say that  $V_{n3} < V_{n2}$  and since  $V_{t2} = V_{t3}$ , the flow deflection angle  $\theta_3 > \theta_2$ . Thus, one can conclude that the streamlines in the non-equilibrium flow behind a straight oblique shock front are curved and continually increase their deflection angle until equilibrium conditions are reached far downstream, as shown above in Figure 17A. One can also conclude that in order to get straight

streamlines after the oblique shockwave in chemical non-equilibrium flow one must have a compression corner as shown above in Figure 17 B. One sees that the shockwave is curved while the streamlines are straight with a constant deflection angle,  $\theta$ . The wave angle,  $\beta$ , of this curve shock wave varies from the frozen flow angle right at the corner, to the equilibrium angle value reached downstream of the corner. One must finally note that the equilibrium shock-wave angle is always less than the frozen wave angle or calorically perfect gas shockwave angle [1].

To sum up, the non-equilibrium flow behind a shock front varies with distance behind the front. Therefore a dimensional scale is introduced into such flows. Bussing and Eherhandt [9] defined a non-equilibrium length scale, relaxation distance, as the distance downstream of the shock front, required for the flow properties to reach 95% of their equilibrium values . This relaxation distance is different for different flows. The shockwave analysis shows that non-equilibrium effects are very important in hypersonic aerial vehicles. This can further be proved by the following example. Say you have a blunt body with a nose radius of 10cm. The approximate shock detachment distance will be on the order of 1cm or less. This indicates that most of the portions of the blunt body flow region will be in chemical non-equilibrium flow. For slender bodies and wings one predicts long regions of chemical non-equilibrium flows downstream from the leading edge further proving the point that chemical non-equilibrium flow dominates the performance of the hypersonic vehicle. Thus it is of utmost importance to choose and design the best materials for applications such as nose cones and leading edges for the future of hypersonic aerial vehicles.

### 1.1.4: Hypersonic Flow Navier-Stokes Equations

Now that one has covered all of the possible different types of shockwaves encountered by hypersonic aerial vehicles, the next step is to go over the following theories, which are some more approximate methods with increasing complexity: Newtonian, Modified Newtonian, Newtonia-Buseman, Tangent-Wedge/Tangent-Cone Methods, Shock-Expansion Method, Small-Disturbance Theory, Blast Wave Theory, Shock-Layer Theory, Method of Characteristics. The most exact of these theories are Euler and Navier-Stokes equations (applied to Viscous Flow with and without chemical reacting flows). All of these theories, derivations, and applications can be found in Anderson[1].

The most important of these theories is the Navier-Stokes equations. Since computers have been able to handle more computationally heavy problems these equations are becoming more popular. This is due to the fact that the Navier-Stokes equations give the exact solution to the entire flowfield including the regions of the flow with chemical reaction present, as well as the boundary layer. The Navier-Stokes equation can also be used to solve the location of the shock. For hypersonic viscous flow with no chemical reactions the governing equations as show below as Eqns. (24)-(34) [1]:

$$\frac{\partial \rho}{\partial t} + \nabla \cdot (\rho \vec{V}) = 0 \quad (24)$$

$$\rho \frac{Du}{Dt} = -\frac{\partial p}{\partial x} + \frac{\partial \tau_{xx}}{\partial x} + \frac{\partial \tau_{yx}}{\partial y} + \frac{\partial \tau_{zx}}{\partial z} \quad (25)$$

$$\rho \frac{Dv}{Dt} = -\frac{\partial p}{\partial y} + \frac{\partial \tau_{xy}}{\partial x} + \frac{\partial \tau_{yy}}{\partial y} + \frac{\partial \tau_{zy}}{\partial z} \quad (26)$$

$$\rho \frac{Dw}{Dt} = -\frac{\partial p}{\partial z} + \frac{\partial \tau_{xz}}{\partial x} + \frac{\partial \tau_{yz}}{\partial y} + \frac{\partial \tau_{zz}}{\partial z} \quad (27)$$

$$\begin{aligned} & \rho \frac{D(e + V^2/2)}{Dt} \\ &= \rho \dot{q} + \frac{d}{dx} \left( k \frac{\partial T}{\partial x} \right) + \frac{d}{dy} \left( k \frac{\partial T}{\partial y} \right) + \frac{d}{dz} \left( k \frac{\partial T}{\partial z} \right) - \nabla \cdot (p\vec{V}) \\ &+ \frac{\partial (u\tau_{xx})}{\partial x} + \frac{\partial (u\tau_{yz})}{\partial x} + \frac{\partial (u\tau_{zx})}{\partial x} + \frac{\partial (v\tau_{xy})}{\partial y} + \frac{\partial (v\tau_{yy})}{\partial y} \\ &+ \frac{\partial (v\tau_{zy})}{\partial y} + \frac{\partial (w\tau_{xz})}{\partial z} + \frac{\partial (w\tau_{yz})}{\partial z} + \frac{\partial (w\tau_{zz})}{\partial z} \end{aligned} \quad (28)$$

where

$$\tau_{xy} = \tau_{yx} = \mu \left( \frac{\partial v}{\partial x} + \frac{\partial u}{\partial y} \right) \quad (29)$$

$$\tau_{xz} = \tau_{zx} = \mu \left( \frac{\partial u}{\partial z} + \frac{\partial w}{\partial x} \right) \quad (30)$$

$$\tau_{yz} = \tau_{zy} = \mu \left( \frac{\partial w}{\partial y} + \frac{\partial v}{\partial z} \right) \quad (31)$$

$$\tau_{xx} = \lambda(\nabla \cdot V) + 2\mu \frac{\partial u}{\partial x} \quad (32)$$

$$\tau_{yy} = \lambda(\nabla \cdot V) + 2\mu \frac{\partial v}{\partial y} \quad (33)$$

$$\tau_{zz} = \lambda(\nabla \cdot V) + 2\mu \frac{\partial w}{\partial z} \quad (34)$$

where  $t$  is time,  $k$  is the thermal conductivity and  $\lambda = -\frac{2}{3}\mu$  is the bulk viscosity coefficient,  $\mu$  is the viscosity,  $\nabla$  is the gradient,  $u$  is the x-component of velocity,  $v$  is the y-component of velocity,  $w$  is the z-component of velocity,  $\dot{q}$  is the volumetric heating that may occur,  $\rho$  is the density,  $e$  is

the internal energy,  $h$  is the specific enthalpy,  $T$  is the temperature,  $p$  is the pressure and  $V$  is the velocity vector.

Upon conducting a boundary layer analysis on a flat plate, analogous to Blasius, the boundary layer thickness in hypersonic flow can be calculated. One finds that the boundary layer thickness is proportional to  $\frac{M_e^2}{\sqrt{Re}}$  [1]. This relation shows that as the Mach # increases the boundary layer becomes thicker and is an order of magnitude higher than the conventional incompressible boundary layer.

Another important aspect of hypersonic is the aerodynamic heating that occurs, with the strongest heating at the stagnation point. By conducting another order of magnitude analysis one find that the wall heat transfer is inversely proportional to the radius of the nose tip and is shown below in Eqn. (35) [1]:

$$q_w \propto \frac{1}{\sqrt{R}} \quad (35)$$

where  $R$  is the radius of the nose, and  $q_w$  is the heat transfer in watts. Looking at this result, one notices that to decrease the heat transfer into the hypersonic vehicle, one needs to increase the radius of the nose.

For hypersonic flow with chemical reaction one gets the same governing equations as hypersonic viscous flow except that the energy equation is modified as shown below in Eqns. (36)-(37) [1]:

$$\begin{aligned}
& \rho \frac{D(e + V^2/2)}{Dt} \\
&= -\nabla \cdot q - \nabla \cdot (p\vec{V}) + \frac{\partial(u\tau_{xx})}{\partial x} + \frac{\partial(u\tau_{yz})}{\partial x} + \frac{\partial(u\tau_{zx})}{\partial x} \\
&+ \frac{\partial(v\tau_{xy})}{\partial y} + \frac{\partial(v\tau_{yy})}{\partial y} + \frac{\partial(v\tau_{zy})}{\partial y} + \frac{\partial(w\tau_{xz})}{\partial z} + \frac{\partial(w\tau_{yz})}{\partial z} \\
&+ \frac{\partial(w\tau_{zz})}{\partial z}
\end{aligned} \tag{36}$$

$$\text{where } q = -k\nabla T + \sum_i \rho_i U_i h_i + q_R \tag{37}$$

where  $t$  is time,  $k$  is the thermal conductivity and  $\lambda = -\frac{2}{3}\mu$  is the bulk viscosity coefficient,  $\mu$  is the viscosity,  $\nabla$  is the gradient,  $u$  is the x-component of velocity,  $v$  is the y-component of velocity,  $w$  is the z-component of velocity,  $q$  is the heat flux-vector,  $q_R$  is the heat flux due to radiation,  $\rho$  is the density,  $e$  is the internal energy,  $h$  is the specific enthalpy,  $T$  is the temperature,  $p$  is the pressure and  $V$  is the velocity vector.

For a chemically reacting flow in nonequilibrium one more equation is needed and that is the species continuity equation shown below as Eqn. (38) [1]:

$$\rho \frac{Dc_i}{Dt} = \nabla \cdot (\rho D_{im} \nabla c_i) + \dot{w}_i \tag{38}$$

where  $t$  is time,  $i$  is the  $i^{\text{th}}$  chemical species,  $\rho$  is the density,  $D_{im}$  is the diffusion velocity of species  $i$  into species  $m$ ,  $\nabla$  is the gradient,  $c$  is the species concentration, and  $\dot{w}_i$  is the finite-rate chemical reaction term. Thus for a chemically reacting flow in nonequilibrium the governing equations are Eqns. (24)-(27), (29)-(34), and finally (36)-(38). Anderson, has also covered effects of wall

catalytic activity, species recombination downstream, and radiative gas dynamics on the hypersonic flow which have not been covered in this dissertation due to the fact that these properties are based on the specific material and flow regime for which data has not been collected. If one would like to know more about these effect one can look at publications and Anderson [1] to find details on these subjects.

### **1.1.5: Summary of Hypersonic Flow Fields**

Figure 18 below shows the different regions of flow for a hypersonic blunt-body. One finds that there are three distinct regions the non-equilibrium, equilibrium and nearly frozen flow. For the non-equilibrium region the flow is chemically reacting and the species present are changing with respect to time and location along the blunt-body, i.e. the flow is not in chemical equilibrium. The equilibrium region, which includes the stagnation point, is the region where the flow is chemically reacting but the species present do not change with respect to time and location along the blunt-body, and thus the flow is in chemical equilibrium. For the nearly frozen flow there is little to no chemical reactions occurring, thus the name frozen.

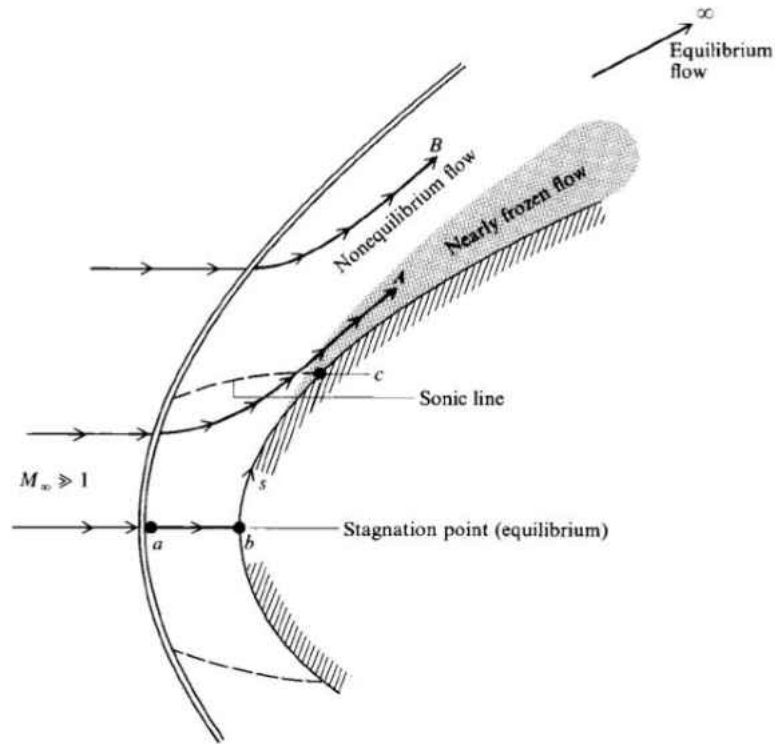


**Figure 18: Different Regions in high-temperature blunt-body flowfield. Reprinted from Hypersonic and High Temperature Gas Dynamics 2<sup>nd</sup> Ed., Copyright (2006), with permission from John D. Anderson, Jr. [1]**

For each of these regions a different set of governing equations are used, and therefore the CFD that is used to needs to be able to detach the area where there is chemically non-equilibrium, equilibrium or frozen flow and solve the appropriate governing equations. This describes the flow field where the hypersonic vehicle is in the continuum range [1]. When a spacecraft on re-entry or aerial hypersonic vehicle flies through the atmosphere, it experiences different flight regime. Therefore, there is no one answer to explain hypersonic flow upon re-entry, rather the re-entry flight path can be broken up to three sections of different flight characteristics. Figure 19 shows the typical flow regimes an aerial vehicle encounters upon re-entry.



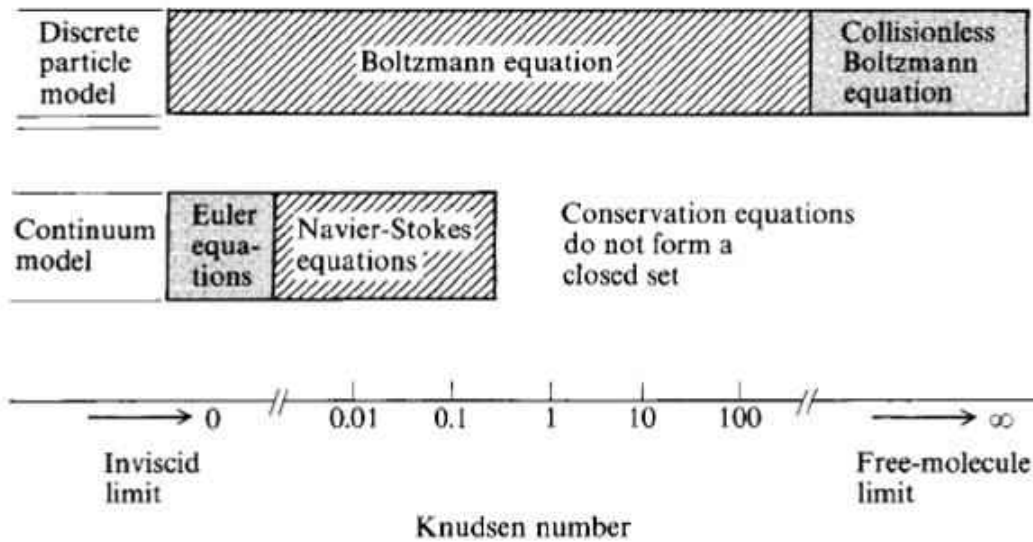


**Figure 19: Different flow regimes. Reprinted from Hypersonic and High Temperature Gas Dynamics 2<sup>nd</sup> Ed., Copyright (2006), with permission from John D. Anderson, Jr. [1]**

Upon re-entry space crafts, such as the space shuttle, first encounter the free molecule regime, where individual molecule's impacts on the surface are important, to the transition regime, where slip effects are important, and finally to the continuum regime. The regime of flight the aerial vehicle is defined by the following similarity parameter, the Knudsen number. The Knudsen number is defined by the following Eqn. (39) [1]:

$$Kn = \lambda / L \quad (39)$$

where  $\lambda$  is the mean free path of the flow and  $L$  is the characteristic length. The different flow regime is defined using the  $Kn$  as shown in Figure 19 above. The free molecule regime occurs when the  $Kn \geq 1$ , the transition regime occurs when  $0.03 > Kn < 1$ , and finally the continuum regime occurs when  $Kn < 0.03$  [1]. This helps to determine what regime is more important at any given point in time during re-entry when doing simulations.

## **1.2: Material Requirements for Hypersonic Vehicles Applications**

Due to all of the phenomena occurring all at once in hypersonic flow, it is very difficult to design vehicles to withstand the extreme conditions. Most materials in this environment will simply melt, oxidize, fail from thermal shock, and at high temperature the mechanical properties of most materials degrade as the temperature increases. In addition to the degradation of the mechanical properties, creep and fatigue also becomes a major issue. Looking through literature one is able to come up with a set of general requirements needed in order to determine if a material is a possible candidate for applications in hypersonic vehicles. Some of the desired material properties were picked based on the performance of materials that were previously used. The material should have a very high melting temperature  $>2000^{\circ}\text{C}$  [11], have a high strength at elevated temperature  $> 300$  MPa at  $1700^{\circ}\text{C}$  [11]. The material should also have high thermal conductivity  $>14.5$  W/mK [12], which is the thermal conductivity of C/C-SiC ceramic composites. Lastly the material should be oxidation resistant,  $< 80$  g/m<sup>2</sup> over 2 hours at  $1400^{\circ}\text{C}$  [13]. Looking at these requirements one finds a group of ultra-high temperature ceramic composites (UHTC), specifically ZrB<sub>2</sub>-SiC ceramic composites, that could fulfill the requirements. These composites have been of high interest to the scientific community for the past few years. This material is relatively cheap and light, making it ideal for aerospace application where weight matters. ZrB<sub>2</sub>-SiC ceramic composites exhibit the following properties: melting temperature  $> 3000^{\circ}\text{C}$  [11], strength  $217\pm 17$  MPa at  $1800^{\circ}\text{C}$  [14], thermal conductivity of 66 W/mK [13], and oxidation resistance of 50g/m<sup>2</sup> over 2 hour at  $1400^{\circ}\text{C}$  [12]. Thus showing ZrB<sub>2</sub>-SiC is an excellent candidate for hypersonic vehicle applications.

### **1.3: Proposed Material Candidate Properties**

This section will present literature search of ZrB<sub>2</sub>-SiC ceramic composites starting with the crystal structure and phase diagrams of each of the phases.

#### **1.3.1: Crystal Structure and Phase Diagram of ZrB<sub>2</sub>, IrB<sub>2</sub>, and SiC**

The crystal structure of ZrB<sub>2</sub> is shown below as Figure 20 [15, 16]. As one can see ZrB<sub>2</sub> consist of layers of Zr and B in the hexagonal structure. ZrB<sub>2</sub> has AlB<sub>2</sub>-type crystal structure and is a member of the space group symmetry P6/mmm and the crystal has a simple hexagonal symmetry of D<sub>6h</sub>. The B rings shown in Figure 20 in blue, has a single Zr atom centered above and below it [16].

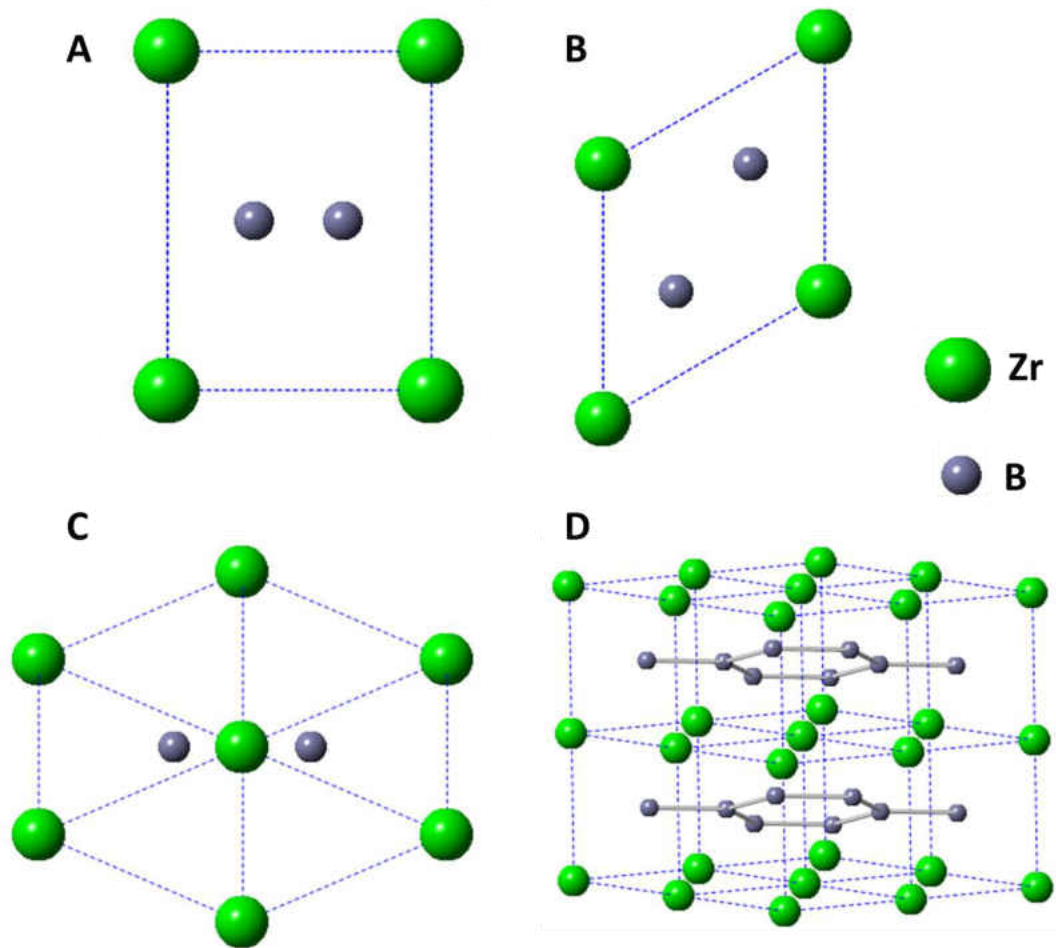


**Figure 20: ZrB<sub>2</sub> crystal structure, where the green balls are Zr atoms and the blue balls are B atoms. ZrB<sub>2</sub> unit cell view from the a or b-plane (A), c-plane (B), 111 plane (C), and a 3D view showing the alternating layers of B and Zr (D).**

The bonding between the Zr and B layer is most likely ionic [16]. The lattice parameters for ZrB<sub>2</sub> calculated both experimentally and theoretically ranges from 3.127 to 3.197Å for *a* and 3.49-3.561Å for *c* [16-21]. The bond length between the boron atoms ranges from 1.818 to 1.83Å and the bond length between Zr and B atoms ranges from 2.529 to 2.546 Å [16-21].

The 6H-SiC crystal structure is shown below as Figure 21 [22]. 6H-SiC is part of the P6<sub>3</sub>mc space group and the C<sup>4</sup><sub>6v</sub> point group with a stacking order of ABCACB [23]. The lattice

parameters for 6H-SiC calculated both experimentally and theoretically ranges from 3.031-3.0817Å for  $a$  and 15.1173-15.11976Å for  $c$  [23-26].

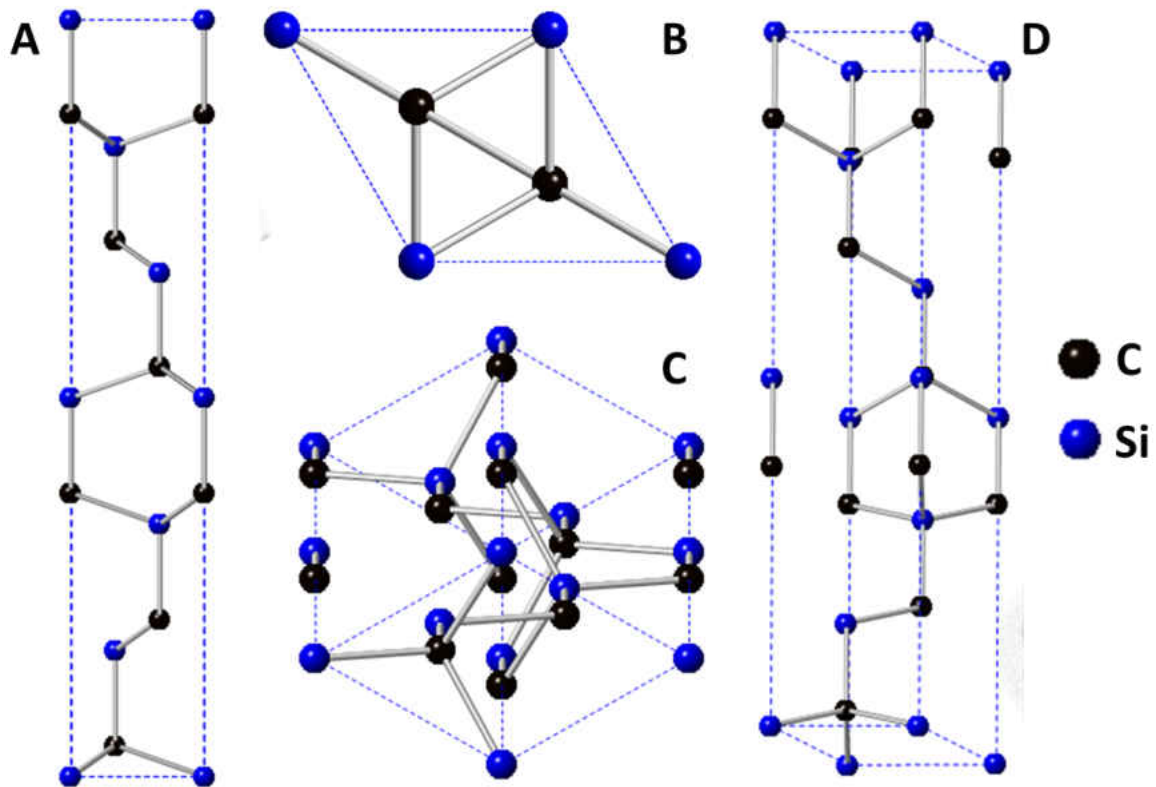


**Figure 21: 6-hexagonal SiC crystal structure looking at the a or b-plane (A), c-plane (B), 111 plane (C), and finally a 3D view of the crystal structure (D) [15]**

The third and final crystal structure one is interested in is the Ir-B crystal structure. There are many different phases of the Ir-B system but the IrB<sub>2</sub> crystal structure is the relevant one here. A new phase of the Ir-B system has recently been synthesized. This new phase is ReB<sub>2</sub>-type IrB<sub>2</sub> and the crystal structure is shown below in Figure 22 [27]. The lattice parameters of this new IrB<sub>2</sub> phase is shown in ref. [27].

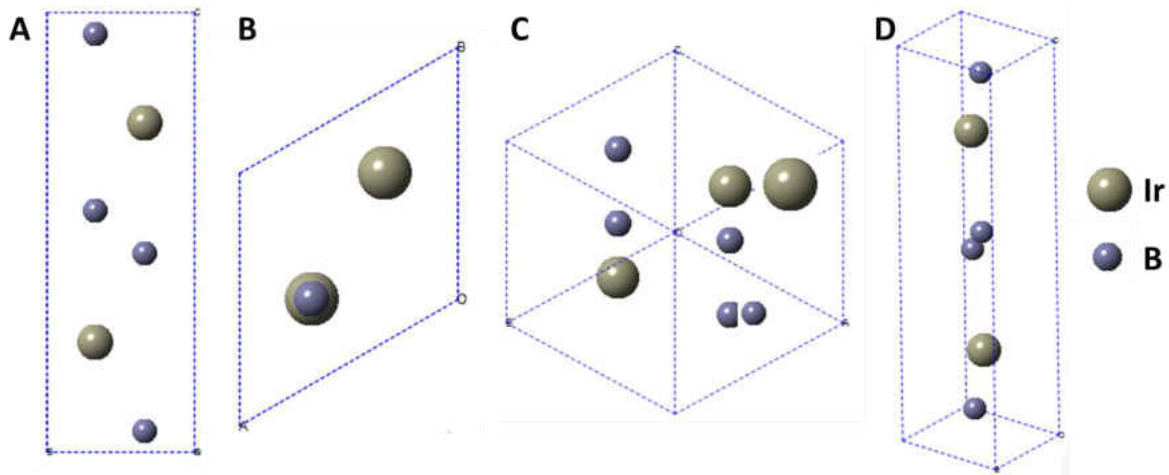


**Figure 22: ReB<sub>2</sub>-type IrB<sub>2</sub> crystal structure looking at the a or b-plane (A), c-plane (B), 111 plane (C) and a 3D view of the structure (D) (from Xie [27])**

A summary table of the lattice parameters for ZrB<sub>2</sub>, 6H-SiC, and ReB<sub>2</sub>-type IrB<sub>2</sub> has been created to be able to compare the different crystal structures of interest and is shown below in Table 1.

**Table 1: Summary of lattice parameters of ZrB<sub>2</sub>, 6H-SiC, and ReB<sub>2</sub>-type IrB<sub>2</sub>**

| Composition                                  | $a$ , Å      | $c$ , Å          |
|----------------------------------------------|--------------|------------------|
| ZrB <sub>2</sub> [16-21]                     | 3.127-3.197  | 3.49-3.561       |
| 6H-SiC [23-26]                               | 3.031-3.0817 | 15.1173-15.11976 |
| ReB <sub>2</sub> -type IrB <sub>2</sub> [28] | 2.926        | 7.543            |

The phase diagrams for ZrB<sub>2</sub> system is shown below in Figure 23. These are essential to determine what molar percentage of ZrB<sub>2</sub> can be produced at different temperatures. This is mostly used by industry to produce these powders.

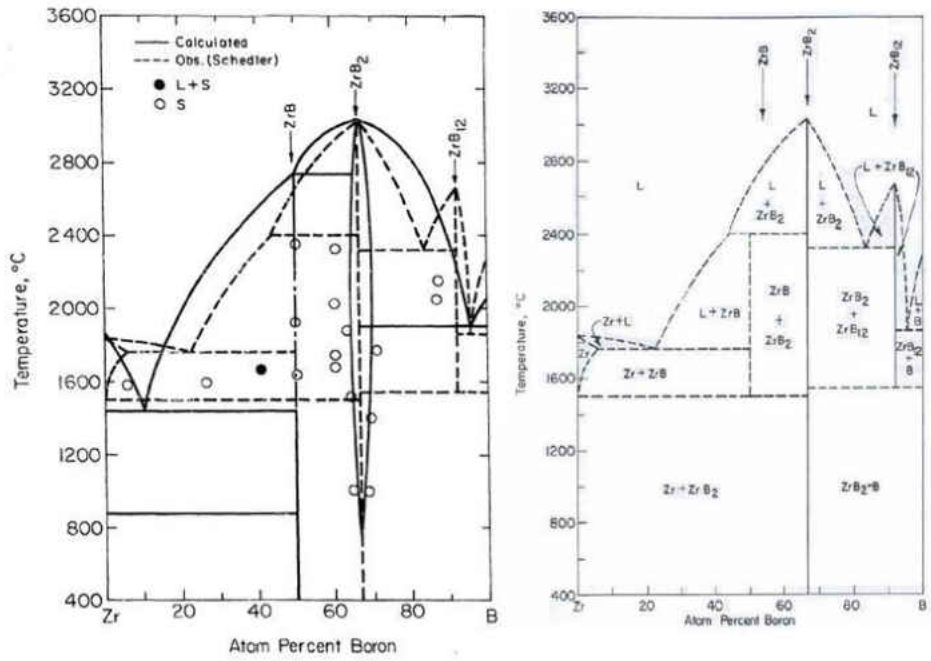


**Figure 23: Phase diagram Zr-B system without labels(a), and with labels of the phases(b)[29, 30]**

The SiC system phase diagram is shown below in Figure 24. This shows the same information as the ZrB<sub>2</sub> phase diagram but for SiC system only. Another SiC phase diagram not shown has also been found by Zou et al [31].

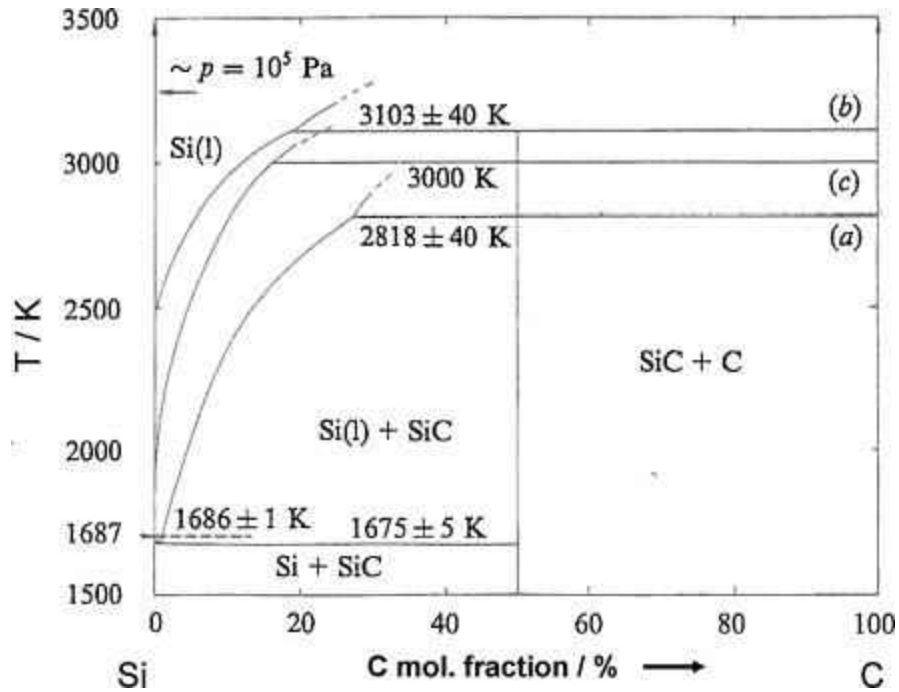


**Figure 24: Si-C binary system Phase Diagram.** Reprinted from *Journal of the European Ceramic Society*, vol. 32, G. Honstein, C. Chatillon, and F. Baillet, "Thermodynamic approach to the vaporization and growth phenomena of SiC ceramics. I. SiC and SiC-SiO<sub>2</sub> mixtures under neutral conditions," pp. 1117-1135, Copyright (2012), with permission from Elsevier. [32]

The ZrB<sub>2</sub>-SiC phase diagram found in literature is shown below in Figure 25.



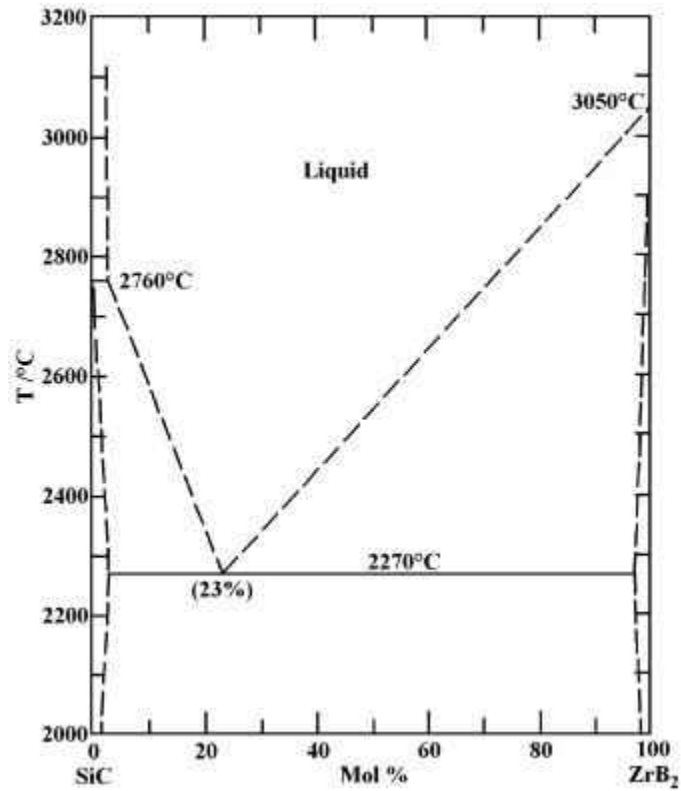


**Figure 25: ZrB<sub>2</sub>-SiC phase diagram. Reprinted from Journal of the European Ceramic Society, vol. 32, Q. Lonné, N. Glandut, and P. Lefort, "Surface densification of porous ZrB<sub>2</sub>-39mol.% SiC ceramic composites by a laser process," pp. 955-963, Copyright (2012), with permission from Elsevier. [33]**

The final phase diagram that one would like to include in this work is the Ir-B system. The Ir-B phase diagram is shown below in Figure 26.

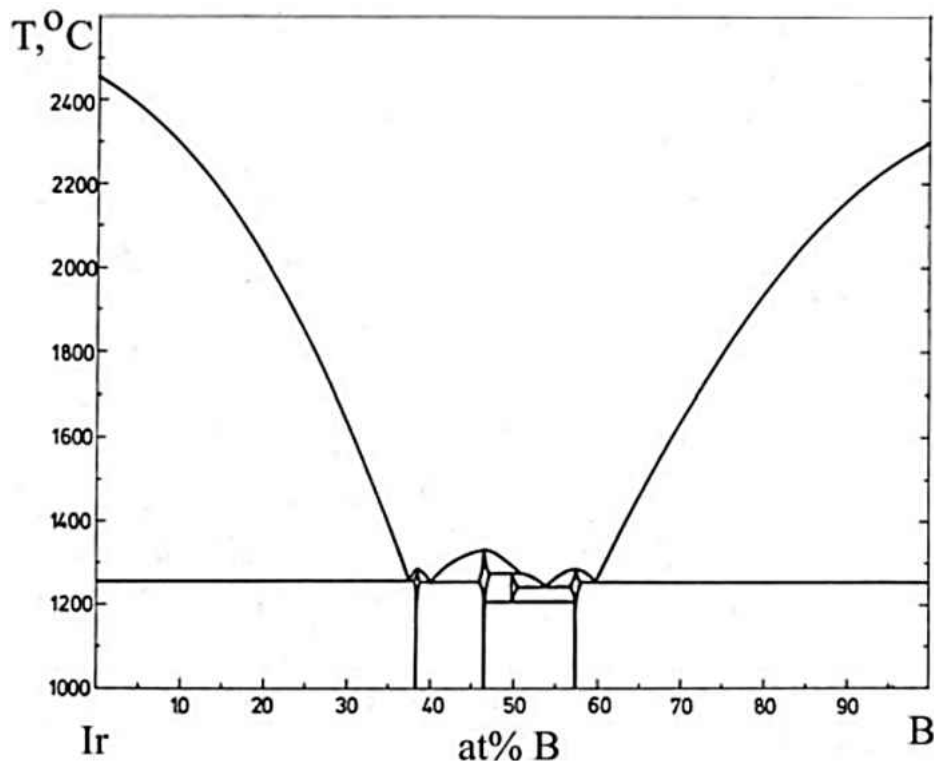


**Figure 26: Ir-B phase diagram. Reprinted from *Journal of the Less Common Metals*, vol. 82, H. Ipsier and P. Rogl, "Constitution diagrams of the binary systems Pd-B and Ir-B," pp. 363, Copyright (1981), with permission from Elsevier. [34, 35]**

### 1.3.2: Mechanochemical Synthesis

Mechanochemical synthesis is the use of mechanical processes to cause or induce chemical reactions to occur near or at room temperature. The mechanical energy is what includes these phase transformations and chemical reactions to occur [36, 37]. The reason this works is that the powder, in the solid phase, can support shear strain/stresses [38]. Therefore mechanical energy can cause chemical reactions to occur: due to the low diffusion distances and that the increases in surface energy effectively lowers the energy to initiate chemical reactions at or near room temperature [36]. There are a few advantages to using mechanochemical synthesis. Firstly, mechanochemical synthesis is more energy efficient compared to traditional high-temperature solid-state synthesis

methods, which require extended high temperature heating [36]. Secondly, the mechanochemical synthesis is a scalable technology that can be used to produce bulk quantities of polymers, alloys, and ceramic materials [36]. Thirdly, mechanochemical synthesis is able to synthesize new nanoscale and non-equilibrium phases. Finally, mechanochemical synthesis does not require solvents; which reduces the production of waste [36]. Although a few models/theories [39, 40] have been proposed with limitations [36], it must be mentioned that the exact mechanism of the mechanochemistry or mechanosynthesis is still not understood fully [36]. Mechanochemistry has been successfully used to produce high performance alloys for aerospace applications [41], ceramic material [42-44], and polymer synthesis [36, 45].

Ball milling is one of the many methods that is used as a part of the mechanochemical synthesis technique; other types of milling used for mechanosynthesis are planetary, shaker, attrition, and pebble mills [36, 46]. Ball milling was found to be able to synthesize many different phases to include equilibrium and non-equilibrium phases, such as metastable, and quasi crystalline phases, as well as solid solutions, amorphous alloys and nanostructures [36, 41]. The mechanical of ball milling is shown below as a schematic as Figure 27.

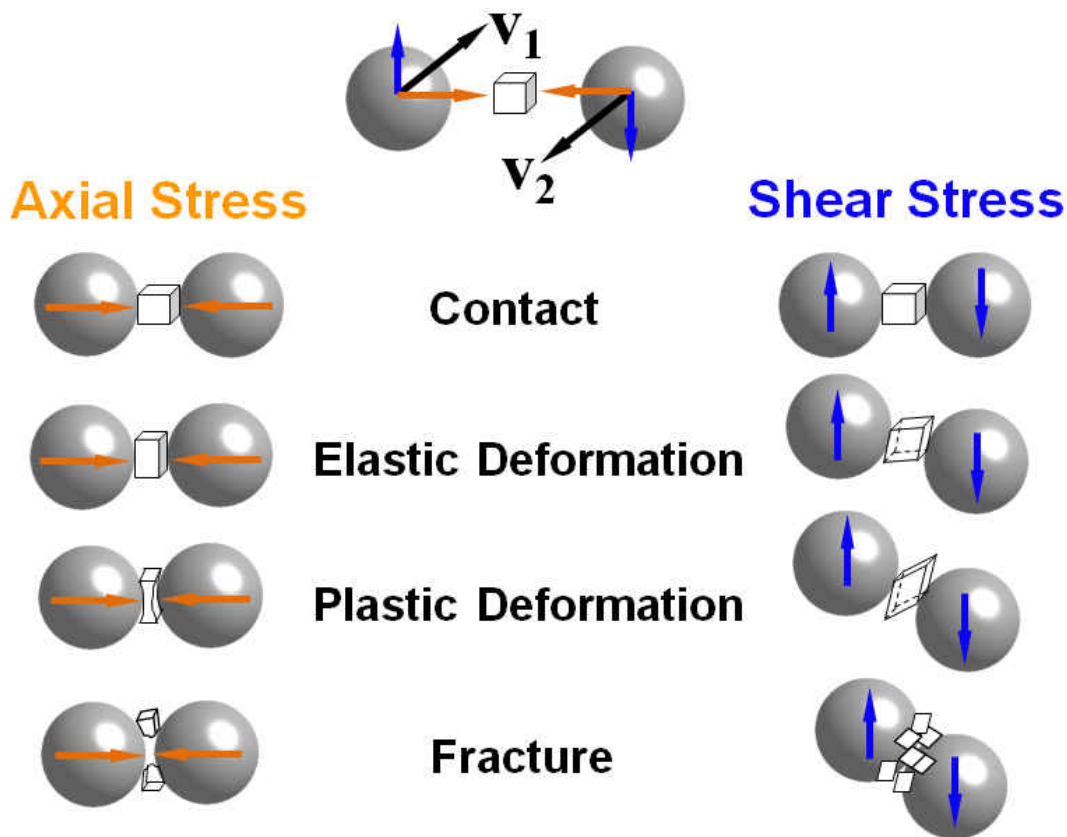


**Figure 27: Mechanisms of ball milling.** Reprinted from “Rhenium, osmium and iridium diborides by mechanochemistry : synthesis, structure, thermal stability and mechanical properties”, Z. Xie, Copyright (2014), with permission from Zhilin Xie. [36]

Ball milling accelerates the kinetics of chemical reactions through dynamic fracturing, deformation, and cold welding of the solid particles [36, 47]. Ball milling has many variables that affect milling that are as following: the milling container, milling medium, ball to powder mass ratio, milling time, milling speed, milling atmosphere, temperature, and powder to container volume ratio [36]. The effects of each of these are described in detail by Xie in [36]. A description of the mechanisms of mechanochemistry is also described in detail by Xie in [36].

As a way to show how powerful this mechanochemistry is, recently a new phase of  $\text{ReB}_2$  was synthesized using this technique [48]. New phases of  $\text{OsB}_2$  [49-53] and  $\text{IrB}_2$  [27, 28] have also

been discovered. Finally  $\text{AlMgB}_{14}$  [54] was also produced using mechanochemistry. These recent discoveries show that mechanosynthesis will lead to many more new materials never thought of or discovered yet.

### 1.3.3: Sintering Processes of $\text{ZrB}_2\text{-SiC}$ , $\text{ZrB}_2\text{-IrB}_2\text{-SiC}$ , and pure $\text{SiC}$ Ceramic Composites

For  $\text{ZrB}_2\text{-SiC}$  ceramic composites the most common method of sintering the material is hot pressing (HP) [55, 56] and spark plasma sintering (SPS) [57-59]. HP uses heating elements along with pressure and vacuum to sinter the material, a schematic is shown below in Figure 28. The disadvantage of HP is that the heating and cooling rates are slow and it takes many hours to even a full day to sinter one sample.

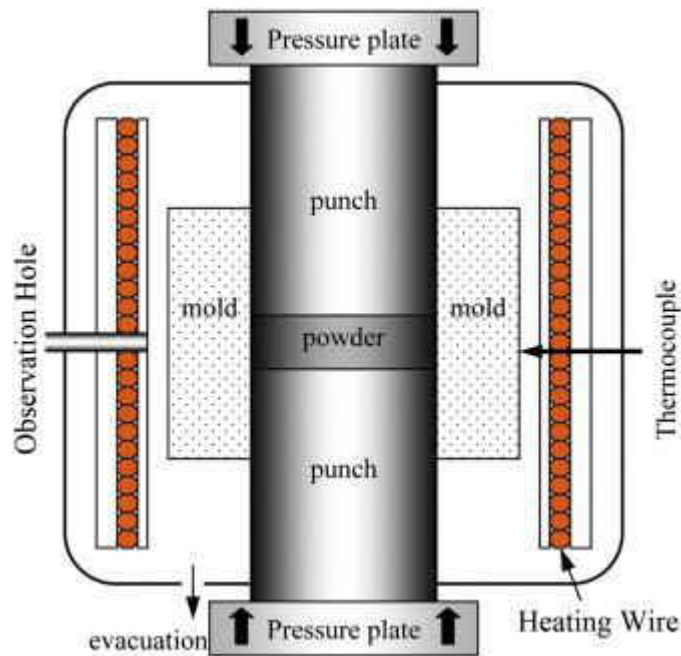


**Figure 28: Hot pressure schematic. Reprinted from *Diamond and Related Materials*, vol. 21, Z. Yuan, Z. Jin, R. Kang, and Q. Wen, "Tribochemical polishing CVD diamond film with FeNiCr alloy polishing plate prepared by MA-HPS technique," pp. 50-57, Copyright (2012), with permission from Elsevier. [60]**

SPS uses pulsing electrical current to heat up a sample along with pressure and vacuum to sinter the material, a schematic is shown below as Figure 29. SPS has many advantages to HP; heating and cooling rate are very high, on the order of 100°C/min, and it take only 1-2hours to produce one full sample with some materials requiring only a few seconds to sinter. As opposed to HP that takes almost a full day to produce a sample. The disadvantages of SPS are that the sample has to be electrically conductive, the samples are usually circular, and the sample size that SPS is able to produce is not as large as in HP. But in recent years larger SPS machines have been developed, capable of producing large samples

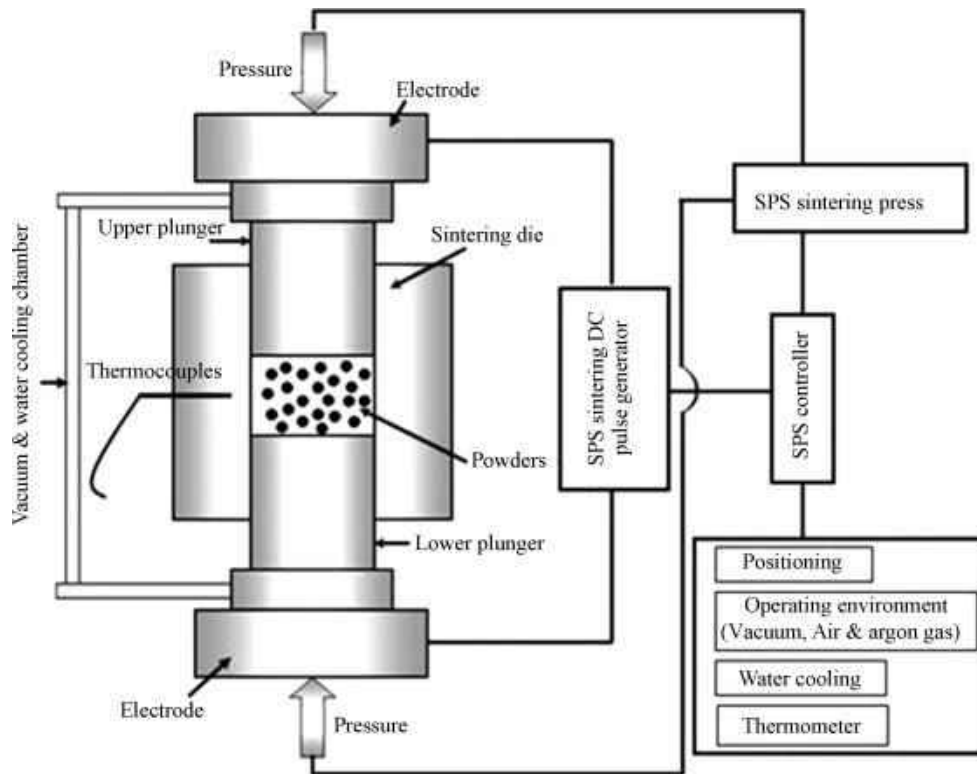


**Figure 29: Spark plasma sintering schematic. Reprinted from *Materials Chemistry and Physics*, vol. 112, X. Dong, F. Lü, L. Yang, Y. Zhang, and X. Wang, "Influence of spark plasma sintering temperature on electrochemical performance of  $\text{La}_{0.80}\text{Mg}_{0.20}\text{Ni}_{3.75}$  alloy," pp. 596-602, Copyright (2008), with permission from Elsevier. [61]**

There are also less comment methods that have been used to produce ZrB<sub>2</sub>-SiC. These methods are reactive hot pressing [62, 63], reactive spark plasma sintering [64-66], colloidal processing [67], combustion synthesis [68, 69], electron beam sintering [70], gel casting based on a double gel network [71], plasma arc welding [72], aqueous tape casting and hot pressing [73], reeducation-carburization route [74], pressure less sintering [75-77], and boro-carbothermal reduction [78, 79].

Apart from the effect of the sintering method on the ZrB<sub>2</sub>-SiC, papers have also investigated the effect of sintering on the microstructure, density of the produced samples, and the mechanical properties of the material [80]. Other effects that have been investigated are the effect of powder processing on the densification [81], creating porous ceramics [82], improving mechanical properties by changing sintering properties [83], and heating rates [84].

In their paper Zhang et al., compare properties of ZrB<sub>2</sub>-SiC produced by SPS and HP [85]. This paper found that both SPS and HP methods produced samples with flexural strength above 700MPa but the SPS sample was sintered for only 20 minutes while the HP sample took 210 minutes to sinter [85].

#### **1.3.4: Mechanical Properties of ZrB<sub>2</sub>, SiC, and ZrB<sub>2</sub>-SiC**

Mechanical properties of major importance for materials are strength, toughness, and hardness. These properties determine the applications of the material under study, thus the reason for including this section in the literature search. For pure ZrB<sub>2</sub> the theoretical density is 6.09 g/cm<sup>3</sup> [86] and the melting temperature is 3100-3500°C [87]. For pure 6H-SiC the theoretical density is

3.21 g/cm<sup>3</sup> [88] and the melting temperature is 2700°C [87]. A summary of the properties of ZrB<sub>2</sub> and 6H-SiC are shown below as Table 2.

**Table 2: Mechanical Properties of ZrB<sub>2</sub> and SiC**

|                                               | ZrB <sub>2</sub>                     | SiC                                   |
|-----------------------------------------------|--------------------------------------|---------------------------------------|
| Young's modulus [89-92]                       | 489-493 GPa                          | 440±20 GPa                            |
| Melting temperature [87]                      | 3100-3500°C                          | 2700°C                                |
| Density [86, 88]                              | 6.09 g/cm <sup>3</sup>               | 3.21 g/cm <sup>3</sup>                |
| Vickers hardness [91, 93]                     | 21-23 GPa                            | 32 GPa                                |
| Fracture toughness [85, 91, 94]               | 5.46-6.02 MPam <sup>1/2</sup>        | 6.8 MPam <sup>1/2</sup>               |
| Fracture strength [85, 91, 94]                | 416-708 MPa                          | 490±70 MPa                            |
| Coeff. of Thermal Expansion(CTE) [19, 91, 95] | 5.9x10 <sup>-6</sup> K <sup>-1</sup> | 4.16x10 <sup>-6</sup> K <sup>-1</sup> |
| Thermal conductivity [93, 94]                 | 60 W/mK                              | 0.9-50 W/mk                           |

There are more papers on the mechanical properties of ZrB<sub>2</sub> and SiC than one can read and collect all of the data. Therefore I am going to summarize the range of Young's modulus, shear modulus, bulk modulus, Poisson's ratio, flexure strength, flexure toughness, hardness, and density that has been found in literature in Table 3. Table 3 values are based on literature of mechanical properties of pure ZrB<sub>2</sub>, pure 6H-SiC, and ZrB<sub>2</sub>-SiC at room temperature only. The values in Table 3 include materials that are porous, fully dense, and that contain impurities causing the density to be above theoretical density. This is the main reason why there is such a wide range of reported values. Another reason for the large range of reported values is that a variety of different methods were used to produce all of these results that include some that varied the sintering properties to find the effect on the mechanical properties of the material.



**Table 3: Summary of mechanical properties of pure ZrB<sub>2</sub>, pure 6H-SiC, and ZrB<sub>2</sub>-SiC ceramic composites at room temperature**

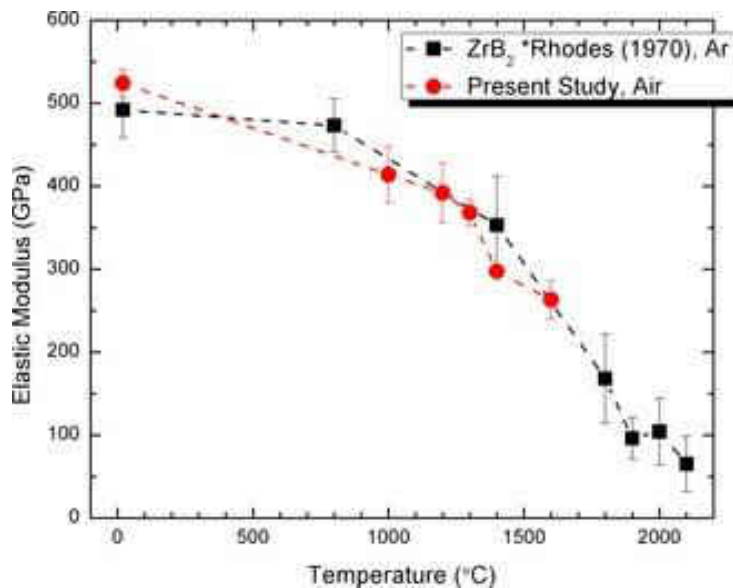
| Composition                           | ZrB <sub>2</sub>          | ZrB <sub>2</sub> -<br>10vol%SiC | ZrB <sub>2</sub> -<br>20vol%SiC | ZrB <sub>2</sub> -<br>30vol%SiC | 6H-SiC              |
|---------------------------------------|---------------------------|---------------------------------|---------------------------------|---------------------------------|---------------------|
| Measured Density (g/cm <sup>3</sup> ) | 5.28-6.26 [56, 96, 97]    | 5.54 [97]                       | 5.72 [97]                       | 5.43 [97]                       | 3.124-3.21 [91]     |
| Young's Modulus                       | 346-550 [56, 96-99]       | 439-453 [97, 98]                | 466-481 [97, 98]                | 484-517 [97, 98]                | 410-475 [91, 97-99] |
| Shear modulus (GPa)                   | 185 [56]                  | -                               | -                               | -                               | -                   |
| Bulk Modulus (GPa)                    | 185 [56]                  | -                               | -                               | -                               | -                   |
| Poisson's Ratio                       | 0.11-0.15 [56]            | -                               | -                               | -                               | -                   |
| Vickers Hardness (GPa)                | 8.3-23.9 [96, 97, 99]     | 13.1-24.9 [97, 98]              | 17.7-26.8 [97, 98]              | 21.7-24.7 [97, 98]              | 15.74-32 [91, 99]   |
| Flexure Strength (MPa)                | 275-565 [56, 96, 97]      | 404-713 [97, 98]                | 359-1003 [97, 98, 100]          | 673-1089 [97, 98, 101]          | 420-800 [91, 102]   |
| Flexure Toughness (MPa)               | 2.3-4.8 [56, 96, 97, 103] | 3.0-4.1 [97, 98]                | 3.3-6.4 [97, 98, 100]           | 3.2-5.3 [97, 98]                | 3.1-7.0 [91, 103]   |

Table 3 above, shows mechanical properties of ZrB<sub>2</sub>-SiC with different volume percent of SiC, other papers have also published results of ZrB<sub>2</sub>-SiC with different weight percent of SiC instead of volume percent. Table 4 below shows all of these mechanical properties found to date on weight percent SiC in ZrB<sub>2</sub>.

**Table 4: Mechanical properties of ZrB<sub>2</sub>-SiC with different weight percent of SiC [99]**

| Composition                | Fracture Toughness (MPa m <sup>1/2</sup> ) | Hardness (GPa) |
|----------------------------|--------------------------------------------|----------------|
| ZrB <sub>2</sub> -5wt%SiC  | 3.31-3.65                                  | 19.05-21.97    |
| ZrB <sub>2</sub> -10wt%SiC | 2.485-2.841                                | 16.47-19.08    |
| ZrB <sub>2</sub> -15wt%SiC | 2.58-3.525                                 | 17.18-17.86    |
| ZrB <sub>2</sub> -20wt%SiC | 1.965-3.162                                | 15.62-15.81    |

An investigation of ZrB<sub>2</sub> flexure strength and elastic modulus was carried out by Neuman from room temperature to 2300°C [104]. The elastic modulus as a function of temperature for pure ZrB<sub>2</sub> is shown below as Figure 30, and the flexure strength as a function of temperature is shown below as Figure 31. Both plot show that the Young's modulus and strength decrease with increase in temperature [104].



**Figure 30: Elastic modulus vs. temperature for ZrB<sub>2</sub>. Reprinted from *Journal of the American Ceramic Society*, vol. 96, E. W. Neuman, G. E. Hilmas, and W. G. Fahrenholtz, "Strength of Zirconium Diboride to 2300°C," pp. 47-50, Copyright (2012), with permission from John Wiley and Sons. [104]**

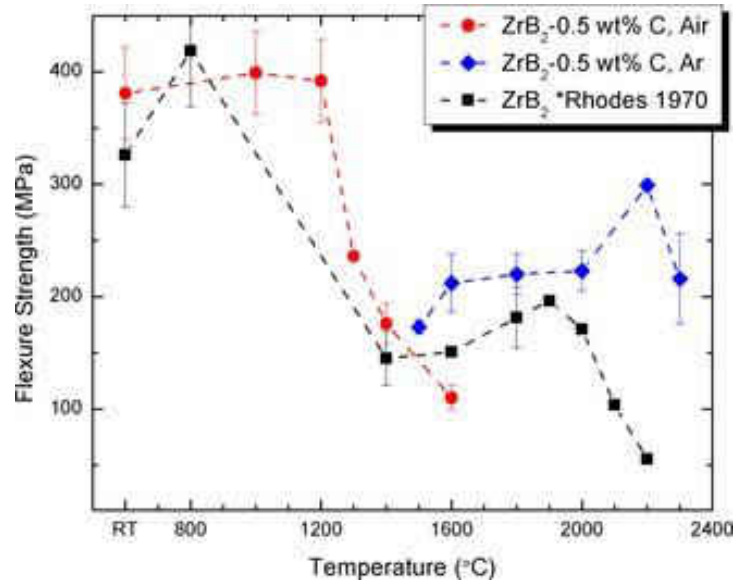


**Figure 31: Flexure strength vs. temperature for ZrB<sub>2</sub>.** Reprinted from *Journal of the American Ceramic Society*, vol. 96, E. W. Neuman, G. E. Hilmas, and W. G. Fahrenholtz, "Strength of Zirconium Diboride to 2300°C," pp. 47-50, Copyright (2012), with permission from John Wiley and Sons. [104]

Now looking at the mechanical properties of ZrB<sub>2</sub>-SiC at elevated temperature one find the same trend as with pure ZrB<sub>2</sub>, that the mechanical properties decline as the temperature increases [105-107]. For ZrB<sub>2</sub>-30vol%SiC the trends of mechanical properties are shown in Figure 32 blow, with A being the Elastic modulus, B being the fracture toughness, C being the flexure strength and D being the oxide thickness for the sample at that temperature.

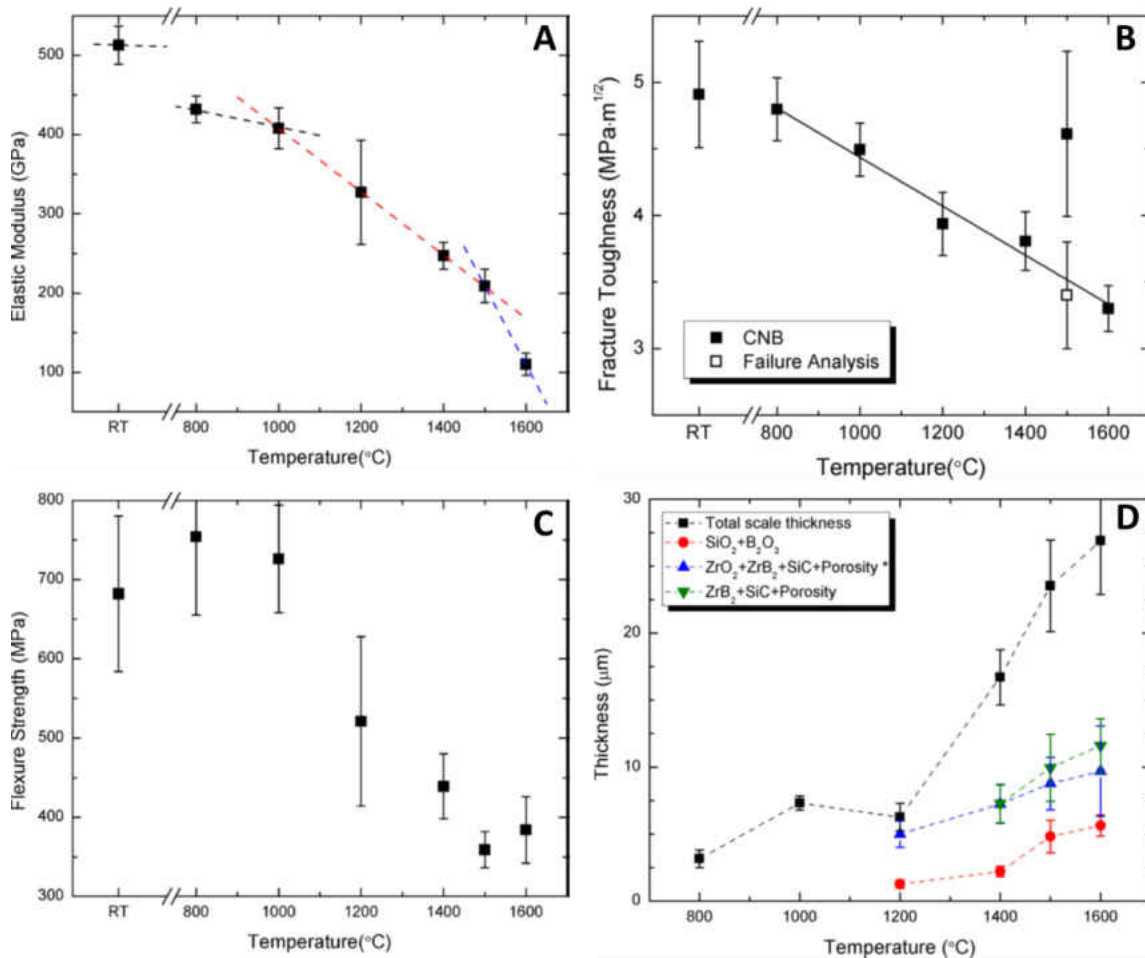


**Figure 32: Summary of trends of the mechanical properties of ZrB<sub>2</sub>-30vol%SiC (A) Young's Modulus [106], (B) Fracture toughness [106], (C) Flexure strength [106], and for completeness the oxide layer thicknesses. Reprinted from *Journal of the European Ceramic Society*, vol. 33, E. W. Neuman, G. E. Hilmas, and W. G. Fahrenholtz, "Mechanical behavior of zirconium diboride–silicon carbide ceramics at elevated temperature in air," pp. 2889-2899, Copyright (2013), with permission from Elsevier. [106]**

Recent papers have reported the results of uniaxial compression and tension tests on ZrB<sub>2</sub>-SiC ceramic composites at room temperature and elevated temperatures [108, 109]. The compression tests were carried out on polished and unpolished ZrB<sub>2</sub>-SiC ceramic composites without any additives and with carbon and SiC fibers [109]. It was found that the polished ZrB<sub>2</sub>-SiC samples without additives performed the best with a room temperature strength of

approximately 3.1 GPa [109]. Figure 33 below shows summary of the compression test results as a function of temperature. Looking at this figure one notices the trend of decreasing strength with increase in temperature; this trend matches well with other literature on elevated temperature properties of ZrB<sub>2</sub>-SiC.

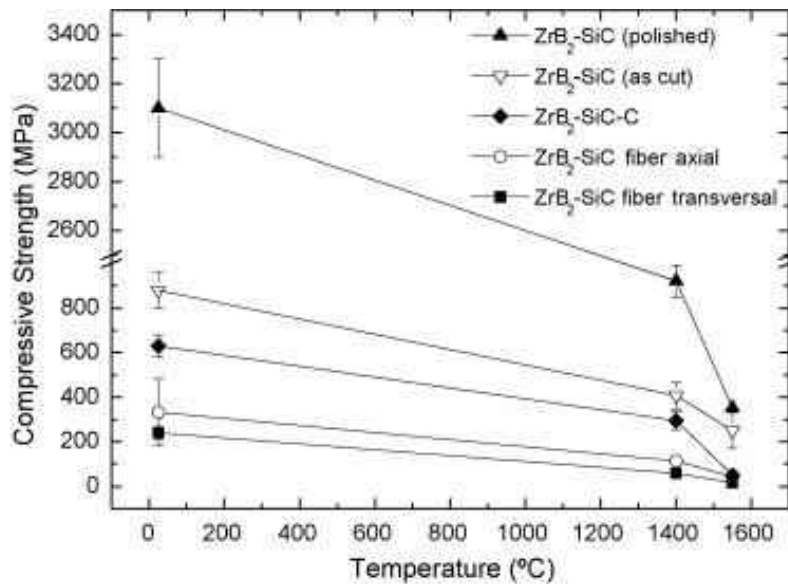


**Figure 33: Compressive strength for different ZrB<sub>2</sub>-SiC composition as a function of temperature. Reprinted from *Journal of the European Ceramic Society*, vol. 31, J. Ramírez-Rico, M. A. Bautista, J. Martínez-Fernández, and M. Singh, "Compressive strength degradation in ZrB<sub>2</sub>-based ultra-high temperature ceramic composites," pp. 1345-1352, Copyright (2011), with permission from Elsevier. [109]**

The tensile test was conducted on ZrB<sub>2</sub>-SiC-graphite composites, and found at room temperature the tensile strength was 120±10MPa, at 1550°C was 60±10MPa, at 1650°C was 40±10MPa, and at 1750°C was 20±10MPa [108].

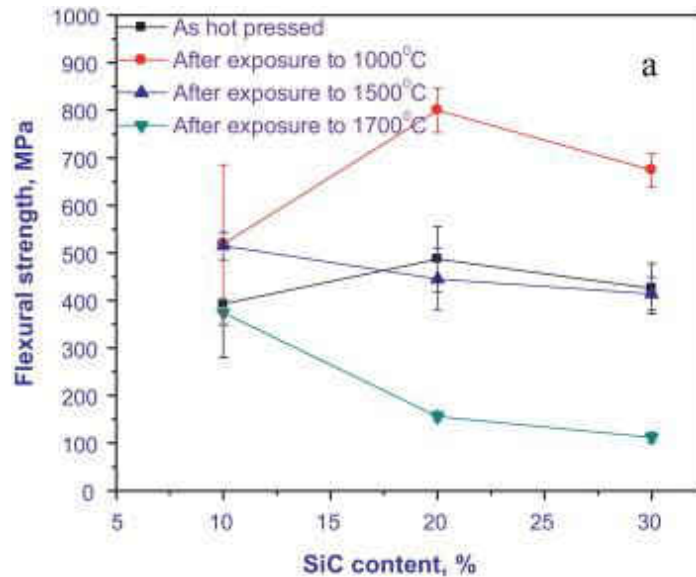


**Figure 34: ZrB<sub>2</sub>-SiC Flexure strength after exposure. Reprinted from *Journal of the European Ceramic Society*, vol. 32, M. Patel, J. J. Reddy, V. V. Bhanu Prasad, and V. Jayaram, "Strength of hot pressed ZrB<sub>2</sub>-SiC composite after exposure to high temperatures (1000–1700°C)," pp. 4455-4467, Copyright (2012), with permission from Elsevier. [107]**

The flexural strength has also been investigated at room temperature after exposure to high temperature, allowing oxide layers to form [107]. One found that as the sample was heated to 1000°C the strength of the samples increased and then decreased again after samples were exposed to higher temperatures [107]. This is mainly due to the fact that at 1000°C the probability of healing flaws is expected to be the highest, and results in the lowest oxide scale thickness [107].

In addition to the investigation of the mechanical properties at room temperature and at elevated temperatures, one has also found papers on the mechanical properties of ZrB<sub>2</sub>-SiC with different SiC particle size [110, 111]. This paper found that as the SiC particles size is increased the mechanical properties of strength, fracture toughness, Young's modulus and hardness all decreased [110, 111]. One also found papers on the effect of the SiC powder used in ZrB<sub>2</sub>-SiC on the composites mechanical properties [110-112]. Papers have also been published on effects of

different additives on the mechanical properties of ZrB<sub>2</sub>-SiC, with CrSi<sub>2</sub> and HfB<sub>2</sub> [113], and carbon nanotubes [114]. The final set of papers reported that other factors that have an effect on ZrB<sub>2</sub>-SiC composite properties is heating rates [84], holding times [115], hot pressing time and temperature [93].

The final section of mechanical properties is creep. There are relatively few papers on creep when compared to the rest of mechanical properties, the first being on the creep behavior of ZrB<sub>2</sub>-SiC. This paper found that between 1500-1600°C, the creep rate increase, which was attributed to the activation energy changing from 364kJ/mol to 639kJ/mol [116]. The lower activation energy refers to ZrB<sub>2</sub> or ZrB<sub>2</sub>-SiC interphase boundary, while the higher activation energy refers to ZrB<sub>2</sub>-ZrB<sub>2</sub> and/or ZrB<sub>2</sub>-SiC boundary sliding [116]. The second paper found was on 4-point flexure creep of ZrB<sub>2</sub>-30vol%SiC in argon [117]. The samples were placed under a static load of 19MPa for 0-100h at 1500 and 1600°C. It was found that the strain rate at 1600°C was 3.7 times higher than 1500°C [117]. Another paper on flexural creep was also found, which used an electromagnetic Lorentz force loading, 20-50MPa at temperature of 1700-2200°C [118]. The activation energy for this flexural creep test was found to be 344±35 kJ/mol, for non-oxidizing conditions as this paper investigated creep in both air and non-oxidizing atmospheres [118]. Long crack behavior of ZrB<sub>2</sub>-SiC was investigated as a function of temperature using a double cantilevered beam with half-chevron-notch initiation zones [119]. The K<sub>R</sub> raised from 0.1 to 0.5 MPa m<sup>1/2</sup>, and is attributed to wake zone toughening up to 1000°C but beyond 1000°C creep zone development became the major fracture mechanism [119]. The final paper one found investigated creep of ZrB<sub>2</sub>-SiC under compressive stress with addition of Si<sub>3</sub>N<sub>4</sub> [120]. It was found that ZrB<sub>2</sub>-SiC had higher creep resistance than ZrB<sub>2</sub>-SiC-Si<sub>3</sub>N<sub>4</sub> [120].

### 1.3.5: Fatigue and Oxidation of ZrB<sub>2</sub>-SiC

Fatigue is a form of failure when a part is subjected to cyclic loading or environmental factors that a part or sample will encounter in the real world. There are many types of fatigue: cyclic loading, thermal cycling, and corrosion and rust resistance. Most of the papers in this section have been found to be mainly about thermal shock resistance. These papers were written by Zimmermann [121] and Meng [122]. Zimmermann also investigated the depth of damage and stiffness as the temperature changed. Meng investigated the strength of samples after a number of thermal shock cycles [122].

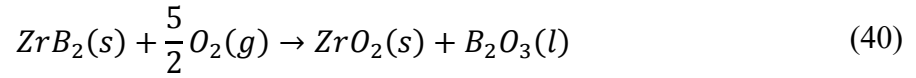
Other types of fatigue are crack growth behavior and Mode I fracture toughness have been investigated by Bird [119] and Kurihara [123], respectively. Environmental and creep effects have also been studied by Orlovskaya [124] on ZrB<sub>2</sub>-30wt%SiC ceramic composites.

Many papers have been published on oxidation results and oxidation resistance of ZrB<sub>2</sub>-SiC ceramic composites. Such papers were written by Mallik [125], Tian [126], Hu [127], Guo [128], Opeka [129], and Han [130]. All of these papers were about oxidation and oxidation resistance. Looking further one finds many more. In addition to just looking at the oxidation mechanisms, tests were conducted with torches and high enthalpy flow using arc-jet test and plasma torch. These tests were done to simulate the intense heating of the leading edge upon re-entry. Looking at the specimen after the testing, one notices the sample is no longer smooth and is charred, showing the effects of oxidation on the sample.

Since ZrB<sub>2</sub>-SiC exposed to high temperatures will be oxidized, one would like to know how the material oxidizes. First looking at the oxidation of each phase separately, starting with

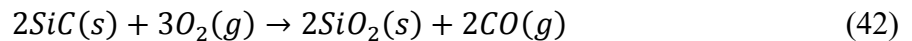


ZrB<sub>2</sub>. ZrB<sub>2</sub> oxidizes through the following chemical reactions shown below as Eqns. (40)-(41) [131]:

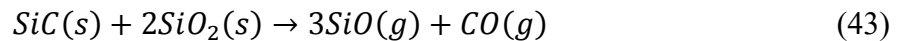


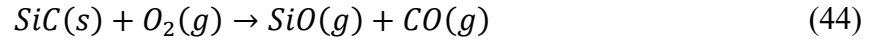
where s stands for solid phase, g stands for gas phase, and l stands for liquid phase of the composition in the reaction. ZrB<sub>2</sub> oxidation in air results in dense adherent oxide scale consisting of two phases, ZrO<sub>2</sub> and B<sub>2</sub>O<sub>3</sub> [131]. At low temperatures (<1000°C), a glassy B<sub>2</sub>O<sub>3</sub> film is observed on top of the (ZrO<sub>2</sub>+B<sub>2</sub>O<sub>3</sub>) scale [131]. But at higher temperatures the B<sub>2</sub>O<sub>3</sub> layer is not present. Over all temperatures a porous ZrO<sub>2</sub> scale is one part of the oxidation product [131]. At low and intermediate temperatures the ZrO<sub>2</sub> pores are filled with B<sub>2</sub>O<sub>3</sub> [131]. The microstructure of ZrO<sub>2</sub> changes from equiaxed grains to columnar grains at higher temperatures [131].

Now looking at the oxidation of SiC by itself, SiC has two types of oxidation behavior, “active” and “passive” at high temperatures [132]. “Passive” oxidation occurs at high oxygen pressures, which occurs within a protective film of SiO<sub>2</sub>(s) that is formed on the surface through the following reaction Eqn. (42) [132]:



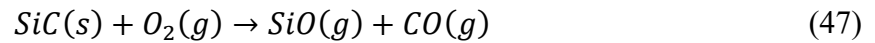
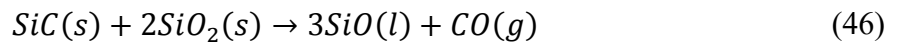
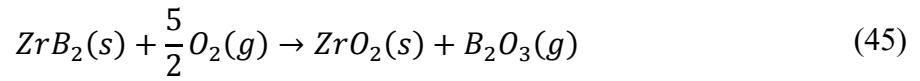
“Active” oxidation occurs at low oxygen potentials and occurs through the following reactions as shown below as Eqns. (43)-(44) [132]:





It has been found that this active oxidation occurs only at oxygen pressures lower than  $3 \cdot 10^{-4}$  atm at a temperature of 1400°C [133].

Now looking into ZrB<sub>2</sub>-SiC one can find it oxidizing through the following reactions as shown below in Eqns. (45)-(47) [134]:



When ZrB<sub>2</sub>-SiC oxidizes it forms many different layers which depends on the percent of SiC content and the oxygen pressure [134].

### 1.3.6: Thermal Properties and Thermal Shock of ZrB<sub>2</sub>-SiC

Due to the high temperature at hypersonic flight the thermal properties and thermal shock of ZrB<sub>2</sub>, SiC and ZrB<sub>2</sub>-SiC are of high interest. For ZrB<sub>2</sub> one can find a paper by Yaun, where he investigated porous ZrB<sub>2</sub> prepared by spark plasma sintering as well as reactive spark plasma sintering [135]. Yaun found that at room temperature ZrB<sub>2</sub> raw powder samples had a thermal conductivity of 56.5W/mK, with a sample porosity of 0.21 [135]. Yaun also found that the heat capacity of ZrB<sub>2</sub> was similar to that reported in the NIST-JANAF tables and the thermal diffusivity was 27.1 mm<sup>2</sup>/s at ambient room temperature and around 18.7 mm<sup>2</sup>/s at 773K [135]. The final result from Yaun was that for porous ZrB<sub>2</sub> samples, the thermal properties trends did not depend on the porosity of the sample [135]. The next paper found on ZrB<sub>2</sub> showed that the thermal

properties is a function of temperature found by radiative measurements by Zhang [136]. Figure 35 below shows the results for the temperature dependence of thermal conductivity and thermal diffusivity of  $ZrB_2$ , one can see that in both cases as the temperature increases the thermal conductivity and diffusivity decreases [136].

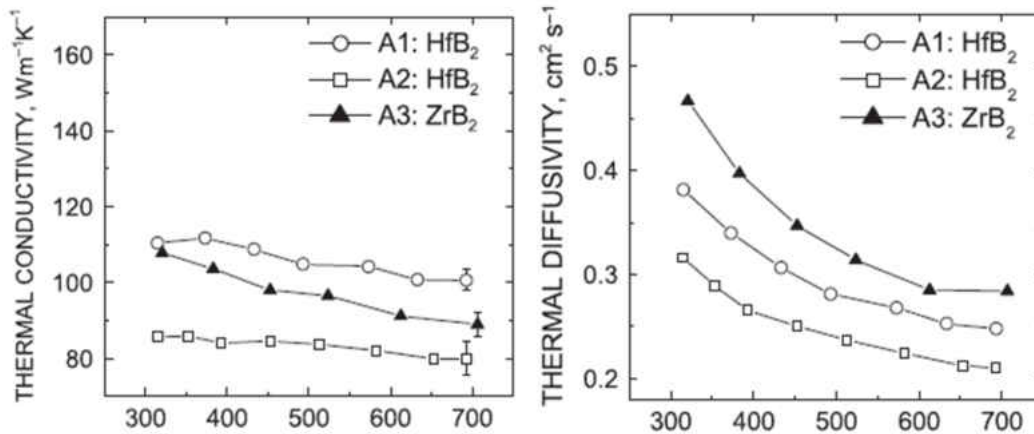


**Figure 35: Thermal conductivity and diffusivity as a function of temperature. Reprinted from *Journal of the American Ceramic Society*, vol. 94, L. Zhang, D. A. Pejaković, J. Marschall, and M. Gasch, "Thermal and Electrical Transport Properties of Spark Plasma-Sintered HfB<sub>2</sub> and ZrB<sub>2</sub> Ceramics," pp. 2562-2570, Copyright (2011), with permission from John Wiley and Sons. [136]**

Zapata-Solvas investigated the coefficient of thermal expansion (CTE) of  $ZrB_2$  ceramics and found that as the temperature increased the CTE increases as well [137]. The value at 200°C was approximately  $6.2 \times 10^{-6} \text{ K}^{-1}$  but increased to approximately  $7.8 \times 10^{-6} \text{ K}^{-1}$  at 2000°C [137]. Zapata also investigated the thermal conductivity and diffusivity, which both showed the same trends as the previous papers [137]. Another paper by Mallik found the same trends as well for thermal conductivity and diffusivity [138].

Now looking at the thermal properties of 6H-SiC, Li investigated thermal expansion and thermal expansion anisotropy of multiple SiC polytypes [95]. Li reported the following for the

average CTE along the c axis of 6H SiC polytype as  $4.16 \times 10^{-6} \text{ }^\circ\text{C}^{-1}$  with an average principle axis CTE of  $4.46 \times 10^{-6} \text{ }^\circ\text{C}^{-1}$  [95]. The 6H SiC polytype thermal expansion anisotropy was found to increase in temperature as a quadratic function with  $0^\circ\text{C}$  having a value of 0.03 and at  $1000^\circ\text{C}$  having a value of 0.08 [95]. A paper by Slack found that the SiC thermal conductivity value is between that of pure Si and pure diamond, and that the heat transport in SiC is caused by phonons [88].

Now looking at the thermal properties of  $\text{ZrB}_2\text{-SiC}$ , one finds many papers. Zapata-Solvas also investigated  $\text{ZrB}_2\text{-20vol\%SiC}$  thermal properties over the temperature range of  $0\text{-}2000^\circ\text{C}$  [137]. The thermal conductivity over this temperature range started at around  $90 \text{ W/mK}$  and decreased with increasing temperature to  $60 \text{ W/mK}$  at  $2000^\circ\text{C}$  [137]. The thermal diffusivity exhibited the same trend with the starting value of  $35 \text{ mm}^2/\text{s}$  to  $15 \text{ mm}^2/\text{s}$  at  $2000^\circ\text{C}$  [137]. Zapata also investigated the CTE of  $\text{ZrB}_2\text{-20vol\%SiC}$  and found at  $200^\circ\text{C}$  the CTE to be approximately  $5.4 \times 10^{-6} \text{ K}^{-1}$  and increased to  $7.0 \times 10^{-6} \text{ K}^{-1}$  at  $1800^\circ\text{C}$  [137]. Just like Zapata, Zhang also investigated the thermal properties of  $\text{ZrB}_2\text{-20vol\%SiC}$  [136]. The trend that Zhang report for thermal diffusivity, and conductivity match that of Zapata with the values having good agreement between the two [136]. Mallik used values from literature and models such as ROM or Kerner's to investigate the CTE of  $\text{ZrB}_2\text{-20vol\%SiC}$ . Mallik's results are as shown below in Figure 36. One can see that the CTE of  $\text{ZrB}_2\text{-20vol\%SiC}$  can vary greatly over a temperature range [138].

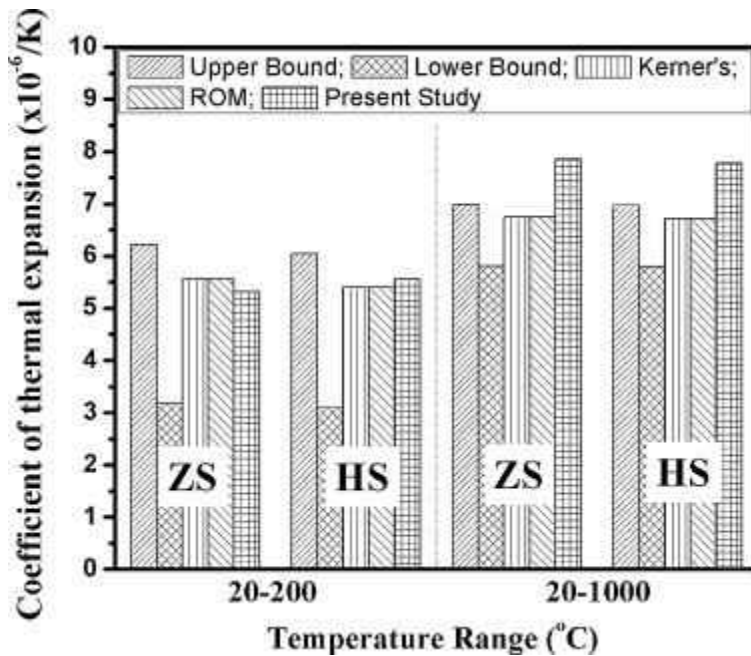


**Figure 36: CTE bar chart of results obtained for the different composite investigated. Reprinted from *Journal of the European Ceramic Society*, vol. 32, M. Mallik, A. J. Kailath, K. K. Ray, and R. Mitra, "Electrical and thermophysical properties of ZrB<sub>2</sub> and HfB<sub>2</sub> based composites," pp. 2545-2555, Copyright (2013), with permission from Elsevier. [138]**

Patel studied ZrB<sub>2</sub>-10vol%SiC-1wt%B<sub>4</sub>C (Z10S), ZrB<sub>2</sub>-20vol%SiC-1wt%B<sub>4</sub>C (Z20S), and ZrB<sub>2</sub>-30vol%SiC-1wt%B<sub>4</sub>C (Z30S) composites sintered using hot press [139]. Patel reports the specific heat capacity, thermal diffusivity, and thermal conductivity of the three mentioned composites, and the results are as shown below as Figure 37 A, B, and C respectively [139]. These trends match the other results reported in literature.

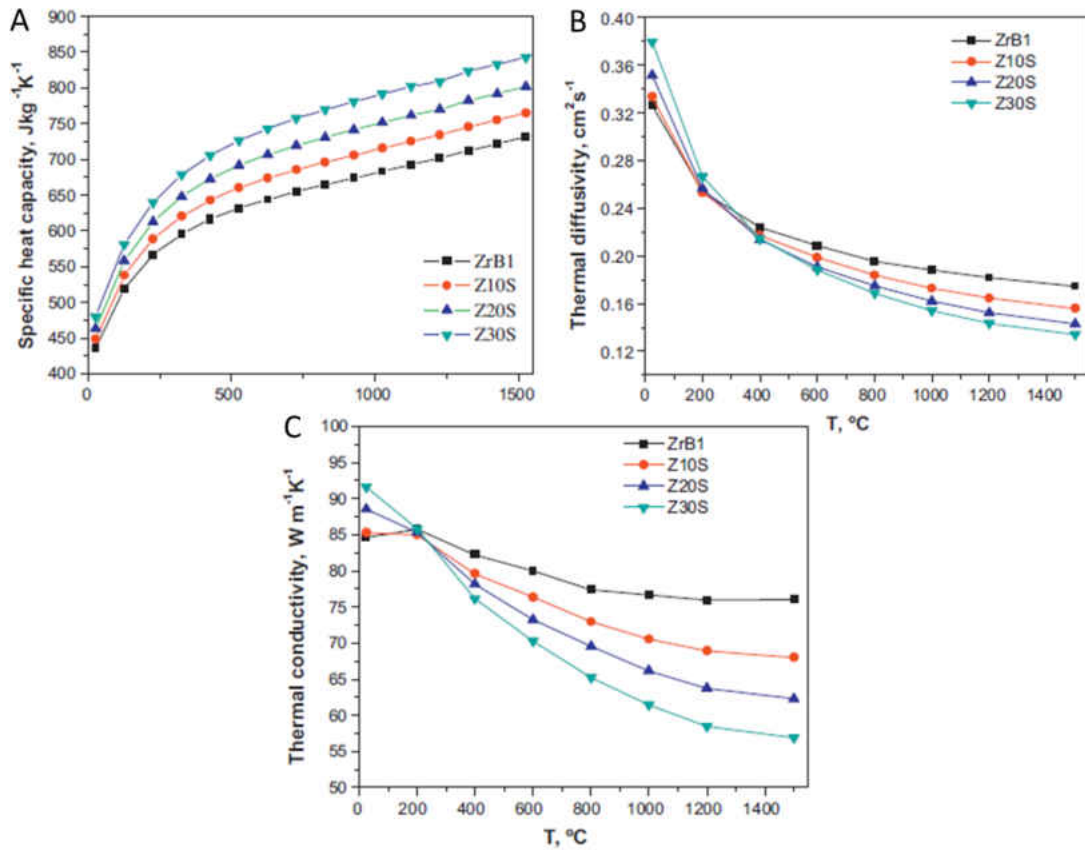


**Figure 37: Specific heat capacity(A), thermal diffusivity (B), and thermal conduction (C) as a function of temperature. Reprinted from *Journal of the European Ceramic Society*, vol. 33, M. Patel, V. V. B. Prasad, and V. Jayaram, "Heat conduction mechanisms in hot pressed ZrB<sub>2</sub> and ZrB<sub>2</sub>SiC composites," pp. 1615-1624, Copyright (2013), with permission from Elsevier. [139]**

The radiative properties of ZrB<sub>2</sub>-SiC were reported by Meng [140]. Meng found that the material's emissivity of ZrB<sub>2</sub>-SiC over the range of 1100-1800°C using Fourier transform infrared (FTIR) measurements was found to be in the range of 0.67-0.91 [140]. The last paper is on the effect of SiC shape and oxidation on the emissivity of ZrB<sub>2</sub>-SiC [141].

Now looking at the thermal shock properties of ZrB<sub>2</sub>-SiC ceramic composites, Zimmermann investigated the thermal shock behavior of both ZrB<sub>2</sub> and ZrB<sub>2</sub>-30vol%SiC, and reported the thermal shock parameters at 138°C, and 202°C with a critical  $\Delta T$  of 385 and 395

respectively [142]. Wang investigated the effect of different quenching media on the thermal shock behavior of  $ZrB_2$ -SiC ceramics, they found that the ceramic strength dropped significantly after water quenching with a temperature difference of about  $275^\circ C$  [143], while the strength of samples after quenching in air and silicone oil only varied a little [143]. The difference in thermal shock behavior is because of the different thermal properties of the quenching media [143]. Meng investigated the repeated thermal shock behaviors of  $ZrB_2$ -SiC and found that as the number of thermal shock cycles increased the strength of the sample afterward increased [122]. This is shown below as Figure 38, the increase of strength with the number of cycles is attributed to the healing of defects from oxides forming [122].

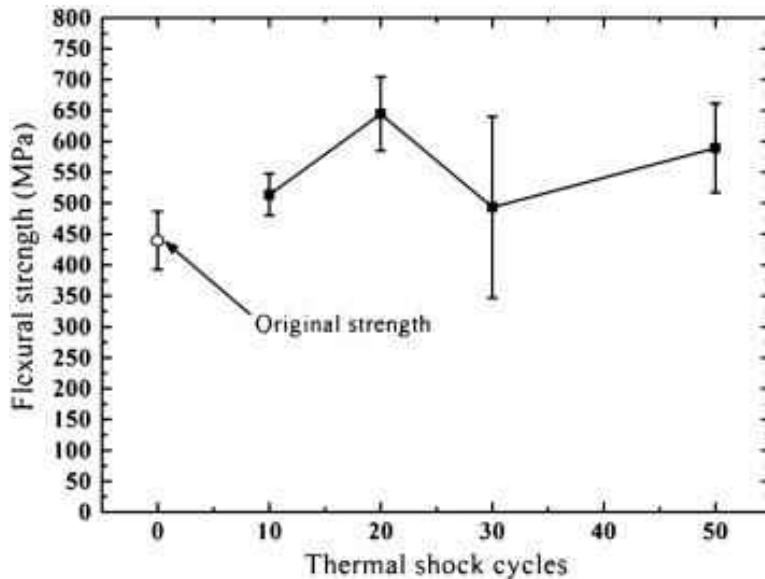


**Figure 38: Thermal shock cycles effect on flexural strength.** Reprinted from *International Journal of Refractory Metals and Hard Materials*, vol. 29, S. Meng, F. Qi, H. Chen, Z. Wang, and G. Bai, "The repeated thermal shock behaviors of a  $ZrB_2$ -SiC composite heated by electric resistance method," pp. 44-48, Copyright (2011), with permission from Elsevier. [122].

$ZrB_2$ -SiC (ZS) and  $ZrB_2$ -SiC-graphite (ZSG) composite have been investigated by Wang, with the ZSG exhibiting better thermal shock resistance than ZS as shown below as Figure 39 [144].

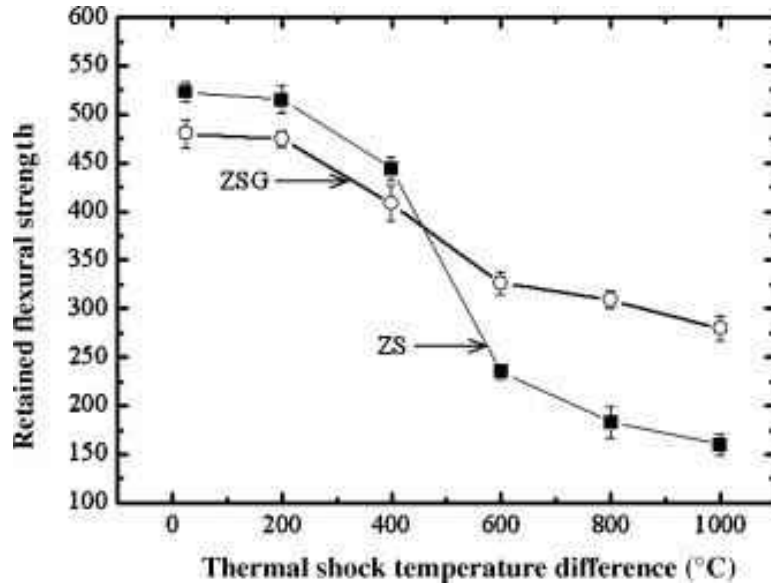


**Figure 39: Thermal shock temperature difference effect on flexure strength. Reprinted from *Materials Chemistry and Physics*, vol. 113, Z. Wang, C. Hong, X. Zhang, X. Sun, and J. Han, "Microstructure and thermal shock behavior of ZrB<sub>2</sub>-SiC-graphite composite," pp. 338-341, Copyright (2009), with permission from Elsevier. [144]**

A few papers have been on modeling of thermal shock [145, 146]. The rest of the papers one found is one other compositions such a ZrB<sub>2</sub>-SiC-graphite [147, 148], HfB<sub>2</sub> [149-151], ZrB<sub>2</sub>-SiC-ZrC [152], ZrB<sub>2</sub>SiC-ZrO<sub>2</sub> [153], and ZrB<sub>2</sub>-SiC-ZrC [154].

### 1.3.7: Ablation and Arc Jet (Arc Heater) Testing of ZrB<sub>2</sub>-SiC

The high temperatures encountered in hypersonic flight causes most materials to ablate. Most of the papers on ultra-high temperature ceramic material ablation properties were found by oxyacetylene torch such as C/C-ZrC-SiC [155], C/ZrB<sub>2</sub>-SiC [156], and C-SiC [157]. Two types of ablative calculations are made: linear ablation rate, shown below as Eqn. (48) and mass ablation rate, shown below as Eqn. (49) [157]:



$$R_l = \frac{\Delta d}{t} \quad (48)$$

$$R_m = \frac{\Delta m}{t} \quad (49)$$

where in Eqn. (48)  $\Delta d$  was the change in the thickness of the sample before and the after the test. In Eqn. (49)  $\Delta m$  is the sample mass change before and after the test, and  $t$  in both equation is the time of the ablation test.

Wei investigated the effect of the environment of an ablation test on 3-D braided C-SiC composites [157]. It was found from this study by Wei that the ablation rates for both linear and mass ablation decreased in oxygen abundant environment when compared to oxygen free environment [157]. This was found to be because under the oxygen free environment, the ablation mechanisms were due to the erosion of the high speed torch, while under abundant oxygen environment the main mechanisms were oxidation erosion [157]. C/C-ZrC-SiC ceramics composites were investigated by Xie [155]. Xie also investigated pure C/C and C/C-SiC composites to compare to C/C-ZrC-SiC and found that C/C-ZrC-SiC have the lowest ablation rates, followed by pure C/C and finally C/C-SiC with the highest ablation rates [155]. Another test with the effect of different environment on C-SiC, C-SiC-ZrO<sub>2</sub>, and C-SiC-ZrB<sub>2</sub> was conducted by Fang in water vapor and in dry air [158]. Fang found that the ablation rates decrease when dry air test results were compared to the water vapor environment test [158]. Tang investigated many different ceramic composites ablation rates using an oxyacetylene torch [159]. Tang looked at the effect of ablation time on the mass erosion or mass ablation rate as shown below as Figure 40. Tang also looked at the ablation rate dependence on the heat flux the sample was exposed to during the ablation test and is shown below as Figure 41.

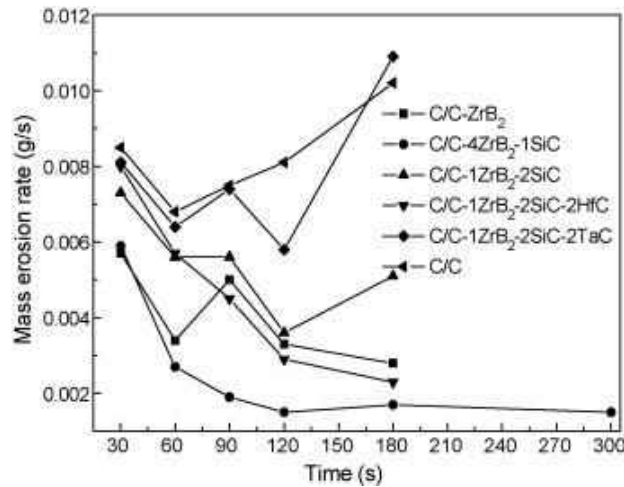


**Figure 40: Mass ablation rate vs. ablation time.** Reprinted from *Materials Science and Engineering: A*, vol. 465, S. Tang, J. Deng, S. Wang, W. Liu, and K. Yang, "Ablation behaviors of ultra-high temperature ceramic composites," pp. 1-7, Copyright (2007), with permission from Elsevier. [159].

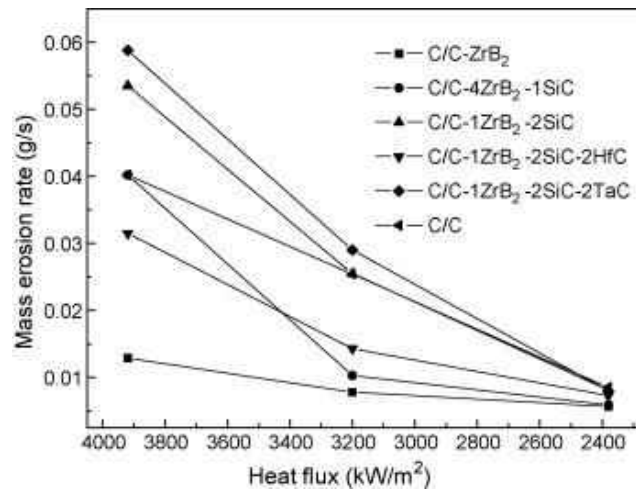


**Figure 41: Mass ablation rate vs. heat flux the sample experienced.** Reprinted from *Materials Science and Engineering: A*, vol. 465, S. Tang, J. Deng, S. Wang, W. Liu, and K. Yang, "Ablation behaviors of ultra-high temperature ceramic composites," pp. 1-7, Copyright (2007), with permission from Elsevier [159].

Many other ceramic composites have been investigated for their ablation properties [141, 160-165]. Now focusing on the composite of interest in the current research, ZrB<sub>2</sub>-SiC, Zhang investigated ZrB<sub>2</sub>-SiC and C/SiC leading edge samples with an arc jet; the samples had a nose

radius of 3.5 mm [166]. The ZrB<sub>2</sub>-SiC samples outperformed C/SiC samples as shown below in Figure 42 [166].

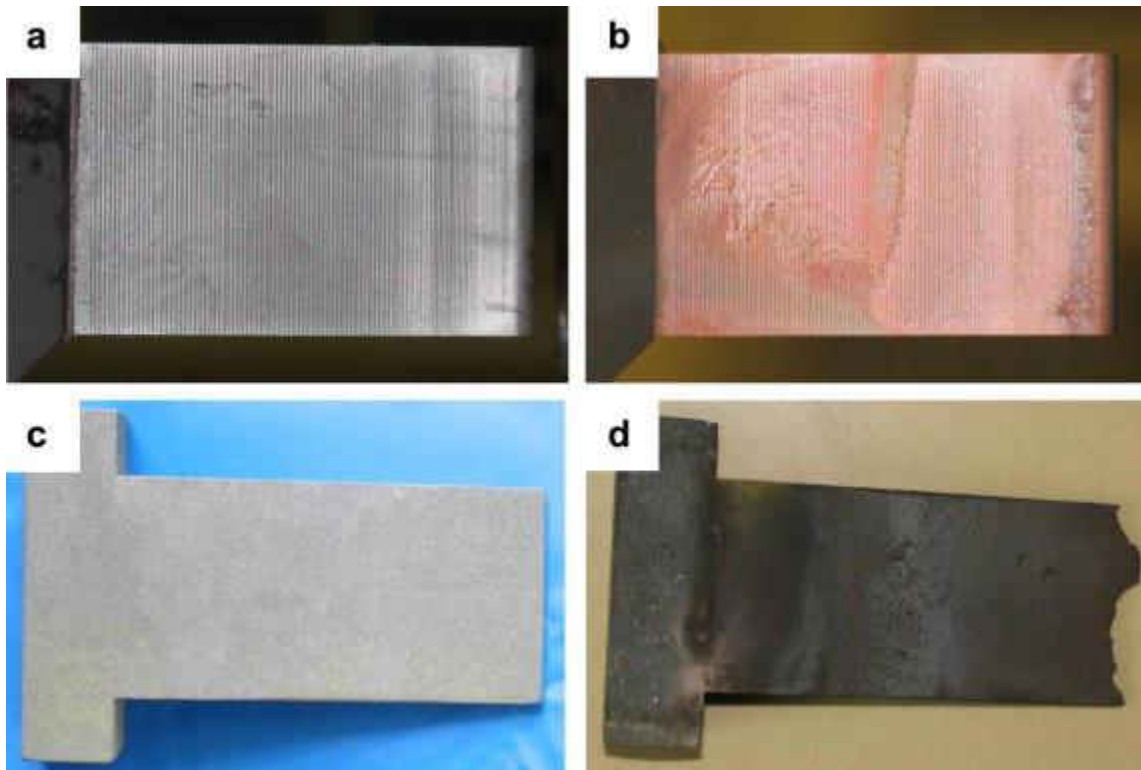


**Figure 42: Sample before test of ZrB<sub>2</sub>-SiC (a), C/C (c), and after for ZrB<sub>2</sub>-SiC (b), and C/C (d). Reprinted from Composites Science and Technology, vol. 68, X. Zhang, P. Hu, J. Han, and S. Meng, "Ablation behavior of ZrB<sub>2</sub>-SiC ultra high temperature ceramics under simulated atmospheric re-entry conditions," pp. 1718-1726, Copyright (2008), with permission from Elsevier [166].**

Zhang also investigated the effect of SiC content in ZrB<sub>2</sub>-SiC on ablation in an oxyacetylene torch [167]. Zhang found that as the SiC composition increases in the composite the ablation rate increased from 0.115 to 0.261 mg/cm<sup>2</sup>s [167].

Jin investigated ZrB<sub>2</sub>-SiC ceramic composites under oxy-acetylene torch varying the nose radius of the samples from 0.15 to 1mm as shown below as Figure 43 [147].

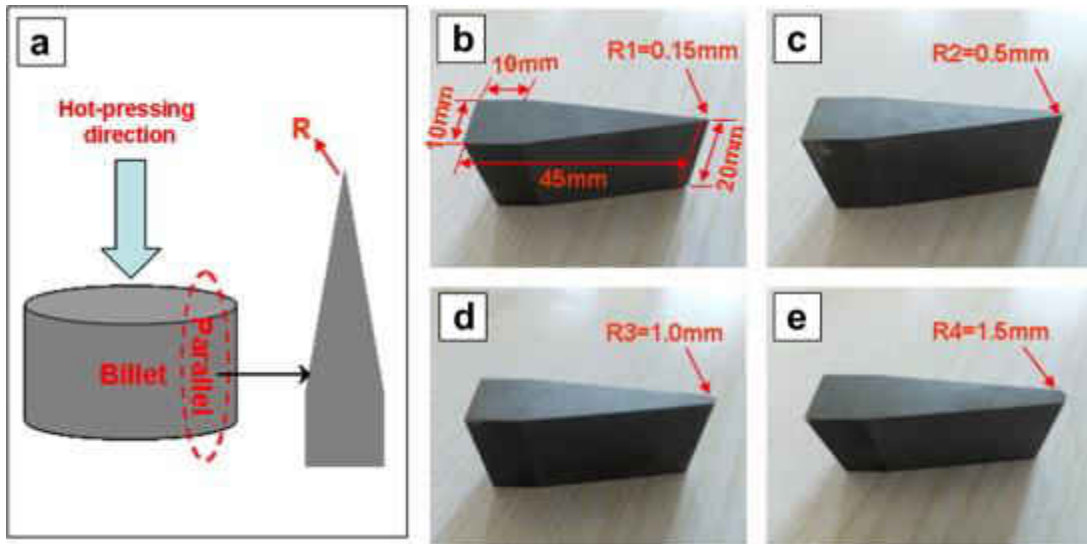


**Figure 43: ZrB<sub>2</sub>-SiC sharp leading edge models with different nose radius. Reprinted from *Journal of Alloys and Compounds*, vol. 566, X. Jin, R. He, X. Zhang, and P. Hu, "Ablation behavior of ZrB<sub>2</sub>-SiC sharp leading edges," pp. 125-130, Copyright (2013), with permission from Elsevier [147].**

The sample with the smallest nose radius had the highest surface temperature, while the largest nose radius sample had the lowest surface temperature, which agrees with theory [147]. The ablation rates had the same trend as the surface temperature, where the rate decreased with increase in sample nose radius [147].

Montevende investigated ZrB<sub>2</sub>-SiC and Si<sub>3</sub>N<sub>4</sub>-MoSi<sub>2</sub> composites ablation in an arc-jet [168]. The sample dimensions used and the picture of the sample in the arc-jet is shown below as Figure 44 [168]. Montevender found that the ZrB<sub>2</sub>-SiC performed better than the Si<sub>3</sub>N<sub>4</sub>-MoSi<sub>2</sub> ceramic composite [168].

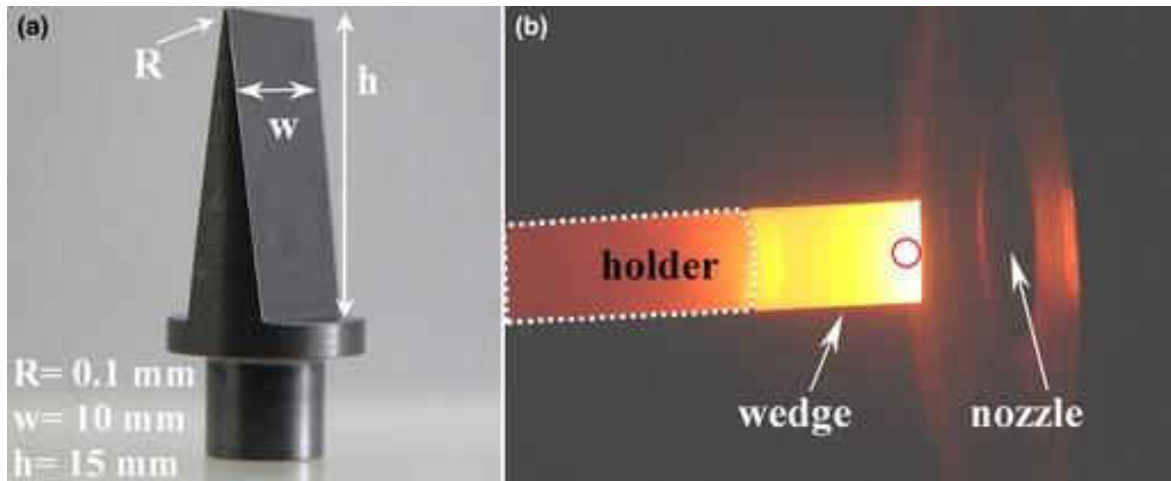


**Figure 44: ZrB<sub>2</sub>-SiC wedge sample on the left and the sample in the arc-jet on the right. Reprinted from *Journal of the American Ceramic Society*, vol. 95, F. Monteverde and R. Savino, "ZrB<sub>2</sub>-SiC Sharp Leading Edges in High Enthalpy Supersonic Flows," pp. 2282-2289, Copyright (2012), with permission from John Wiley and Sons [168].**

The final paper one found on ablation of ZrB<sub>2</sub>-SiC composites is by Hu [169]. Hu investigated the effect of SiC content on the ablation and oxidation behavior [169]. Two different test conditions were investigated in an arc jet, the first is with a heat flux of 4.78 MW/m<sup>2</sup> and enthalpy 27.9 MJ/kg; the second test had a heat flux of 3.8 MW/m<sup>2</sup> and enthalpy of 20.8 MJ/kg [169]. The trend that was found for both test conducted showed that ZrB<sub>2</sub>-30vol%SiC had the best ablation performance followed by ZrB<sub>2</sub>-15vol%SiC, and finally ZrB<sub>2</sub>-10vol%SiC with the worst ablation rate [169].

Arc-jets are an important part of testing material for hypersonic vehicles applications, and most closely simulate the conditions experienced during hypersonic flight. Thus one conducted a literature search for arc jet experiments, but one only found a few papers on the topic. This is mainly due to the fact that arc jet experiments are relatively expensive for the academic research community. The first paper one found on testing of ZrB<sub>2</sub>-SiC was an experiment conducted in

DLR, in Germany, on an Huels type arc-heater and the sample with 5mm radius reached temperatures of 1500K [170]. The DLR facility experiments used a total enthalpy of 20MJ/kg and Mach number of 3.9 and is described in great detail by Esser and Gulhan [171]. A secondary test was conducted at Naples SER with a total power of 28kW, freestream enthalpy of 10.3 MJ/kg and another with total power of 22 kW, freestream enthalpy of 7.3MJ/kg [170]. For the 28kW run a hemisphere and cone shaped samples were used and reach temperatures of 2053K and 2013K respectively [170]. The samples tested in the 28kW run are shown below in Figure 45, with the shear stress plot show [170]. For the 22kW run the same two shapes were used and the samples reached temperature of 1823K and 1819K respectively [170].

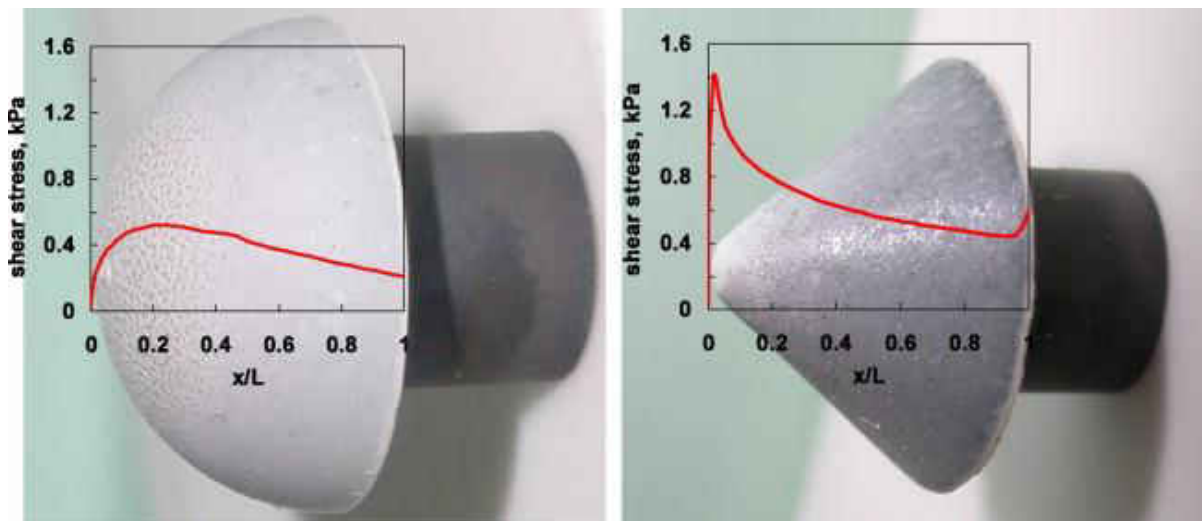


**Figure 45: the hemisphere and cone samples used in the 28kW test. Reprinted from *Aerospace Science and Technology*, vol. 14, R. Savino, M. De Stefano Fumo, D. Paterna, A. Di Maso, and F. Monteverde, "Arc-jet testing of ultra-high-temperature-ceramics," pp. 187, Copyright (2010), with permission from Elsevier Paris. [170]**

Another paper on  $ZrB_2$ -SiC ceramic composites testing with arc-jet was found by Monteverde [172]. The tests were performed at the University of Naples 80KW plasma torch

[172]. The nose radius of the samples was 5 and 0.5mm for the hemisphere and cone respectively [172]. The hemisphere reach a temperature of 2053K while the cone reached a temperature of 2083K during the experiment [172]. Figure 46 shows the sample before and after the test for both the cone and hemisphere.

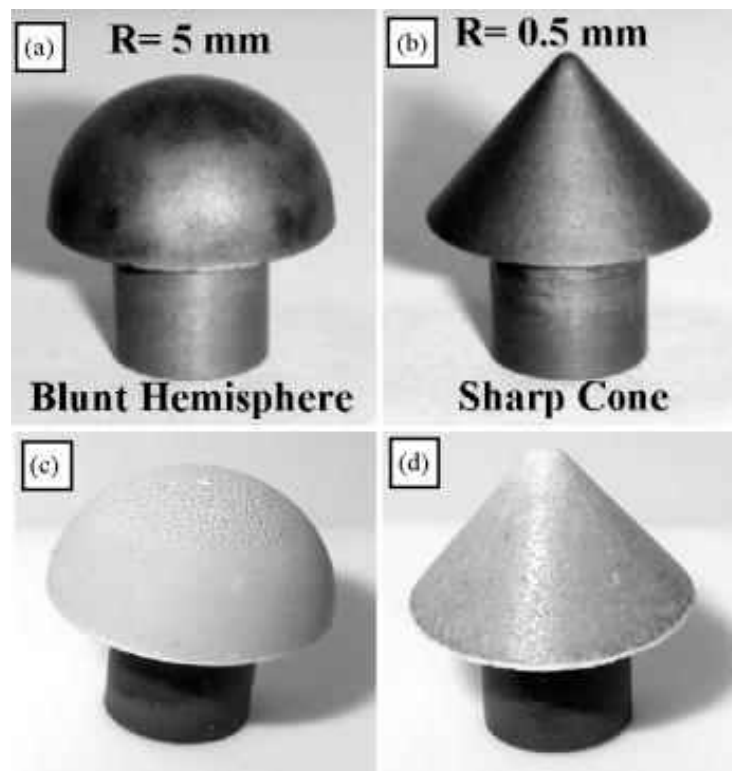


**Figure 46:** the samples before (a and b) and after the test (c and d). Reprinted from *Journal of the European Ceramic Society*, vol. 30, F. Monteverde, R. Savino, M. D. S. Fumo, and A. Di Maso, "Plasma wind tunnel testing of ultra-high temperature  $ZrB_2$ -SiC composites under hypersonic re-entry conditions," pp. 2313-2321, Copyright (2010), with permission from Elsevier [172]

Another paper was written by Monteverde on  $ZrB_2$ -SiC ceramic testing in an arc-jet [173]. This experiment Monteverde tested a Hemispheric  $ZrB_2$ -SiC sample with a nose radius 7.5mm [173]. During the experiment the sample reached 1900°C with a flow enthalpy of 20MJ/kg for 1

minute [173]. After the test the sample was investigated by SEM-EDS, and a oxide scale of zirconia of 20 $\mu$ m was found [173].

Mo-Si-B and ZrB<sub>2</sub>-SiC ceramic composites coated with Mo has been investigated by Ritt at the HyMETS at NASA Langley research center [174]. The samples were exposed to almost 3.5MW/cm<sup>2</sup> heat fluxes for 20 minutes with surface temperature reaching 1500-1650°C [174]. The results of these experiments shows that Mo-Si-B based coating improved the oxidation resistance of ZrB<sub>2</sub>-SiC samples, with the oxide scale on the order of 25 $\mu$ m instead of the typical hundreds of microns reported in prior studies [174].

The next paper one finds is on hemispherical with a radius of 7.5mm of HfB<sub>2</sub> and HfC based ultra-high temperature ceramics [175]. This paper tested HfB<sub>2</sub> and HfC with 5vol%MoSi<sub>2</sub> ceramic composites and they were tested in a plasma torch with enthalpy range of 20-28MJ/kg and an arc total power of 38-51kW [175]. The maximum temperature of the composites test was 1900-2400°C [175]. The samples were also evaluated using SEM-EDS to determine the oxide layer thickness, which was found to be 15 $\mu$ m, for the sample exposed to a 8MJ/kg enthalpy flow from the torch [175].

Another paper on HfB<sub>2</sub> based composites were investigated by Gash and Johnson at NASA Ames facility [176]. The addition of SiC, TaSi<sub>2</sub> and Ir were investigated to find which had the best oxidation performance in the NASA Ames AFH arc jet facility and were exposed to a heat flux of approximately 250W/cm<sup>2</sup> for 5 minutes [176]. The research found that the composites with the addition had oxides thickness reduced by approximately 3 times that of the baseline [176]. Figure



47 below shows the samples surface of the composites tested after the 5 minute exposure to the arc-jet.

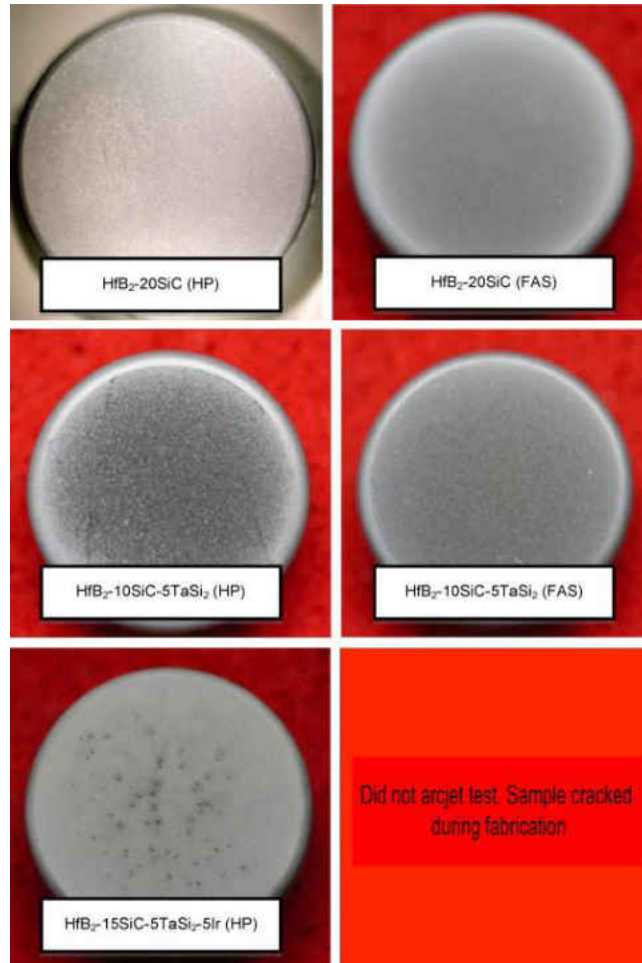


**Figure 47: Images of the samples surfaces after exposure to arc-jet for 5 minutes. Reprinted from *Journal of the European Ceramic Society*, vol. 30, M. Gasch and S. Johnson, "Physical characterization and arcjet oxidation of hafnium-based ultra high temperature ceramics fabricated by hot pressing and field-assisted sintering," pp. 2337-2344, Copyright (2010), with permission from Elsevier [176]**

In addition to the experiments, CFD simulations have been conducted to match the conditions in the experiments. The main goals of these simulations have been to find the catalytic recombination of oxygen for the materials in the ceramic composites [170, 172, 173, 175, 177].

Other papers on Arc-jet are mostly on the calibration, upgrades and additions to the facility already in place [178, 179].

#### **1.4: Raman Spectroscopy**

Now looking at the Raman Spectroscopy of ZrB<sub>2</sub>-SiC, one only finds SiC peaks, since ZrB<sub>2</sub> has not been previously reported as Raman active. This means either that ZrB<sub>2</sub> does not have any peaks at all in the spectra or the peaks are so small that they are not noticeable compared to the intensity of the SiC peaks [180, 181]. Conducting a search about this composition, one finds that each of the SiC polytypes have their own Raman spectra, due to their stacking order, and are different from each other, even though most of the time they share the same peak position. One can find the basic theory of Raman spectroscopy in the following references [182-188].

##### **1.4.1: Phonon Dispersion Curve for 6H-SiC**

To fully understand the Raman spectra of SiC one must first look at the phonon dispersion curve. The phonon dispersion curve not only gives the frequencies of optic modes but also acoustic branches [189].  $\alpha$ -SiC crystals are represented by a number of Si-C double layers in the unit cell and the letter H and R to specific the lattice structure [190]. The unit cell of  $n$ H and  $3n$ R polytypes contains  $n$  formula units (Si-C) and the unit cell length along the c-axis is  $n$  times longer than the basic polytype of 3C-SiC. Looking specifically at 6H-SiC polytype, this is the polytype of interest for the research presented in this dissertation, one finds that the crystal structure belongs to the  $P6_3mc$  space group with 12 atoms per a unit cell resulting in 33 long-wavelength optic modes [191]. 27 of the 33 optic modes are active in first-order Raman scattering [192]. The extent of the Brillouin zone for 6H-SiC is determined by looking at the maximum wave vector of the Brillouin

zone of  $\pi/c$  the length of the axial dimensions of the 6H-SiC unit cell,  $c$  [189-191]. Thus, the Brillouin zone for 6H-SiC extends to  $6\pi/c$ . Since the Brillouin zone for 6H-SiC extends past the maximum of  $\pi/c$  the Brillouin zone is therefore folded 5 times and a reduced wave vector is defined as  $x=q/q_{\max}$ . [189-193]. Because  $2\pi/c$  is a reciprocal lattice vector, therefore the pseudomomentum vectors  $q=0, 2\pi/c, 4\pi/c,$  and  $6\pi/c$  are all equivalent to  $q=0$  in the Brillouin zone [191]. Therefore, based on the reduced wave vector one finds the  $x$ -values that are accessible to Raman scattering measurements  $x=0, 0.33, 0.67,$  and  $1$  [191]. The phonon dispersion curve is shown below as Figure 48. The phonon branches of the dispersion curves are labelled from top to bottom as shown in Figure 48: axial optic (single), planar optic (double), axial acoustic (single), and planar acoustic (double) [191].

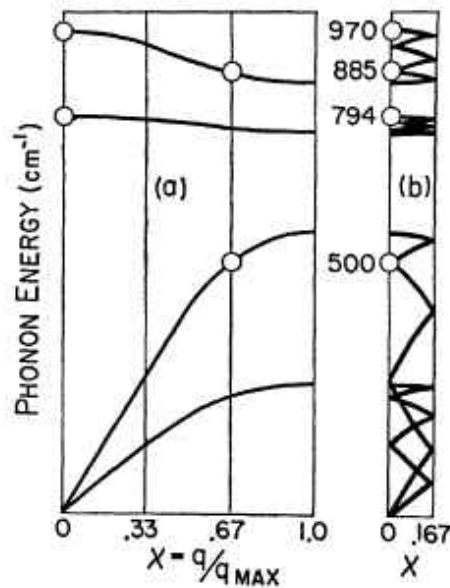


**Figure 48: 6H-SiC phonon dispersion curve. Reprinted from *Physical Review*, vol. 170, D. W. Feldman, J. H. Parker, W. J. Choyke, and L. Patrick, "Raman Scattering in 6H-SiC," pp. 698-704, Copyright (1968), with permission from American Physical Society [191].**

Now that the 6H-SiC phonon dispersion curve has been defined one can list the distribution and symmetry type of the phonon modes found in the dispersion curve. Based on the work by Patrick, the  $A_1$  and  $E_1$  modes should be assigned to the  $x=0$  or  $0.67$ , and  $E_2$  modes to  $x=0.33$  or  $1$  [193]. One should also know that at the  $x=0.33$  and  $0.67$  there is a double set of representations because of the energy discontinuities at these internal boundaries [191]. There are shown below in Table 5.

**Table 5: 6H-SiCphonon symmetry modes [191]**

| Branch          | X=0            | X=0.33 | X=0.67 | X=1   |
|-----------------|----------------|--------|--------|-------|
| Axial optic     | $A_1$ (strong) | $2B_1$ | $2A_1$ | $B_1$ |
| Planar optic    | $E_1$ (strong) | $2E_2$ | $2E_1$ | $E_2$ |
| Axial Acoustic  | $A_1$ (ac)     | $2B_1$ | $2A_1$ | $B_1$ |
| Planar acoustic | $E_1$ (ac)     | $2E_2$ | $2E_1$ | $E_2$ |

The  $A_1$  and  $B_1$  symmetry modes are axial modes while the doubly degenerate  $E_1$  and  $E_2$  modes are planar and finally the  $B_1$  modes are not observable in Raman [191].

#### **1.4.2: Strong and Weak Modes and Anisotropy of 6H-SiC Raman Modes**

The Raman modes can be characterized into strong and weak modes. The main difference between the strong and weak modes is typically determined by intensities of the peaks. In the case of 6H-SiC the difference between the strong and weak peaks is on the order of  $\sim 10^2$  [191]. The strong and weak modes can also be determined not only by the differences in the intensity but also by the following criteria. The weak modes appear with short wavelength,  $x \neq 0$ , from the stand point of the large-zone [191]. While from the stand point of the Brillouin-zone the motion is intracell with equivalent atoms in all unit cells vibrating in phase [191]. This intercell motion whether it be

absent or present, is also used to determine if the mode is strong and weak [191]. This intercell motion in the weak modes is what causes high anisotropy [191].

In Polar uniaxial crystals, optical modes can be classified based on the dominance of the following: (a) long-range electrostatic fields, or (b) crystal anisotropy [191, 194]. Loudon found for the limiting cases that the dependence of phonon frequency propagation and polarization directions simplifies to the following two cases:  $(a) \gg (b)$  or  $(b) \gg (a)$  [194]. The (a) and (b) refers the sentence on the classification of the dominance of the optical modes in polar uniaxial crystals. Applying these limiting cases to 6H-SiC one find that all of the optical modes satisfy one or the other of these conditions dictated by Loudon, and described above. For the  $(a) \gg (b)$  limiting conditions one finds that this corresponds to the strong  $x=0$  modes; While the  $(b) \gg (a)$  is assigned to the  $x \neq 0$  weak modes of 6H-SiC [191]. To conclude this discussion one can group the optical modes the same way weather by the large-zone method or by Loudon limits [191].

These two optical mode groups defined above, described above, have different propagation behavior in the general direction of  $\theta \neq 0^\circ$  or  $90^\circ$ ; where  $\theta$  is the angel between the c-axis of the 6H-SiC unit cell and the propagation vector [191]. This angular dependence of these optical modes is shown as Figure 49 [191]. The strong modes motion of atoms is determined by the propagation vector, while the weak modes are characterized by the axis of the crystal [191].

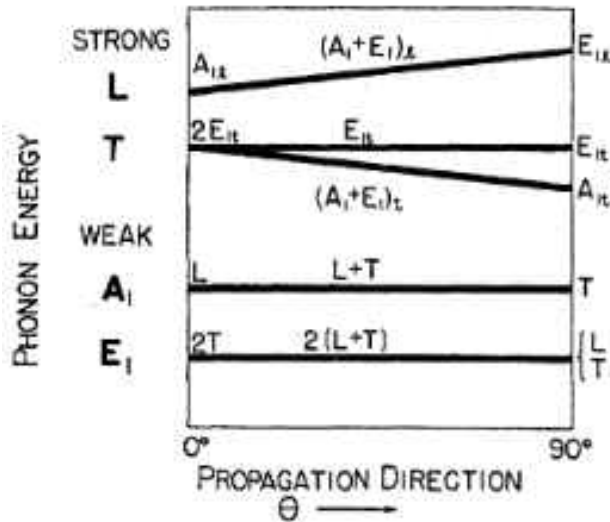


**Figure 49: Angular dependence of the strong  $A_1$  and  $E_1$  modes with that of weak modes of  $A_1$  and  $E_1$ . Reprinted from *Physical Review*, vol. 170, D. W. Feldman, J. H. Parker, W. J. Choyke, and L. Patrick, "Raman Scattering in 6H-SiC," pp. 698-704, Copyright (1968), with permission from American Physical Society [191]**

Looking at only the strong modes one found that they are mainly longitudinal or transverse due to the long-range electric field, but have a mixed symmetry ( $A_1+E_1$ ) [191]. Due to this long-range electric field there is a large separation in the frequency of longitudinal and transverse modes [191]. One also finds that these modes have a small dependence of frequency on the angle  $\theta$  [191]. This is due to the low but measurable anisotropy of the strong modes at  $x=0$  [191].

For the weak modes with the limiting case of  $(b) \gg (a)$ , are mainly axial or planar vibrational motions [191]. They primarily vibrate along or perpendicular to the c-axis of the 6H-SiC unit cell [191]. These weak modes experience a large separation in frequency but this time it is due to the high anisotropy [191]. These weak modes have a constant symmetry and thus in general the propagation direction has no effect, as show in Figure 49.

### 1.4.3: 6H-SiC Raman Modes Notation and Selection Rules

The x, y, and z axes are fixed by the 6H-SiC crystal structure with the c-axis corresponding to the z axis. For the propagation and polarization a symbol system is used. This system is described in detail by Damen [195], where a 4 letter symbol system is used. An example of this symbol is say x(zx)y, the part with x(--y) is the propagation part, and the part with -(zx)- is the polarization par [191]. The physical meaning of x(--y) is that the light incident along the x axis is scattered long the y axis and the part with -(zx)- means that the polarization directions of incident and scattering light are z and x, respectively [191]. For this example the scattering plane of xy, and conservation laws determine the phonon propagation direction in the plane [191]. The photon polarization directions, -(zx)-, determine one component of a tensor. For this polarization-change tensor given in Damen [195] show that for this component, the Raman scattered mode would have E<sub>1</sub> symmetry [191]. Table 6 below show the list of allowed normal-mode symmetry or symmetries for each tensor component [191].

**Table 6: Identification of phonon symmetry and propagation directions and the significance of polarization and propagation symbols for their identification [191]**

| Polarization symbol | Phonon symmetry                 | Propagation symbol | Propagation angle, $\theta$ |
|---------------------|---------------------------------|--------------------|-----------------------------|
| -(xx)-              | A <sub>1</sub> , E <sub>2</sub> | x(--y)             | 90°                         |
| -(yy)-              | A <sub>1</sub> , E <sub>2</sub> | z(--x)             | 45°                         |
| -(zz)-              | A <sub>2</sub>                  |                    |                             |
| -(xy)-              | E <sub>2</sub>                  |                    |                             |
| -(yz)-              | E <sub>1</sub>                  |                    |                             |
| -(zx)-              | E <sub>1</sub>                  |                    |                             |

The number of possible Raman lines is greater for 6H-SiC than for wurtzite because the normal modes are  $6(A_1+B_1+E_1+E_2)$  instead of  $2(A_1+B_1+E_1+E_2)$  [191]. The only issue is being able to distinguish between several normal modes of the same symmetry mode, which is the reason for introducing the large zone [191]. Using the polarization and propagation directions shown in Table 6 above one gets the following schematic of the Raman spectra of 6H-SiC, as shown below as Figure 50.

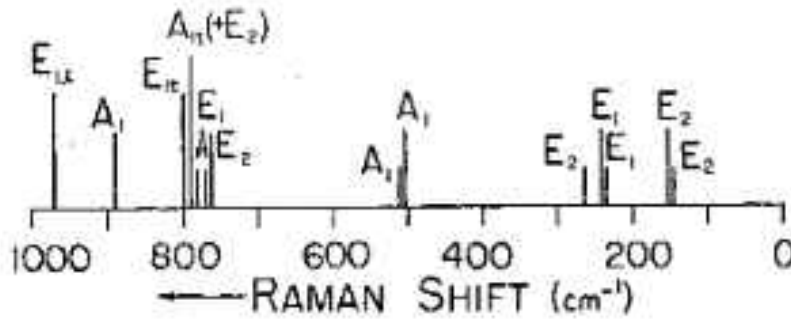


**Figure 50: Schematic showing all 15 lines, with rough classification into four degrees of relative intensity. Reprinted from *Physical Review*, vol. 170, D. W. Feldman, J. H. Parker, W. J. Choyke, and L. Patrick, "Raman Scattering in 6H-SiC," pp. 698-704, Copyright (1968), with permission from American Physical Society [191]**

Table 7 below show the assignment of all of the 6H-SiC weak modes.

**Table 7: Energies ( $\text{cm}^{-1}$ ) of weak phonon modes with this presentations and assignments to the values of  $x=q/q_{\text{max}}$ : N.O. stands for not observed, and F. stands for forbidden [191]**

| Branch          | $x=0.33$            | $x=0.67$            | $x=1$              |
|-----------------|---------------------|---------------------|--------------------|
| Axial optic     | B <sub>1</sub> F.   | A <sub>2</sub> 889  | B <sub>1</sub> F.  |
|                 | B <sub>1</sub> F.   | A <sub>1</sub> N.O. |                    |
| Planar optic    | E <sub>2</sub> 788  | E <sub>1</sub> 777  | E <sub>2</sub> 766 |
|                 | E <sub>2</sub> N.O. | E <sub>1</sub> 769  |                    |
| Axial acoustic  | B <sub>1</sub> F.   | A <sub>1</sub> 508  | B <sub>1</sub> F.  |
|                 | B <sub>1</sub> F.   | A <sub>1</sub> 504  |                    |
| planar acoustic | E <sub>2</sub> 149  | E <sub>1</sub> 241  | E <sub>2</sub> 262 |
|                 | E <sub>2</sub> 145  | E <sub>1</sub> 236  |                    |



To sum up the description of the phonon dispersion curve, Feldman made an experimental data plot of the dispersion curve in the large zone and is shown below as Figure 51.

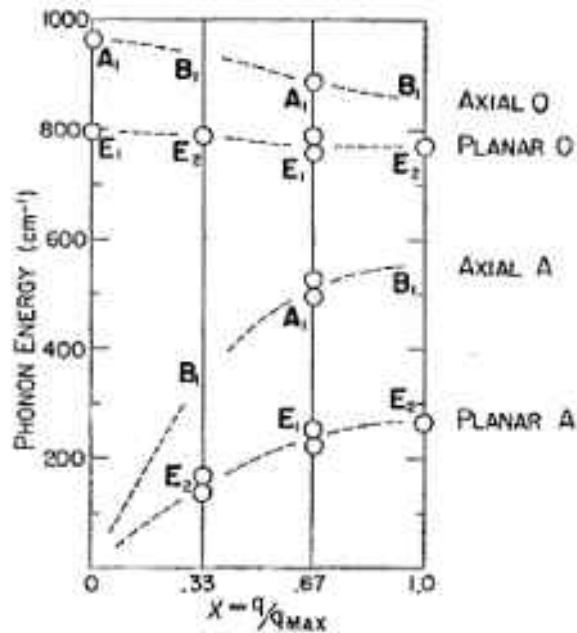


**Figure 51: Experimental dispersion curve. Reprinted from *Physical Review*, vol. 170, D. W. Feldman, J. H. Parker, W. J. Choyke, and L. Patrick, "Raman Scattering in 6H-SiC," pp. 698-704, Copyright (1968), with permission from American Physical Society [191].**

#### 1.4.4: Raman Spectra of 6H-SiC

The Raman spectrum for 6H-SiC is shown below as Figure 52 [190, 191]

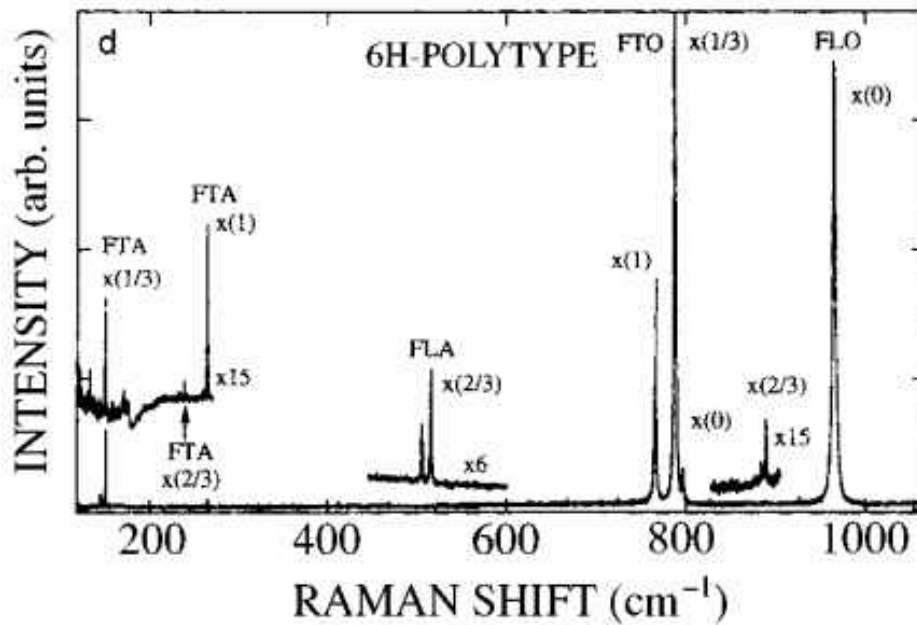


**Figure 52: 6H-SiC experimental Raman spectra. Reprinted from *physica status solidi (a)*, vol. 162, S. Nakashima and H. Harima, "Raman Investigation of SiC Polytypes," pp. 39-64, Copyright (2001), with permission from John Wiley and Sons [190]**

Table 8 below shows the observed peak positions for multiple polytypes of SiC. This is important so that one can see how close some of the peak positions for different polytypes are to each other. This is important when investigating the Raman spectra of 6H-SiC, so that one will not miss label or misinterpret the Raman spectra.

**Table 8: Experimental Raman peak positions for multiple polytypes of SiC [190]**

| Polytype | z=q/q <sub>b</sub> | Frequency(cm <sup>-1</sup> ) |              |                |             |
|----------|--------------------|------------------------------|--------------|----------------|-------------|
|          |                    | Planar acoustic              | planar optic | axial acoustic | axial optic |
|          |                    | FTA                          | FTO          | FLA            | FLO         |
| 3C       | 0                  | -                            | 796          | -              | 972         |
| 2H       | 0                  | -                            | 799          | -              | 968         |
|          | 1                  | 264                          | 764          | -              | -           |
| 4H       | 0                  | -                            | 796          | -              | 964         |

| Polytype | z=q/q <sub>b</sub> | Frequency(cm <sup>-1</sup> ) |              |                |             |
|----------|--------------------|------------------------------|--------------|----------------|-------------|
|          |                    | Planar acoustic              | planar optic | axial acoustic | axial optic |
|          |                    | FTA                          | FTO          | FLA            | FLO         |
|          | 2/4                | 196,204                      | 776          | -              | -           |
|          | 4/4                | 266                          | -            | 610            | 838         |
| 6H       | 0                  | -                            | 797          | -              | 965         |
|          | 2/6                | 145,150                      | 789          | -              | -           |
|          | 4/6                | 236,241                      | -            | 504,514        | 889         |
|          | 6/6                | 266                          | 767          | -              | -           |
| 8H       | 0                  | -                            | 796          | -              | 970         |
|          | 2/8                | 112,117                      | 793          | -              | -           |
|          | 4/8                | 203                          | -            | 403,411        | 917,923     |
|          | 6/8                | 248,252                      | -            | -              | -           |
|          | 8/8                | 266                          | 768          | 615            | -           |
| 15R      | 0                  | -                            | 797          | -              | 965         |
|          | 2/5                | 167,173                      | 785          | 331,337        | 932,938     |
|          | 4/5                | 255,256                      | 769          | 569,577        | 860         |
| 21R      | 0                  | -                            | 797          | -              | 967         |
|          | 2/7                | 126,131                      | 791          | 241,250        | -           |
|          | 4/7                | 217,220                      | 780          | 450,458        | 905,908     |
|          | 6/7                | 261                          | 767          | 590,594        | -           |

The hexagonality of the SiC polytype can be determined based on the mode with the maximum intensity. This is used to help identify the polytype of SiC present in the material being investigated.

Table 9 below shows the corresponding polytype, the maximum intensity mode and the hexagonality of that polytype; which is invaluable when identify polytypes present in SiC [190].

**Table 9: The hexagonality and the reduced wave vector of the folded modes which show the strongest intensity of each branch (ref 12 in Nakashima)[190]**

| polytype                            | $x = q/q_B$ for $I_{\max}$ mode | hexagonality |
|-------------------------------------|---------------------------------|--------------|
| 4H: 22                              | $2/4 = 0.5$                     | 0.5          |
| 15R: $(32)_3$                       | $2/5 = 0.4$                     | 0.4          |
| 6H: 33                              | $2/6 = 0.33$                    | 0.33         |
| 21R: $(34)_3$                       | $2/7 = 0.28$                    | 0.28         |
| 8H: 44                              | $2/8 = 0.25$                    | 0.25         |
| 27R: $(22\ 23)_3$                   | $4/9 = 0.44$                    | 0.44         |
| 33R: $(33\ 32)_3$                   | $4/11 = 0.36$                   | 0.36         |
| 45R: $[(32)_2 23]_3$                | $6/15 = 0.4$                    | 0.4          |
| 51R <sub>1</sub> : $[(33)_2 32]_3$  | $6/17 = 0.353$                  | 0.353        |
| 51R <sub>3</sub> : $(43\ 32\ 23)_3$ | $6/17 = 0.353$                  | 0.353        |
| 66R: $[(33)_2(32)_2]_3$             | $8/22 = 0.364$                  | 0.364        |

Nakashima has also mentioned methods on how to identify the SiC polytypes based on the Raman spectra collect [190]. This method is as follows for polytypes with longer periods:

1. The period is estimated from the Frequency Transverse Acoustic (FTA) and Frequency Transverse Optic (FTO) frequencies
2. Possible model structures are listed up and the observed spectrum is compared with those calculated for these model structure [196, 197]

The method for common polytypes with shorter periods is as follows:

1. Obtain the precise frequency values of the FTA and FTO modes in order to determine the period
2. Seek a folded mode which has the maximum intensity

3. Then use the simple rule that the reduced wave vector of the folded mode with a maximum intensity,  $x=q/q_{\max}$  is equal to the hexagonality of the polytype (ref 12 of Nakashima)

Being able to identify what polytypes are present in SiC is very important since it will have an effect on the data you're collecting and the type of analysis to conduct. This is also useful if the specific polytype of a sample of SiC is unknown, one can identify it. This fact can also be used to determine if a sample of known polytype of SiC has only that polytype or is a mixture of multiple polytypes.

Experimental results have also shown Raman to be useful in identifying if a crystal is disordered or not. This was done with 6H-SiC by Nakashima and is shown below Figure 53 [190]. Where Figure 53A shows heavy disordering of a crystal for the FTA modes and Figure 53B shows heavy disordering of a crystal for the FTO modes. Looking at this Figure 53 one can clearly see the difference between a disordered crystal and a crystal that is not. The disordered crystal peak is much broader and the intensity is much lower. This is true for both the FTO and FTA modes. This crystal disorder is from a stacking disorder of SiC crystal itself [190].

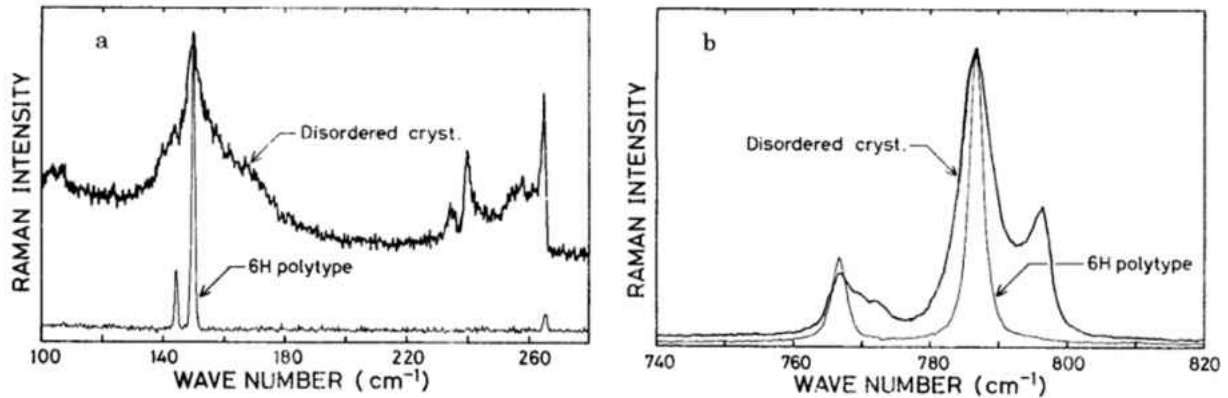


**Figure 53: Raman spectra of a heavily disordered SiC crystal for FTA modes (A), and FTO modes (B). Reprinted from *physica status solidi (a)*, vol. 162, S. Nakashima and H. Harima, "Raman Investigation of SiC Polytypes," pp. 39-64, Copyright (2001), with permission from John Wiley and Sons [190]**

In addition to being able to determine if the crystal is disordered or not one can also determine the stress in the crystals. These effects have been studied to great depths and will be discussed in depth in 1.6: Raman Piezo-Spectroscopy section of this dissertation. Continuing the investigation of 6H-SiC Raman spectra one finds that changing the temperature of the material changes the peak position of the material. This was experimentally shown below Figure 54, one can see in this figure that there is a slight shifting in the peak position. This occurs in both heating and cooling. The peak position shifts to a higher wavenumber upon heating SiC and shifting to a lower wavenumber upon cooling SiC.

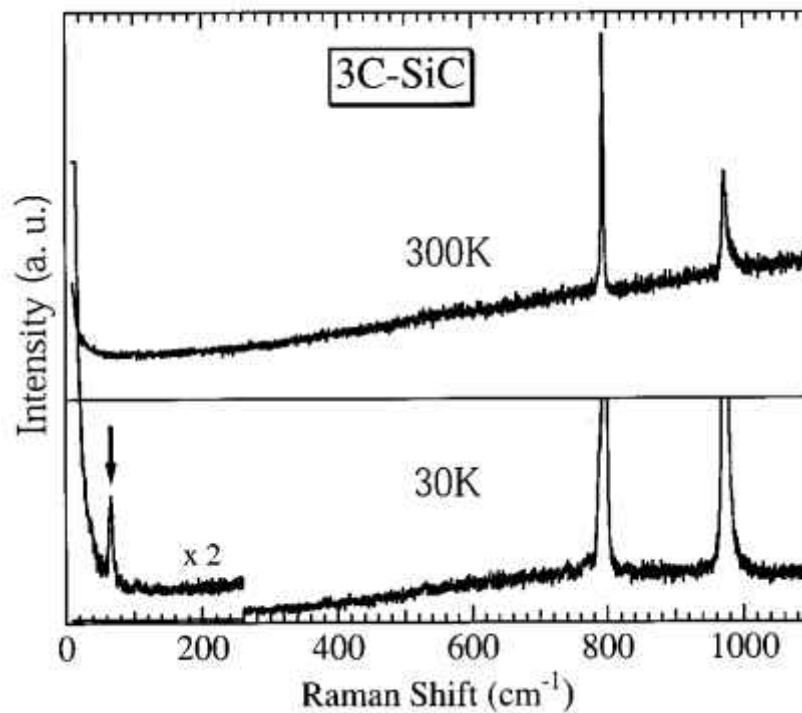


**Figure 54: Effect of temperature on SiC Raman spectra. Reprinted from *physica status solidi (a)*, vol. 162, S. Nakashima and H. Harima, "Raman Investigation of SiC Polytypes," pp. 39-64, Copyright (2001), with permission from John Wiley and Sons [190]**

### **1.5: Thermal Residual Stresses in ZrB<sub>2</sub>-SiC Ceramic Composites**

Looking at this Table 2 above in the mechanical properties section, one notices that the Young's modulus and the coefficient of thermal expansion (CTE) are very different. Looking at theory for composites one sees that since the Young's modulus and CTE are different, thermal residual stresses will develop. These stresses develop due to the mismatch in Young's Modulus and CTE, and occurs as the sample cools down from the sintering temperature [198, 199]. This is due to the fact thermal stresses are internal stresses that arise when a constraint on dimensional change of a body. In the absence of this constraint, the body can experience free thermal strain without any accompanying thermal stress [199]. The following constraint can have its origin in:

temperature gradient, crystal structure anisotropy, phase transformations resulting in volume change, and a composite material made of dissimilar materials. In the case of ZrB<sub>2</sub>-SiC, the last constraint is the reason for the thermal stress in the composite [200]. This is of interest since mechanical properties are known to be affected by residual stresses in ceramic composites [200]. With this in mind one would like to calculate the residual stresses in ZrB<sub>2</sub>-SiC. Assuming the composite as an assembly of elastic spheres of uniform size, embedded in an infinite elastic continuum one gets the following Eqns. (50)-(52) shown below, from the theory of elasticity, as described by Chawla [199]:

$$P = \frac{(\alpha_m - \alpha_p)\Delta T}{\left[ \frac{0.5(1 + \nu_m) + (1 - 2\nu_m)V_p}{E_m(1 - V_p)} + \frac{1 - 2\nu_p}{E_p} \right]} \quad (50)$$

where  $P$  is the thermal residual stress in the particulate phase,  $\alpha$  is the coefficient of thermal expansion (CTE),  $\Delta T$  is the temperature change between the sintering temperature and room temperature ( $\Delta T = -1930^\circ\text{C}$ ),  $\nu$  is the Poisson's ratio of the material,  $V_p$  is the volume fraction of the particulate phase,  $E$  is the Young's modulus of the material, subscripts  $m$  is used to identify the matrix phase and  $p$  is used for the spherical phase. For the matrix phase both radial and tangential with respect to the center of the spherical phase direction stresses are presented by Eqns. (51)-(52), respectively:

$$\sigma_{rad} = \frac{P}{1 - V_p} \left[ \frac{a^3}{r^3} - V_p \right] \quad (51)$$

$$\sigma_{tan} = -\frac{P}{1 - V_p} \left[ \frac{a^3}{r^3} + V_p \right] \quad (52)$$



where  $\sigma_{rad_m}$  and  $\sigma_{tan_m}$  are the radial and tangential thermal residual stress in the matrix phase,  $P$  is the compressive thermal residual stress in the spherical grain,  $V_p$  is the volume fraction of the particulate phase,  $a$  is the radius of the particulate grain,  $r$  is the radial distance from the center of the spherical grain, subscripts  $m$  is used to identify the matrix phase and  $p$  is used for the spherical phase. Due to the imposed boundary conditions used by Chawla, assuming that the stress vanishes at the free surface (the radius of the matrix grain and using the equilibrium equation), one gets a tangential and radial component of stress inside the matrix [199]. In addition, Chawla equations do not take into account the near-neighboring grains and their effect on the residual stresses. As well as the calculation is not an average stress calculation but a local maximum residual stress calculation. Therefore, values calculated using these Eqns. (50)-(52) will overestimate values measured experimentally.

Another model to consider is one developed by Sergio [201], which were derived using a stochastic analysis for particulate composites starting with the thermal strain in a binary composites with different CTE [202]:

$$P = -3f_m K^* (\alpha_m - \alpha_p) \Delta T \quad (53)$$

where  $P$  is the compressive thermal residual stress in the particulate phase,  $f_m$  is the volume fraction of matrix phase in the composite,  $K^*$  is the effective bulk modulus defined in Eqn. (54),  $\alpha$  is the CTE,  $\Delta T$  is the temperature change between the sintering temperature and room temperature ( $\Delta T = -1930^\circ\text{C}$ ). The equation for the effective bulk modulus is expressed below as Eqn. (54):

$$K^* = \frac{K_m K_p}{K_p f_p + K_p f_p n_m + K_p n_m + K_m f_m n_m} \quad (54)$$

where  $K^*$  is the effective bulk modulus,  $K$  is the bulk modulus of the phases, and  $f_m$  and  $f_p$  are the volume fractions of the matrix and particulate phases in the composite, respectively,  $n_m$  is defined in Eqn. (55):

$$n_m = \frac{2(1 - 2v_m)}{1 + v_m} \quad (55)$$

The thermal residual stresses in the matrix phase of the composite is given by Eqn. (56):

$$\sigma_m = 3f_p K^* (\alpha_m - \alpha_p) \Delta T \quad (56)$$

where  $P$  is the thermal residual stress in the particulate phase,  $f_p$  is the volume fraction of particulate phase in the composite,  $K^*$  is the effective bulk modulus defined in Eqn. (54),  $\Delta T$  is the temperature change between the sintering temperature and room temperature ( $\Delta T = -1930^\circ\text{C}$ ). This model by Sergio [22] is the calculation of the average thermal residual stresses. This model also has its limitations in that the fact that it does not consider effects from near-neighboring grains or grains that interconnected, since the main assumption is that you have a particulate surrounded by an infinite matrix with no other particulate nearby or interconnecting grains of the particulate. This can pose a problem of over or under predicting the thermal residual stresses in the composite depending on the properties of the phases in the composite.

To find the stress at the interface of the two phases one needs to set the thermal stresses in each phase equal to each other [203]. In doing so one gets the following Eqn. (57):

$$\sigma_{p,eq} = \sigma_{m,eq} = \frac{(\alpha_m - \alpha_p) \Delta T}{\frac{1}{E_p} + \frac{1}{E_m}} \quad (57)$$

where  $\sigma_{p,eq}$  and  $\sigma_{m,eq}$  is the stress in SiC and ZrB<sub>2</sub> phase respectively,  $E$  is the Young's modulus of the material,  $\Delta T$  is the temperature change between the sintering temperature and room temperature ( $\Delta T = -1930^\circ\text{C}$ ),  $\alpha$  is the coefficient of thermal expansion (CTE) subscripts  $m$  is used to identify the matrix phase and  $p$  is used for the spherical phase.

Looking at Eqn.(50), Eqn.(53), and Eqn. (57) above one sees that these equations are only a function of the change in temperature from the sintering temperature to the sample's current temperature (usually room temperature), the volume percent of the particles (SiC in ZrB<sub>2</sub>) the Young's Modulus and the CTE. This shows that one can change the residual stresses by changing the  $\Delta T$  and the amount of SiC in the ZrB<sub>2</sub>. Finally one can see that, since CTE of ZrB<sub>2</sub> > SiC, upon cooling from sintering temperature to room temperature, SiC will be in uniform compressive stress and ZrB<sub>2</sub> will have compressive stresses in the radial direction and tensile stresses in the tangential direction. These stresses in the end affect the ultimate strength through its effects on both the interface sliding stress and matrix cracking stress [200]. Thus the residual stresses in ZrB<sub>2</sub>-SiC are intergranular stresses of type II residual stress [204].

The statistical properties of residual stresses in ceramic materials has been modeled by Ortiz [205]. Ortiz modeled the distributions of residual stresses induced by thermal and elastic anisotropy as well as microcracking for two different temperature drops using a Finite Element Model of a hexagonal grain [205]. Ortiz's model predicted that all of the residual stresses induced by thermal and elastic anisotropy as well as microcracking from temperature drops followed a Gaussian or normal distribution [205].

## 1.6: Raman Piezo-Spectroscopy

Now that one knows that residual stresses are important and the type of residual stress, one would like to determine the actual stresses in the sample. There are many different methods to find the residual stresses, which are as follows: Hole drilling, Curvature, X-ray diffraction (ZRD), Hard X-rays, Neutrons, Ultrasonics, Magnetic, and finally Raman [204]. Table 10 below gives a summary of various techniques and their attributes in finding the residual stresses.

**Table 10: Various techniques and attributes for finding residual stresses [204]**

| <b>Method</b>                                                 | <b>Penetration</b>                                          | <b>Spatial Resolution</b>                                 | <b>Accuracy</b>                                                                                            |
|---------------------------------------------------------------|-------------------------------------------------------------|-----------------------------------------------------------|------------------------------------------------------------------------------------------------------------|
| Hole drilling (distortion caused by stress relaxation)        | ~1-2 x hole diameter                                        | 50 $\mu$ m depth                                          | $\pm$ 50MPa, limited by reduced sensitivity with increasing depth                                          |
| Curvature (distortion as stress arise or relax)               | 0.1-0.5 of thickness                                        | 0.05 of thickness ; no lateral resolution                 | Limited by minimum measurable curvature                                                                    |
| X-ray diffraction (atomic strain gauge)                       | <50 $\mu$ m[Al]; <5 $\mu$ m[Ti]; < 1mm (with layer removal) | 1mm laterally; 20 $\mu$ m depth                           | $\pm$ 20MPa, limited by non-linearities in $\sin^2\Psi$ or surface conditions                              |
| Hard X-ray (atomic strain gauge)                              | 150-50mm (Al)                                               | 20 $\mu$ m lateral to incident beam; 1mm parallel to beam | $\pm$ 10*10 <sup>-6</sup> strain, limited by grain sampling statistics                                     |
| Neutrons (atomic strain gauge)                                | 200mm (Al); 25mm(Fe); 4mm(Ti)                               | 500 $\mu$ m                                               | $\pm$ 50*10 <sup>-6</sup> strain, limited by counting statistics and reliability of stress free references |
| Ultrasonics (stress related changes in elastic wave velocity) | >10cm                                                       | 5mm                                                       | 10%                                                                                                        |
| Magnetic (variations in magnetic domains with stress)         | 10mm                                                        | 1mm                                                       | 10%                                                                                                        |
| Raman                                                         | <1 $\mu$ m                                                  | <1 $\mu$ m approx.                                        | $\Delta\lambda$ 0.1cm <sup>-1</sup> =50MPa                                                                 |

Looking at the table above one sees that Raman spectroscopy is an excellent choice for finding intergranular stress with high special resolution, and reasonable accuracy; as well as get stress directly.

### 1.6.1: The Origin of Raman Piezo-Spectroscopy

When a sample exposed to radiation is stressed, the virtual states are changed as compared to the unstressed virtual state, as shown below as Figure 55. These changes in the virtual states and hence change of the wavelength is the basis of Raman piezo-spectroscopy.

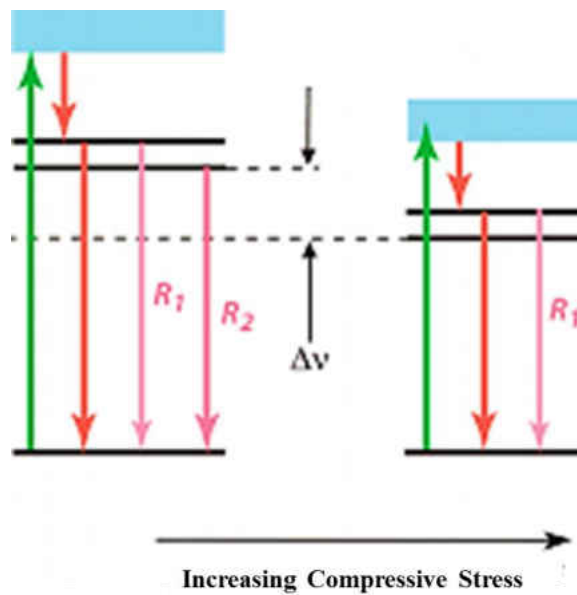


**Figure 55: Effect of stress on virtual states [206]**

The cause of the change in virtual states is when a unit cell has a load applied to it, as shown as P in Figure 56 below.

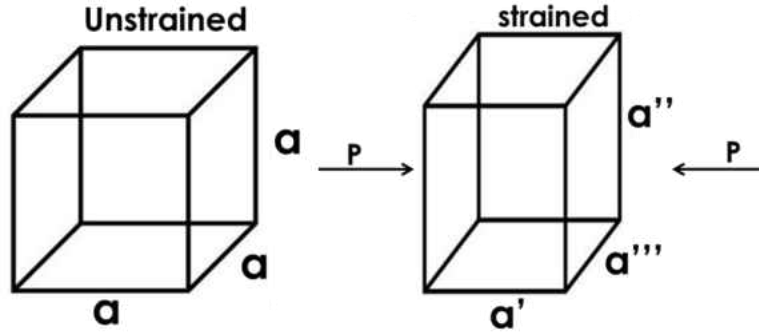


**Figure 56: Strained and unstrained unit cell**

The unit cell is strained and thus the bond length is changed and therefore the forcing constant changes. Thus the frequency of the vibration of the material is changed and therefore a shift in the peak position is observed in the Raman spectra, when compared to the Raman spectra of the unstressed material. If the new peak position of the stressed material is related to the initial unstressed peak position through a Taylor series expansion one would get the following Eqn. (58) [207]:

$$v = v_0 + \left(\frac{\partial v}{\partial \sigma_{ij}}\right)_0^0 \sigma_{ij} + \frac{1}{2} \left(\frac{\partial^2 v}{\partial \sigma_{ij} \partial \sigma_{kl}}\right)_0^0 \sigma_{ij} \sigma_{kl} + \dots \quad (58)$$

If one would take the second derivative and higher order terms to be so small, then we can neglect them one gets the following Eqn. (59) [207]:

$$\left(\frac{\partial v}{\partial \sigma_{ij}}\right)_0 = \frac{v - v_0}{\sigma_{ij}} \quad (59)$$

Now rearranging the equation and solving for the change in  $\nu$  one gets the following equation 47 and replacing the partial derivative of the change in peak position with change in stress for a constant,  $\Pi$  one gets Eqn. (60) shown below [208-210]:

$$\Delta\nu = \Pi_{ij}\sigma_{ij} \quad (60)$$

where  $\Delta\nu$  is the observed change in the peak position,  $\sigma_{ij}$  is stress components, and  $\Pi_{ij}$  is the piezo-spectroscopic coefficients and is a tensor with nine components. Eqn. (79) is only valid when one knows the orientation of the material, usually when one is investigating a single crystal. But most commonly one is investigating a material with random crystal structure orientation, thus the directional information from the material is lost. Therefore, the following Eqn. (61) is valid in such a case [208-210]:

$$\Delta\nu = \Pi \langle \sigma \rangle \quad (61)$$

Since the directional information is lost one is able to only obtain average results and therefore the  $\Pi$ , and  $\sigma$  are the average values of piezo-spectroscopic coefficient and stress. One must also note that the Eqn. (61) is for hydrostatic stresses only. Therefore if bending is being used as the method to determine the piezo-spectroscopic coefficient a correction needs to be made to the Eqn. (61). This correction is shown below as Eqn. (62), where the piezo-spectroscopic coefficient is multiplied by 3. This Eqn. (62) is valid for piezo-spectroscopic coefficient found by applying a stress via bending:

$$\Delta\nu = 3\Pi \langle \sigma \rangle \quad (62)$$

Now solving Eqn. (62) for stress one gets the following Eqn. (63):

$$\langle \sigma \rangle = \frac{\Delta \nu}{3\Pi} \quad (63)$$

Eqn. (63) shows a linear relationship between the changes in peak position and stress, and also shows that based on the change in the peak position and a known piezo-spectroscopic coefficient one can find the stress of the material. Usually the piezo-spectroscopic coefficient is found with a calibration experiment where a known stress is applied to the material and the observed frequency shift is noted. Thus when the frequency shift is plotted versus the stress, the slope is the piezo-spectroscopic coefficient.

Since this research is focusing on ceramic composites one would like to look into the derivation of the piezo-spectroscopic equation for composites. Starting with Eqn. (60) and conducting an orthogonal coordinate transformation one gets the following Eqn. (64) [209]:

$$\Delta \nu = \Pi_{ij} a_{ik} a_{jl} \sigma_{kl} \quad (64)$$

Now looking at matrix with a fibrous inclusion, which is not the same exact problem as with ZrB<sub>2</sub>-SiC, the cross sectional view is similar. A schematic of a composite with a fibrous inclusion is shown below as Figure 57.



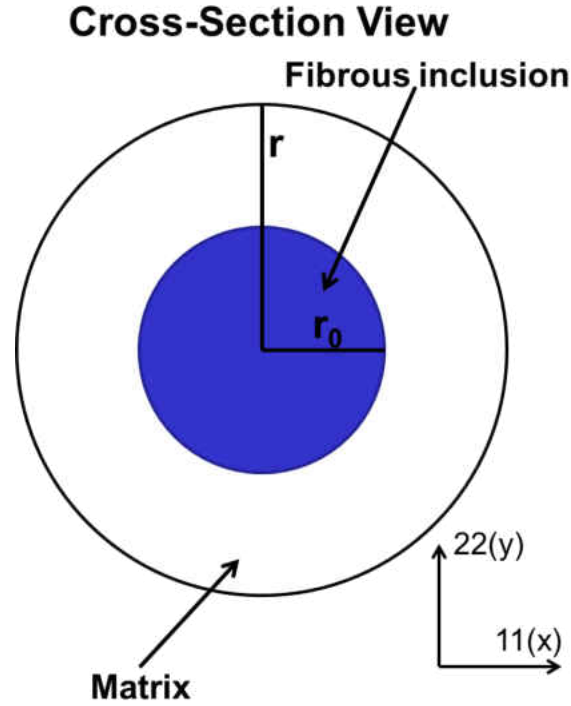


**Figure 57: Schematic of a composite with a fibrous inclusion**

For matrix stresses due to the presence of fibrous inclusions one gets the following equation for the stress in composites as shown below in Eqn. (65) [209]:

$$\sigma_{11} = -\sigma_{22} = \frac{\sigma_0 r_0^2}{r^2}; \sigma_{33}=0 \quad (65)$$

Now applying Eqns. (64) and (65) one gets the following Eqn. (66) for the change in peak position [209]:

$$\Delta v = (\Pi_{22} - \Pi_{11})(a_{21}^2 - a_{22}^2)\sigma_{11} + (\Pi_{33} - \Pi_{11})(a_{31}^2 - a_{32}^2)\sigma_{22} \quad (66)$$

This equation is valid for ceramic composites, and thus valid for the ZrB<sub>2</sub>-SiC. But since most composite materials have randomly oriented grains, one is not able to get directional

information and therefore one can only get average information and thus Eqn. (62) is the equation that is valid for this research.

### **1.6.2: Laser Penetration Depth**

The most important part of Raman piezo-spectroscopy is that you make sure you are collecting spectrum from the correct volume of the material. This is because the computation of numerical stress values from the measurements using micro-Raman spectra is impaired by the averaging over the finite sample volume being probed [211, 212]. If the correct volume is not sampled then one will not be able to determine the piezo-spectroscopic coefficient accurately and end up with the wrong stress calculation in the end. Typically the diameter of the focused laser beam is  $1\mu\text{m}$  but the penetration depth can vary from tens of nanometers to several millimeters and thus we can sample a potentially large volume of the strained structure [213]. This can be shown by looking at Figure 58, one can see that if a spectra is taken at the first spot with just one grain one gets an accurate spectra. But if one takes a spectra say the same spot but this time a second grain is present then the Raman spectra will change as shown in the figure. This change resulted in a peak broadening because the extra grain has a different stress state. Thus showing that the volume for which the spectra is collected is very important.

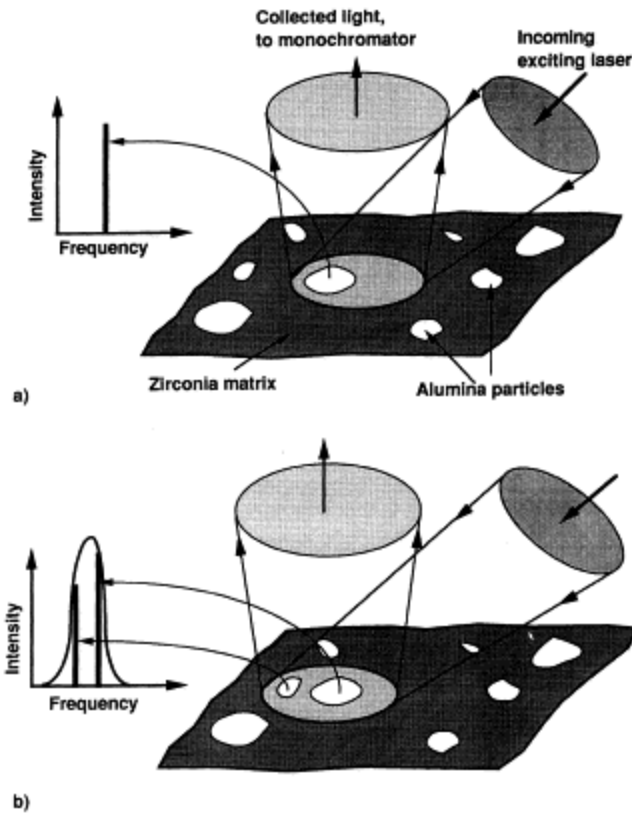


**Figure 58: Laser volume effect on Raman spectra. Reprinted from *Acta Materialia*, vol. 46, V. Sergo, G. Pezzotti, O. Sbaizero, and T. Nishida, "Grain size influence on residual stresses in alumina/zirconia composites," pp. 1701-1710, Copyright (1998), with permission from Elsevier [201]**

Now that one knows the laser volume is important one would like to know how it is calculated. This is a function of the laser beam diameter and the laser penetration depth. The laser beam diameter is dictated by the objective lens being used. For example the laser beam diameter is much larger when using a 5x objective lens than when one used a 50x objective lens. The optics not only dictate the laser beam diameter (lateral spatial resolution) but also dictates the depth into the material from which the spectra is collected [214]. There are a few methods to estimate the penetration depth of the laser. The first by Wolf where the depth of penetration is estimated based on the properties of the material being exposed. The expression given by Wolf calculates the laser

penetration depth as an approximation based on the absorption coefficient of the material and is shown below as Eqn. (67) [215, 216]:

$$d_p = \frac{-\ln(0.1)}{2\alpha} = \frac{2.3}{2\alpha} \quad (67)$$

where  $d_p$  is the penetration depth, and  $\alpha$  is the absorption coefficient of the material at the specific laser or excitation wavelength. The absorption coefficient for most materials are a function of temperature and wavelength of the excitation source, thus based on Eqn. (67) the penetration depth can greatly vary within the same material. For crystalline silicon with a excitation source wavelength of 514.5 nm the penetration depth is on the order of 770nm, to give the perspective of how deep the laser can penetrate [215]. Harima found for a 6H-SiC with a 500nm laser that the penetration depth is approximately 2mm and the absorption coefficient of 6H-SiC [216]. Sridhara found for seven laser wavelengths of 325-356.4 nm the 6H-SiC laser penetration depth at room temperature ranged from 4.3-11  $\mu\text{m}$  [217].

Another method to estimate the penetration depth is to use the numerical aperture of the objective lens being used. Everall gave an approximation for the depth of focus based on the numerical aperture (NA). Everall assumed that for an objective lens with a NA of 0.9-0.95 (typical for high NA objective) that only 86% of the intensity of the laser is transmitted through the lens; one gets that the probed volume is defined by a laser diameter expressed by the following Egn (68) [218]:

$$\text{Laser Diameter} \approx \frac{1.22\lambda}{NA} \quad (68)$$

where  $\lambda$  is the laser wavelength, and NA is the numerical aperture. The depth of focus can then be approximated by the expression Egn. (69) below [218]:

$$\text{depth of focus} \approx \frac{4\lambda}{NA^2} \quad (69)$$

where again  $\lambda$  is the laser wavelength, and NA is the numerical aperture. These approximations stem from the fact that for a diffraction-limited laser focal volume that the dimensions of the focal region depend only on the NA of the focusing lenses and the degree of which the laser fills that objective lens [218]. The main reason for wanting to know the laser penetration depth is that when one is doing piezospectroscopic coefficient calibration and determining residual stresses from Raman, the knowledge of where the response is coming from is very important. Since the volume of response probed can and will change the results obtained for measurements, especially stresses, the data will be interpreted wrongly. For example say that one wants the average stress of the bulk material, but are only collecting the stress from a few grains below the material's surface. Without knowing the probed volume or taking into account the probed volume, one will not be obtaining the correct information, giving rise to wrong values for stress in the end. That is why knowing the penetration depth is so important.

Everall also discussed another method based on the refraction-limited depth resolution. This method is based on the numerical aperture of the objective lens being used and the index of refraction of the sample,  $n$ , and is defined in the Egn. (70) [218]:

$$DR = \Delta \left[ \sqrt{\frac{NA^2(n^2 - 1)}{(1 - NA^2)} + n^2} - n \right] \quad (70)$$

where  $DR$  is the depth resolution,  $n$  is the refraction of the material being investigated,  $NA$  is the numerical aperture of the objective lens being used, and  $L$  the location of the laser beam focus distance below the sample surface.

The attainable resolution depth is usually a lot less than the lateral resolution; the depth of field of the optics and the details of optical scattering within the probed volume of the sample, which results in the depth of field of the optics being the limiting factor [214]. Thus reiterating the point that the knowledge of laser penetration depth is essential in determining the stress state in the material as well as when calibrating the piezospectroscopy coefficient.

### **1.6.3: Piezo-Spectroscopy Found in Publications**

ZrB<sub>2</sub>-SiC ceramic composites have residual stresses due to the mismatch of the coefficient of thermal expansion and the Young's modulus, and the difference between the sintering or processing temperature and room temperature. Since the residual stress distribution can affect the mechanical properties of the material, one would naturally want to find the distribution so that it can be altered to meet the specifications wanted. These residual stresses can be found using Raman spectroscopy, which is the method that will be used in the proposed research to find the residual stresses in ZrB<sub>2</sub>-SiC ceramic composites. The first paper one finds from Liu is about 6H-SiC peak dependence on hydrostatic pressure from 1 atm to 95 GPa [219]. The spectra dependence on the pressure is shown below in Figure 59A, and Figure 59B shows the results of the pressure dependence on LO-TO peak splitting [219].

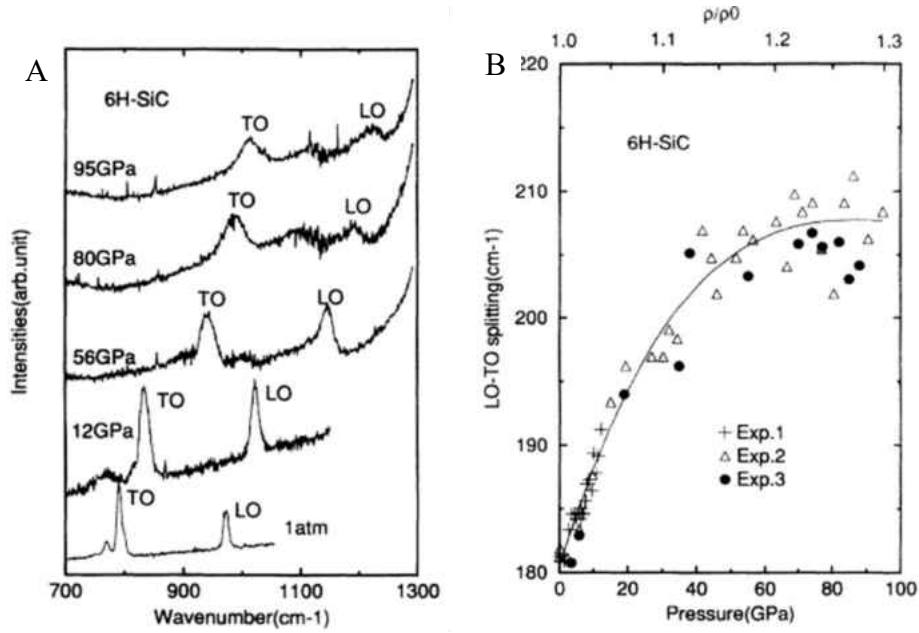


**Figure 59: Raman spectra dependence on pressure (A) and the LO-TO splitting dependence on pressure (B). Reprinted from *Physical Review Letters*, vol. 72, J. Liu and Y. K. Vohra, "Raman Modes of 6H Polytype of Silicon Carbide to Ultrahigh Pressures: A Comparison with Silicon and Diamond," pp. 4105-4108, Copyright (1994), with permission from American Physical Society [219]**

Liu also performed a curve fitting of the results with a quadratic fit and is shown below as Eqn.

(71) [219]:

$$\begin{aligned}\omega_{LO} &= 970.1 + 3.83P - 0.013P^2 \\ \omega_{TO} &= 789.2 + 3.11P - 0.009P^2\end{aligned}\tag{71}$$

where P is the measured pressure in GPa. Another study of 6H-SiC was done by DiGregorio where he found the FLO phonon mode to have piezospectroscopic coefficient of  $4.28 \pm 0.22 \text{ cm}^{-1}\text{GPa}^{-1}$  and  $3.53 \pm 0.21 \text{ cm}^{-1}\text{GPa}^{-1}$  for the FTO phonon mode [220]. Grodecki investigated 6H-SiC crystals grown in the c-face (001) direction under uniaxial stress [221]. The stress was applied in the parallel and perpendicular to the c-axis, the results are shown in Figure 60 [221]. Figure 60A shows the Raman spectra for the X and Y directions, and Figure 60B shows the peak position dependence

on stress for the X and Y propagation directions [221]. The resulting coefficient obtained for the X propagation direction are  $0.44\text{-}2.58\text{ cm}^{-1}\text{GPa}^{-1}$  and depend on the whether the uniaxial stress is applied parallel or perpendicular to the c-axis [221]. For the Y propagation direction the coefficients are  $0.38\text{-}1.13\text{ cm}^{-1}\text{GPa}^{-1}$  [221]. The values report from previous results were for the LO phonon modes  $3.8\text{ cm}^{-1}\text{GPa}^{-1}$  and for the TO phonon mode  $3.1\text{ cm}^{-1}\text{GPa}^{-1}$  [221].

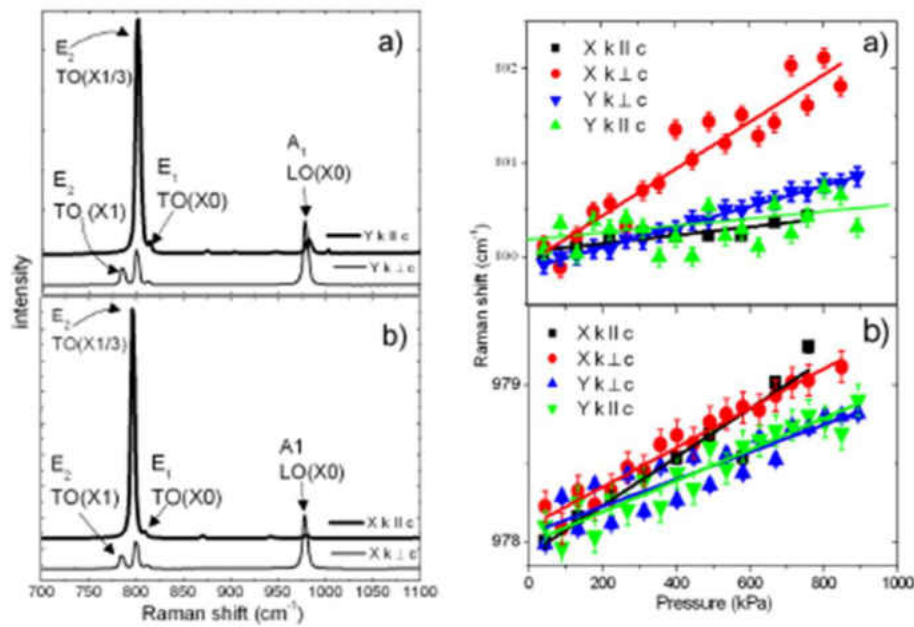


**Figure 60: The Raman spectra of the X and Y propagation direction (Left) and the peak position shift dependence on pressure for the X and Y propagation direction (Right) [221]**

The next paper one comes across is by Limarga on the piezo-spectroscopic coefficient of tetragonal-prime yttria-stabilized zirconia [210]. Limarga found the piezo-spectroscopic coefficient to be as shown in Figure 61 for each of the Raman bands [210].



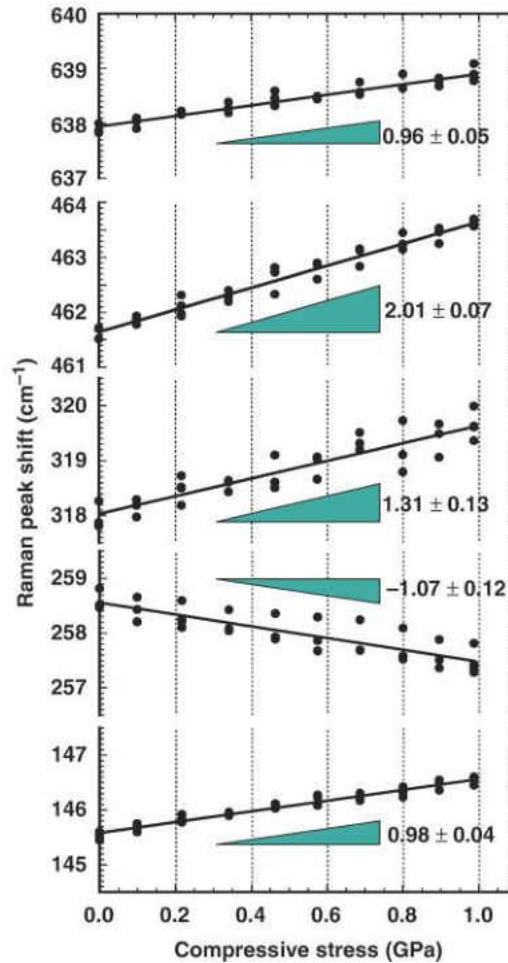


**Figure 61: Stress dependence of Raman frequency with the slope representing the piezo-spectroscopic coefficients. Reprinted from *Journal of the American Ceramic Society*, vol. 90, A. M. Limarga and D. R. Clarke, "Piezo-Spectroscopic Coefficients of Tetragonal-Prime Yttria-Stabilized Zirconia," pp. 1272-1275, Copyright (2007), with permission from John Wiley and Sons [210]**

Limarga not only investigated the peak shift but also the peak splitting, peak width, and peak intensity dependence on compressive stress to 1GPa, with the results shown in Figure 62 below [210]. Lastly Limarga investigated whether the spectra changed before, and after the compressive stress and the spectra was found to be the same thus meaning that no plastic deformation was encounter by the sample [210].

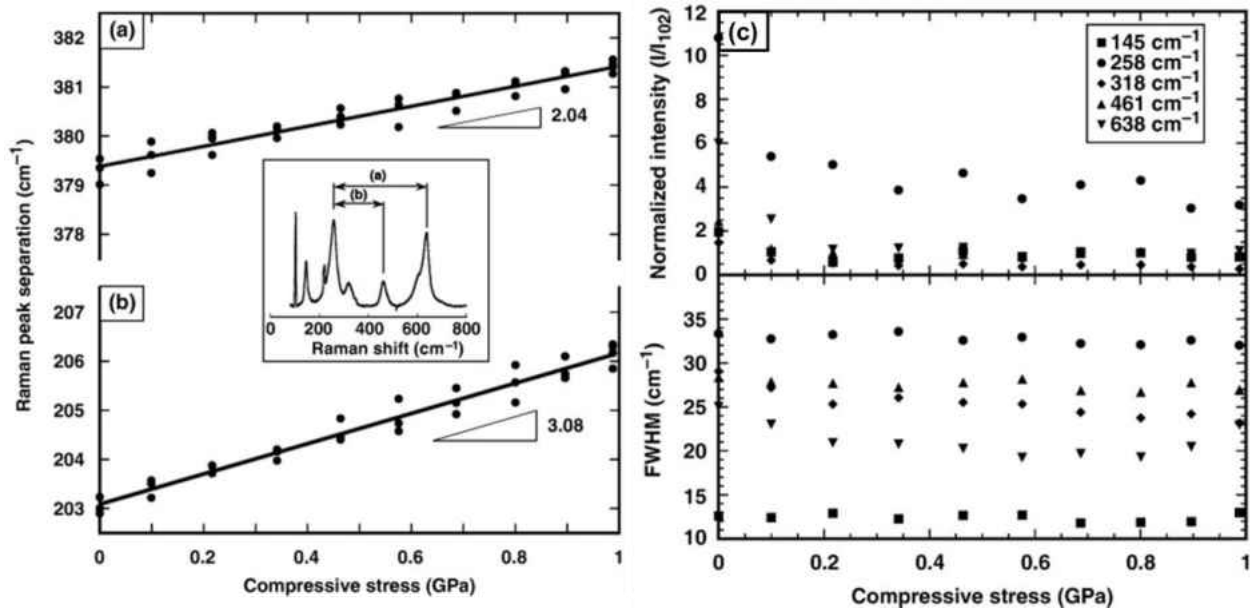


**Figure 62: peak splitting (A), peak intensity (B), and peak width (C) dependence on stress.**  
 Reprinted from *Journal of the American Ceramic Society*, vol. 90, A. M. Limarga and D. R. Clarke,  
 "Piezo-Spectroscopic Coefficients of Tetragonal-Prime Yttria-Stabilized Zirconia," pp. 1272-1275,  
 Copyright (2007), with permission from John Wiley and Sons [210]

Watts investigated  $\text{ZrB}_2\text{-SiC}$  using Raman spectroscopy to evaluate the residual stresses in the SiC phase of the composite [181]. Watts used the results found by Liu shown in Eqn. (71) and the unstressed and stressed peak position shown below as Figure 63 [181].

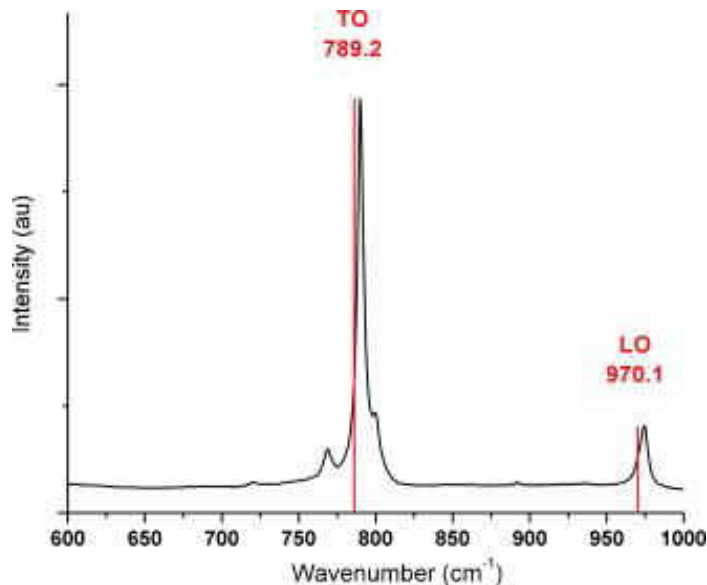


**Figure 63: Raman pattern for 6H SiC from a hot pressed ZrB<sub>2</sub>-SiC composite with unstressed peak positions identified with lines. Reprinted from *Journal of the European Ceramic Society*, vol. 30, J. Watts, G. Hilmas, W. G. Fahrenholtz, D. Brown, and B. Clausen, "Stress measurements in ZrB<sub>2</sub>-SiC composites using Raman spectroscopy and neutron diffraction," pp. 2165-2171, Copyright (2010), with permission from Elsevier [181]**

The residual stresses of ZrB<sub>2</sub>-SiC were calculated from neutron diffraction and Raman. For Raman the residual stresses was calculated to be 810MPa which is higher compared to that calculated from neutron diffraction analysis of 775MPa [181]. Other materials have been investigated such as carbon [222, 223], Si [224, 225], Si<sub>3</sub>N<sub>4</sub> [226, 227], Al<sub>2</sub>O<sub>3</sub> [227], LaCoO<sub>3</sub> [228], LaGaO<sub>3</sub> [229], ZrO<sub>2</sub> [210, 230, 231], GaN [232] SrAl<sub>12</sub>O<sub>3</sub>/ZrO<sub>2</sub> system [233], β-Si<sub>3</sub>N<sub>4</sub> [207, 234], alpha-Quartz [235], ceria-stabilized zirconia [236], alumina [237], alumina-alumina titanate laminates [238], and Alumina/zirconia composites [201, 239]. This shows that this method has been widely investigating and a very useful method to find residual stresses especially in ZrB<sub>2</sub>-SiC ceramic composites used for this research.

### **1.7: Effect of Residual Stress on Mechanical Properties in Ceramic Composites**

Many models have been proposed to estimate or calculate the increase in fracture toughness based on the effects of residual stress. The main mechanisms for increase in fracture toughness particulate-reinforced ceramic composites is crack front deflection [240-243] and crack deflection along the grain boundary has also been observed [240, 244]. However, the crack deflection due to crack deflection front is considered the dominate toughening mechanism [240].

A few models have been proposed in literature to predict the increase in mechanical properties, such as fracture toughness and fracture strength. Some models are as follows: Faber and Evans [241], Budiansky [245], Wei and Becher [242], Virkar and Johnson [246], and finally Evals, Culter, and Virkar [247, 248]. Most of these models take into account only a portion of the mechanism that are acutely occurring. Such as the Faber and Evans model is based on a geometrical treatment of a crack deflection from its main crack plane and ignores the local stress field at and near the interface between the matrix and the particulate phases [240]. Wei and Becher considered the thermal residual stresses as the major cause of the crack deflection [240]. These models all have some draw backs when being implemented. Two relatively recent models presented by Pezzotti [249] and Taya [240] aimed to increase the accuracy of predicting increase in fracture toughness specifically in particulate-reinforced ceramic composites.

The paper by Pezzotti deals with the system of  $\text{Al}_2\text{O}_3/\text{ZrO}_3$  composites [227]. In order to find the dependence of the fracture strength on residual stress Pezzotti first experimentally measured the fracture strength and fracture toughness. Following this the average residual stresses were determined using a stochastic model, first developed by Kreher and Pompe [202], analogous to the

one used by Sergio [201]. Pezzotti proposed a model to predict the increase in strength of the  $\text{Al}_2\text{O}_3/\text{ZrO}_3$  composite due to elastic residual stresses. The model was based on the possible strengthening effect arising from shielding of the microcrack by local (compressive) residual stresses as shown in the schematic below as Figure 64 [249].

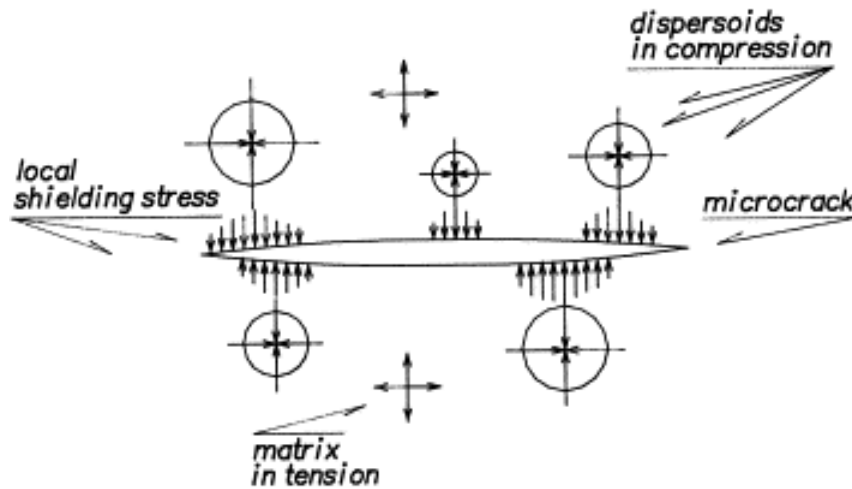


**Figure 64: Schematic of shielding of a microcrack with local (compressive) residual stresses.** Reprinted from *Journal of the European Ceramic Society*, vol. 19, G. Pezzotti, V. Sergio, O. Sbaizero, N. Muraki, S. Meriani, and T. Nishida, "Strengthening contribution arising from residual stresses in  $\text{Al}_2\text{O}_3/\text{ZrO}_2$  composites: a piezo-Spectroscopy investigation," pp. 247-253, Copyright (1999), with permission from Elsevier [249]

Based on this idea of shielding of the microcrack by local compressive residual stresses, Pezzotti developed a model to predict the change in the strength of the material or effect of residual stress on the mechanical property of the composite. The model Pezzotti developed is described by the following Eqns. (72)-(74) [249]:

$$\Delta K = 2\sigma_R \Phi \sqrt{\frac{a_0}{\pi}} \quad (72)$$

where  $\Delta K$  is the increase of fracture toughness,  $a_0$  is the size of the formed microcrack,  $\Phi$  is a constant depending upon the shape of the microcrack ( $\Phi \approx 2$  for a shielded microcrack), and finally

$\sigma_R$  is the shielding closure stress component [249].  $\sigma_R$  is expressed in the following Eqn. (73) as a function of the maximum residual stress  $\sigma_{max}$ , the average grain size of the particulate  $d$ , and finally the average distance between near-neighboring grains  $\Delta$  [249]:

$$\sigma_R = \left( \frac{\sigma_{max}}{2} \right) \left[ \frac{2d}{\Delta - d} \right]^3 \quad (73)$$

The  $\sigma_{max}$  is determined using the model given by Chawla and is describe above as Eqn. (50). Pezzotti finally related this increase in fracture toughness to an increase in strength through the following expression shown below as Eqn. (74) [249]:

$$\Delta\sigma = \frac{\Delta K}{Y\sqrt{a_o}} \quad (74)$$

where  $\Delta\sigma$  is the increase in strength of the composite,  $\Delta K$  is the increase in fracture toughness,  $Y$  is the geometric factor, and  $a_o$  is the size of the critical microcrack. Based on this model Pezzotti predicted the strength of the  $Al_2O_3/ZrO_3$  composite as a function of the volume fraction of  $Al_2O_3$  and compared it to measured strength values found in experiments. The model and the experiments results were plotted and are shown below as Figure 65 [249].

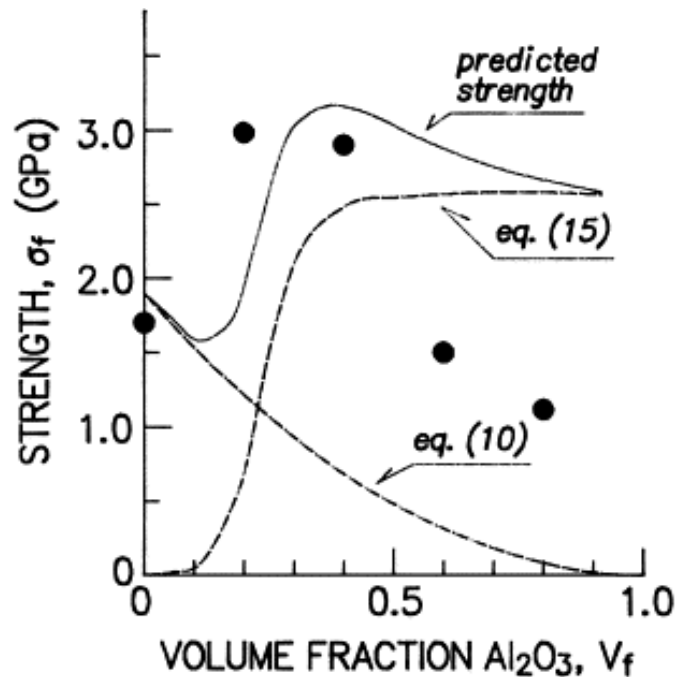


**Figure 65: Comparison of experimental data of fracture strength to the theoretical predictions.** Reprinted from *Journal of the European Ceramic Society*, vol. 19, G. Pezzotti, V. Sergo, O. Sbaizero, N. Muraki, S. Meriani, and T. Nishida, "Strengthening contribution arising from residual stresses in  $\text{Al}_2\text{O}_3/\text{ZrO}_2$  composites: a piezo-Spectroscopy investigation," pp. 247-253, Copyright (1999), with permission from Elsevier [249]

As one can see from Figure 65 the experimental results and theoretical values do not match very well.

The paper by Taya deals specifically with  $\text{TiB}_2\text{-SiC}$  ceramic composites [240]. In this model Taya first determines the average thermal residual stresses in the matrix and reinforcement by using Eshelby's model [240, 250]. Then applies the calculated thermal residual stresses in the matrix of the composites to calculate the stress intensity factor reduction [240]. In this calculation of the stress intensity factor reduction, Taya considers a semi-infinite crack surrounded by a particulate-reinforcement ceramic composites with a thermal residual stress distribution [240]. This is shown graphically in the Figure 66A below. Then assuming a uniform residual compressive

stress acting in the normal direction to the crack propagation plane, shown in Figure 66B below [240].

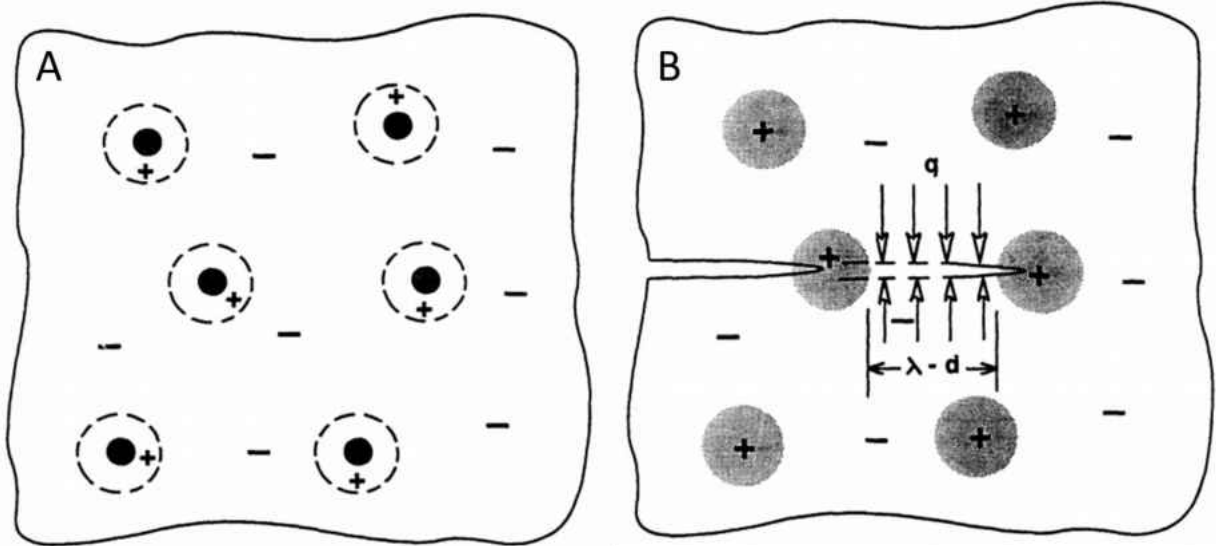


**Figure 66: Schematic of a thermal residual stresses in a particulate-reinforced ceramic composite (A) and semi-infinite crack advancing through a matrix compressive region toward articulate tensile region (B). Reprinted from Journal of the American Ceramic Society, vol. 73, M. Taya, S. Hayashi, A. S. Kobayashi, and H. S. Yoon, "Toughening of a Particulate-Reinforced Ceramic-Matrix Composite by Thermal Residual Stress," pp. 1382-1391, Copyright (2005), with permission from John Wiley and Sons. [240]**

The following model was developed as shown below as Eqn. (75) [240]:

$$\Delta K_1 = 2q \sqrt{\frac{2(\lambda - d)}{\pi}} \quad (75)$$

where  $\Delta K_1$  can be an increase or decrease in fracture toughness,  $q$  is the local average compressive stress,  $\lambda$  is the average interparticulate distance, and  $d$  is the average diameter of the particles of the particulate-reinforcement phase.



Now applying this model Taya achieved better approximation of experimentally measured crack growth values compared to that of other models. This is shown below in Figure 67 as the solid line.

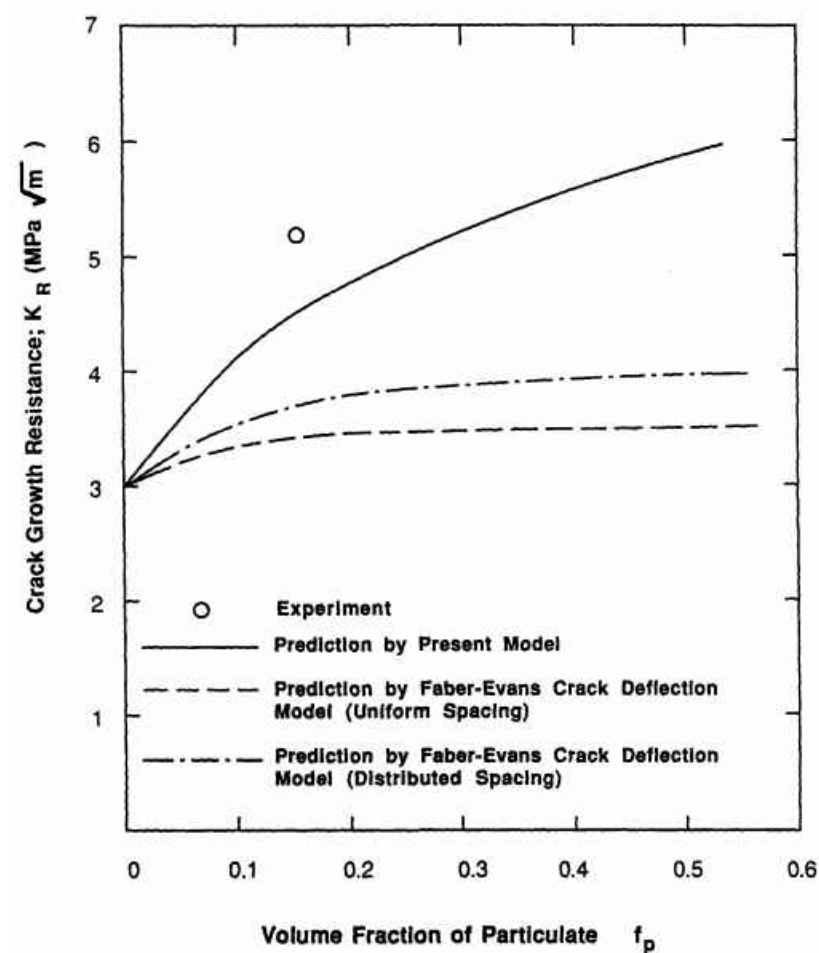


Figure 67: Comparison of crack growth resistance measured experimentally and calculated using models. Reprinted from Journal of the American Ceramic Society, vol. 73, M. Taya, S. Hayashi, A. S. Kobayashi, and H. S. Yoon, "Toughening of a Particulate-Reinforced Ceramic-Matrix Composite by Thermal Residual Stress," pp. 1382-1391, Copyright (2005), with permission from John Wiley and Sons. [240]

## **CHAPTER 2: EXPERIMENTAL PROCEDURE**

This section of the dissertation describes the research procedure used for all experiments conducted.

### **2.1: Processing the ZrB<sub>2</sub>-SiC Ceramic Composites Samples**

Spark Plasma Sintering (SPS) technique was used to process pure SiC, and ZrB<sub>2</sub>-SiC (17, 32, and 45vol%) composites. For the pure SiC samples, as received powders (H.C. Starck- Alpha-SiC Grade UF-10) were packed into a graphite die for sintering. The samples were consolidated using an SPS furnace (FCT HPD 25; FCT Systeme GmbH, Rauenstein, Germany) under vacuum (~5 Pa). The pure SiC samples were then sintered at 2150 °C, 50 MPa with a dwell time of 20 minutes. The heating rate was 100°C/min during heating and cooling. Above 1500°C the heating rate was reduced to 50°C/min. The ZrB<sub>2</sub>-SiC composite were prepared in three batches by weighting the ZrB<sub>2</sub> powder (H.C. Starck-ZrB<sub>2</sub> Grade B) and the SiC powder (H.C. Starck- Alpha-SiC Grade UF-10) in a certain proportion, and grinding them together in a plastic bottle, using ZrO<sub>2</sub>-Y<sub>2</sub>O<sub>3</sub> balls and acetone as a milling media. After 48 hours of milling, the batches were dried and sieved to break up the agglomerates. The sieved powders were loaded in a graphite die, using graphite foil as an intermediate layer between the die and powder. The ZrB<sub>2</sub>-SiC (17, 32, and 45vol%) samples were sintered at 1950°C, 50 MPa, with a heating and cooling rate of 100°C/min, and a dwell time of 15 minutes. After grinding/removal the graphite foil from the surface of the sintered samples, the density of the samples was determined using liquid immersion technique.

## **2.2.: Fracturography analysis and microstructure determination**

Scanning electron microscope (Zeiss-SEM) was used for the analysis of fracture surfaces of the ZrB<sub>2</sub>-17, 32, and 45 vol% SiC bars after mechanical testing. Backscattered SEM images (Using a Tescan Vega SEM), were used to determine the near-neighbor distance between SiC grains. This was done by analyzing the micrographs using the Adobe Photoshop software; 100 measurements were made to obtain a statistical data set.

## **2.3: Calibration of Piezo-Spectroscopy Coefficient via 3-Point Bending**

This section will cover the process for calibrating a bending device to conduct the experiment to determine the piezo-spectroscopy coefficient. Finally, this section will describe the procedure used to determine the piezo-spectroscopy coefficient.

### **2.3.1: *In-Situ* 3-Point Bending Device: Design and Calibration**

For the design of the loading device for 3 point bending of ceramic samples, the following set of requirements was used: the sample dimensions used for 3 point bending in the device should be in the range of 3x4x45 mm to 2x2.5x35 mm, the maximum stress that can be applied to the sample should be 100 MPa to 360 MPa, thus the maximum load, for the load cell used in the device should be able to apply a maximum load of 70N. Additionally, the device should fit below the optical microscope lenses that the ceramic sample could be illuminated by the laser light via Raman spectrometer coupled with the optical microscope. The dimensions for the bending device to fit below the microscope are limited to 85x220x480 mm. The surface of the bending bar exposed to the laser radiation has to be under tensile stress so that the effect of the tension on the vibrational

properties of the material as well as a redistribution of the residual micro-stresses under tensile load can be detected.

A device was created to place a specimen under *in-situ* three-point bending to simultaneously perform Raman spectroscopy to investigate the change in vibrational response at different applied stresses. The device consists of a rotary M drive motor which turns two large gears which both are mounted to an aluminum plate. Each of the large gears has a long screw attached in the center of each gear with the load cell platform attached to both screws. This allows the motor to create a linear displacement via screws and gears to load the ceramic bar. This is the most plausible method since it has the ability to provide a digital interface to accurately apply a load with great precision. Using a computer controlled input to the M Drive motor, vertical motion can be applied to the load cell to begin loading the specimen. Due to the gearing setup in the device, a small loading rate can be achieved which is especially important for brittle ceramics. The applied load is measured using the load cell that converts force into a digital signal. A schematic of the three-point loading (Figure 68a) and a picture of the device (Figure 68b) is shown. Also, the device coupled with the InVia Renishaw Raman Spectrometer is also shown (Figure 68c).

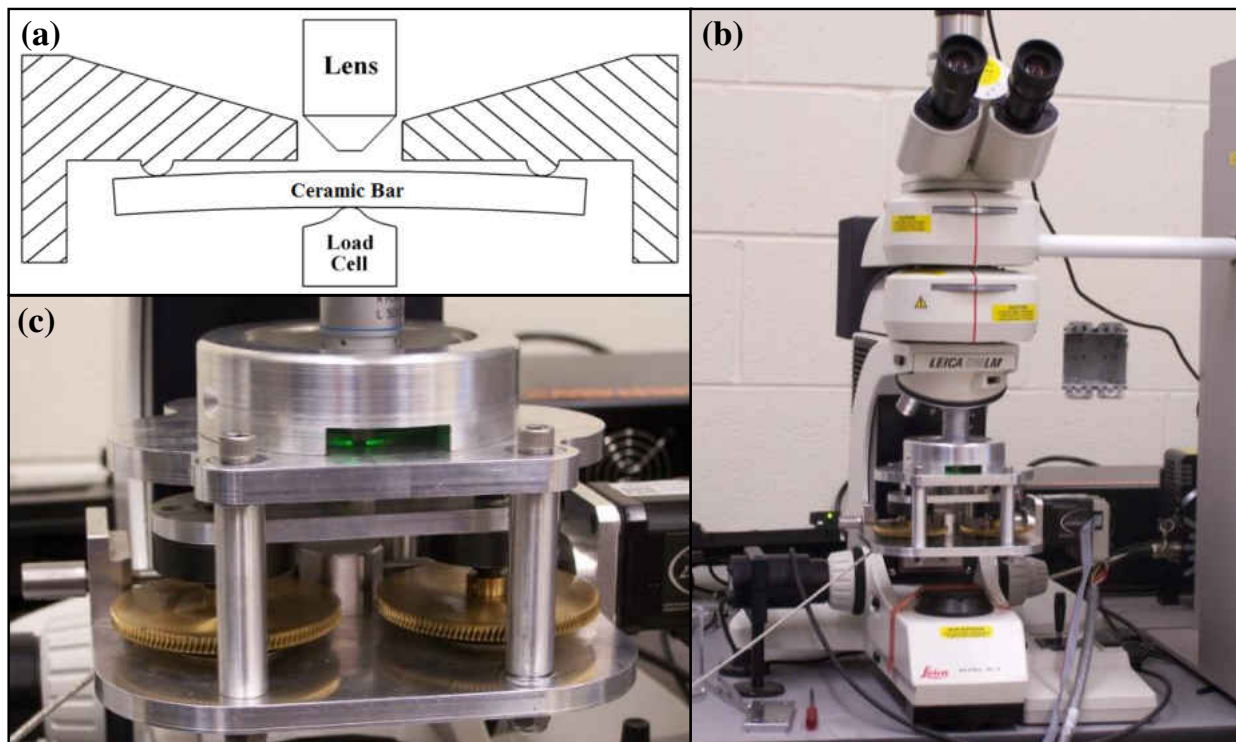


**Figure 68: (a) Schematic of loading ceramic bar in three point bending for collection of *in-situ* scattered light. (b) A photograph of the *in-situ* loading device. (c) Loading device coupled with Leica optical microscope connected to InVia micro-Raman spectrometer.**

The Raman spectrometer system uses a 532 nm laser to excite the sample, a single spectrograph fitted with holographic notch filters, and a Leica optical microscope rigidly mounted and optically coupled to the spectrometer. The generated laser power was 25mW. Before collecting the spectra of the ceramics, the spectrometer was calibrated with a Si standard using a Si peak position at  $520.3 \text{ cm}^{-1}$ . The average collection time for a single spectrum was 300 s for both  $\text{ZrB}_2+10\text{wt}\%\text{SiC}$  and  $\text{LaCoO}_3$  ceramics. The 50x long range lens with a working distance of 13mm was used for illumination of the spot of 3-4 $\mu\text{m}$  in diameter.

After the *in-situ* bending device was developed, the calibration of the device was performed to verify that the applied load and deformation are correctly measured. Since the output of the

load cell initially produced a voltage, a correlation from voltage to force was calculated. To do this, weights were applied by screwing off the load cell cap and placing an acrylic platform that provided a flat surface to apply various weights. A series of weights from 10 g to 200 g was placed on the acrylic platform and the corresponding voltage was recorded to verify that the measured voltage is accurate. Based on the measured data, it was established that in order to obtain the force in Newton's, the voltage output of the load cell has to be multiplied by eight (Figure 69).

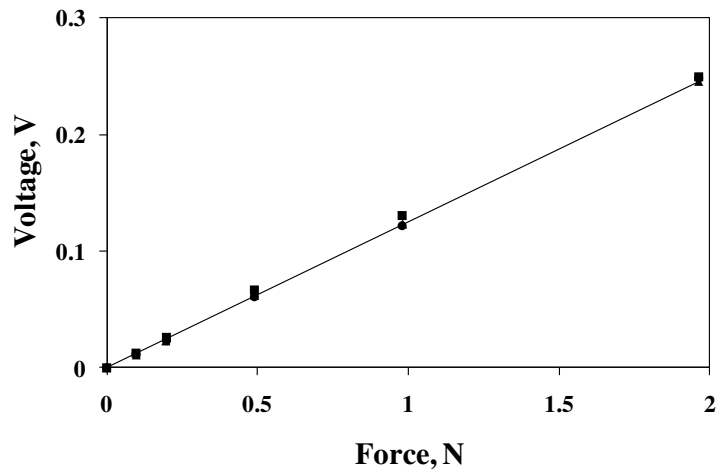


**Figure 69: Force applied versus voltage output for calibration of the load cell.**

In order to further verify the correctness of the measured stress and strain by the *in-situ* bending device, selected materials with a known Young's modulus were used to perform the bending tests. Stress was applied by the load cell, and resulting strain was measured by an attached strain gauge. The foil strain gauge was mounted with cyanoacrylate adhesive strain gauge glue on the tensile surface of the sample. The wires of the strain gauge and a programmable power supply that outputted 4 V and 0.2 A were attached to an Omega BCM-1 in a quarter bridge configuration. A Flute 114 Mutli-meter was also attached to read the output voltage produced by the strain gauge.

This setup is shown in (Figure 70). After the stress-strain data were collected, the slope of the stress-strain curve was determined and Young's modulus was calculated.

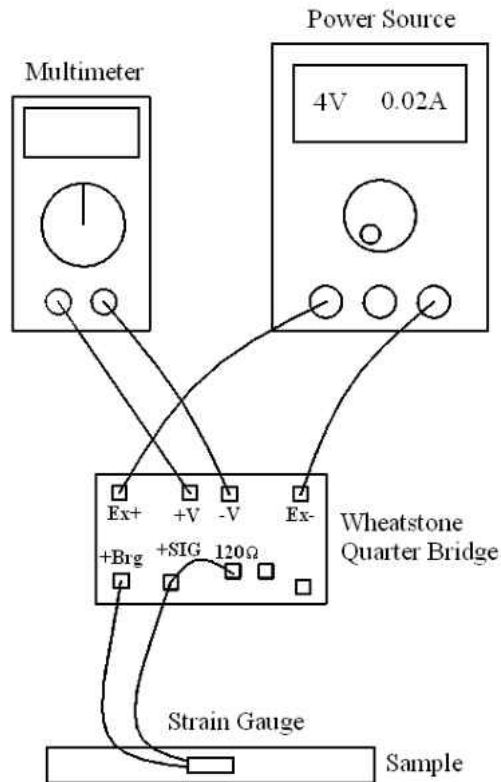


**Figure 70: Strain measurement setup for the sample under investigation.**

Further, the measured Young's modulus values were compared to those published in the literature or measured by other techniques. Few materials were selected as materials of choice for calibration and verification of *in-situ* bending device. Aluminum 2024 T3 (Al) was chosen as an example of a soft and ductile material, as well as brittle ceramics, such as  $\text{La}_{0.8}\text{Sr}_{0.2}\text{Ga}_{0.8}\text{Mg}_{0.2}\text{O}_3$ ,  $\text{La}_{0.8}\text{Ca}_{0.2}\text{CoO}_3$ , and  $\text{B}_4\text{C}$ . The Young's modulus of Al was reported to be 73.1 GPa [251], for  $\text{La}_{0.8}\text{Sr}_{0.2}\text{Ga}_{0.8}\text{Mg}_{0.2}\text{O}_3$  was reported to be 175 GPa [252], for  $\text{La}_{0.8}\text{Ca}_{0.2}\text{CoO}_3$  was reported to be 135 GPa [253], and for  $\text{B}_4\text{C}$  it was reported to be 450 GPa [253].

Each sample was loaded and unloaded five times using the *in-situ* bending device so that the stress-strain deformation curves could be collected for these materials for multiple times (Figure 71). By comparing the reference data measured in the literature to the experimental data obtained in the present research, one can see that the measured values of Young's Moduli of the four materials deviated by 6% of the data published in the literature. Thus, the calibration results show that the device performs very well and can be reliable for *in-situ* bending under laser radiation.

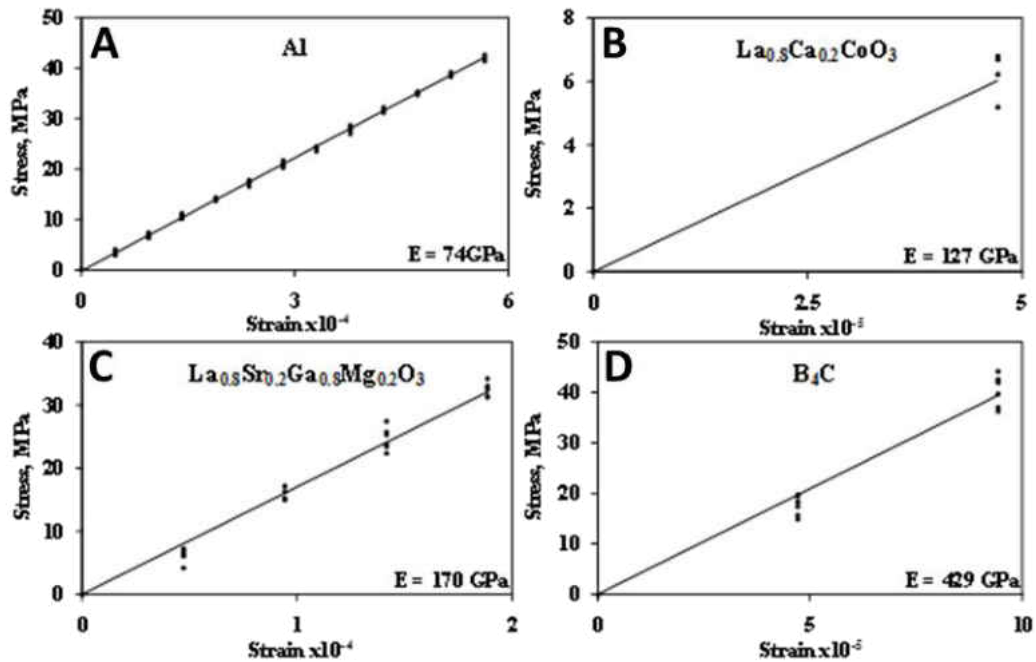


**Figure 71:** Stress-strain deformation curves obtained by loading (A) Al, (B)  $\text{La}_{0.8}\text{Ca}_{0.2}\text{CoO}_3$ , (C)  $\text{La}_{0.8}\text{Sr}_{0.2}\text{Ga}_{0.8}\text{Mg}_{0.2}\text{O}_3$ , and (D)  $\text{B}_4\text{C}$  samples using the *in-situ* loading device. The Young's moduli of the samples obtained from the measurements showed a good coincidence with the published data on the same materials.



### 2.3.2: Determination of Laser Penetration Depth

To estimate the laser penetration depth, wedge samples were produced using 4mmx1.5mmx20mm bar samples of both pure SiC, and ZrB<sub>2</sub>-17, 32, and 45 vol% SiC ceramic composites. The bar was mounted in an epoxy mold at a 5° angle (Figure 72), then covered with epoxy. Once hardened, the bar was ground to create a wedge sample as shown in Figure 72. To ensure that the tip of wedge was as thin as possible the sample length was measured in 30 minute interval while using 75, 45, and 30 μm diamond discs for grinding. Once the sample length began to decrease, it was assumed that, the thinnest possible wedge tip had been reached. The wedge sample surface was then further polished using 9, 3, and 1μm diamond suspensions. The measurements of the laser penetration depth in the samples were performed using the following experimental set up of the Renishaw Raman spectrometer system: 100x objective lens were used to focus the laser beam of 50 or 100% available laser power during 15 to 60 secs exposure time. Spectra were acquired starting from the wedge tip, where the thickness of the sample was minimal, along the central line of the sample. In the first 500μm from the wedge tip the spectra were acquired every 20μm. After 500μm, the step was changed to 50μm. After the spectra were collected, the samples were removed from the epoxy and the thickness versus distance from the wedge tip was measured using optical microscopy. It was determined that the thinnest section of the samples varied in the range of 20 μm from one side and increased to 1,500 μm on the other side. The normalized area of the Raman peaks were plotted as a function of sample thickness in order to determine the thickness of the wedge sample where the intensity of the Raman peak reached the maximum value, as this is an indication of the laser penetration depth of that material. In our experiments, the thinnest portion of the sample at the wedge tip was ~20μm and for the

spectrometer set up no difference in the intensity of the collected Raman peak as a function of sample's thickness was observed. Thus, it was concluded that the laser penetration depth was less than  $20\mu\text{m}$  and could not be explicitly determined.

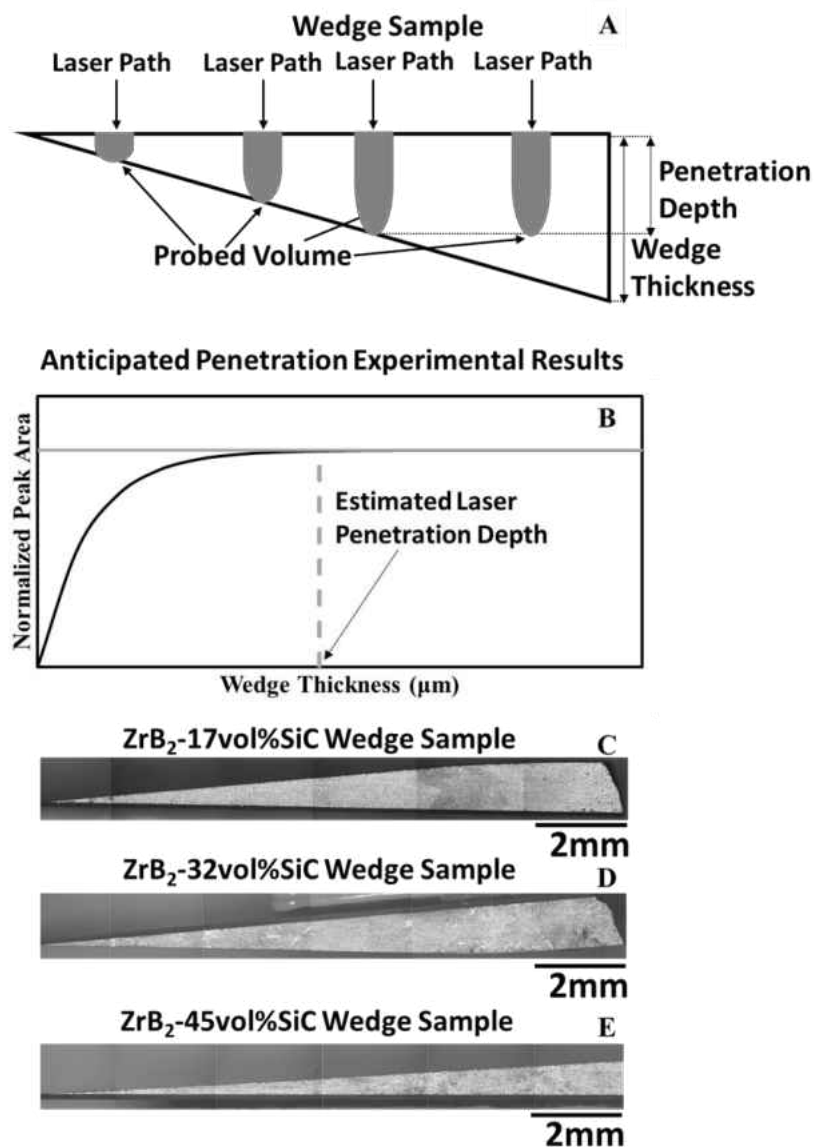


**Figure 72: Wedge sample schematic (A), anticipated penetration depth (B), optical micrographs of produced wedge samples for  $\text{ZrB}_2$ -17vol%SiC (C),  $\text{ZrB}_2$ -32vol%SiC (D), and  $\text{ZrB}_2$ -45vol%SiC (E) ceramic composites**

**2.3.3: Piezo-Spectroscopy Coefficient Determination Procedure and Collection of the Distribution of Thermal Residual Stresses**

The internal/thermal residual stresses in the material will be determined from Raman piezospectroscopy data using the linear expression below [201, 209, 210]:

$$\Delta\nu = \Pi \langle \sigma \rangle \quad (76)$$

where  $\Delta\nu$  is the difference in Raman active peak positions of the stressed material and the stress-free material,  $\Pi$  is the average piezospectroscopic coefficient for the material, and  $\langle \sigma \rangle$  is the mean or average internal stress in the material. A predetermined stress was applied using the *in-situ* 3-point bending device and the corresponding shift,  $\Delta\nu$ , of the Raman peak was measured. Then, the average piezospectroscopic coefficient was calculated using Eqn (77):

$$\Pi = 3 \frac{\partial(\Delta\nu)}{\partial\sigma} \quad (77)$$

where the derivative  $\frac{\partial(\Delta\nu)}{\partial\sigma}$  is the slope of the change in Raman peak position as a function of applied stress. As the data collected from the surface under uniaxial tension was used for the calculation of piezospectroscopic coefficients, a factor 3 was added to the Eqn. (77), as typically the piezospectroscopic coefficient is calculated for hydrostatic stress state.

The average piezospectroscopic coefficients were determined from calibration measurements made separately for pure SiC, ZrB<sub>2</sub>-17, 32, and 45 vol% SiC ceramic composites using 5X and 50X objective lenses on the optical microscope. The first set of measurements, labelled 5X, were collected using a Leica 5X lens, with a 15mm working distance and a laser spot diameter of ~20 $\mu$ m. The Raman spectra were collected using static scan setting, 50% laser power, and 50 second exposure time. To find the piezospectroscopic coefficient a 3-point bending device was used to apply loads to the specimens, as described by Fist [254]. The measurements were

made by keeping the selected spot constant throughout the entire loading of the sample. Stresses were applied between 0-300MPa at 50MPa intervals, with collection of Raman spectra at each step. To gather statistically representative results, 10 separate loadings were conducted, and then for each stress the average peak position was determined. The second set of measurements, labelled 50X, were collected using a Leica 50x lens, with a 13mm working distance and laser spot diameter of  $\sim 2\mu\text{m}$ . The Raman spectra were collected using a static scan setting, 50% laser power, and 50 second exposure time. The same 3-point bending device was used to apply a load to the sample. The applied stresses were 0-300MPa with a 100MPa step size. For each applied stress 100 different random spots were selected to collect the Raman spectra from.

## **2.4: Raman Spectra Collection, Raman Map Collection and the 2D Mapping of Thermal Residual Stress of ZrB<sub>2</sub>-SiC Ceramic Composites**

This section will cover how the Raman spectra, Raman 2D maps and the 2D maps of thermal residual stresses of SiC in ZrB<sub>2</sub>-SiC were produced for this research.

### **2.4.1: Collection of Raman Spectra and the Optimization of Parameters for Collecting 2D Raman Maps of ZrB<sub>2</sub>-SiC**

The Renishaw in-Via micro-Raman Spectrometer system was used to study the vibrational spectra of the ZrB<sub>2</sub>-17vol%SiC ceramic composites. The Raman microscope system comprises of a laser (532 nm Silicon laser) to excite the sample, a single spectrograph fitted with an edge filter, and an optical microscope (a Leica microscope with a motorized XYZ mapping stage) rigidly mounted and optically coupled to the spectrograph [255] (Figure 73).

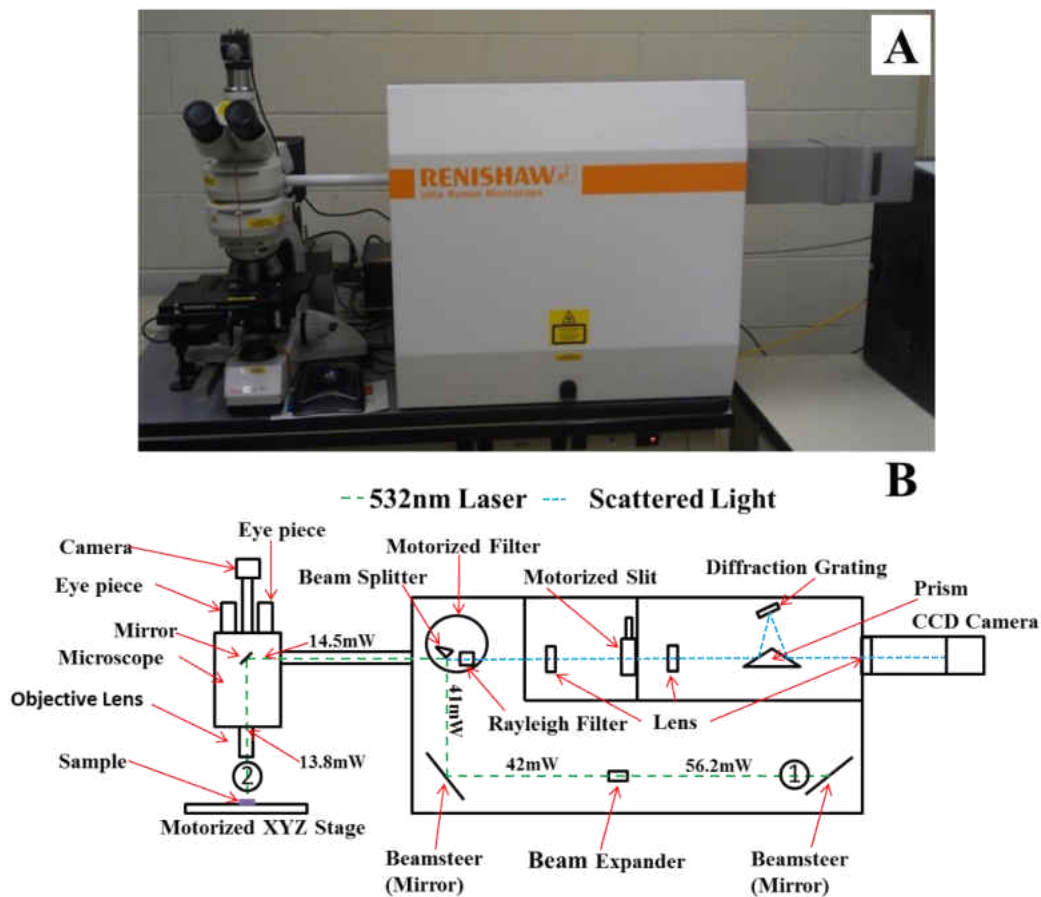


**Figure 73: Raman Spectrometer (A), Schematic of spectrometer with the laser power labelled throughout (B)**

The maximum generated power by the laser is 100mW. The laser power at different intensities of the laser were measured both after the first mirror (location 1 in Figure 73) and at the exit of the objective lens of the microscope (location 2 in Figure 73) is shown in Table 11. 100% laser power was used for all measurements in this paper.

**Table 11: Laser power through spectrometer**

| Laser Intensity (%) | Laser Power after First Beamsteer (mW)* | 5x Sample Laser Power (mW)** |
|---------------------|-----------------------------------------|------------------------------|
| 100                 | 57                                      | 13.2                         |
| 50                  | 28.5                                    | 7.09                         |
| 10                  | 5.83                                    | 1.24                         |
| 5                   | 2.86                                    | 0.59                         |
| 1                   | 0.519                                   | 0.1                          |
| 0.5                 | 0.261                                   | 0.05                         |
| 0.1                 | 0.0535                                  | 0.01                         |

\*Taken at spot #1 as shown in the schematic of spectrometer (Figure 73)

\*\*Taken at spot #2 as shown in the schematic of spectrometer (Figure 73)

The average collection time for a single spectrum varied from 30 to 84 s per point. The incident and scattered beams were focused with a microscope having a 100x objective lens, which allowed keeping a laser spot as low as 1–2 $\mu\text{m}$  (Figure 80C). All measurements were performed at room temperature. Before the ZrB<sub>2</sub>-17vol%SiC measurements, the spectrometer was calibrated with a Si standard calibration source was used at the Si band position of 520.3  $\text{cm}^{-1}$ . This system offers many advantages, such as (i) automated Raman mapping collection option by using an automated XYZ stage linked to WIRE, Renishaw's software, (ii) laser auto focusing feature, (iii) WIRE software's ability to conduct analysis directly within the software through curve fitting and its ability to remove irregularity or errors due to cosmic rays in the collected spectra; (iv) the stage's high resolution of 100 nm in X, Y, and Z directions, (v) as well as the ability of the system to edit the parameters of the spectrum collected using the WIRE software. The software allows the user to change the following parameters of spectra collected: (a) laser intensity (power), by increasing/decreasing the percentage of laser power which the sample experiences during spectrum collection; (b) Raman shift range that is used for the spectra collection, i.e. 100-2000 $\text{cm}^{-1}$ , 50-4000 $\text{cm}^{-1}$ , or other; (c) sample exposure time for how long the sample is exposed to the laser for

spectrum collection. Besides these three parameters used for setting up the experiment, other important parameters which need to be used are: (d) the time required for the collection of a single spectrum; (e) the total time required for the collection of a whole map; (f) as well as resolution steps. The time for a single spectral collection varies from 30 to 74 s. Two-dimensional (2D) map can be produced by setting up the area on the sample surface where the spectra are to be collected. The total collection time of the whole maps varied from 1.18 to 16.41 hours in the current experiments. The resolution set up for the mapping experiment was varied from 1  $\mu\text{m}$  step size for the lowest resolution step to 0.5  $\mu\text{m}$  resolution step; while the Renishaw system allowed up to 0.1  $\mu\text{m}$  resolution step, this however would tremendously increase the collection time as well as cause the overlap of many collected spectra as the laser spot size was higher than 1  $\mu\text{m}$ .

Well-polished surface of  $\text{ZrB}_2$ -17vol%SiC was produced by mechanical polishing using diamond paste with 30, 9, 6, 3, and 1  $\mu\text{m}$  sizes of the diamond particles. Since the 100x objective lens was used for the area mapping experiments it was possible to keep the spot size of the laser as small as 1.5  $\mu\text{m}$  in the experiments. During the experiments, the system was set up to take spectra from all points in the area of interest on the surface of  $\text{ZrB}_2$ -17vol%SiC composite material. Two different types of scans were used for spectra collection during the 2D mapping experiment. One was a static scan which allowed to center the collection of spectrum at  $900\text{cm}^{-1}$  Raman shift with  $\pm 420$ -442 range collected, thus limiting the collected spectrum to  $456$ - $1320\text{ cm}^{-1}$  range of the wavenumbers. Another type of the collected spectrum was a so-called “extended scan”, which allows the user to establish the required spectral range of interest to be mapped. Autofocusing was used to collect the Raman spectra because it maintains a good focus on the sample surface during mapping experiments. To produce 2D maps and fir the collected data, Renishaw WIRE software

with a mixed Lorentzian and Gaussian peak fitting function was used. The fitting procedure allowed for precise determination of four peaks' parameters, such as peak intensity, peak position, peak width or full width at half maximum (FWHM), as well as to calculate the area below the peak. In the current paper only peak intensity maps were used for analysis of the results to establish the best practices for creation of Raman maps.

#### **2.4.2: Collection of 2D Raman Maps of ZrB<sub>2</sub>-SiC Ceramic Composites**

A Renishaw in-Via micro-Raman spectrometer system was used to study the vibrational spectra of the SiC, ZrB<sub>2</sub>-SiC (17, 32, and 45vol%) ceramic composites. The Raman microscope system comprises of a laser (532 nm silicon laser) to excite the sample, a single spectrograph fitted with an edge filter, and an optical microscope (a Leica microscope with a motorized XYZ mapping stage) rigidly mounted and optically coupled to the spectrograph [255]. The maximum generated power by the laser is 100mW, and 100% laser power was used for all measurements [256]. The average collection time for a single spectrum was 20s per point. The incident and scattered beams were focused with a microscope having a 100x objective lens, which produced a laser spot diameter as low as 1–2 $\mu$ m [256]. All measurements were performed at room temperature. Before the measurements, the spectrometer was calibrated with a Si standard calibration source and using the Si band position at 520.3 cm<sup>-1</sup>. The stage has high resolution positioning of 100 nm in X, Y, and Z directions.

Well-polished surfaces of SiC, ZrB<sub>2</sub>-SiC (17, 32, and 45vol%) were produced using diamond paste with 30, 9, 6, 3, and 1  $\mu$ m size diamond particles. During the experiments, the system was set up to record spectra from all points in the area of interest on the surface of SiC,



ZrB<sub>2</sub>-SiC (17, 32, and 45vol%) composite materials. Autofocusing was used to collect the Raman spectra. To produce 2D maps and collect data, the Renishaw WIRE software with a mixed Lorentzian and Gaussian peak fitting function was used. The fitting procedure allowed for precise determination of four peak parameters, peak intensity, peak position, peak width or full width at half maximum (FWHM), and the area below the peak. Within the defined area, 900 points were taken, with a resolution step size of 0.7 $\mu$ m, taking a total of ~12 hours for data collection. Since the laser spot size is on the order of 1-2 $\mu$ m and map resolution (distance between centers of laser spots) is 0.7 $\mu$ m, there is a small overlapping of probe volume for neighboring measurement positions. To create maps of peak position, peak width, and peak intensity, the 6H-SiC Frequency Longitudinal Optic (FLO) 965cm<sup>-1</sup> peak was used for curve fitting. In order to create an accurate peak position map to show only the SiC phase, a filtering method was used based on peak position, peak width and peak intensity as well as a filter using a combination of all three. This filtering method will be described in detail in the results section of this dissertation.

## **2.5: Determining the Mechanical Properties of the Produced ZrB<sub>2</sub>-SiC Ceramic**

### **Composites**

The Young's, bulk, and shear moduli along with the Poisson's ratio of the materials were measured at room temperature using a Resonant Ultrasound Spectroscopy (RUS). Which is a highly accurate method for determining the elastic properties from the resonant spectra of a sample of known mass, geometry, and dimensions [203, 257, 258]. The composite pellets of 20 mm in diameter and 2-3 mm thick were placed on 3 transducers of which one of them was sending out an ultrasonic waves at sweeping frequency and the other two transducers recorded the natural

frequencies at which the sample was vibrating. For determining the elastic moduli of the examined materials from resonant spectra, it was assumed that the composite pellets were isotropic, and thus, only two elastic constants, i.e.,  $C_{11}$  and  $C_{44}$  are required. From the known sample dimensions, density, and a set of “guessed” elastic constants  $C_{11}$ , and  $C_{44}$ , the first 40 resonant frequencies were calculated for each sample. A multidimensional software Quasar RuSpec (Magnaflux Quasar Systems, Albuquerque, NM) that iteratively minimizes error between the measured and calculated resonant frequencies by changing the initially “guessed” elastic constants, was used to determine elastic constants for the set of measured resonant frequencies of the sample. The elastic constants  $C_{11}$  and  $C_{44}$  were further used to calculate Young’s, shear and bulk moduli and Poisson’s ratio of the composite samples. It is worth noting here that the fitting error, i.e. the root-mean-square (RMS) error between the measured and calculated resonant frequencies, never exceeded 0.3% for all of the tested samples.

Bars with dimensions of 2x2.5x25mm were machined out of the SPS samples by Prematech Advanced Ceramics, MA. Flexure strength was measured using a four-point test technique in accordance with the EN843-1 standard. Five samples were used for room temperature testing for each composition. The crosshead speed was set to 0.5mm/min.

Fracture toughness was measured using the Single Edge V Notch Beam (SEVNB) technique in accordance with the CEN/TS 14425-5 standard. A single notch was made on the 2 mm side of the 2x2.5x25mm bar as near to the center as possible with a depth between 20 to 40 % of the total depth of the bar, since it was shown that within this range the depth of the notch has no influence on the measured  $K_{Ic}$  values [259]. A diamond saw was used to make the initial 0.5

mm depth notch, after that the final 1 to 1.5 mm depth notch with  $\sim 45\mu\text{m}$  tip radius was produced by manually cutting using the razor blade with 15 and then 3  $\mu\text{m}$  diamond paste deposited. Five samples were tested at room temperature with the crosshead speed of 0.5mm/min.

## **2.6: Processing and Preparing the $\text{ZrB}_2\text{-IrB}_2\text{-SiC}$ Ceramic Composites**

This section of the dissertation will cover the how the  $\text{ZrB}_2\text{-IrB}_2\text{-SiC}$  ceramic composite powders were produced.

### **2.6.1: Synthesis of $\text{IrB}_2$ Powders**

The  $\text{IrB}_2$  powders were produced using a synthesized using mechanochemical synthesis. A high energy ball mill was utilized to do the mechanochemical synthesis. The ball mill used was the Spex 8000 miller/mixer shown below as Figure 74A. The Ir powders (Precious Metal Purchase, 99.9% pure) and B powders (Alfa Aesar, 99% pure, -325 mesh, amorphous and crystalline) were loaded into an Ar filled glovebox. Then powders were then loaded into a WC vial with two WC milling balls under the Ar atmosphere. The vial already have Ir and B powders on the wall from previous milling experiments. This reduced contamination of WC in the powders after milling. The WC vial is used is shown below as Figure 74B. The ratio of Ir:B powders loaded into the vial were 1:3, with the total powder weight being 12g. Once loaded into the vial the powders were then seal into the vial using a rubber gasket and Teflon tape to prevent leaks around the threads of the lid. Once the lid was tighten down electrical tape was then used to make sure the lid is sealed and stayed on. The vial was then loaded into the high energy ball mill and was milled for 30 hours. During the milling process the mill was on for 30 minutes and then rested for 30 minutes. This cycle of on and off was continued until 30 hours of total milling time was reached. This on/off

cycling was done to extend the life of the mill and to prevent the temperature of the mill and the vial from getting too hot during the milling process.

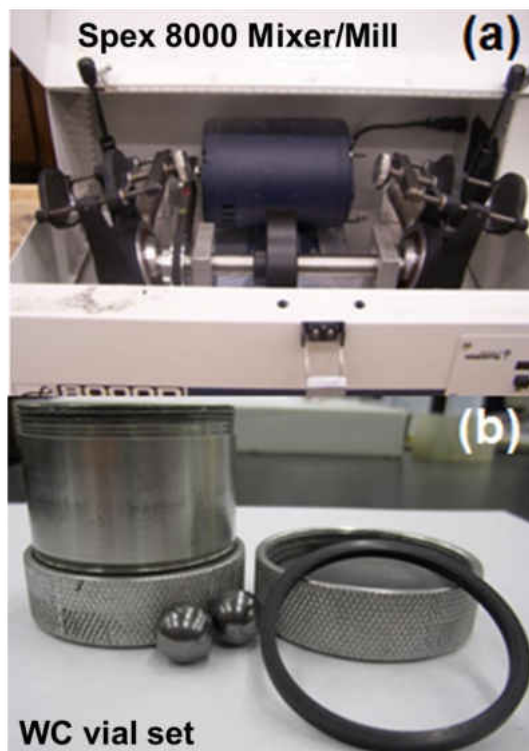


**Figure 74: Spex 8000 Mixer/Mill (A) and WC vial set (B): pictures taken by Zhilin Xie**

After the 30 hours of milling the powder was then removed from the vial by again using a glovebox with Ar atmosphere to prevent an oxidation of the powders as the diameter of the powders is very fine. The powders were then loaded into a bag to be seal and used for later. This process was developed by Zhilin Xie and is also described in [27, 28]. An in depth analysis of the phases present in the powder after this process is shown by Zhilin Xie in [27, 28].

### 2.6.2: Preparing the ZrB<sub>2</sub>-IrB<sub>2</sub>-SiC Powder

The ZrB<sub>2</sub>-2.1vol%IrB<sub>2</sub>-32vol%SiC composite were prepared in three batches by weighting the ZrB<sub>2</sub> powder (H.C. Starck-ZrB<sub>2</sub> Grade B), the SiC powder (H.C. Starck- Alpha -SiC Grade UF-10), and the IrB<sub>2</sub> powder, synthesized as described in the previous section in a certain proportion. The combined powders were then grinding together in a plastic bottle, using ZrO<sub>2</sub>-Y<sub>2</sub>O<sub>3</sub> balls and acetone as a milling media. After 48 hours of milling, the batches were dried and sieved to break up the agglomerates. The sieved powders were loaded in a graphite die, using graphite foil as an intermediate layer between the die and powder and then sintered using SPS. The parameters used to sinter the samples will be described in the results section of this work.

### 2.6.3: XRD and XRD Refinement of ZrB<sub>2</sub>-IrB<sub>2</sub>-SiC

A Rigaku MiniFlex6000 was used to collect the XRD pattern from the ZrB<sub>2</sub>-2.1vol%IrB<sub>2</sub>-20vol%SiC samples, shown below as Figure 75.



**Figure 75: Rigaku MiniFlex6000 XRD machine**

Before the XRD of the samples were taken the samples were grinded to remove the graphite foil off the sample using 125, 75, 45, and 30 $\mu$ m diamond discs. The XRD was taken from the bulk of the produced ZrB<sub>2</sub>-2.1vol%IrB<sub>2</sub>-32vol%SiC ceramic composites samples. Two samples were chosen to take the XRD patterns from. They were the samples at 1950°C due to the sampling losing mass during the sintering process and the 1500°C with 5 minutes dwell time. The XRD patterns of the two samples were collect of the following range of 2 $\theta$  angles, 15°-145° and each pattern took a total of 45 minutes to collect. The samples were then refined using the HighScore software by PANalytical. The following phases were assumed to be present for the refinement process: IrB<sub>1.1</sub>, ZrB<sub>2</sub>, 6H-SiC, IrB<sub>1.35</sub>, and ReB<sub>2</sub>-tyoe IrB<sub>2</sub> phases.

## **CHAPTER 3: RESULTS**

This section of the dissertation discusses and presents the results of the research conducted.

### **3.1: Sintering and Microstructure of ZrB<sub>2</sub>-SiC Ceramic Composites Samples by SPS**

This section will cover the sintering and the microstructure of the samples produced by SPS.

#### **3.1.1: Sintering of ZrB<sub>2</sub>-SiC Ceramic Composites Samples by SPS**

The shrinkage of the ZrB<sub>2</sub>-SiC ceramics during spark plasma sintering is shown in Figure 76. Both the pressure profile and temperature profiles, along with the shrinkage of the sample, are shown as a function of sintering time. The sample was heated from 400°C to the sintering temperature of 1950°C in 15 min, then dwelled at 1950°C for 15 min, and then cooled down back to 400°C in 15 min. A pressure of 50MPa was applied during the heating, when the temperature was at 1000°C, held constant for the remainder of the run until the temperature during cooling reached 1000°C, then the pressure was gradually removed.

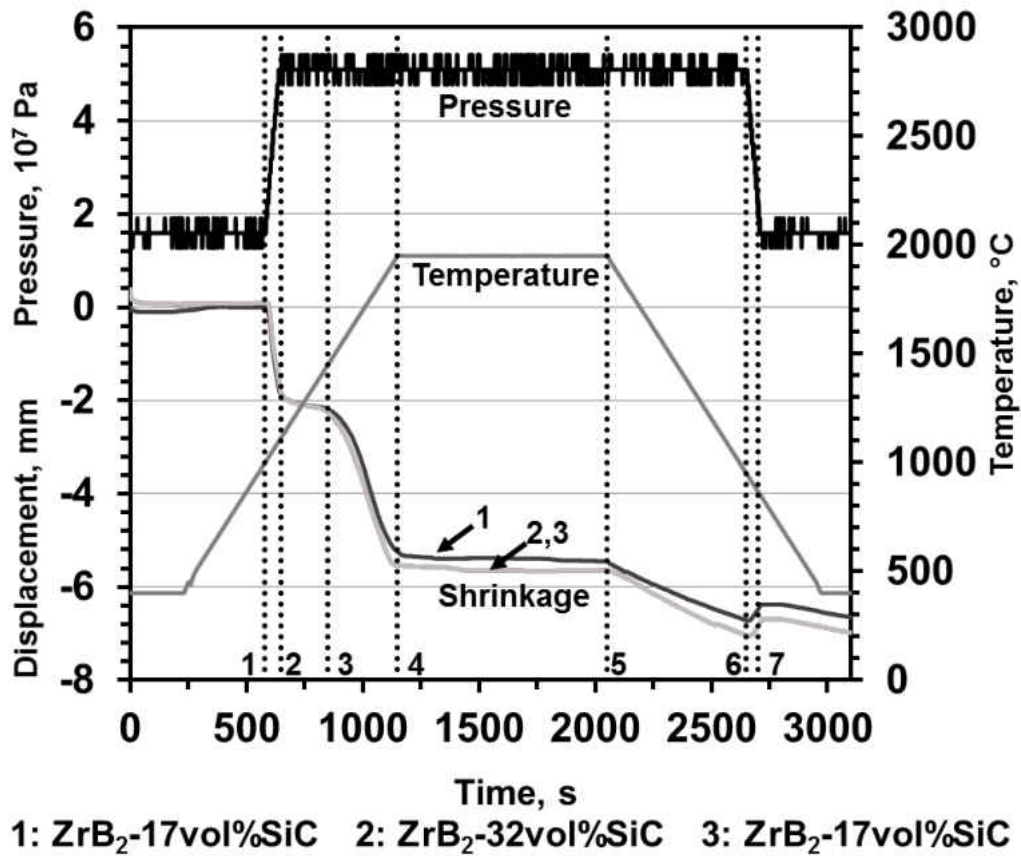


**Figure 76: The pressure, temperature, and shrinkage plots showing the sintering parameters of three  $\text{ZrB}_2$ -17, 32, and 45vol%SiC ceramic composites by SPS**

The highest shrinkage rate was at 1500°C. All three  $\text{ZrB}_2$ -17, 32, and 45 vol% SiC composites showed the same shrinkage behavior. The two plots for  $\text{ZrB}_2$ -32 and 45 vol% SiC compositions were completely coincided and can not be distinguished from Figure 76, but the  $\text{ZrB}_2$ -17vol% SiC showed slight different behavior. The difference might be due to different weight of powder placed in the graphite die for sintering.



### 3.1.2: Microstructure of ZrB<sub>2</sub>-SiC Ceramic Composites Samples by SPS

The properties of SiC and ZrB<sub>2</sub>-SiC (17, 32, and 45vol%) ceramics after sintering are presented in Table 12. The pure SiC ceramics has 32.2±4.0% porosity, while the three ZrB<sub>2</sub>-SiC composites were more dense.

**Table 12: Density, porosity, and grain size of the SiC and ZrB<sub>2</sub>-SiC ceramics**

| Composition                 | Density (g/cm <sup>3</sup> ) | Porosity (%) | SiC Grain Size (μm) |
|-----------------------------|------------------------------|--------------|---------------------|
| SiC                         | 2.18±0.13                    | 32.19±3.9    | -                   |
| ZrB <sub>2</sub> -17vol%SiC | 5.39±0.01                    | 3.63±0.1     | 1.48±1.0            |
| ZrB <sub>2</sub> -32vol%SiC | 4.96±0.03                    | 3.93±0.5     | 1.83±1.4            |
| ZrB <sub>2</sub> -45vol%SiC | 4.67±0.04                    | 2.78±0.8     | 2.12±1.48           |

The representative microstructure along with Frequency Transverse Optic (FTO) and FLO Raman peaks of SiC for all four ceramics are shown in Figure 77. The pores are clearly visible in pure SiC ceramics (Figure 77A) an increasing number of SiC grains in the ZrB<sub>2</sub> composites, apparent as the darker phase in optical microscope images. There was no significant difference in Raman spectra of SiC for all four compositions, but it was found that not only were the FTO (789cm<sup>-1</sup>) and FLO (965cm<sup>-1</sup>) peaks present, but also two small peaks (767cm<sup>-1</sup>, and 797cm<sup>-1</sup>) around the FTO peak appeared, indicating the presences of the hexagonal 6H polytype of SiC phase in all four compositions [190] (Figure 77A-D).

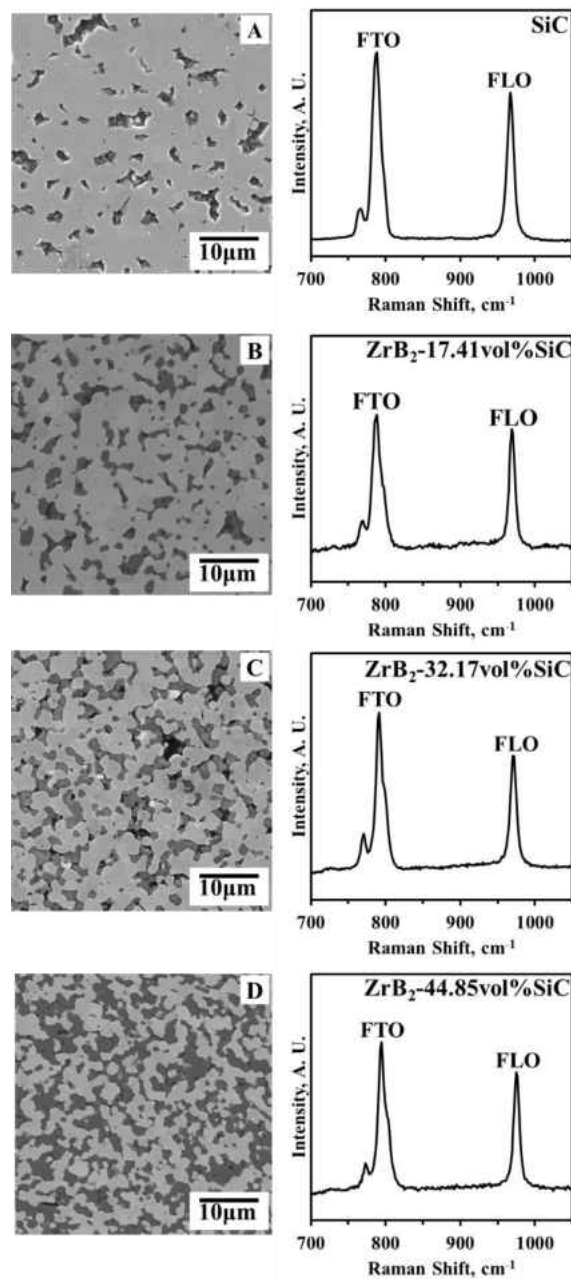


**Figure 77: SEM micrographs and Raman Spectra (100% laser power, 20s exposure, and 100-1050 $\text{cm}^{-1}$  Raman Shift Range): (A) SiC ; (B)  $\text{ZrB}_2$ -17 vol%SiC; (C)  $\text{ZrB}_2$ -32 vol%SiC; (D)  $\text{ZrB}_2$ -45 vol%SiC.**

The microstructure of three  $\text{ZrB}_2$ -SiC ceramic composites is shown in Figure 78. The SiC grains are homogeneously distributed in the  $\text{ZrB}_2$ . The sintered ceramic composites have a porosity

of less than 4% [260]. The measured grain sizes of the SiC are  $\sim 1.48 \pm 1.0 \mu\text{m}$ ,  $1.83 \pm 1.4 \mu\text{m}$ , and  $2.12 \pm 1.48 \mu\text{m}$  for ZrB<sub>2</sub>-17vol%SiC, ZrB<sub>2</sub>-32vol%SiC, and ZrB<sub>2</sub>-45vol%SiC ceramic composites respectively [260]. While the size of ZrB<sub>2</sub> grains is about 5-7 $\mu\text{m}$  for ZrB<sub>2</sub>-17vol%SiC ceramics (Figure 78A). The ZrB<sub>2</sub> grain size decreased to 2-3 $\mu\text{m}$  for the ZrB<sub>2</sub>-32vol%SiC and for ZrB<sub>2</sub>-45vol%SiC composites.

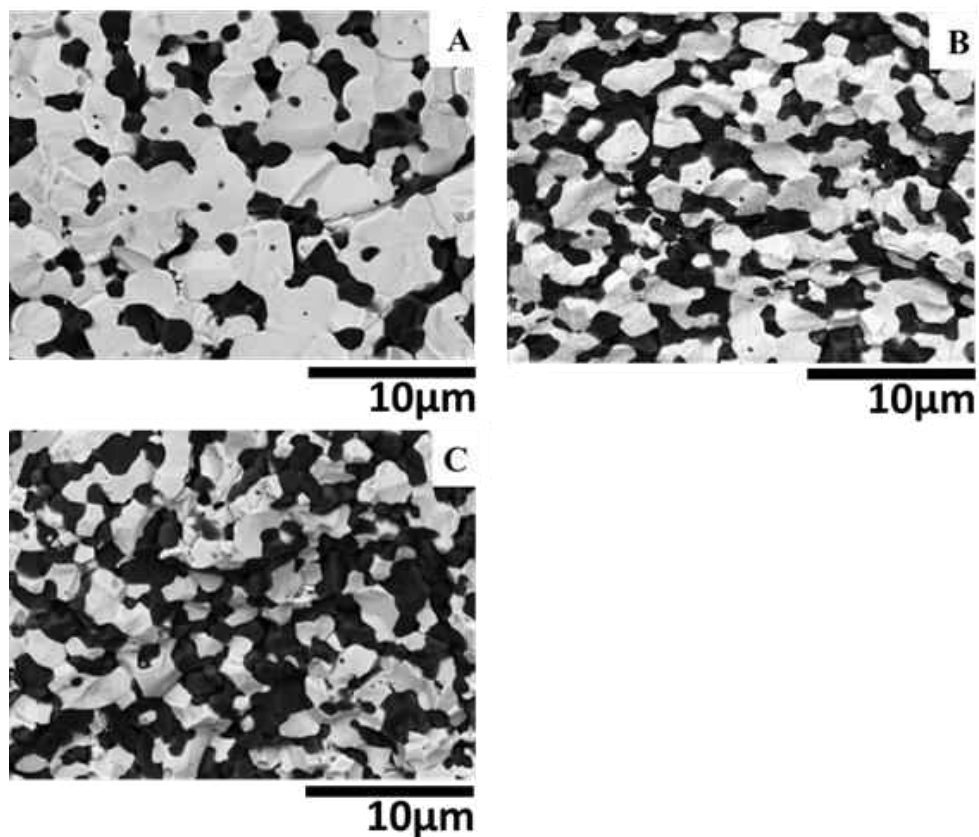


**Figure 78: SEM backscattered micrographs of ZrB<sub>2</sub>-17vol%SiC (A), ZrB<sub>2</sub>-32vol%SiC (B), and ZrB<sub>2</sub>-45vol%SiC (C) ceramic composites, respectively. Dark grains belong to SiC phase, and the light grains belong to ZrB<sub>2</sub> matrix phase**

### 3.2: Calibration of Piezo-Spectroscopy Coefficient via 3-Point Bending

In order to calculate the piezospectroscopic coefficients for both pure SiC and for ZrB<sub>2</sub>-17, 32, and 45vol%SiC ceramic composites the measurements of the FLO 6H-SiC peak position as a function of applied uniaxial stress were performed using an *in-situ* 3-point bending device as shown in Figure 79.

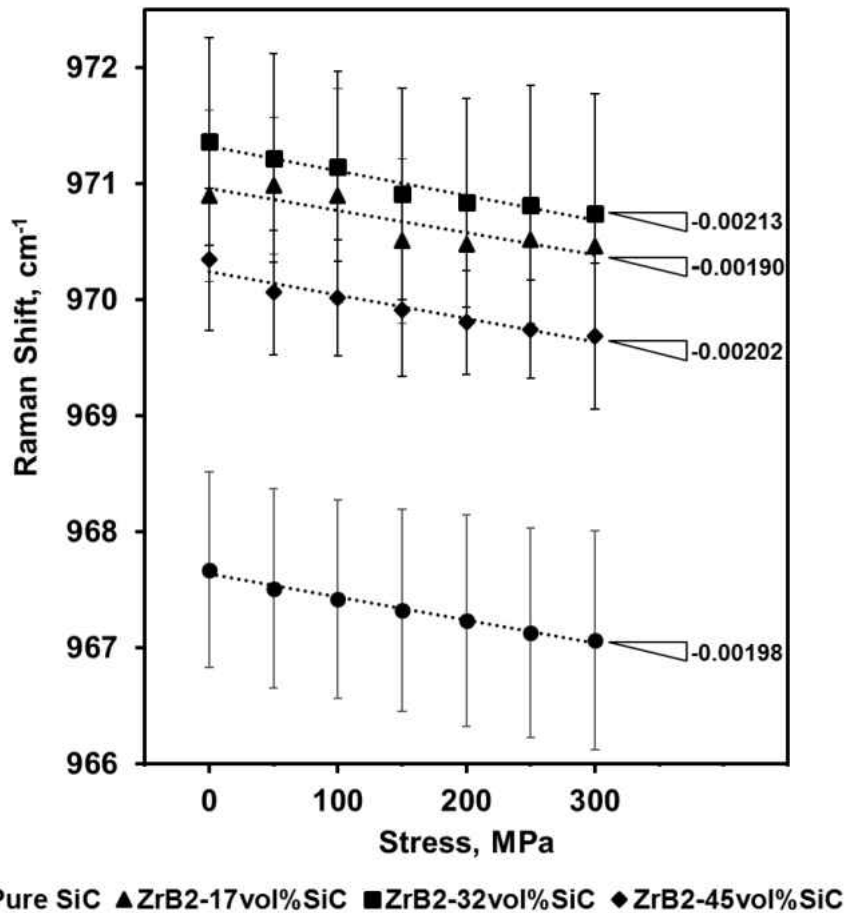


Figure 79: 6H-SiC FLO peak position as a function of applied stress for pure SiC and ZrB<sub>2</sub>-17, 32, and 45vol%SiC ceramic composites

The peak shifts to lower wavenumbers as the applied stress increases to 300 MPa, indicating the presence of tensile stresses in the SiC grains on the surface of the samples. While the position of the FLO SiC peak is a function of the ceramic compositions, the calculated slope for all four materials are similar. The slopes of the four plots are equal to the derivative  $\frac{\partial(\Delta\nu)}{\partial\sigma}$ , where  $\Delta\nu = \nu - \nu_0$ , where  $\nu_0$  is the peak position for zero applied stress and  $\nu$  is the peak position for applied stress. The piezospectroscopic coefficients measured using the four different ceramic compositions are presented in Table 13.

**Table 13: Piezospectroscopy coefficients  $\Pi$  of SiC phase measured in pure SiC and three ZrB<sub>2</sub>-SiC ceramic composites**

| # | Composition                 | $\Pi$ , (GPa <sup>-1</sup> *cm <sup>-1</sup> ) |
|---|-----------------------------|------------------------------------------------|
| 1 | Pure SiC                    | -5.94±3.3                                      |
| 2 | ZrB <sub>2</sub> -17vol%SiC | -5.7±3.0                                       |
| 3 | ZrB <sub>2</sub> -32vol%SiC | -6.39±3.5                                      |
| 4 | ZrB <sub>2</sub> -45vol%SiC | -6.06±3.1                                      |

### **3.3: Raman Line and 2D mapping of Thermal Residual Stress of ZrB<sub>2</sub>-SiC Ceramic Composites**

This section will cover the results of the Raman maps in terms of what the optimized collection parameters are. The filtering method used to eliminate the ZrB<sub>2</sub> data point from the maps to obtain only the SiC data point. Then the maps obtained using the filtering method described and finally the thermal residual stress maps created based on the collected maps and the obtain piezospectroscopic coefficient from the previous section.

### 3.3.1: Optimization of Parameters for Collecting 2D Raman Maps of ZrB<sub>2</sub>-SiC

The scanning electron microscope (SEM) micrographs of ZrB<sub>2</sub>-17vol%SiC ceramic composites are shown in Figure 80C. As one can see from Figure 80C the distribution of SiC strengthening phase in ZrB<sub>2</sub> matrix is rather homogeneous and the grain size of SiC is  $1.48 \pm 0.98$   $\mu\text{m}$ . The typical spectra collected from three locations are marked as #1, and #2 on the optical micrograph, and the corresponding 2D Raman Map (Figure 80A and B) is shown in Figure 80D, and E. The spectrum taken from spot #1 corresponds to the 6H-polytype SiC phase and the spectrum taken from spot #2 corresponds to the spectrum of ZrB<sub>2</sub> phase (Figure 80E). Thus, the micro-Raman spectroscopy helps to identify the presence of different polytypes of SiC phase with great precision in microscopic locations. It is also interesting to notice, that while in many existing publications [180, 181] it was stated that the ZrB<sub>2</sub> is not Raman active, in all of our experiments two peaks at  $791\text{cm}^{-1}$  and  $1150\text{cm}^{-1}$  always appeared during the measurements affecting the results of the fitting and map's creation. Thus, we report them here. Those two peaks are very weak but they always appear when ZrB<sub>2</sub> surface, whether ZrB<sub>2</sub>-SiC composite or pure ZrB<sub>2</sub> ceramic is used for spectra collection. As we have an overlapping effect of the weak  $791\text{cm}^{-1}$  peak of ZrB<sub>2</sub> (Figure 80E) and strong  $791\text{cm}^{-1}$  Frequency Transverse Optic (FTO) SiC peak.

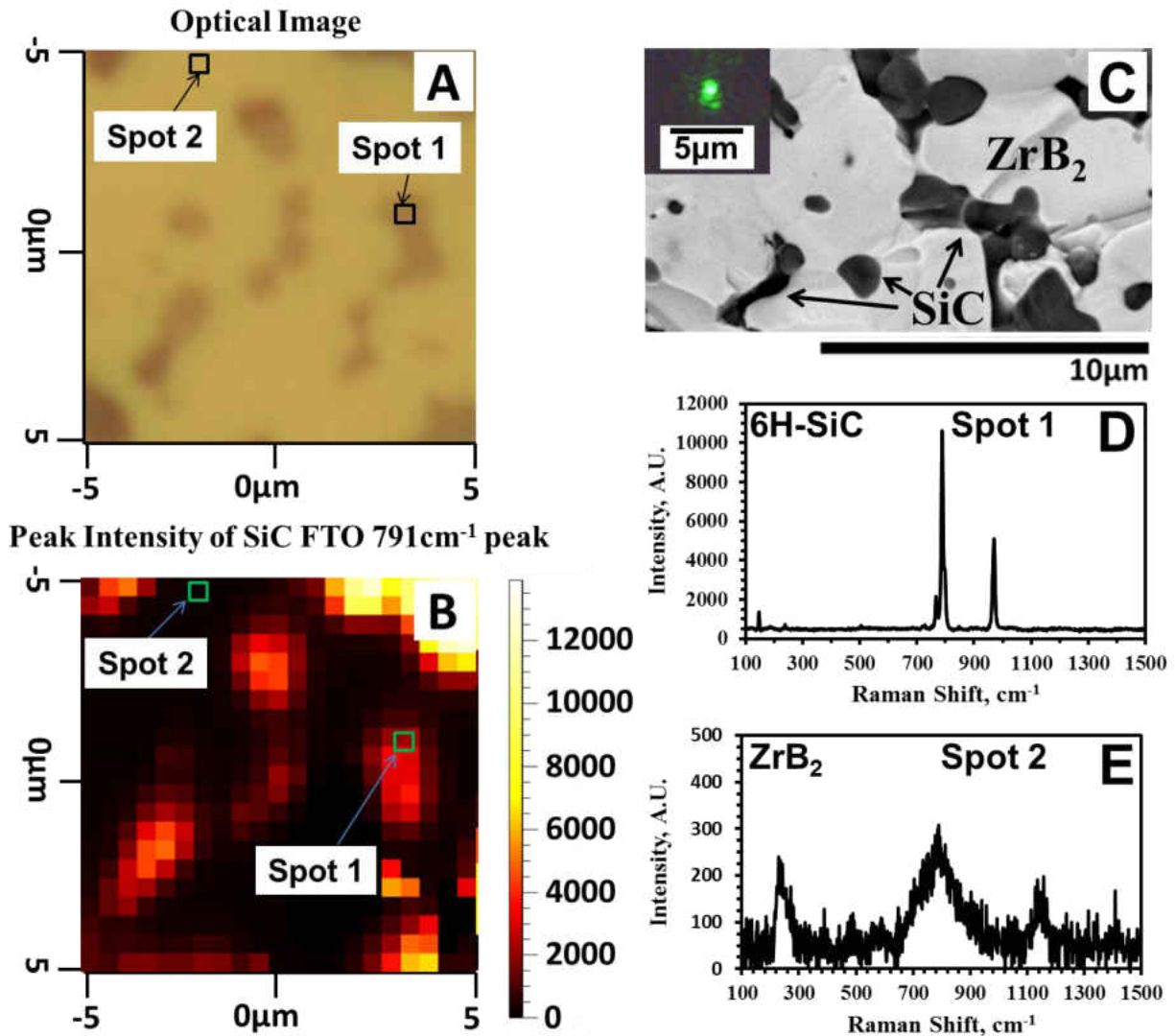


**Figure 80: (A) Optical image of mapping area, (B) 791cm-1 peak intensity map, (C) SEM backscattered image of ZrB<sub>2</sub>-17vol %SiC, the insert shows a laser spot size taken using 100x objective lens, (D) Typical Raman spectra for SiC phase, (E) Typical Raman spectra for ZrB<sub>2</sub> phase**

To find the best mapping parameters to optimize the mapping procedure, the first experiment was performed to verify how the resolution of point collection would affect the map quality. Figure 81 shows the examples of three maps of peak intensity and peak width of 791cm<sup>-1</sup> SiC peak collected from 10x10μm representative area of ZrB<sub>2</sub>-17vol%SiC ceramic composite.

Both 1 $\mu\text{m}$ , 0.7 $\mu\text{m}$ , and 0.5 $\mu\text{m}$  steps were used for these collections, and as one can see all three peak intensity maps reflected rather correctly the location of SiC grains, which are clearly visible on the corresponding optical micrographs. The 1 $\mu\text{m}$  resolution step gave the least precise quality of the map, as each step in the map represented 1x1 $\mu\text{m}^2$  area of the surface, thus it is only 10 areas are shown per line. The quality of the peak intensity map improves as the resolution is increased therefore maps at 0.7 $\mu\text{m}$  and especially at 0.5 $\mu\text{m}$  resolution steps are more detailed and precise. Thus for peak intensity maps both of the three resolution steps provide sufficient quality of the data. However, as one can see from Figure 81, the peak width maps show different results. For 1 $\mu\text{m}$  step size of mapping, too many data points show very low FWHM values, 9.1%, thus a very high percentage of the data was not valid.



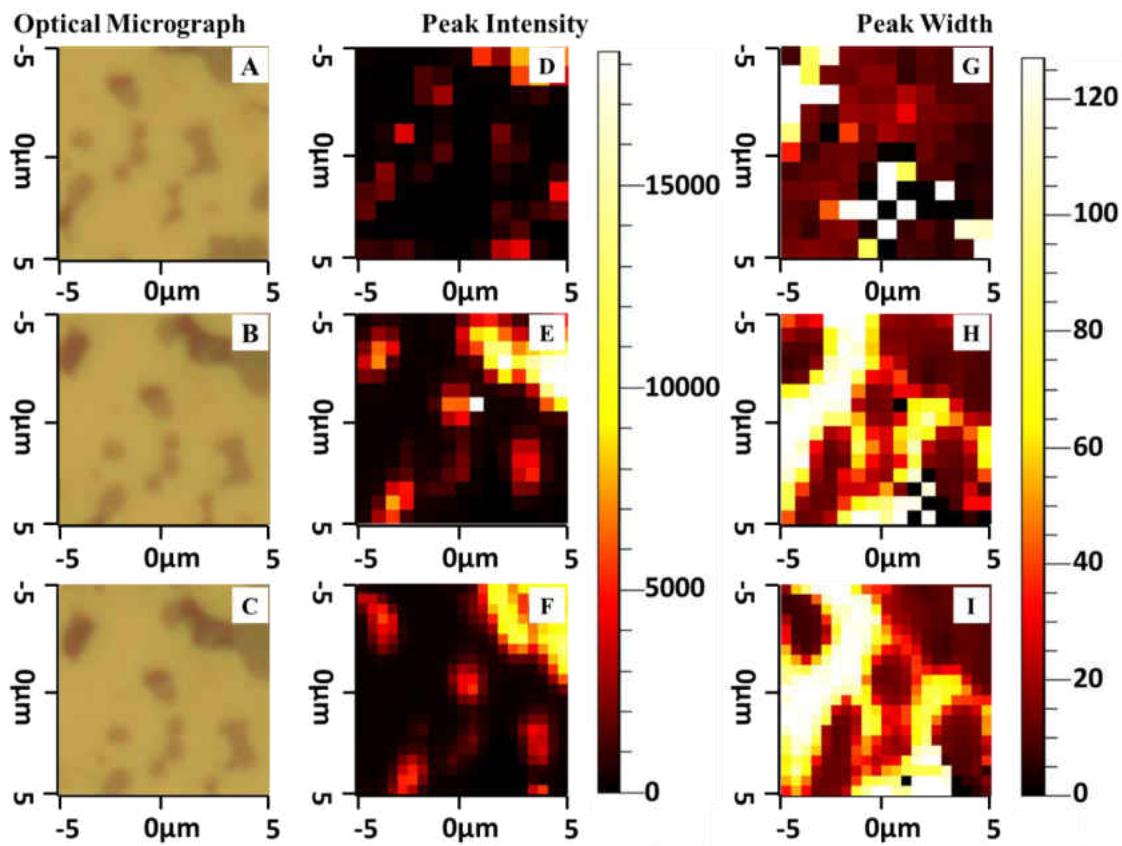


**Figure 81: Raman maps of  $ZrB_2$ -17vol%SiC with different step sizes: (A-C) optical micrograph corresponding to the maps in the same row,  $791\text{ cm}^{-1}$  peak intensity maps are shown with step sizes of  $1\text{ }\mu\text{m}$  (D),  $0.7\text{ }\mu\text{m}$  (E),  $0.5\text{ }\mu\text{m}$  (F), and  $791\text{ cm}^{-1}$  peak width maps are shown with step sizes of  $1\text{ }\mu\text{m}$  (G),  $0.7\text{ }\mu\text{m}$  (H),  $0.5\text{ }\mu\text{m}$  (I)**

When  $0.7\text{ }\mu\text{m}$  step size was used for the data collection, the percentage of the invalid or questionable data points decreased to 4%, thus improving the quality of the peak width map. When the step size decreased to  $0.5\text{ }\mu\text{m}$ , only 6 points out of 441 (1.4%) total data points provided wrong results. Thus  $0.5\text{ }\mu\text{m}$  step size resolution is the best from the point of view of the quality of the data, however the time required to collect spectra is significantly longer when  $0.5\text{ }\mu\text{m}$  step size resolution is used (Table 14) in which case to collect  $10\times 10\text{ }\mu\text{m}$  area map a total of 4.3 hours and 441 data points are necessary.

**Table 14: Investigation of step size on Raman mapping parameters used**

| Step Size( $\mu\text{m}$ ) | Scan Type | Exposure Time(sec) | Raman Shift Range( $\text{cm}^{-1}$ ) | Number of Spectra Collected | Total Experiment Time |
|----------------------------|-----------|--------------------|---------------------------------------|-----------------------------|-----------------------|
| 0.5                        | Static    | 30                 | 456-1320                              | 441                         | 15494s (4.3hrs.)      |
| 0.7                        | Static    | 30                 | 456-1320                              | 225                         | 7903s (2.2 hrs.)      |
| 1                          | Static    | 30                 | 456-1320                              | 121                         | 4246s (1.18hrs.)      |

Another point of interest for collecting good quality maps was collection time. While some of the ceramic compounds such as  $\text{LaCoO}_3$  or  $\text{La}_{0.8}\text{Ca}_{0.2}\text{CoO}_3$  perovskites are weakly Raman active and require a longer collection time of 300 seconds or longer [228], other ceramics and semiconductors, such as Si are very Raman active and therefore require very short collection time such as 1 second. SiC ceramic Raman activity is relatively good and one can collect a Raman spectrum with sufficient intensities of the peaks within 30-60 seconds per collection step. Yet it was interesting to compare the quality of the maps if one used different collection times to see if the maps are different, and if increasing collection time would improve the quality of the map. Figure 82 shows the peak intensity and Full Width at Half Maximum maps collected for 30 and 60 seconds collection time at  $0.7\mu\text{m}$  resolution steps. As one can see from Figure 82, the quality of both maps are identical both for 30 and 60 seconds, therefore the shorter collection time would be more preferable, as the collection time of the  $10\times 10\mu\text{m}$  area increased from 2.2 hours to 4.07 hours when the collection time for a single spectrum increased from 30 to 60 seconds.

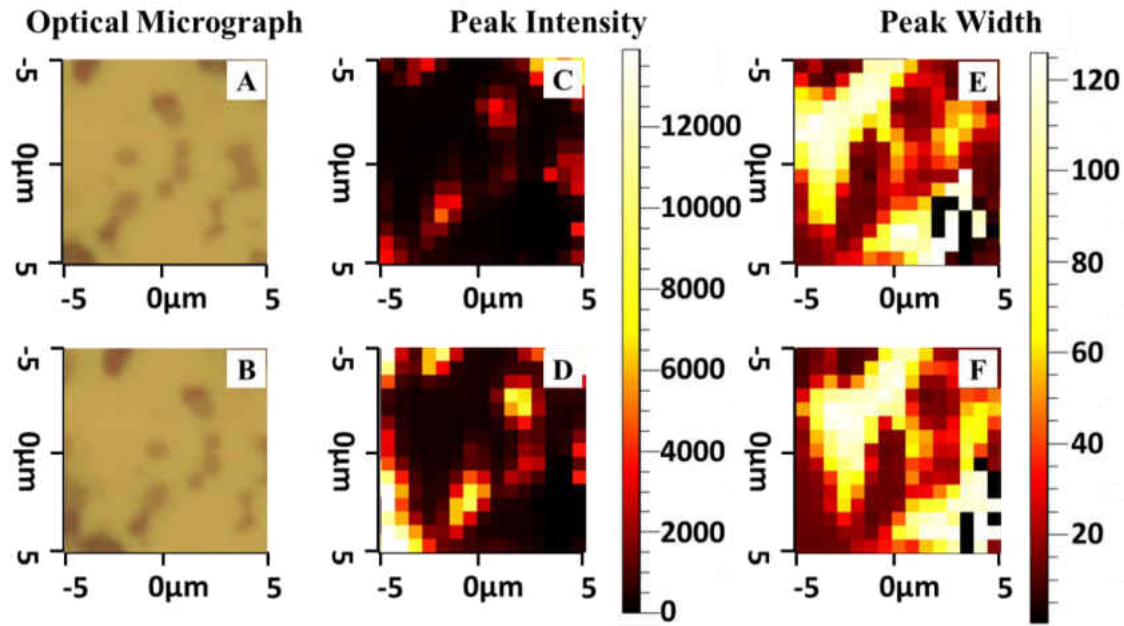


**Figure 82: Raman maps of  $ZrB_2$ -17vol%SiC created using static scan and  $0.7\mu m$  resolution step size with different scan exposure times : (A,B) optical micrograph corresponding to the maps in the same row,  $791cm^{-1}$  peak intensity maps for 30 sec (C) and 60sec (D), and  $791cm^{-1}$  peak width maps for 30 sec (E) and 60 sec (F)**

Another option of interest for different mapping parameters is given by the Renishaw software, the acquisition of the spectra might be done either in static or extended modes. With static mode one needs to center at the wavenumber of interest, and, then, the software will define the whole range, usually within  $\pm 400cm^{-1}$  Raman shift. This option is very often more preferable as it allows for faster collection times. With the extended mode one determines the whole range of the spectrum collection, thus it is possible to collect much longer ranges of the spectrum, which is impossible with the static mode. Figure 83 and Table 15 shows the comparison between maps collected using static and extended collection modes taken both at 30 sec and 60 sec collection times.

**Table 15: Investigation of scanning parameters on Raman mapping for 0.5, 0.7, and 1 $\mu$ m resolution**

| Step Size( $\mu$ m) | Scan Type | Exposure Time(sec) | Raman Shift Range( $\text{cm}^{-1}$ ) | Number of Spectra Collected | Total Experiment Time |
|---------------------|-----------|--------------------|---------------------------------------|-----------------------------|-----------------------|
| 0.5                 | Static    | 30                 | 456-1320                              | 441                         | 16500s (4.58hrs.)     |
| 0.5                 | Static    | 60                 | 456-1320                              | 441                         | 28742s (7.98hrs.)     |
| 0.5                 | Extended  | 30                 | 750-1050                              | 441                         | 20309s (5.64hrs.)     |
| 0.5                 | Extended  | 60                 | 750-1050                              | 441                         | 28742s (7.98 hrs.)    |
| 0.7                 | Static    | 30                 | 456-1320                              | 225                         | 7903s (2.2 hrs.)      |
| 0.7                 | Static    | 60                 | 456-1320                              | 225                         | 14650s (4.07hrs.)     |
| 0.7                 | Extended  | 30                 | 750-1050                              | 225                         | 18556s (5.15hrs.)     |
| 0.7                 | Extended  | 60                 | 750-1050                              | 225                         | 21984s (6.12hrs.)     |
| 1                   | Static    | 30                 | 456-1320                              | 121                         | 4264s (1.18hrs.)      |
| 1                   | Static    | 60                 | 456-1320                              | 121                         | 7893s (2.19hrs.)      |
| 1                   | Extended  | 30                 | 750-1050                              | 121                         | 5588s (1.55hrs.)      |
| 1                   | Extended  | 60                 | 750-1050                              | 121                         | 9875s (2.74 hrs.)     |

As one can see there is almost no difference in quality of the maps, as both modes provide adequate and necessary information about the peak parameters, such as peak intensity of the SiC phase. For the maps created using 60 sec collection times the intensity of the peaks were higher in comparison with maps created using 30 sec collection times, thus the maps look much brighter. However, with 60 s spectral collection time requires longer overall collection times, thus it is clear that 30 s spectral collection time and static scan would be sufficient to create high-quality maps in the ZrB<sub>2</sub>-SiC system.

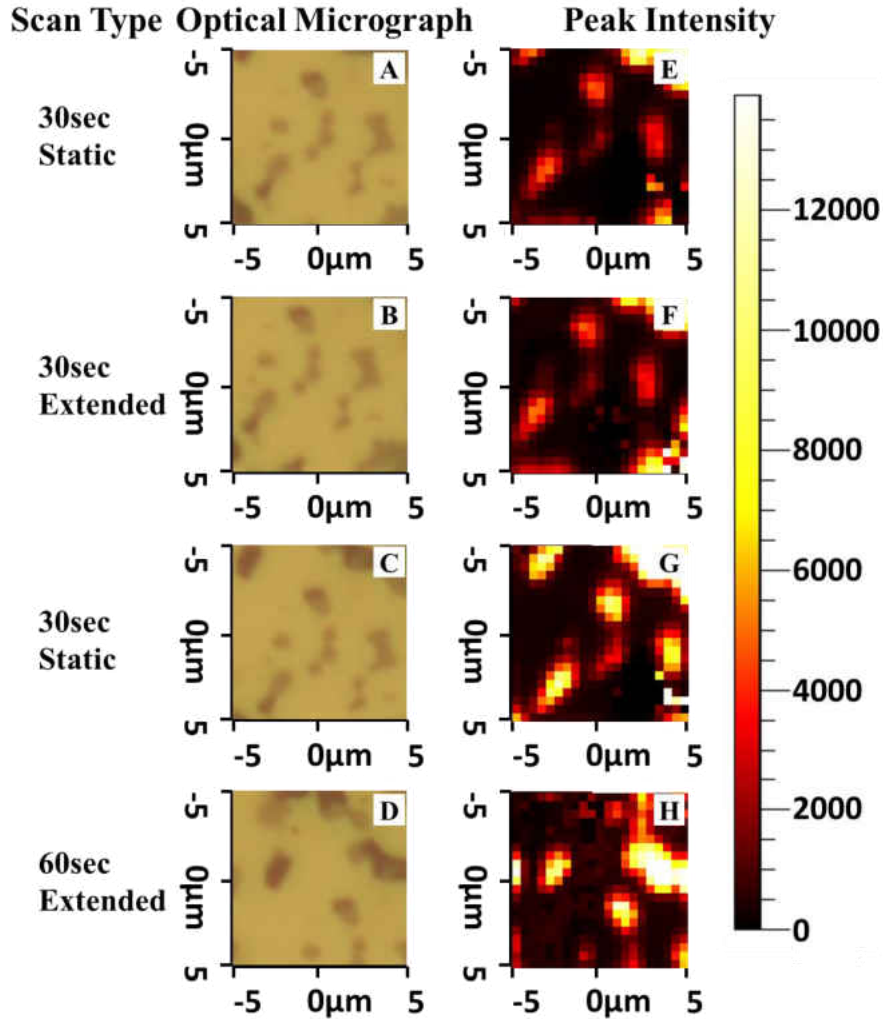


**Figure 83: Raman maps of  $ZrB_2$ -17vol%SiC created using different scanning parameters as shown in the first column with a resolution step size of  $0.5\ \mu\text{m}$ : (A-D) optical micrograph corresponding to the maps in the same row,  $791\text{cm}^{-1}$  peak intensity maps (E-H)**

Then finally one wanted to verify if the system is robust and stable enough to allow collection of maps from a larger area, where longer period of time would be required for data acquisition. Therefore we chose  $20 \times 20\ \mu\text{m}$  area on the polished surface of  $ZrB_2$ -17vol%SiC ceramics and collected maps using  $0.7\ \mu\text{m}$  and  $0.5\ \mu\text{m}$  steps size (Figure 84). As one can see, the resulting 2D maps correspond very well with the optical images of the composite, thus even when

longer periods of time (up to 16.41 hours) are required for collection (Table 16), the Renishaw spectrometer would allow data collection with a high quality.

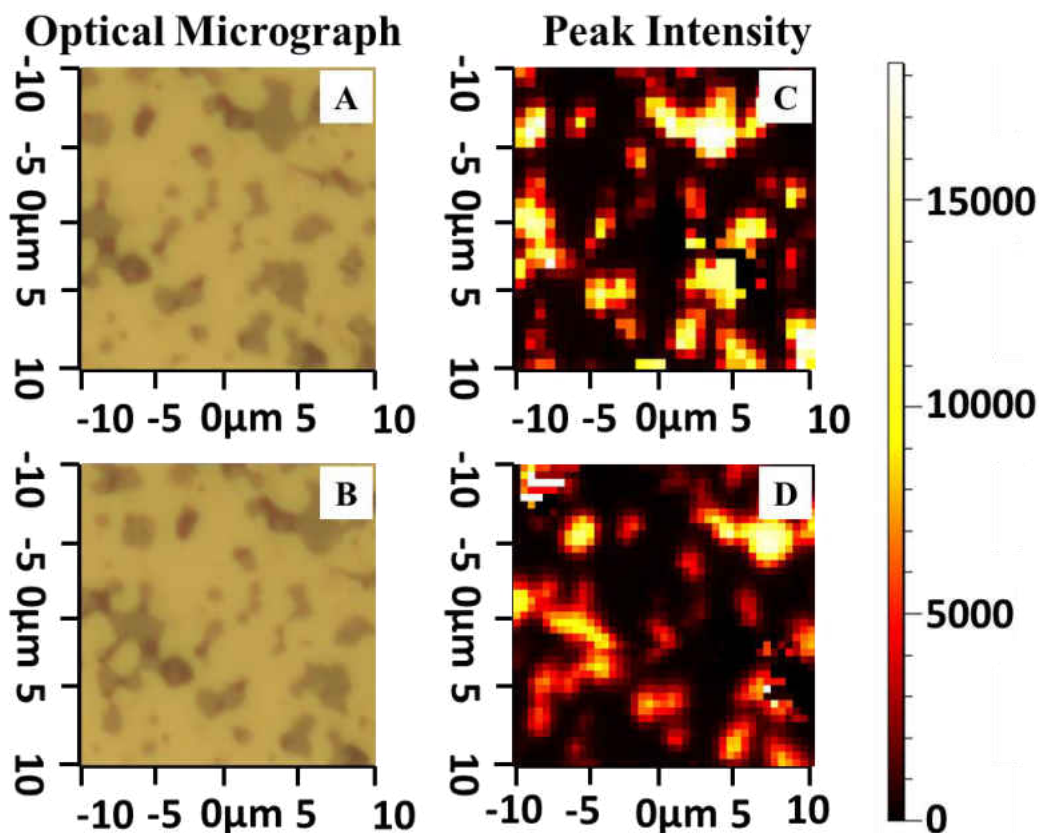


Figure 84: Comparison step size on the Raman maps of SiC FTO  $791\text{cm}^{-1}$  Peak Intensity of ZrB<sub>2</sub>-17vol%SiC: (A,B) Optical micrographs that's correspond to the maps on the right in the same row, (C) 0.7 $\mu\text{m}$  resolution, (D) 0.5 $\mu\text{m}$  resolution

Table 16: Investigation of resolution between spectra on Raman mapping for larger area

| Step Size( $\mu\text{m}$ ) | Scan Type | Exposure Time(sec) | Raman Shift Range( $\text{cm}^{-1}$ ) | Number of Spectra Collected | Total Experiment Time |
|----------------------------|-----------|--------------------|---------------------------------------|-----------------------------|-----------------------|
| 0.5                        | Static    | 30                 | 456-1320                              | 1681                        | 59059s (16.41hrs.)    |
| 0.7                        | Static    | 30                 | 456-1320                              | 900                         | 31603s (8.78hrs.)     |

### **3.3.2: Raman Mapping Methodology of Selection of Proper Data Points (Band) Filtering**

2D Raman maps were generated on the polished surfaces of the composite ceramics based on the following procedure. The FLO SiC peak was used for generation of 2D Raman maps (Figure 85A), where a  $20 \times 20 \mu\text{m}^2$  area was used to collect 900 data points using the Wire Renishaw software (Figure 86B).

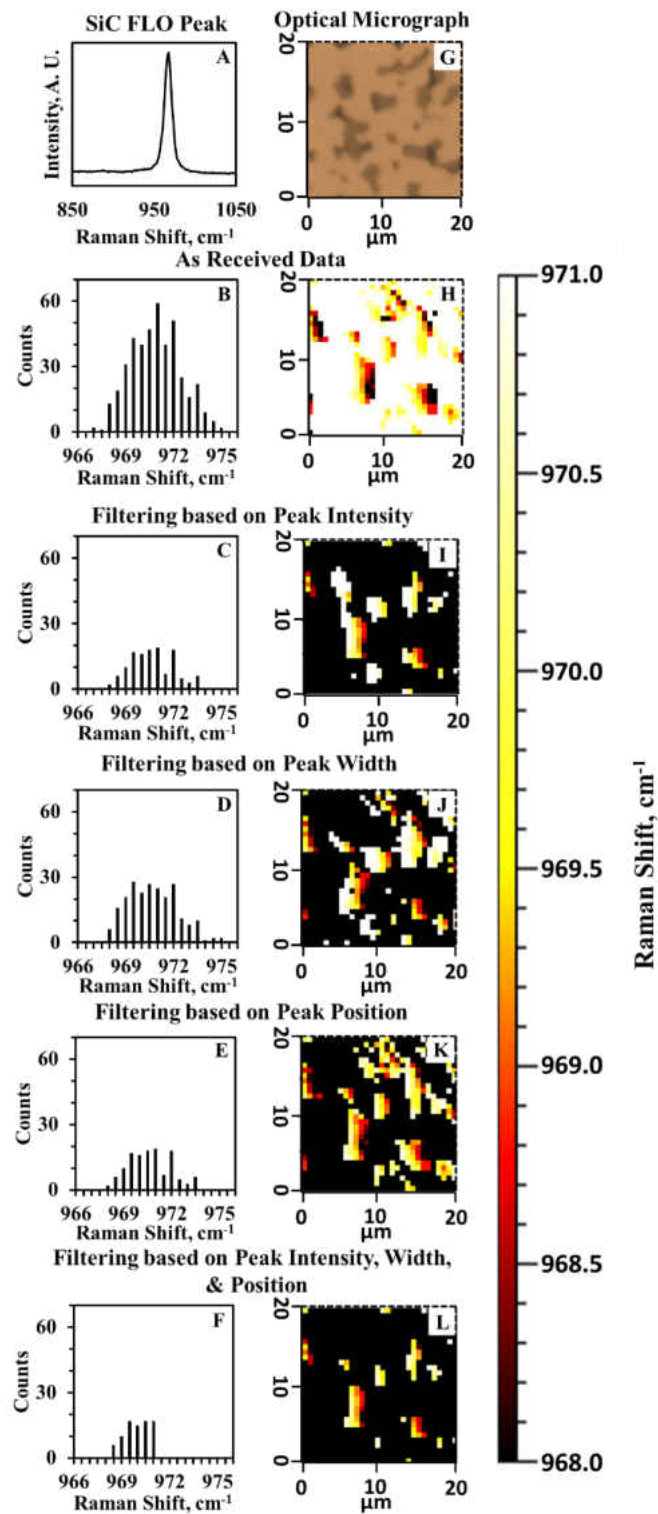


Figure 85:  $\text{ZrB}_2\text{-17vol\%SiC}$  distribution of peak position based on filtering



The choice of FLO SiC peak was made because of the most easy curve fitting procedure for this peak in comparison with other overlapping peaks of SiC phase. The collected data points were used to create intensity, Full Width at Half Maximum (FWHM), and peak position 2D maps. Before the three types of 2D maps were created for the four compositions, a procedure was established for the elimination of the non-representative data points collected during raw data collection, as the use of such data points resulted in a degradation of the quality of the maps. Therefore, the following procedure was developed to filter unwanted data points and improve the quality of the 2D maps that were used for the thermal residual stresses analysis in ZrB<sub>2</sub>-SiC ceramic composites. The procedure used for generation of such maps is described below. First all, as received data points were considered as valid and unfiltered 2D maps were created. An example of the distribution of the data points and a resulting 2D maps of FLO SiC peak position is shown in Figure 86H. This peak position map was created using all 900 data points, where the distribution/range of peak positions varied from 967cm<sup>-1</sup> to 975cm<sup>-1</sup>. Upon analysis of the individual data points, it was determined that some of these spectra did not provide a good representation of FLO SiC peak on the basis of both its intensity, FWHM, and positions and they were filtered out of the data pool. The filtering was performed based on the criteria for the peak intensity (Figure 86C), Peak Width at Half Maximum (Figure 86D), peak position (Figure 86E) and also when all three parameters (peak intensity, FWHM, and a peak position) were combined together and used for filtering of data for 2D map creation. The first filtering was performed using the intensity of the FLO peak as an indicator. In such peak intensity filtering the following criteria was used: if the intensity of the SiC peak in all four ceramics compositions was below 500 arbitrary units (a.u.) (on a scale 20-10000 a.u. intensity range) then the corresponding data point was

removed from the data set without further consideration. After such filtering, the range of the FLO peak positions decreased to 968-973.5 $\text{cm}^{-1}$  (Figure 86C). The filtered data was used for the FLO peak position 2D maps (Figure 86I). The next filtering step was to eliminate unsuitable peaks from the pool of data based on their peaks being too broad. The need for such filtering arose because of the automatic curve fitting where the program created data points even for the cases where peaks were not clearly present, thus creating broad and low intensity peaks. Peaks with a 9-12  $\text{cm}^{-1}$  Raman Shift Peak Width at Half Maximum were accepted as peaks belonging to SiC, and those broader than 12  $\text{cm}^{-1}$  were filtered out, leaving only 229 data points out of the total 900. The representative map of the peak position created using these 229 data points is shown in Fig. 2J. Similar filtering, based on the peak position of the FLO SiC peak was 968-971  $\text{cm}^{-1}$ . This procedure eliminated another 661 data points, thus leaving only 239 data points in the pool after peak position filtering. The last filtering, presented in Fig. 2F, was performed using a combination of peak intensity, Peak Width at Half Maximum, and peak position criteria, where 818 data points were eliminated, and those FLO SiC peaks that were used were found to be in the 968.5–971  $\text{cm}^{-1}$  Raman shift range. Based on the above filtering, a 2D map of the SiC peak position, using only these 82 data points was generated (Figure 86L). By comparing all 5 maps created using the different subsets of the data points, it was concluded that the 2D map (Figure 86L) created by using the last filtering procedure (Figure 86F), best represented the corresponding optical image. Therefore, the procedure was adopted to be used for all further 2-D maps presented in this paper.

### **3.3.3: 2D Raman Maps: Peak Intensity, Peak Width, and Peak Position**

The optical micrographs of the pure SiC (Figure 86A), and ZrB<sub>2</sub>-SiC (17, 32, and 45vol%) (Figure 86E, I, and M, respectively) are shown in Figure 86. The corresponding 2D map of the peak

intensity, peak width, and peak position of all four ceramics are shown below the corresponding optical images.

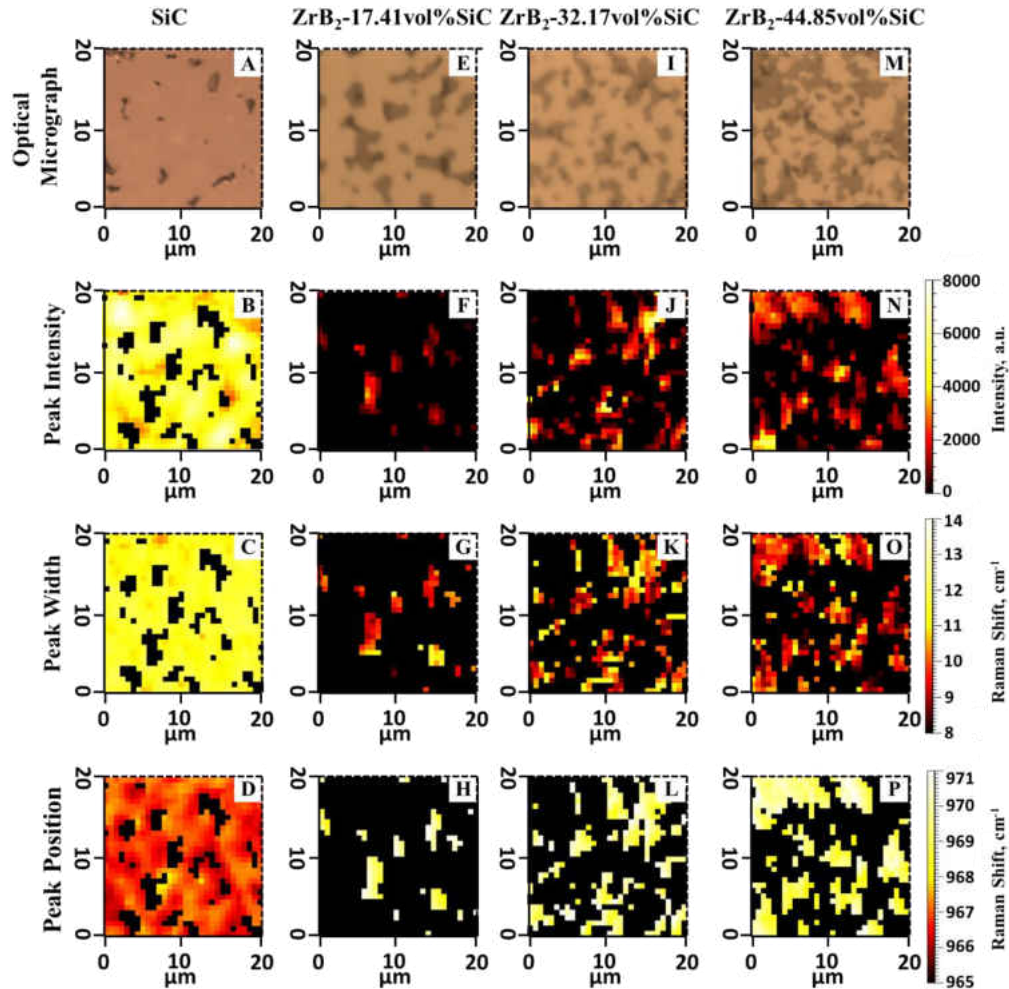


**Figure 86: Comparison of pure SiC, and ZrB<sub>2</sub>-SiC composites: SiC (A) optical image, (B) Peak Intensity map, (C) Peak Width map, (D) Peak Position map, ZrB<sub>2</sub>-17vol%SiC (E) optical image, (F) Peak Intensity map, (G) Peak Width map, (H) Peak Position map; ZrB<sub>2</sub>-32vol%SiC (I) optical image, (J) Peak Intensity map, (K) Peak Width map (L) Peak Position map; ZrB<sub>2</sub>-45vol%SiC (M) optical image, (N) Peak Intensity map, (O) Peak Width map, (P) Peak Position map**

All four 2D maps of the peak intensity of FLO SiC peak are presented using the same intensity scale, which is shown on the right side of the maps. The intensity of the FLO peak is the highest in the case of pure SiC and the lowest in the case of the ZrB<sub>2</sub>-17vol%SiC, while changing in the

composition from 17vol% to 32vol% to 45vol% of SiC content in ZrB<sub>2</sub>-SiC ceramic composite. The Peak Width at Half Maximum is also the broadest for pure SiC (11-12 cm<sup>-1</sup>), but decreased to a much lower values of 8-10 cm<sup>-1</sup> when SiC grains are surrounded by a ZrB<sub>2</sub> matrix in the ZrB<sub>2</sub>-SiC composites. A similar trend can be seen for the 2D maps of the FLO peak position, which will be used for the calculation of the thermal residual stresses in the composite.

### **3.3.4: Calculation of Thermal Residual Stresses in SiC Grains of ZrB<sub>2</sub>-SiC Ceramic Composites Based on Previously Published SiC Piezospectroscopy Coefficients**

The FLO peak position in pure SiC is shifted to a wavenumber of 966.01±0.6cm<sup>-1</sup> and, as it is single phase SiC, we can assume it does not possess thermal residual stresses caused by the mismatch of the properties of two different phases. At the same time, the FLO position of SiC is shifted to the higher wavenumbers in the case of ZrB<sub>2</sub>-SiC ceramic composites. The average shift is > 3 Raman wavenumbers from 966.01cm<sup>-1</sup> in pure SiC to higher than 969cm<sup>-1</sup> in ZrB<sub>2</sub>-SiC ceramics. The data on peak position is presented in Table 17 and the graphical representation of these results is shown in Figure 87A (shown as the circles).

**Table 17: Thermal Residual Stresses in SiC estimated from the shift in the FLO peak position of 6H-SiC using both theoretically calculated and experimentally measured piezospectroscopic coefficients**

| Composition                 | Volume Percent SiC (%) | Average SiC FLO Peak Position (cm <sup>-1</sup> ) | $\Delta\nu$ (cm <sup>-1</sup> ) | Measured value based on [220] (MPa) | Measured value based on [219] (MPa) | Calculated value based on [199] (MPa) | Calculated value based on [201] (MPa) |
|-----------------------------|------------------------|---------------------------------------------------|---------------------------------|-------------------------------------|-------------------------------------|---------------------------------------|---------------------------------------|
| SiC                         | 100                    | 966±0.6                                           | 0                               | 0                                   | 0                                   | 0                                     | 0                                     |
| ZrB <sub>2</sub> -17vol%SiC | 17                     | 969.72±0.8                                        | 3.706±0.004                     | -866±238                            | -937±263                            | -1495                                 | -955                                  |
| ZrB <sub>2</sub> -32vol%SiC | 32                     | 969.67±0.8                                        | 3.656±0.004                     | -854±231                            | -925±255                            | -1233                                 | -748                                  |
| ZrB <sub>2</sub> -45vol%SiC | 45                     | 969.41±0.7                                        | 3.396±0.003                     | -794±225                            | -859±249                            | -1002                                 | -582                                  |

Besides the experimental peak positions we also show calculated peak positions calculated using theoretical values of thermal residual stresses. Using the value of the thermal residual stresses in SiC grains for the three ZrB<sub>2</sub>-SiC (17, 32, and 45vol%) ceramic composites by Eqns. (53)-(55), the FLO SiC peak positions were back calculated using Eqns. (78) and (79) in order to compare the peak positions both experimentally measured and predicted by theory [201, 219, 220]. Using the FLO SiC peak positions of pure SiC 966.01±0.6cm<sup>-1</sup> as the zero stress peak position, the peak position in the three ceramic composites were calculated and are shown in Figure 87A.

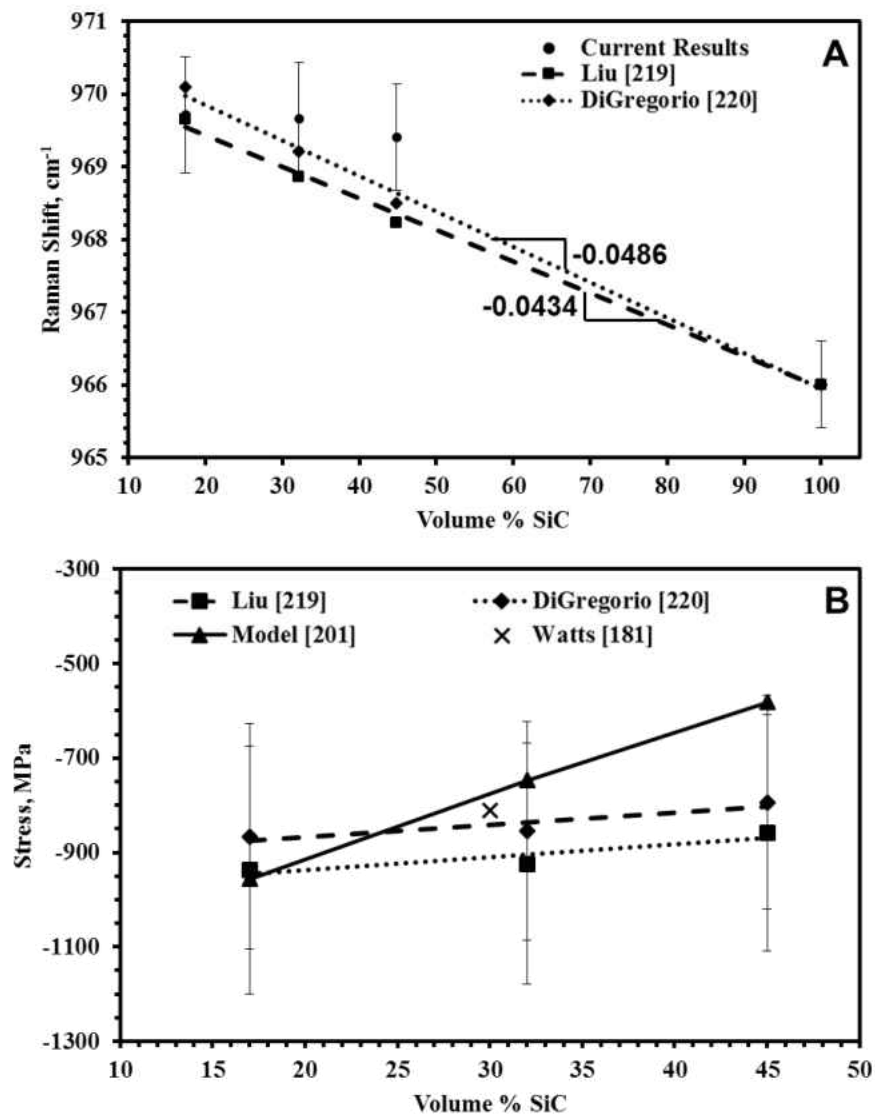


**Figure 87: Comparison of Raman peak position measured and calculated for different volume fractions of SiC (A) and thermal residual stresses of ZrB<sub>2</sub>-SiC ceramic composites calculated using experimental peak positions and the model [201] along with calculated thermal residual stress of ZrB<sub>2</sub>-30vol%SiC [181] (B), two piezospectroscopic coefficients were used [219, 220].**

Along with the data obtained from 2D maps shown in Figure 86D, H, L, and P, which show a matching trend with similar results published in Ref. [261]. From the comparison of both

experimental and theoretical results, there is a rather good correspondence, and the values of piezospectroscopy coefficients are rather close to each other.

Based on the Raman shift of measured 6H-SiC FLO peak position, the thermal residual stresses were calculated using piezospectroscopy coefficients measured in [219, 220]. One of the piezospectroscopy coefficients was presented by a quadratic equation as shown below in Eqn. (78) [219], and another one was measured to be equal to  $4.28 \pm 0.22 \text{ cm}^{-1}\text{GPa}^{-1}$  [220]:

$$\omega_{LO} = 970.1 + 3.83P - 0.013P^2 \quad (78)$$

where  $\omega_{LO}$  is the frequency of the FLO mode of SiC in the ZrB<sub>2</sub>-SiC composites  $970.1\text{cm}^{-1}$  is the zero-stress frequency of the FLO mode, and P is the stress in GPa. Then the following procedure was used to estimate thermal residual stresses in three ZrB<sub>2</sub>-SiC ceramic composites, as described below. Eqn. (78) was modified in the way that the frequency of the FLO Raman mode of SiC at zero stress, presented in the equation as  $970.1\text{cm}^{-1}$  was replaced by  $966.01 \pm 0.6\text{cm}^{-1}$  as measured in our own experiments on pure SiC. This discrepancy between published value [219] and our own measurements can be attributed to the differences in the SiC materials used in these experiments, but also the use of two completely different spectrometers. That is why the observed difference in three wavenumbers are not really significant, however, we used experimentally measured values to perform more precise evaluations. Then the  $\Delta\omega_{LO}$  was calculated as the difference between peak position of FLO SiC peak for pure SiC and the three ZrB<sub>2</sub>-SiC ceramic composites, then Eqn. (78) was used to obtain the stress value. The results are presented in Figure 87B (shown as the squares) and the numerical values of stresses are listed in the Table 17.

To calculate the thermal residual stress using the piezospectroscopy coefficient from [220], a simplified approach was used and the thermal residual stress in pure SiC was assumed to be equal to zero, then the difference between FLO SiC peak positions of pure SiC  $966.01 \pm 0.6 \text{ cm}^{-1}$  and FLO SiC peak position of ZrB<sub>2</sub>-SiC (17, 32, and 45vol%) are given in Eqn. (79):

$$\Omega^{LO} - \Omega_0^{LO} = X(4.28 \pm 0.22) \text{ cm}^{-1} \text{ GPa}^{-1} \quad (79)$$

where  $\Omega^{LO}$  and  $\Omega_0^{LO}$  are the frequencies of the FLO mode with (ZrB<sub>2</sub>-SiC) and without (pure SiC) respectively, and X is the calculated stress in GPa. Then, the equation was solved for X and the calculated data are presented in Figure 87B (shown as the diamond) and the numerical values are given in Table 17. The values of thermal compressive residual stress in SiC grains were calculated to be equal to -793.56 to -865.97 MPa and -858.6 to -937.2 using two different piezospectroscopy coefficients as given in Refs.[219, 220] respectively, which showed rather close values. A similar value of the compressive residual stresses in SiC grains of ZrB<sub>2</sub>-30vol%SiC ceramic composites is reported, where the stress equal to 810 MPa was measured by using Raman spectroscopy [181] and shown graphically in Figure 87B.

For comparison, the values of estimated thermal residual stress in SiC grains using two different models [199, 201] and calculated using Eqn. (50) and Eqns. (53)-(55) are also presented in Table 17. The calculated stress given by Eqn. (50) [199] provides overestimated values in comparison with the numbers obtained using Raman spectroscopy. Such an overestimate might be based on the fact that in the model used for the calculation, the matrix phase (ZrB<sub>2</sub>) fully surrounds the spherical particle (SiC), but in reality, ZrB<sub>2</sub>-SiC ceramic composite, even in a 17vol% of SiC phase, SiC grains are in contact with each other (Figure 77B). It is possible to expect that as the



amount of SiC increases, the continuous contact between SiC grains are established (Figure 77C and D). Thus it is necessary to use the properties of the ZrB<sub>2</sub>-SiC composite as a matrix phase instead of using the properties of pure ZrB<sub>2</sub>. If such an approach is used, the value of thermal residual compressive stresses decreases significantly from -1495; -1232; and -1002 MPa using properties of pure ZrB<sub>2</sub> phase as a matrix [6] to -1216; -804; and -518 MPa where the properties of the ZrB<sub>2</sub>-17vol%, 32vol%, 45vol% SiC matrix phase were derived using the rules of mixture approach, respectively. The calculations using Eqns. (53)-(55) [201] give a better approximation, but it shows slightly overestimated value of stress for the composite with 17vol%SiC phase. However, when amount of SiC phase increases in the composite, the calculated values become underestimated (Table 17). This is graphically shown in Figure 87B as the solid black line. The thermal residual stresses calculated from measured peak position shift using two piezospectroscopy coefficients and theoretical thermal residual stresses calculated using model presented in [201] exhibit good correspondence.

### **3.3.5: Determination of the Distribution of Thermal Residual Stresses and Resulting 2D Thermal Residual Stress Maps of ZrB<sub>2</sub>-SiC Ceramic Composites**

Once the piezospectroscopic coefficients are known, the average thermal residual stresses,  $\sigma_r$  in SiC grains of ceramic composites can easily be calculated by using the following:

$$\sigma_r = \frac{\Delta v}{\Pi} \quad (80)$$

For comparison, the theoretical values of the average thermal residual stresses were calculated using Eqn.(81) [201], and the elastic properties of pure ZrB<sub>2</sub> and pure SiC reported in [262]:

$$\sigma_r = -3f_m K^* (\alpha_m - \alpha_p) \Delta T \quad (81)$$

where  $f_m$  is the volume fraction of matrix phase in the composite,  $K^*$  is the effective bulk modulus defined in Eqn. (82),  $\alpha$  is the CTE,  $\Delta T$  is the temperature change between the sintering temperature and room temperature ( $\Delta T = -1930^\circ\text{C}$ ). The equation for the effective bulk modulus is expressed below:

$$K^* = \frac{K_m K_p}{K_p f_p + K_p f_p n_m + K_p n_m + K_m f_m n_m} \quad (82)$$

where  $K^*$  is the effective bulk modulus,  $K$  is the bulk modulus of the phases, and  $f_m$  and  $f_p$  are the volume fractions of the matrix and strengthening phases in the composite, respectively,  $n_m$  is defined in Eqn. (83):

$$n_m = \frac{2(1 - 2\nu_m)}{1 + \nu_m} \quad (83)$$

where  $\nu_m$  is the Poisson's ratio of the matrix phase. For experimental values of average thermal residual stresses in ZrB<sub>2</sub>-17, 32, and 45vol%SiC the four different piezospectroscopic coefficients were used. The results of such calculations are shown in Table 18. The best fit between experimental results and theoretically calculated values exists for the case when the piezospectroscopic coefficient of the specific composition was used to determine the experimental value of thermal residual stresses.

**Table 18: Calculated values of thermal residual stresses in SiC grains of three ZrB<sub>2</sub>-SiC ceramic composites using piezospectroscopic coefficients  $\Pi$  from Table 13 without external applied load**

| Composition                 | Thermal Residual Stresses (MPa) |                           |                                |                                |                                |                                          |
|-----------------------------|---------------------------------|---------------------------|--------------------------------|--------------------------------|--------------------------------|------------------------------------------|
|                             | Model [201]                     | Using $\Pi$ from Table 13 |                                |                                |                                | $\Pi = \#2,3,4$<br>Composition Dependent |
|                             |                                 | #1 SiC                    | #2 ZrB <sub>2</sub> -17vol%SiC | #3 ZrB <sub>2</sub> -32vol%SiC | #4 ZrB <sub>2</sub> -45vol%SiC |                                          |
| ZrB <sub>2</sub> -17vol%SiC | 956                             | 859±310                   | 895±323                        | 798±288                        | 842±304                        | 895±323                                  |
| ZrB <sub>2</sub> -32vol%SiC | 748                             | 850±256                   | 885±267                        | 790±238                        | 833±251                        | 790±238                                  |
| ZrB <sub>2</sub> -45vol%SiC | 582                             | 751±219                   | 783±228                        | 698±204                        | 736±215                        | 736±215                                  |

It means that  $\Pi_{ZrB_2-17vol\%SiC}$  coefficient was used to determine the experimental value of thermal residual stresses in ZrB<sub>2</sub>-17vol%SiC,  $\Pi_{ZrB_2-32vol\%SiC}$  was used for ZrB<sub>2</sub>-32vol%SiC, and  $\Pi_{ZrB_2-45vol\%SiC}$  was used for ZrB<sub>2</sub>-45vol%SiC. The corresponding experimental and theoretical values of thermal residual stresses along with their distribution are shown in Figure 88. For the determination of the statistical distribution of thermal residual stresses, the Raman spectra were collected from 100 randomly chosen single SiC grains. As the SiC grain size was on the average about 2 $\mu$ m, a laser spot of about 2 $\mu$ m (50X objective lens) used. The statistical distribution of the stresses is shown in Figure 88B, where the absolute values were taken to make the thermal residual stresses positive. The plots are presented as a normal distribution with the average values and standard deviations being equal to our experimental values (Figure 88A), with the absolute average values of the thermal residual stresses being the highest for ZrB<sub>2</sub>-17vol%SiC and the lowest one for ZrB<sub>2</sub>-45vol%SiC.

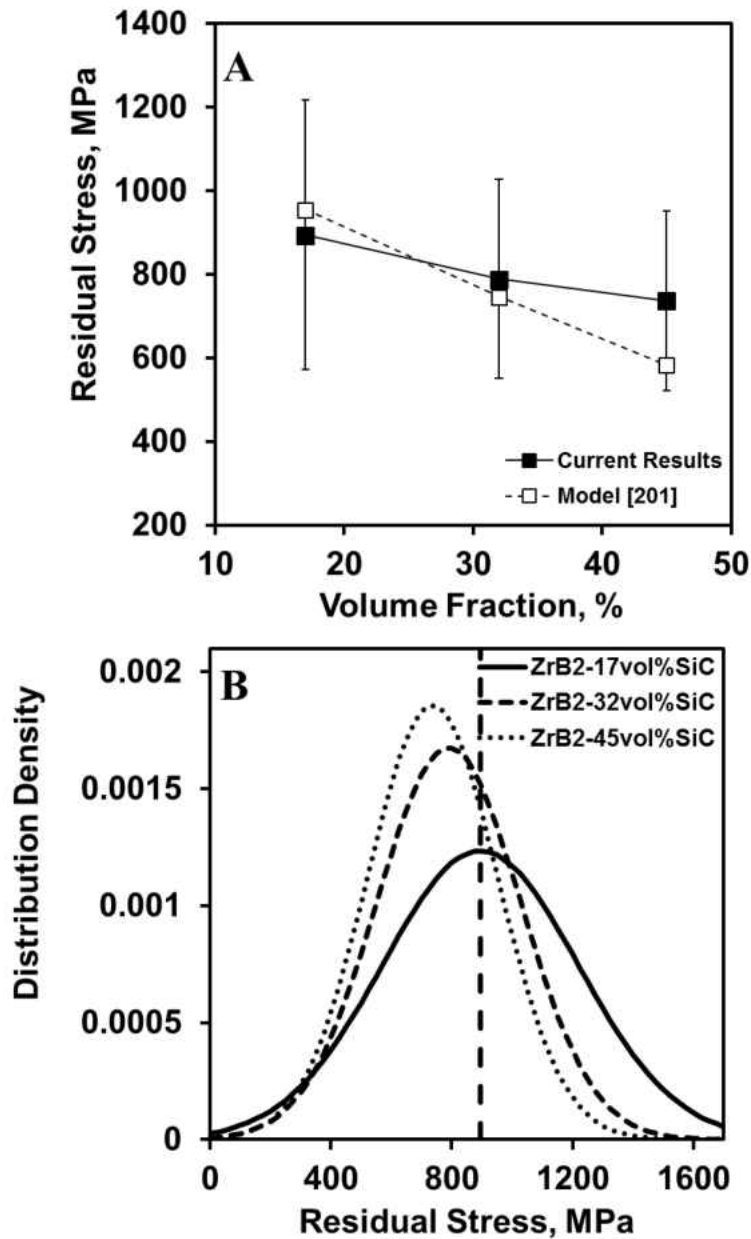


**Figure 88: Comparison of average thermal residual stresses (A), and distribution of thermal residual stresses of ZrB<sub>2</sub>-17, 32, and 45vol%SiC at 0 MPa applied load (B)**

Figure 89 shows 2D and line maps of the thermal residual stresses for selected areas at the surface of the ZrB<sub>2</sub>-SiC ceramic composites. The zero-stress 966cm<sup>-1</sup> FLO SiC peak position, measured positions of each point used in the map's creations, and the piezospectroscopy

coefficients obtained in this work were all used to calculate the thermal residual stresses. As the volume percentage of SiC phase increases in the ZrB<sub>2</sub>-SiC composites the average values of the thermal residual stresses decreases.

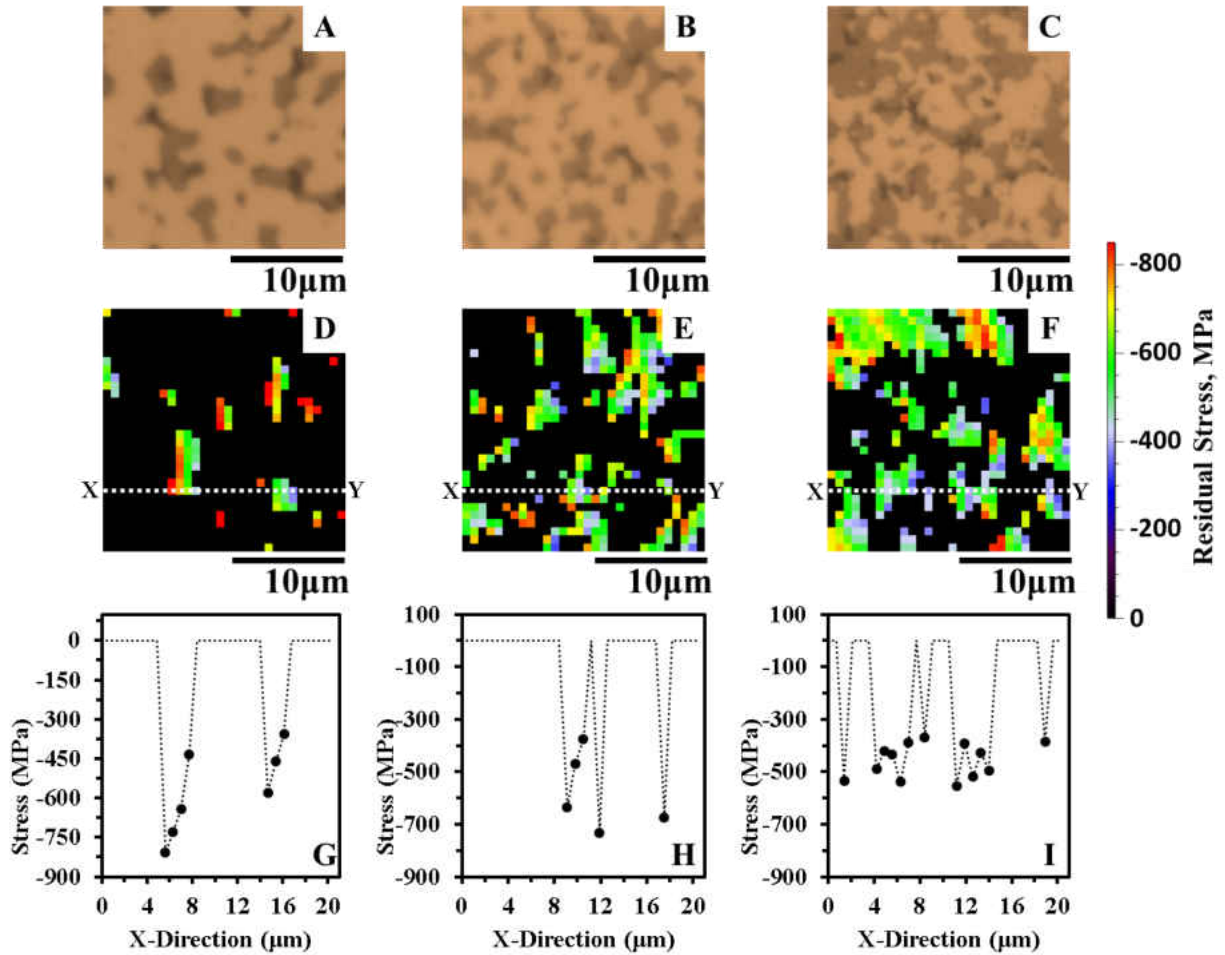


**Figure 89:** Optical micrographs of ZrB<sub>2</sub>-17vol%SiC (A), ZrB<sub>2</sub>-32vol%SiC (B), and ZrB<sub>2</sub>-45vol%SiC (C), the 2D maps of thermal residual stress in ZrB<sub>2</sub>-17vol%SiC (D), ZrB<sub>2</sub>-32vol%SiC (E), and ZrB<sub>2</sub>-45vol%SiC (F), and line maps along X-Y line of 2D maps for ZrB<sub>2</sub>-17vol%SiC (G), ZrB<sub>2</sub>-32vol%SiC (H), and ZrB<sub>2</sub>-45vol%SiC (I)

### **3.4: Statistical Distribution of Thermal Residual Stress in SiC Grains Under Applied Load in ZrB<sub>2</sub>-SiC Ceramic Composites**

In addition to measurements of thermal residual stresses where no external load was applied, experiments were performed to determine if and how an applied stress affects the statistical distribution of thermal residual stresses in ZrB<sub>2</sub>-SiC composites. In order to be able to estimate the effect of external stress, the ZrB<sub>2</sub>-SiC ceramic composites were loaded to 200 MPa and further to 300 MPa using 3-point bending and, while under constant stress, Raman spectra were collected from 100 randomly chosen SiC grains. The stresses were calculated using corresponding piezospectroscopic coefficients for each of the three ZrB<sub>2</sub>-17, 32, and 45 vol% SiC composites. The calculated stresses from the shift of the Raman peak contains two stress components – one contribution from the thermal residual stresses and other from the applied external load. Therefore, to determine the distribution of thermal residual stresses both as a function of the composition of ceramic and as a function of applied stress, the corresponding values of applied stress were subtracted from the stress calculated by Raman piezospectroscopy. The corresponding distributions of thermal residual stresses both under no stress and under 200 MPa and 300 MPa applied stress for three ZrB<sub>2</sub>-SiC ceramic composites are shown in Figure 90 and Table 19, no noticeable difference can be found between the distributions of stresses in each composite at different applied stresses. Thus the conclusion can be made that there is no redistribution of thermal residual stresses under applied load, when the applied stress is up to 300 MPa in tension.

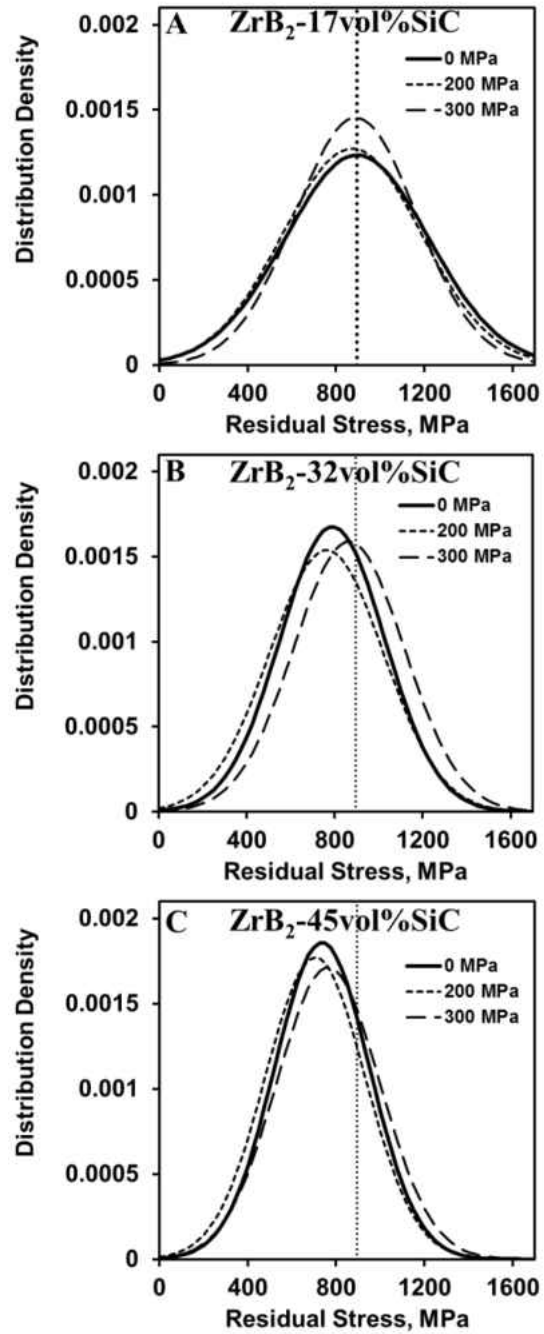


**Figure 90: Experimentally measured re-distribution of thermal residual stresses as a function of applied tensile stress for (A) ZrB<sub>2</sub>-17vol%SiC, (B) ZrB<sub>2</sub>-32vol%SiC, (C) ZrB<sub>2</sub>-45vol%SiC ceramic composites**

**Table 19: Calculated thermal residual stresses in SiC grains of three ZrB<sub>2</sub>-SiC ceramic composites as a function of applied bending stress**

| Composition                 | Thermal Residual Stress (MPa)        |                                        |                                        |
|-----------------------------|--------------------------------------|----------------------------------------|----------------------------------------|
|                             | $\sigma_{\text{appl}} = 0\text{MPa}$ | $\sigma_{\text{appl}} = 200\text{MPa}$ | $\sigma_{\text{appl}} = 300\text{MPa}$ |
| ZrB <sub>2</sub> -17vol%SiC | 895±323                              | 872±314                                | 889±274                                |
| ZrB <sub>2</sub> -32vol%SiC | 790±238                              | 763±260                                | 865±251                                |
| ZrB <sub>2</sub> -45vol%SiC | 736±215                              | 706±225                                | 765±233                                |

### **3.5: Mechanical Properties of the Produced SPS ZrB<sub>2</sub>-SiC Ceramic Composites**

The elastic properties of ZrB<sub>2</sub>-17, 32, and 45vol%SiC ceramic composites, measured Resonant Ultrasonic Spectroscopy (RUS) are shown in Figure 91. The Young's modulus decreases when the content of SiC phase is increased as shown in Figure 91A. This decrease is consistent with the rule of mixture as, for example, the Young's Modulus of ZrB<sub>2</sub> larger (520 GPa [262]) than that of the 6H-SiC phase (410 GPa [262]). At the same time, the Poission's ratio increases as the SiC content is increased, as the increasing amount of the more compliant SiC phase in the particulate composite shown in Figure 91A. The bulk and shear moduli as a function of volume percent of SiC is shown in Figure 91B. It shows that as the volume percent of SiC increases, the bulk and shear moduli values decreases. The measured properties correspond well with the previously reported data on similar composites [58, 65, 73, 83, 98, 114, 263].



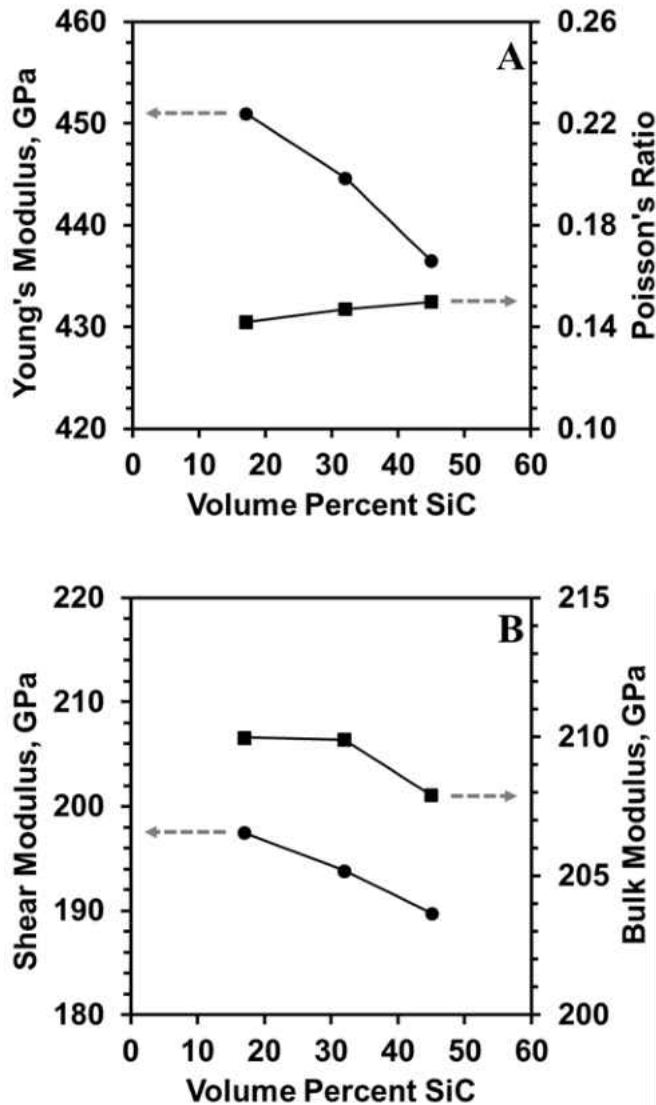


**Figure 91: Elastic properties: (A) Young's modulus and Poisson's ratio; (B) shear and bulk moduli of ZrB<sub>2</sub>-17, 32, and 45vol%SiC ceramic composites.**

The instantaneous strength and fracture toughness of ZrB<sub>2</sub>-SiC ceramic composites are shown in Figure 92. The 4-point bending strength values are shown in Figure 92A as a function of the composites' composition. The strength of the ZrB<sub>2</sub>-17vol%SiC and ZrB<sub>2</sub>-32vol%SiC composites are equal to 585±88 MPa, and 552±59 MPa, respectively, whereas the ZrB<sub>2</sub>-

45vol%SiC composite shows a significant improvement in strength, as the measured values are equal to  $751 \pm 81$  MPa. The fracture toughness of ZrB<sub>2</sub>-SiC ceramic composites is shown in Figure 92B as a function of composition, and the measured values are equal to  $2.54 \pm 0.29$  MPa·m<sup>1/2</sup>,  $2.64 \pm 0.27$  MPa·m<sup>1/2</sup>, and  $2.90 \pm 0.34$  MPa·m<sup>1/2</sup> for ZrB<sub>2</sub>-17, 32, and 45vol%SiC respectively.

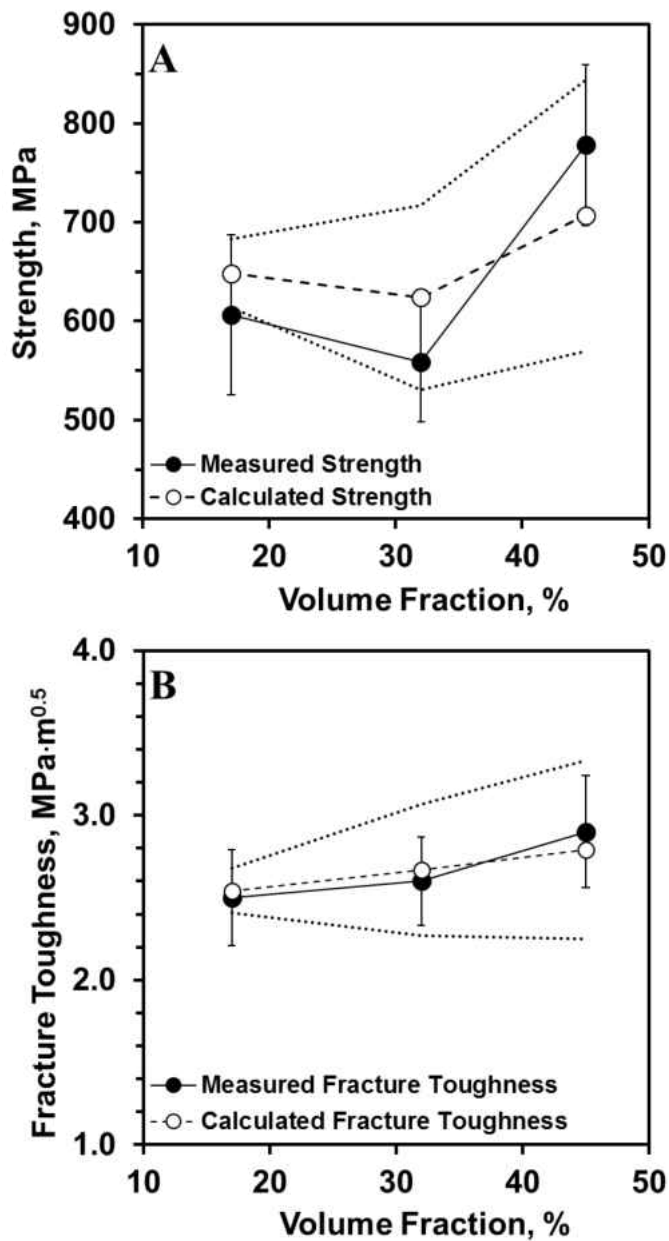


**Figure 92: 4-point bending strength (A) and fracture toughness (B) of ZrB<sub>2</sub>-17, 32, and 45vol%SiC ceramic composites. ● – measured values, ○ – estimated values accounting the effect of the thermal residual stresses in SiC grains, the dotted lines are the upper and lower bounds of uncertainty for the calculated values of fracture strength and fracture toughness.**

Thus, a slight increase in fracture toughness is observed when the SiC phase content is increased. As ZrB<sub>2</sub>-SiC ceramic composites are brittle materials, the strength of ZrB<sub>2</sub>-SiC could be described by the following well known equation:

$$\sigma_s = \frac{K_{1C}}{\psi\sqrt{a}} \quad (84)$$

where  $K_{1C}$  is the fracture toughness of the material;  $\psi$  is the geometrical coefficient dependent on the shape of the critical defect when  $\psi=1.264$  for the assumed to be semi-circular surface defect; and  $a$  is a radius of the surface critical defect that serves as the fracture origin during the failure event, The size of the critical defect  $a$  could be both evaluated using Eqn. (84), or it could be directly measured using the size of the fracture origin identified from the fracture surface by SEM. The calculated values were equal to 12  $\mu\text{m}$ , 14  $\mu\text{m}$ , and 9  $\mu\text{m}$  using Eqn. (84), while measured values using fractography results (Figure 93) were equal to 9.62  $\mu\text{m}$ , 11.44  $\mu\text{m}$ , and 9.75  $\mu\text{m}$  (Figure 93B, D, and F) for ZrB<sub>2</sub>-17, 32, and 45vol%SiC respectively, thus showing the excellent coincidence in both cases for the estimation of critical defect size in ZrB<sub>2</sub>-SiC ceramic composites.

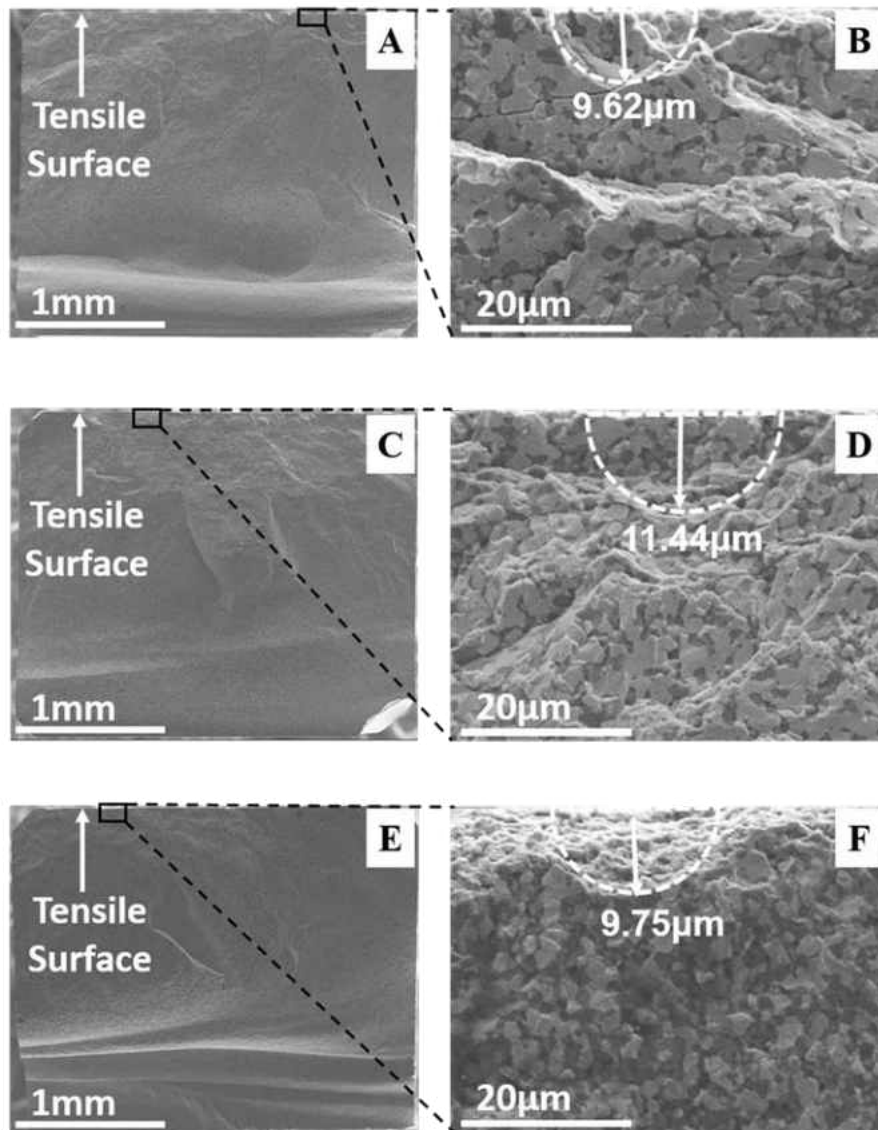


**Figure 93: Fractography of  $ZrB_2$ -SiC ceramic composites. SEM micrographs of the whole fracture surfaces with areas indicated for locations of possible fracture origins (A, C, E) and the micrographs of the fracture origins (B, D, F) of the  $ZrB_2$ -17vol%SiC (A, B);  $ZrB_2$ -32vol%SiC (C, D);  $ZrB_2$ -45vol%SiC (E, F) tested in 4-point bending.**

It was established in [240, 249] that when a crack propagates in two phase composites, an increase or decrease in fracture toughness could be achieved depending on the values of thermal effective residual stresses acting in the material [240, 249]. In our work we use the following Eqn:

$$\Delta K_{1c} = 2\sigma_{eff} \sqrt{\left(\frac{2(\Delta - d)}{\pi}\right)} \quad (85)$$

where  $\Delta K_{1c} = K_{1c} - K_0$  ( $K_0$  is the fracture toughness of the hypothetical matrix material when no residual stress is present, and  $K_{1c}$  is the fracture toughness of the particulate composite),  $\sigma_{eff}$  is an effective residual compressive stress components in the ZrB<sub>2</sub> matrix phase (while the average thermal residual stress state in the ZrB<sub>2</sub> matrix is still tensile),  $\Delta$  is an average near-neighbor distance between SiC grains, and  $d$  is the size of SiC grains. The average effective residual stress  $\sigma_{eff}$  in the matrix could be expressed by the following equation:

$$\sigma_{eff} = \sigma_r \left(\frac{\Delta}{d}\right)^{-3} \quad (86)$$

as the compressive component of residual stress in ZrB<sub>2</sub> matrix phase decreases with the third power of the distance from the center of the grain [249]. Thus the Eqn. (85) can be rewritten as:

$$\Delta K_{1c} = 2\sigma_r \left(\frac{\Delta}{d}\right)^{-3} \sqrt{\left(\frac{2(\Delta - d)}{\pi}\right)} \quad (87)$$

and than, the fracture toughness of ZrB<sub>2</sub>-SiC ceramic composites can be represented by:

$$K_{1c} = K_o + 2\sigma_r \left(\frac{\Delta}{d}\right)^{-3} \sqrt{\left(\frac{2(\Delta - d)}{\pi}\right)} \quad (88)$$

Using Eqn. (88), the fracture toughness of ZrB<sub>2</sub>-SiC ceramic composites can be evaluated and the calculated  $K_{1c}$  values can be compared with experimentally measured values in order to validate the proposed model. As most of the parameters in Eqn. (88) can be determined experimentally and

unknown  $K_0$  can be found by fitting the data, the model can be used to evaluate the increase in fracture toughness of ZrB<sub>2</sub>-SiC ceramic composite due to presence of thermal residual stresses. Note that  $\sigma_r$ ,  $\Delta$ , and  $d$  are all known parameters in Eqn (88) as their values for all three ZrB<sub>2</sub>-SiC compositions were measured and  $K_0$  was determined by fitting the calculated values of fracture toughness to the fracture toughness measured experimentally. The least-squares method was used to obtain the best fit, where the sum of squared residuals was minimized, where the residual is the difference between the measured and calculated (Eqn. (88))  $K_{IC}$  values. The values of  $\Delta$ ,  $d$ , and  $K_0$  are listed in Table 20. The calculated  $K_{IC}$  values obtained using Eqn (88) are shown in Figure 92B. As both  $\sigma_r$ ,  $\Delta$ , and  $d$  all have a statistical distribution of their values, as do the experimentally measured  $K_{IC}$  values, it is important to perform an error propagation or uncertainty analysis to determine the uncertainty in the calculated  $K_{IC}$  values. The standard deviation of calculated  $K_{IC}$  value could be determined using the following expression [264]:

$$StDev(K_{1C}) = \sqrt{\left[\frac{\partial K_{1C}}{\partial \sigma_r} * StDev(\sigma_r)\right]^2 + \left[\frac{\partial K_{1C}}{\partial \Delta} * StDev(\Delta)\right]^2 + \left[\frac{\partial K_{1C}}{\partial d} * StDev(d)\right]^2} \quad (89)$$

where  $\frac{\partial K_{1C}}{\partial \sigma_r}$ ,  $\frac{\partial K_{1C}}{\partial \Delta}$ , and  $\frac{\partial K_{1C}}{\partial d}$  are the partial derivatives of  $K_{IC}$  (88) with respect to  $\sigma_r$ ,  $\Delta$ , and  $d$ , respectively. By calculating the standard deviation of the variables in the parentheses of Eqn (89), the uncertainty of the  $K_{IC}$  values are shown in Figure 92B using the data for  $\sigma_r$ ,  $\Delta$ ,  $d$ , and  $K_0$  from Table 20. There is an excellent match between the measured and calculated fracture toughness of ZrB<sub>2</sub>-SiC ceramic composites.

**Table 20: The summary of the parameters used for the calculation of  $K_{1C}$  (Eqn. (88))**

| Composition                     | $K_{1C}^*$<br>(MPa*m <sup>1/2</sup> ) | $d^\dagger$ (μm) | $\Delta^\ddagger$ (μm) | $K_0^*$<br>(MPa*m <sup>1/2</sup> ) |
|---------------------------------|---------------------------------------|------------------|------------------------|------------------------------------|
| ZrB <sub>2</sub> -<br>17vol%SiC | 2.54±0.29                             | 1.48±1.0         | 5.36±2.85              | 2.48                               |
| ZrB <sub>2</sub> -<br>32vol%SiC | 2.64±0.27                             | 1.83±1.4         | 3.93±1.64              |                                    |
| ZrB <sub>2</sub> -<br>45vol%SiC | 2.9±0.34                              | 2.12±1.48        | 3.49±1.54              |                                    |

\* The  $K_{1C}$  is an experimentally measured fracture toughness

†  $d$  is an average size of SiC grains

‡  $\Delta$  is an average distance between SiC grains in ZrB<sub>2</sub>-SiC ceramic composites

\*  $K_0$  is a fracture toughness of an hypothetical ZrB<sub>2</sub> matrix material without residual stresses and  $\sigma_r$  values used in the  $K_{1C}$  calculation are taken from Table 19 corresponding to the data when  $\sigma_{app} = 0$  MPa.

The calculated fracture toughness, accounting for the presence of thermal residual stresses, showed an excellent correspondence with the experimentally measured results. These results were used to evaluate strength of the ZrB<sub>2</sub>-SiC ceramic composite using Eqn. (84) and estimate the surface critical defect size, which was assumed to be a constant for each composition. The calculated strength values are shown in Figure 92A. The uncertainty of strength values are also shown in Figure 92A as dotted lines, when the strength is calculated using Eqn (84) and uncertainty is determined using the following Eqn. (90) [264]:

$$StDev(\sigma) = \sqrt{\left[ \frac{\partial \sigma}{\partial K_{1C}} * StDev(K_{1C}) \right]^2} \quad (90)$$

As one can see from Figure 92A, there is good correlation between the calculated and experimental strength values can be found.

### **3.6: Sintering and Preliminary XRD Results of ZrB<sub>2</sub>-IrB<sub>2</sub>-SiC Ceramic Composites**

This section will cover the results of the sintering of ZrB<sub>2</sub>-5wt%IrB<sub>2</sub>-20wt%SiC ceramic composites and the X-Ray Diffraction (XRD) patterns of the produced composites.

#### **3.6.1: Spark Plasma Sintering of the ZrB<sub>2</sub>-IrB<sub>2</sub>-SiC Ceramic Composites**

In sintering the new ZrB<sub>2</sub>-2.1vol%IrB<sub>2</sub>-32vol%SiC one used the sintering properties to sintering the ZrB<sub>2</sub>-32vol%SiC ceramic composites. These parameters are 1950°C sintering temperature with 100°C/min heating/cooling rate, 20 minute dwell time, and 50MPa pressure. The shrinkage plot for these shrinkage parameters is shown below as Figure 94. One found that the sample melted and broke the graphite die being used during the sintering process. This was the so called first cycle of sintering as shown in the Figure 94A. Upon removal of the sample from the die one finds that mass of the sample decreased slightly. Which leads one to believe that some material have melting and left the sample during the sintering process. Since sintering of ZrB<sub>2</sub>-32vol%SiC did not have anything melting or reacting with the graphite die when it was sintered. Therefore, it lead to the concluding that the extra phase added in of IrB<sub>2</sub> is want melted. The sample was sintered again to make sure it was as dense as possible even though some of the material melted and was removed from the sample. This so call second cycle is shown below as Figure 94B.



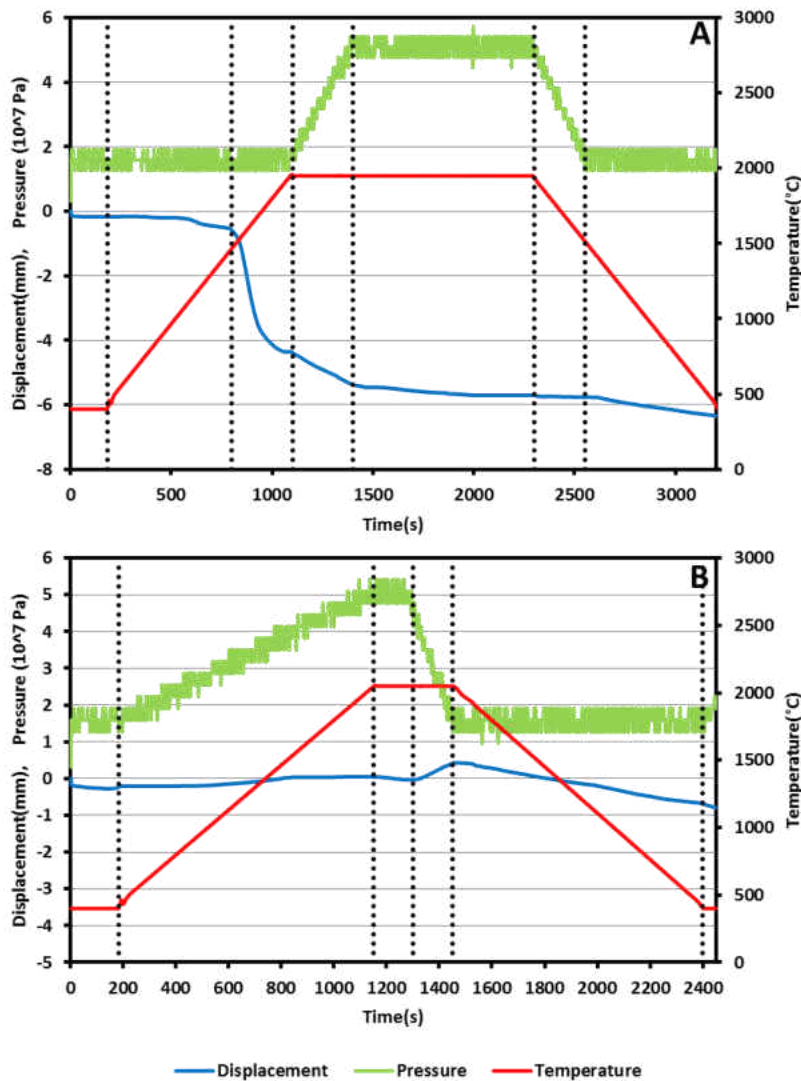


**Figure 94: Shrinkage plot for 1950 $^{\circ}$ C sintering temperature, 1<sup>st</sup> cycle (A), and 2<sup>nd</sup> cycle (B)**

Since the first sample melted at a sintering temperature of 1950 $^{\circ}$ C, one decided that a lower sintering temperature was necessary. In order to determine a lower sintering temperature one looked at the derivative of the displacement plot and found the maximum shrinkage occurred around 1500 $^{\circ}$ C. Naturally one choose this as the next sintering temperature. The shrinkage plot of this 1500 $^{\circ}$ C temperature, 5 minute dwell time is shown below as Figure 95.

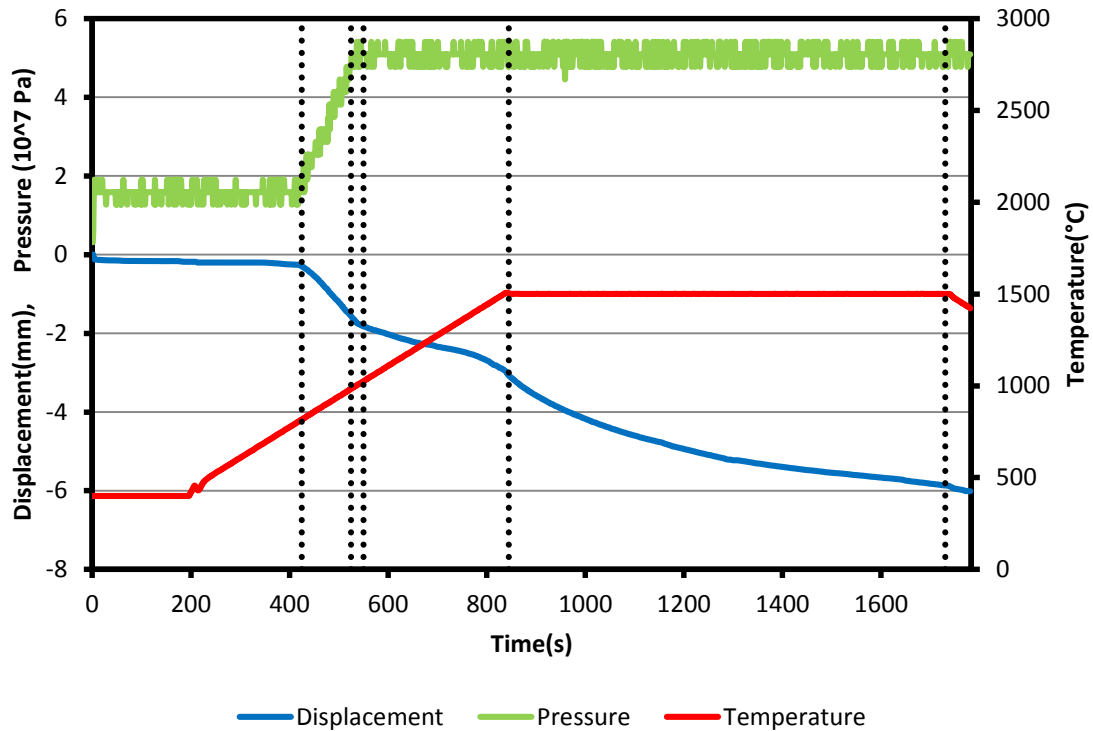


**Figure 95: Shrinkage plot for 1500 $^{\circ}$ C sintering temperature**

From this one can see looking at the displacement only that the sample is has not fully densified due to the small slope in the displacement plot. Thus, one decided to increase the sintering temperature to 1600 $^{\circ}$ C with a dwell time of 10 minutes. This shrinkage plot is shown below as Figure 96.

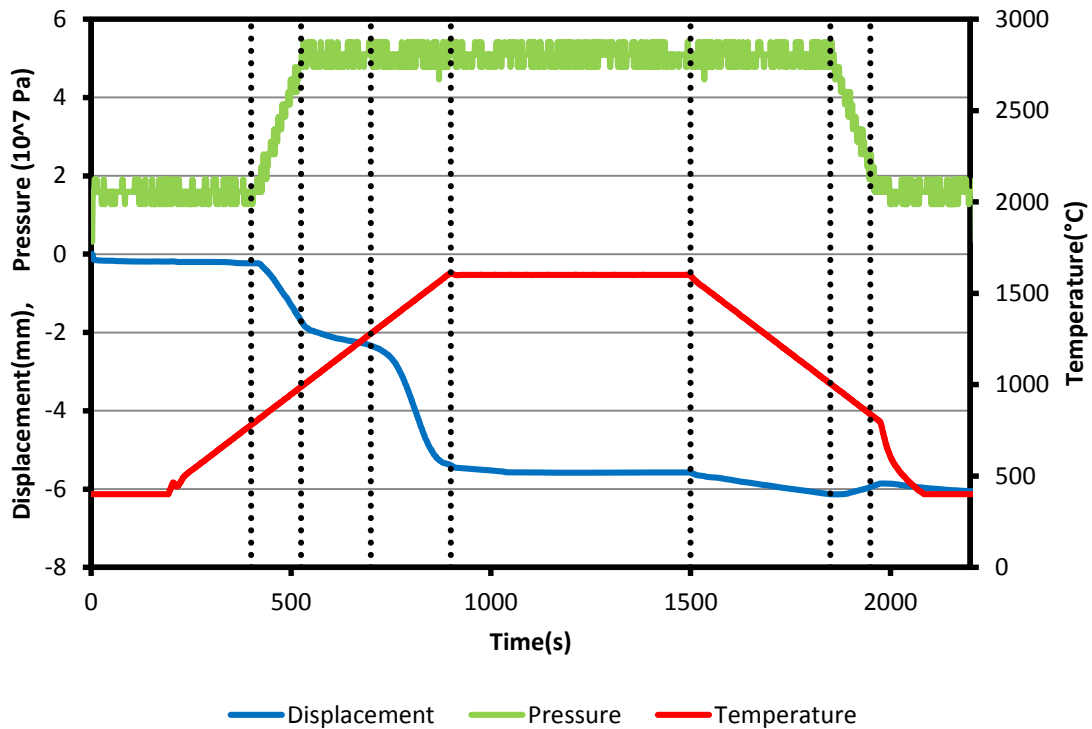


**Figure 96: Shrinkage plot for 1600°C sintering temperature**

To further determine the optimum sintering temperature of  $ZrB_2$ -2.1vol%IrB<sub>2</sub>-32vol%SiC one decided to investigate 1700°C for a sintering temperature. The shrinkage plot is shown below as Figure 97.

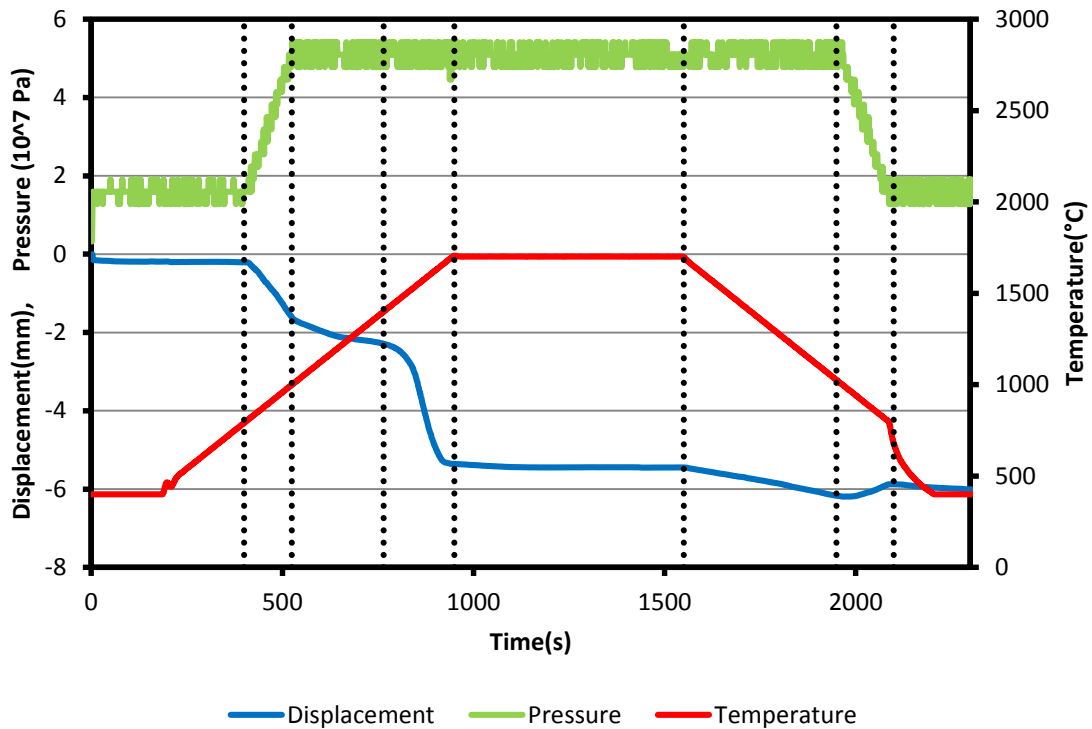


**Figure 97: Shrinkage plot for 1700°C sintering temperature**

The final sintering temperature investigated is 1800°C and the shrinkage plot is shown below as Figure 98. This final temperature was investigated to see the upper limit of sintering temperature at which the sample does not melt to the graphite die.

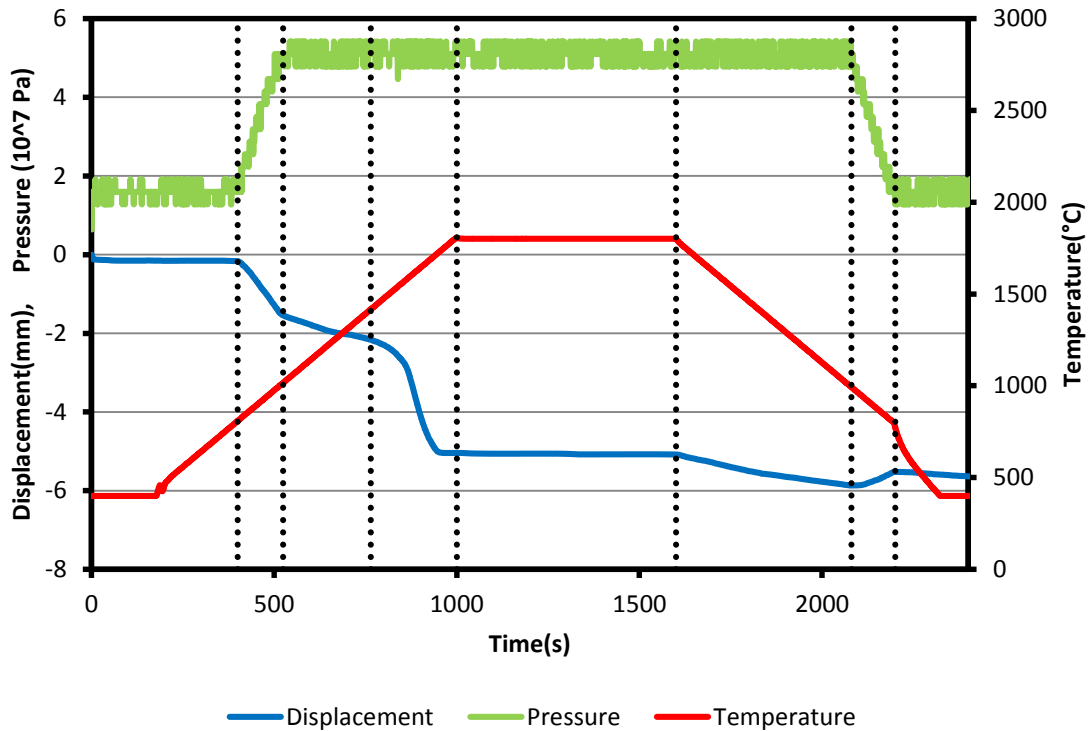


**Figure 98: Shrinkage plot for 1800°C sintering temperature**

One last sample was sintered at 1500°C sintering temperature, with the shrinkage plot shown below as Figure 99. The reason for sintering another the sample at 1500°C is to match the dwell times of 10 minutes for the other sintering temperature of 1600°C, 1700°C, and 1800°C. Upon looking at this shrinkage plot for this sample sintered at 1500°C and 10 minute dwell one see on the displacement plot that the has not fully occurred yet. There is a relatively large slope in the displacement plot which supports this. Therefore one can without a doubt determine that 1500°C is not the optimum sintering temperature. This suggests that there is some grain growth or some other mechanism causing the sample to not densify fully. Since when one looks at the shrinkage plot for 1500°C with 5 minutes dwell, Figure 95, one does not see this large slope one sees a nearly flat slope which suggest that the sample at 5 minute dwell has fully densified.

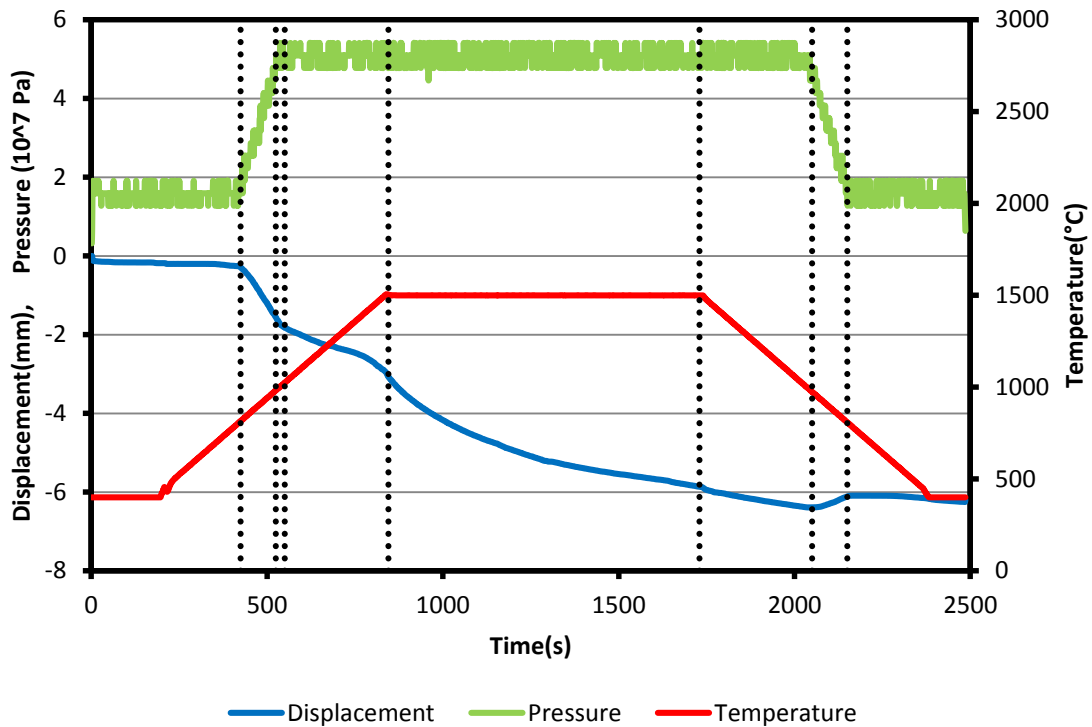


**Figure 99: Shrinkage plot for 1500°C sintering temperature with 10 minute dwell**

Once all of the sintering was completed one needed to determine what was the optimum sintering temperature and that is determined by finding the density and porosity of the sintered samples. The density was found using Archimedes method and is described in detail in the following ref. [265]. The results of the measured densities of the sintered samples are shown below as Table 21. The theoretical density was calculated using the rule of mixtures for  $ZrB_2$ -2.1vol% $IrB_{1.35}$ -32vol%SiC and was found to be  $5.28\text{g/cm}^3$ . The reason that one used  $IrB_{1.35}$  instead of  $IrB_2$  in calculating the theoretical density is because at the one does not know what phases of the Ir-B system are present. One can only guess that the phases present are: Ir, B, IrB,  $IrB_{1.1}$ ,  $IrB_{1.35}$ , and  $IrB_2$ . Thus one chooses  $IrB_{1.35}$  to be more conservative. Before the density was measured for the samples one grinded the graphite foal off the sample using 125, 75, 45, and  $30\mu\text{m}$  diamond discs. The porosity of the

samples were then calculated based on the measured density and the calculated theoretical density, with the results are also shown in below in Table 21. Upon looking at this Table 21 and comparing all of the results one finds that the sintering temperature with the lowest porosity and highest density is 1600°C. Thus, based on the sintering of 6 samples one has determined that the optimum sintering temperature is 1600°C with a dwell time of 10 minutes.

**Table 21: Density and porosity of ZrB<sub>2</sub>-5wt%IrB<sub>2</sub>-20wt%SiC ceramic composites sintered by SPS**

| Sintering Temperature (°C) | Dwell Time (mins.) | Density (g/cm <sup>3</sup> ) | Porosity (%) |
|----------------------------|--------------------|------------------------------|--------------|
| 1950                       | 20                 | 4.9596                       | 6.07%        |
| 1500                       | 5                  | 4.901                        | 7.18%        |
| 1600                       | 10                 | 4.9198                       | 6.82%        |
| 1700                       | 10                 | 4.911                        | 6.99%        |
| 1800                       | 10                 | 4.9164                       | 6.89%        |

### 3.6.2: XRD Patterns of the ZrB<sub>2</sub>-IrB<sub>2</sub>-SiC Ceramic Composites

In order to determine what phases are present in the newly sintered materials one conducted an XRD analysis of the two selected samples. The two samples were the one sample sintered at 1950°C and 1500°C. These two samples were chosen since they were the two extreme temperature that were used to sinter the samples. Another reason is that at the 1950°C temperature samples one would like to determine what exactly melted to the graphite die and with phase analysis using XRD one can be more certain as to what happened. One also choose 1500°C because one wants to make sure that IrB<sub>2</sub> phase was successfully sintered in the sample. The XRD plot is shown below as Figure 100 for the 1950°C sample;

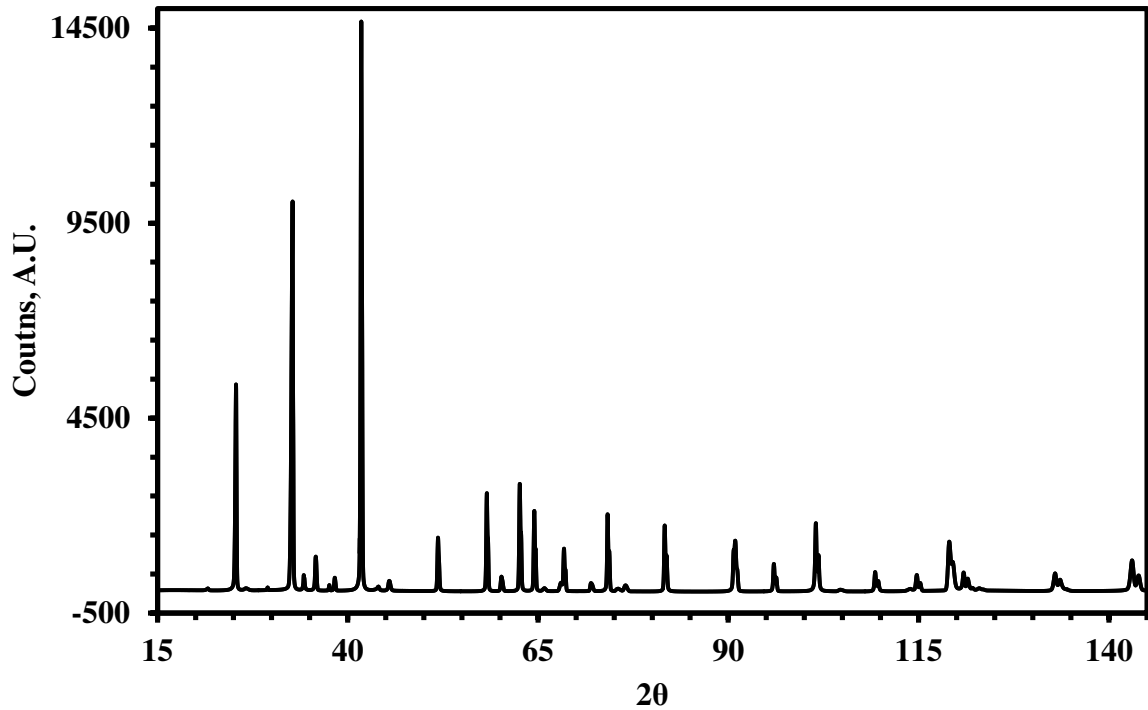


**Figure 100: XRD results for the 1950°C samples with phase identification**

The XRD plot below as Figure 101 for the 1500°C sample. Where in both figure the large sharp peaks are from the  $ZrB_2$  and  $SiC$  phases, while the lower intensity peaks are from the  $IrB_2$  phase. Refinement of these XRD patterns needs to be conducted in order to determine the phases present. This however will be for future work and will not be shown.



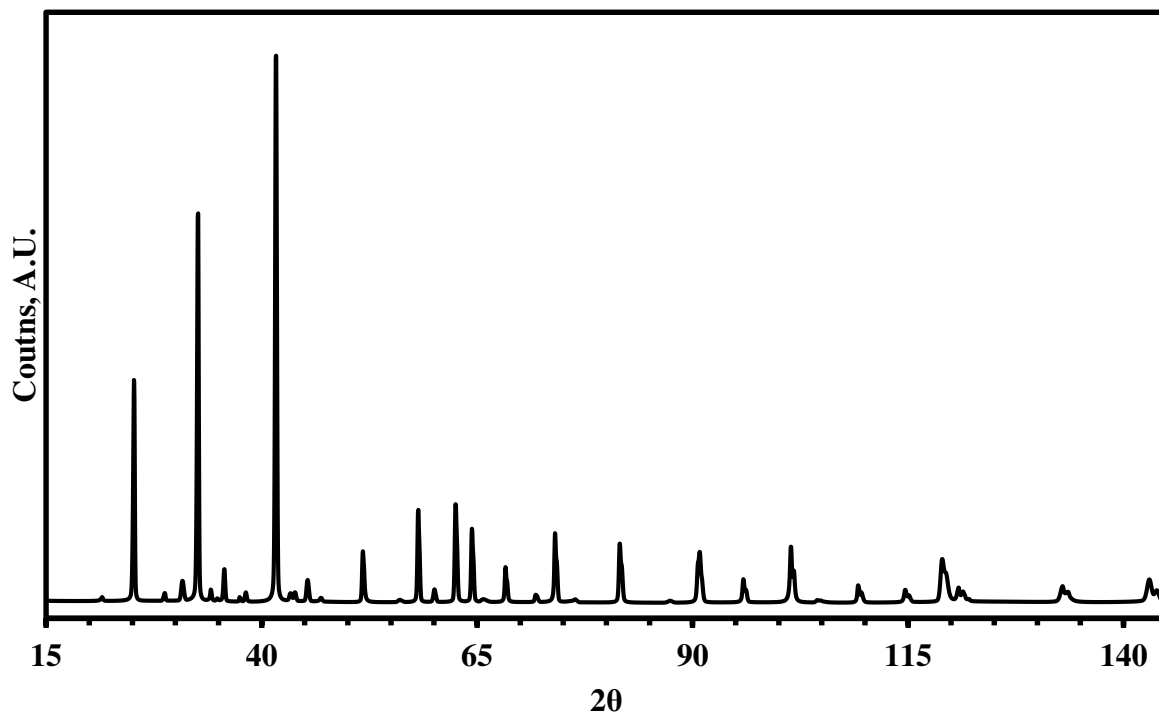


**Figure 101: XRD results for the 1500°C samples with phase identification**

## CHAPTER 4: CONCLUSIONS

ZrB<sub>2</sub>-SiC UTHC composites with applications for hypersonic vehicles as leading edges and nose cones were investigated. ZrB<sub>2</sub>-17, 32, and 45vol%SiC powders were sintered using SPS with a sintering temperature of 1950°C. The sintered samples were near fully dense, with porosity less than 4%. Pure SiC was also sintered using SPS in order to determine the piezospectroscopic coefficient of pure SiC and compare that to the piezospectroscopic coefficient of SiC in ZrB<sub>2</sub>-SiC ceramic composites. The pure SiC sintered samples have a porosity of ~30%. ZrB<sub>2</sub>-17, 32, and 45vol%SiC mechanical properties of fracture strength, fracture toughness, Young's modulus, shear modulus, bulk modulus, and Poisson's ratio were measured. The fracture strength was measured using 4-point bending and was found that as the percent SiC content is increased in the composites from ZrB<sub>2</sub>-17vol%SiC to ZrB<sub>2</sub>-45vol%SiC the fracture strength increased from 584±88 MPa to 751±81 MPa. The fracture toughness was determined using SEVNB and it was also found that as the percent SiC content is increased in the composites from ZrB<sub>2</sub>-17vol%SiC to ZrB<sub>2</sub>-45vol%SiC the fracture toughness increased from 2.54±0.29 MPa\*m<sup>1/2</sup> to 2.9±0.34 MPa\*m<sup>1/2</sup>. The elastic properties of Young's, shear, and bulk moduli as well as Poisson's ratio were all determined used RUS. For the ZrB<sub>2</sub>-SiC ceramic composites it was observed that as the percent SiC content was increased the values of bulk modulus as well as Poisson's ratio increased, while Young's and shear moduli decreased with increase of SiC content. The measured elastic properties of ZrB<sub>2</sub>-SiC ceramic composites range from 437-451 GPa for Young's modulus, 190-197 GPa for shear modulus, 208-210 GPa for bulk modulus, and 0.142-0.15 for Poisson's ratio.

Experiments were conducted to find the optimum parameters for collecting Raman maps on ZrB<sub>2</sub>-17vol%SiC ceramic composites using the Renishaw inVia microRaman. The parameters

of interest were: exposure time, scan type, resolution step size, and finally, the area of the map collected. Upon completion of the study we found that an exposure time of 30 seconds, with static scan type and 0.7 $\mu\text{m}$  or 0.5 $\mu\text{m}$  resolution step size achieved the best results. If the quality of the map is of importance and there is no significant time constraints to the map collection, one recommends 0.5 $\mu\text{m}$  step size as this gives the highest accuracy. But if time is of importance, then one recommends 0.7 $\mu\text{m}$  resolution step size, since this gives adequate accuracy while taking a lot less time to complete the collection of the data.

2D Raman maps of peak position, peak intensity, and Peak Width at Half Maximum of the Raman active and stress sensitive FLO SiC peak were taken. A filtering technique was used to improve the quality of the maps. Thermal residual stresses in ZrB<sub>2</sub>-SiC (17, 32, and 45vol%) were estimated using piezospectroscopic equations derived in other work by Liu [219] and by DiGregorio [220] and the measured peak positions taken from the obtained 2D Raman maps. These values were compared to the values of thermal residual stresses using the theoretical approaches developed by Chawla [199] and Sergio [201]. The measured values best match those calculated using the method in [201]. These calculated values of thermal residual stresses are -955 MPa, -748 MPa, and -582 MPa for ZrB<sub>2</sub>-17, 32, and 45vol%SiC respectively. Finally, the stressed peak positions were back calculated to compare to the measured values from the 2D Raman maps and those corresponding to the positions obtained from the theoretical equations.

The piezospectroscopic coefficients of SiC were investigated in pure SiC and ZrB<sub>2</sub>-SiC ceramic composites using an *it-situ* 3-point bending device. One determined the piezospectroscopic coefficient to be  $-5.94 \pm 3.278 \text{ GPa}^{-1} \cdot \text{cm}^{-1}$  for pure SiC,  $-5.7 \pm 2.99 \text{ GPa}^{-1} \cdot \text{cm}^{-1}$  for ZrB<sub>2</sub>-17vol%SiC,

$-6.39 \pm 3.52 \text{ GPa}^{-1} \cdot \text{cm}^{-1}$  for ZrB<sub>2</sub>-32vol%SiC, and  $-6.06 \pm 3.06 \text{ GPa}^{-1} \cdot \text{cm}^{-1}$  for ZrB<sub>2</sub>-45vol%SiC. It was determined that the overall piezospectroscopic coefficient to be used was pure SiC. Using the determined piezospectroscopic coefficient the thermal residual stresses were recalculated and were found to be  $-859 \pm 310 \text{ MPa}$ ,  $-850 \pm 256 \text{ MPa}$ , and  $-751 \pm 219 \text{ MPa}$  for ZrB<sub>2</sub>-17, 32, and 45vol%SiC respectively. These values were then compared to the previously used model by Sergio and excellent correspondence was observed. In addition to the calculated thermal residual stresses, 2D thermal stress maps were calculated using the 2D Raman peak positions maps. Additionally line maps were created at the same location for each of the 2D thermal stress maps to show the thermal residual stress distribution along the specified line. From this one can see that ZrB<sub>2</sub>-17vol%SiC had the highest thermal residual stresses with the least amount of SiC grains present; while ZrB<sub>2</sub>-45vol%SiC has the lowest thermal residual stresses with the highest count of SiC grains. ZrB<sub>2</sub>-32vol%SiC fell in between ZrB<sub>2</sub>-17 and 45vol%SiC when looking at the maximum value of thermal stresses and amount of SiC grains present. Using these maps a distribution of thermal residual stresses were produced using statistical analysis and assuming a normal distribution. From the results it was determined that the assumption of a normal distribution was correct.

The effect of applied load on the distribution of thermal residual stresses of SiC grains in ZrB<sub>2</sub>-17, 32, and 45vol%SiC ceramic composites were investigated. The results show that as tensile load is applied there is no re-distribution of thermal residual stresses in the three composites that were investigated. The effect of residual stress on the fracture strength and fracture toughness of ZrB<sub>2</sub>-17, 32, and 45vol%SiC were investigated. A simple model was developed to correlate the average thermal residual stresses to a predicted fracture toughness and then fracture. This was done

using the measured average SiC grain size, the average distance between near-neighboring SiC grains, and observed defects in ZrB<sub>2</sub>-17, 32, and 45vol%SiC ceramic composites. The fracture toughness and fracture strength values calculated using this simple model correlated well with those determined experimentally. The results for ZrB<sub>2</sub>-17, 32, and 45 vol%SiC ceramic composites show that they are indeed candidate materials for hypersonic vehicle applications.

The IrB<sub>2</sub> powders were produced using high-energy ball milling and were then combined with ZrB<sub>2</sub> and SiC powders to produce a new composite. This new ceramic composite of ZrB<sub>2</sub>-2.1vol%IrB<sub>2</sub>-32vol%SiC was sintered at different temperatures using SPS. The sintering at different temperatures was done to find the optimum sintering parameters that produced a composite with highest density. The optimum sintering temperature based on the current experiment was found to be 1600°C with a dwell time of 10 minutes. At this sintering temperature of 1600°C the porosity was found to be ~6.82%. The XRD patterns of the bulk of the samples sintered at 1500°C and 1950°C were collected to determine the phases present in the sample. The ground work for future work on the new ZrB<sub>2</sub>-2.1vol%IrB<sub>2</sub>-32vol%SiC has been laid with the successful sintering of this new composite. The future work will include fully characterizing the new material's mechanical and elastic properties, as well as to determine the effect of the new phase of IrB<sub>2</sub> on the thermal residual stresses of SiC in the new composite.

The following is suggested as future work: Test the ZrB<sub>2</sub>-17, 32, and 45vol%SiC in an arc-jet to determine the material performance in high enthalpy flow; which matches the heat transfer rates and flow conditions in hypersonic flight. The novel ZrB<sub>2</sub>-IrB<sub>2</sub>-SiC ceramic composite should be fully characterized by determining the following: the elastic properties, fracture strength and

toughness, microstructure, the phases present in the material, and finally the thermal residual stresses. Then test the novel  $\text{ZrB}_2\text{-IrB}_2\text{-SiC}$  ceramic composites in the arc-jet/heater at the same conditions as the  $\text{ZrB}_2\text{-SiC}$  ceramic composites and compare their performance. Specifically, the ablation rates and the thickness scale of the oxide layers.

## **APPENDIX: COPYRIGHT PERMISSION LETTERS**

Richard P Stadelmann  
12124 Fountainbrock Blvd Apt. 208  
Orlando, FL 32825

October 21, 2015

Dr. John D. Anderson Jr.  
Smithsonian National Air and Space Museum  
Independence Ave at 6<sup>th</sup> St, SW  
Washington, DC 20560

Dear Dr. Anderson:

I am completing a doctoral dissertation at the University of Central Florida entitled "ZrB<sub>2</sub>-SiC Based Ultra High Temperature Ceramic Composites: Mechanical Performance and Measurements and Design of Thermal Residual Stresses for Hypersonic Vehicle Applications" I would like your permission to reprint in my thesis/dissertation excerpts from the following:

J. D. Anderson, *Hypersonic and high temperature gas dynamics 2<sup>nd</sup> Edition*. Reston, Virginia :AIAA , 2006.

The excerpts to be reproduced are:

|              |              |
|--------------|--------------|
| Figure 1.13  | Figure 14.4b |
| Figure 1.14  | Figure 14.6  |
| Figure 1.16  | Figure 14.7  |
| Figure 1.18  | Figure 14.8a |
| Figure 1.19  | Figure 14.8b |
| Figure 1.20  | Figure 14.10 |
| Figure 2.2   | Figure 14.11 |
| Figure 2.4   | Figure 15.5  |
| Figure 11.9  | Figure 15.7  |
| Figure 14.3  | Figure 15.8  |
| Figure 14.4a | Figure 15.18 |

The requested permission extends to any future revisions and editions of my thesis/dissertation, including non-exclusive world rights in all languages. These rights will in no way restrict republication of the material in any other form by you or by others authorized by you. Your signing of this letter will also confirm that you own the copyright to the above-described material.



If these arrangements meet with your approval, please sign this letter where indicated below and return it to me in the enclosed return envelope. Thank you for your attention in this matter.

Sincerely,



Richard P Stadelmann

---

PERMISSION GRANTED FOR THE USE REQUESTED ABOVE: *FOR EDUCATIONAL*

By: *John D. Anderson Jr.*  
John D. Anderson Jr., PhD

*PURPOSES.*  
*JDA.*

Date: *Oct. 22, 2015*

**ELSEVIER LICENSE  
TERMS AND CONDITIONS**

Oct 21, 2015

---

This is a License Agreement between Richard Stadelmann ("You") and Elsevier ("Elsevier") provided by Copyright Clearance Center ("CCC"). The license consists of your order details, the terms and conditions provided by Elsevier, and the payment terms and conditions.

**All payments must be made in full to CCC. For payment instructions, please see information listed at the bottom of this form.**

|                                              |                                                                                                                                                                                           |
|----------------------------------------------|-------------------------------------------------------------------------------------------------------------------------------------------------------------------------------------------|
| Supplier                                     | Elsevier Limited<br>The Boulevard, Langford Lane<br>Kidlington, Oxford, OX5 1GB, UK                                                                                                       |
| Registered Company Number                    | 1982084                                                                                                                                                                                   |
| Customer name                                | Richard Stadelmann                                                                                                                                                                        |
| Customer address                             | 12124 Fountinabrook Blvd.<br>ORLANDO, FL 32825                                                                                                                                            |
| License number                               | 3733670582789                                                                                                                                                                             |
| License date                                 | Oct 21, 2015                                                                                                                                                                              |
| Licensed content publisher                   | Elsevier                                                                                                                                                                                  |
| Licensed content publication                 | Journal of the European Ceramic Society                                                                                                                                                   |
| Licensed content title                       | Thermodynamic approach to the vaporization and growth phenomena of SiC ceramics. I. SiC and SiC-SiO <sub>2</sub> mixtures under neutral conditions                                        |
| Licensed content author                      | G. Honstein, C. Chatillon, F. Baillet                                                                                                                                                     |
| Licensed content date                        | May 2012                                                                                                                                                                                  |
| Licensed content volume number               | 32                                                                                                                                                                                        |
| Licensed content issue number                | 5                                                                                                                                                                                         |
| Number of pages                              | 19                                                                                                                                                                                        |
| Start Page                                   | 1117                                                                                                                                                                                      |
| End Page                                     | 1135                                                                                                                                                                                      |
| Type of Use                                  | reuse in a thesis/dissertation                                                                                                                                                            |
| Intended publisher of new work               | other                                                                                                                                                                                     |
| Portion                                      | figures/tables/illustrations                                                                                                                                                              |
| Number of figures/tables/illustrations       | 1                                                                                                                                                                                         |
| Format                                       | both print and electronic                                                                                                                                                                 |
| Are you the author of this Elsevier article? | No                                                                                                                                                                                        |
| Will you be translating?                     | No                                                                                                                                                                                        |
| Original figure numbers                      | Figure 1                                                                                                                                                                                  |
| Title of your thesis/dissertation            | ZrB <sub>2</sub> -SiC BASED ULTRA HIGH TEMPERATURE CERAMIC COMPOSITES: MECHANICAL PERFORMANCE AND MEASUREMENT AND DESIGN OF THERMAL RESIDUAL STRESSES FOR HYPERSONIC VEHICLE APPLICATIONS |
| Expected completion date                     | Nov 2015                                                                                                                                                                                  |
| Estimated size (number of pages)             | 250                                                                                                                                                                                       |
| Elsevier VAT number                          | GB 494 6272 12                                                                                                                                                                            |
| Permissions price                            | 0.00 USD                                                                                                                                                                                  |
| VAT/Local Sales Tax                          | 0.00 USD / 0.00 GBP                                                                                                                                                                       |

**ELSEVIER LICENSE  
TERMS AND CONDITIONS**

Oct 21, 2015

This is a License Agreement between Richard Stadelmann ("You") and Elsevier ("Elsevier") provided by Copyright Clearance Center ("CCC"). The license consists of your order details, the terms and conditions provided by Elsevier, and the payment terms and conditions.

**All payments must be made in full to CCC. For payment instructions, please see information listed at the bottom of this form.**

|                                              |                                                                                                                                                                                           |
|----------------------------------------------|-------------------------------------------------------------------------------------------------------------------------------------------------------------------------------------------|
| Supplier                                     | Elsevier Limited<br>The Boulevard, Langford Lane<br>Kidlington, Oxford, OX5 1GB, UK                                                                                                       |
| Registered Company Number                    | 1982084                                                                                                                                                                                   |
| Customer name                                | Richard Stadelmann                                                                                                                                                                        |
| Customer address                             | 12124 Fountinabrook Blvd.<br>ORLANDO, FL 32825                                                                                                                                            |
| License number                               | 3733670693072                                                                                                                                                                             |
| License date                                 | Oct 21, 2015                                                                                                                                                                              |
| Licensed content publisher                   | Elsevier                                                                                                                                                                                  |
| Licensed content publication                 | Journal of the European Ceramic Society                                                                                                                                                   |
| Licensed content title                       | Surface densification of porous ZrB <sub>2</sub> -39mol.% SiC ceramic composites by a laser process                                                                                       |
| Licensed content author                      | Quentin Lonné, Nicolas Glandut, Pierre Lefort                                                                                                                                             |
| Licensed content date                        | April 2012                                                                                                                                                                                |
| Licensed content volume number               | 32                                                                                                                                                                                        |
| Licensed content issue number                | 4                                                                                                                                                                                         |
| Number of pages                              | 9                                                                                                                                                                                         |
| Start Page                                   | 955                                                                                                                                                                                       |
| End Page                                     | 963                                                                                                                                                                                       |
| Type of Use                                  | reuse in a thesis/dissertation                                                                                                                                                            |
| Intended publisher of new work               | other                                                                                                                                                                                     |
| Portion                                      | figures/tables/illustrations                                                                                                                                                              |
| Number of figures/tables/illustrations       | 1                                                                                                                                                                                         |
| Format                                       | both print and electronic                                                                                                                                                                 |
| Are you the author of this Elsevier article? | No                                                                                                                                                                                        |
| Will you be translating?                     | No                                                                                                                                                                                        |
| Original figure numbers                      | Figure 11                                                                                                                                                                                 |
| Title of your thesis/dissertation            | ZrB <sub>2</sub> -SiC BASED ULTRA HIGH TEMPERATURE CERAMIC COMPOSITES: MECHANICAL PERFORMANCE AND MEASUREMENT AND DESIGN OF THERMAL RESIDUAL STRESSES FOR HYPERSONIC VEHICLE APPLICATIONS |
| Expected completion date                     | Nov 2015                                                                                                                                                                                  |
| Estimated size (number of pages)             | 250                                                                                                                                                                                       |
| Elsevier VAT number                          | GB 494 6272 12                                                                                                                                                                            |
| Permissions price                            | 0.00 USD                                                                                                                                                                                  |
| VAT/Local Sales Tax                          | 0.00 USD / 0.00 GBP                                                                                                                                                                       |

**ELSEVIER LICENSE  
TERMS AND CONDITIONS**

Oct 23, 2015

---

This is a License Agreement between Richard Stadelmann ("You") and Elsevier ("Elsevier") provided by Copyright Clearance Center ("CCC"). The license consists of your order details, the terms and conditions provided by Elsevier, and the payment terms and conditions.

**All payments must be made in full to CCC. For payment instructions, please see information listed at the bottom of this form.**

|                                              |                                                                                                                                                                                           |
|----------------------------------------------|-------------------------------------------------------------------------------------------------------------------------------------------------------------------------------------------|
| Supplier                                     | Elsevier Limited<br>The Boulevard, Langford Lane<br>Kidlington, Oxford, OX5 1GB, UK                                                                                                       |
| Registered Company Number                    | 1982084                                                                                                                                                                                   |
| Customer name                                | Richard Stadelmann                                                                                                                                                                        |
| Customer address                             | 12124 Fountinabrook Blvd.<br>ORLANDO, FL 32825                                                                                                                                            |
| License number                               | 3734811435627                                                                                                                                                                             |
| License date                                 | Oct 23, 2015                                                                                                                                                                              |
| Licensed content publisher                   | Elsevier                                                                                                                                                                                  |
| Licensed content publication                 | Journal of the Less Common Metals                                                                                                                                                         |
| Licensed content title                       | Constitution diagrams of the binary systems Pd□B and Ir□B                                                                                                                                 |
| Licensed content author                      | H Ipsier, P Rogl                                                                                                                                                                          |
| Licensed content date                        | November–December 1981                                                                                                                                                                    |
| Licensed content volume number               | 82                                                                                                                                                                                        |
| Licensed content issue number                | n/a                                                                                                                                                                                       |
| Number of pages                              | 1                                                                                                                                                                                         |
| Start Page                                   | 363                                                                                                                                                                                       |
| End Page                                     | 0                                                                                                                                                                                         |
| Type of Use                                  | reuse in a thesis/dissertation                                                                                                                                                            |
| Portion                                      | figures/tables/illustrations                                                                                                                                                              |
| Number of figures/tables/illustrations       | 2                                                                                                                                                                                         |
| Format                                       | both print and electronic                                                                                                                                                                 |
| Are you the author of this Elsevier article? | No                                                                                                                                                                                        |
| Will you be translating?                     | No                                                                                                                                                                                        |
| Original figure numbers                      | Table 1 and Table 2                                                                                                                                                                       |
| Title of your thesis/dissertation            | ZrB <sub>2</sub> -SiC BASED ULTRA HIGH TEMPERATURE CERAMIC COMPOSITES: MECHANICAL PERFORMANCE AND MEASUREMENT AND DESIGN OF THERMAL RESIDUAL STRESSES FOR HYPERSONIC VEHICLE APPLICATIONS |
| Expected completion date                     | Nov 2015                                                                                                                                                                                  |
| Estimated size (number of pages)             | 250                                                                                                                                                                                       |
| Elsevier VAT number                          | GB 494 6272 12                                                                                                                                                                            |
| Permissions price                            | 0.00 USD                                                                                                                                                                                  |
| VAT/Local Sales Tax                          | 0.00 USD / 0.00 GBP                                                                                                                                                                       |
| Total                                        | 0.00 USD                                                                                                                                                                                  |

Richard P Stadelmann  
12124 Fountainbrook Blvd Apt. 208  
Orlando, FL 32825

October 21, 2015

Dr Zhilin Xie  
1713 Tealvriar Ave.  
Ovideo, FL 32765

Dear Dr. Xie:

I am completing a doctoral dissertation at the University of Central Florida entitled "ZrB<sub>2</sub>-SiC Based Ultra High Temperature Ceramic Composites: Mechanical Performance and Measurements and Design of Thermal Residual Stresses for Hypersonic Vehicle Applications" I would like your permission to reprint in my thesis/dissertation excerpts from the following:

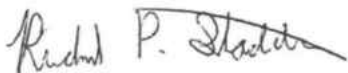
*Z. Xie, Rhenium, osmium and iridium diborides by mechanochemistry : synthesis, structure, thermal stability and mechanical properties: University of Central Florida, Orlando, FL, 2014.*

The excerpts to be reproduced are:  
Figure 13

The requested permission extends to any future revisions and editions of my thesis/dissertation, including non-exclusive world rights in all languages. These rights will in no way restrict republication of the material in any other form by you or by others authorized by you. Your signing of this letter will also confirm that you own the copyright to the above-described material.

If these arrangements meet with your approval, please sign this letter where indicated below and return it to me in the enclosed return envelope. Thank you for your attention in this matter.

Sincerely,



Richard P Stadelmann

---

PERMISSION GRANTED FOR THE USE REQUESTED ABOVE:

By:   
\_\_\_\_\_  
Zhilin Xie, PhD

Date: 10/21/2015

**ELSEVIER LICENSE  
TERMS AND CONDITIONS**

Oct 21, 2015

---

This is a License Agreement between Richard Stadelmann ("You") and Elsevier ("Elsevier") provided by Copyright Clearance Center ("CCC"). The license consists of your order details, the terms and conditions provided by Elsevier, and the payment terms and conditions.

**All payments must be made in full to CCC. For payment instructions, please see information listed at the bottom of this form.**

|                                              |                                                                                                                                                                                           |
|----------------------------------------------|-------------------------------------------------------------------------------------------------------------------------------------------------------------------------------------------|
| Supplier                                     | Elsevier Limited<br>The Boulevard, Langford Lane<br>Kidlington, Oxford, OX5 1GB, UK                                                                                                       |
| Registered Company Number                    | 1982084                                                                                                                                                                                   |
| Customer name                                | Richard Stadelmann                                                                                                                                                                        |
| Customer address                             | 12124 Fountinabrook Blvd.<br>ORLANDO, FL 32825                                                                                                                                            |
| License number                               | 3733241499751                                                                                                                                                                             |
| License date                                 | Oct 20, 2015                                                                                                                                                                              |
| Licensed content publisher                   | Elsevier                                                                                                                                                                                  |
| Licensed content publication                 | Diamond and Related Materials                                                                                                                                                             |
| Licensed content title                       | Tribochemical polishing CVD diamond film with FeNiCr alloy polishing plate prepared by MA-HPS technique                                                                                   |
| Licensed content author                      | Zewei Yuan, Zhuji Jin, Renke Kang, Quan Wen                                                                                                                                               |
| Licensed content date                        | January 2012                                                                                                                                                                              |
| Licensed content volume number               | 21                                                                                                                                                                                        |
| Licensed content issue number                | n/a                                                                                                                                                                                       |
| Number of pages                              | 8                                                                                                                                                                                         |
| Start Page                                   | 50                                                                                                                                                                                        |
| End Page                                     | 57                                                                                                                                                                                        |
| Type of Use                                  | reuse in a thesis/dissertation                                                                                                                                                            |
| Portion                                      | figures/tables/illustrations                                                                                                                                                              |
| Number of figures/tables/illustrations       | 1                                                                                                                                                                                         |
| Format                                       | both print and electronic                                                                                                                                                                 |
| Are you the author of this Elsevier article? | No                                                                                                                                                                                        |
| Will you be translating?                     | No                                                                                                                                                                                        |
| Original figure numbers                      | Figure 3                                                                                                                                                                                  |
| Title of your thesis/dissertation            | ZrB <sub>2</sub> -SiC BASED ULTRA HIGH TEMPERATURE CERAMIC COMPOSITES: MECHANICAL PERFORMANCE AND MEASUREMENT AND DESIGN OF THERMAL RESIDUAL STRESSES FOR HYPERSONIC VEHICLE APPLICATIONS |
| Expected completion date                     | Nov 2015                                                                                                                                                                                  |
| Estimated size (number of pages)             | 250                                                                                                                                                                                       |
| Elsevier VAT number                          | GB 494 6272 12                                                                                                                                                                            |
| Permissions price                            | 0.00 USD                                                                                                                                                                                  |
| VAT/Local Sales Tax                          | 0.00 USD / 0.00 GBP                                                                                                                                                                       |
| Total                                        | 0.00 USD                                                                                                                                                                                  |

**ELSEVIER LICENSE  
TERMS AND CONDITIONS**

Oct 21, 2015

This is a License Agreement between Richard Stadelmann ("You") and Elsevier ("Elsevier") provided by Copyright Clearance Center ("CCC"). The license consists of your order details, the terms and conditions provided by Elsevier, and the payment terms and conditions.

**All payments must be made in full to CCC. For payment instructions, please see information listed at the bottom of this form.**

|                                              |                                                                                                                                                                                           |
|----------------------------------------------|-------------------------------------------------------------------------------------------------------------------------------------------------------------------------------------------|
| Supplier                                     | Elsevier Limited<br>The Boulevard, Langford Lane<br>Kidlington, Oxford, OX5 1GB, UK                                                                                                       |
| Registered Company Number                    | 1982084                                                                                                                                                                                   |
| Customer name                                | Richard Stadelmann                                                                                                                                                                        |
| Customer address                             | 12124 Fountinabrook Blvd.<br>ORLANDO, FL 32825                                                                                                                                            |
| License number                               | 3733250256521                                                                                                                                                                             |
| License date                                 | Oct 20, 2015                                                                                                                                                                              |
| Licensed content publisher                   | Elsevier                                                                                                                                                                                  |
| Licensed content publication                 | Materials Chemistry and Physics                                                                                                                                                           |
| Licensed content title                       | Influence of spark plasma sintering temperature on electrochemical performance of La <sub>0.80</sub> Mg <sub>0.20</sub> Ni <sub>3.75</sub> alloy                                          |
| Licensed content author                      | Xiaoping Dong, Fanxiu Lü, Liying Yang, Yanghuan Zhang, Xinlin Wang                                                                                                                        |
| Licensed content date                        | 1 December 2008                                                                                                                                                                           |
| Licensed content volume number               | 112                                                                                                                                                                                       |
| Licensed content issue number                | 2                                                                                                                                                                                         |
| Number of pages                              | 7                                                                                                                                                                                         |
| Start Page                                   | 596                                                                                                                                                                                       |
| End Page                                     | 602                                                                                                                                                                                       |
| Type of Use                                  | reuse in a thesis/dissertation                                                                                                                                                            |
| Intended publisher of new work               | other                                                                                                                                                                                     |
| Portion                                      | figures/tables/illustrations                                                                                                                                                              |
| Number of figures/tables/illustrations       | 1                                                                                                                                                                                         |
| Format                                       | both print and electronic                                                                                                                                                                 |
| Are you the author of this Elsevier article? | No                                                                                                                                                                                        |
| Will you be translating?                     | No                                                                                                                                                                                        |
| Original figure numbers                      | Figure 1                                                                                                                                                                                  |
| Title of your thesis/dissertation            | ZrB <sub>2</sub> -SiC BASED ULTRA HIGH TEMPERATURE CERAMIC COMPOSITES: MECHANICAL PERFORMANCE AND MEASUREMENT AND DESIGN OF THERMAL RESIDUAL STRESSES FOR HYPERSONIC VEHICLE APPLICATIONS |
| Expected completion date                     | Nov 2015                                                                                                                                                                                  |
| Estimated size (number of pages)             | 250                                                                                                                                                                                       |
| Elsevier VAT number                          | GB 494 6272 12                                                                                                                                                                            |
| Permissions price                            | 0.00 USD                                                                                                                                                                                  |
| VAT/Local Sales Tax                          | 0.00 USD / 0.00 GBP                                                                                                                                                                       |

**JOHN WILEY AND SONS LICENSE  
TERMS AND CONDITIONS**

Oct 21, 2015

---

This Agreement between Richard Stadelmann ("You") and John Wiley and Sons ("John Wiley and Sons") consists of your license details and the terms and conditions provided by John Wiley and Sons and Copyright Clearance Center.

|                                       |                                                                                                                                                                                           |
|---------------------------------------|-------------------------------------------------------------------------------------------------------------------------------------------------------------------------------------------|
| License Number                        | 3733250503561                                                                                                                                                                             |
| License date                          | Oct 20, 2015                                                                                                                                                                              |
| Licensed Content Publisher            | John Wiley and Sons                                                                                                                                                                       |
| Licensed Content Publication          | Journal of the American Ceramic Society                                                                                                                                                   |
| Licensed Content Title                | Strength of Zirconium Diboride to 2300°C                                                                                                                                                  |
| Licensed Content Author               | Eric W. Neuman, Gregory E. Hilmas, William G. Fahrenholtz                                                                                                                                 |
| Licensed Content Date                 | Dec 12, 2012                                                                                                                                                                              |
| Pages                                 | 4                                                                                                                                                                                         |
| Type of use                           | Dissertation/Thesis                                                                                                                                                                       |
| Requestor type                        | University/Academic                                                                                                                                                                       |
| Format                                | Print and electronic                                                                                                                                                                      |
| Portion                               | Figure/table                                                                                                                                                                              |
| Number of figures/tables              | 2                                                                                                                                                                                         |
| Original Wiley figure/table number(s) | Figure 2 Figure 3                                                                                                                                                                         |
| Will you be translating?              | No                                                                                                                                                                                        |
| Title of your thesis / dissertation   | ZrB <sub>2</sub> -SiC BASED ULTRA HIGH TEMPERATURE CERAMIC COMPOSITES: MECHANICAL PERFORMANCE AND MEASUREMENT AND DESIGN OF THERMAL RESIDUAL STRESSES FOR HYPERSONIC VEHICLE APPLICATIONS |
| Expected completion date              | Nov 2015                                                                                                                                                                                  |
| Expected size (number of pages)       | 250                                                                                                                                                                                       |
| Requestor Location                    | Richard Stadelmann<br>12124 Fountinabrook Blvd.<br>Apt. 208<br><br>ORLANDO, FL 32825<br>United States<br>Attn: Richard Stadelmann                                                         |
| Billing Type                          | Invoice                                                                                                                                                                                   |
| Billing Address                       | Richard Stadelmann<br>12124 Fountinabrook Blvd.<br>Apt. 208<br><br>ORLANDO, FL 32825<br>United States<br>Attn: Richard Stadelmann                                                         |
| Total                                 | 0.00 USD                                                                                                                                                                                  |



**ELSEVIER LICENSE  
TERMS AND CONDITIONS**

Oct 21, 2015

This is a License Agreement between Richard Stadelmann ("You") and Elsevier ("Elsevier") provided by Copyright Clearance Center ("CCC"). The license consists of your order details, the terms and conditions provided by Elsevier, and the payment terms and conditions.

**All payments must be made in full to CCC. For payment instructions, please see information listed at the bottom of this form.**

|                                              |                                                                                                                                                                                           |
|----------------------------------------------|-------------------------------------------------------------------------------------------------------------------------------------------------------------------------------------------|
| Supplier                                     | Elsevier Limited<br>The Boulevard, Langford Lane<br>Kidlington, Oxford, OX5 1GB, UK                                                                                                       |
| Registered Company Number                    | 1982084                                                                                                                                                                                   |
| Customer name                                | Richard Stadelmann                                                                                                                                                                        |
| Customer address                             | 12124 Fountinabrook Blvd.<br>ORLANDO, FL 32825                                                                                                                                            |
| License number                               | 3733250701735                                                                                                                                                                             |
| License date                                 | Oct 20, 2015                                                                                                                                                                              |
| Licensed content publisher                   | Elsevier                                                                                                                                                                                  |
| Licensed content publication                 | Journal of the European Ceramic Society                                                                                                                                                   |
| Licensed content title                       | Mechanical behavior of zirconium diboride-silicon carbide ceramics at elevated temperature in air                                                                                         |
| Licensed content author                      | Eric W. Neuman, Gregory E. Hilmas, William G. Fahrenholtz                                                                                                                                 |
| Licensed content date                        | December 2013                                                                                                                                                                             |
| Licensed content volume number               | 33                                                                                                                                                                                        |
| Licensed content issue number                | 15-16                                                                                                                                                                                     |
| Number of pages                              | 11                                                                                                                                                                                        |
| Start Page                                   | 2889                                                                                                                                                                                      |
| End Page                                     | 2899                                                                                                                                                                                      |
| Type of Use                                  | reuse in a thesis/dissertation                                                                                                                                                            |
| Intended publisher of new work               | other                                                                                                                                                                                     |
| Portion                                      | figures/tables/illustrations                                                                                                                                                              |
| Number of figures/tables/illustrations       | 4                                                                                                                                                                                         |
| Format                                       | both print and electronic                                                                                                                                                                 |
| Are you the author of this Elsevier article? | No                                                                                                                                                                                        |
| Will you be translating?                     | No                                                                                                                                                                                        |
| Original figure numbers                      | Figures 6, 8, 9, and 10                                                                                                                                                                   |
| Title of your thesis/dissertation            | ZrB <sub>2</sub> -SiC BASED ULTRA HIGH TEMPERATURE CERAMIC COMPOSITES: MECHANICAL PERFORMANCE AND MEASUREMENT AND DESIGN OF THERMAL RESIDUAL STRESSES FOR HYPERSONIC VEHICLE APPLICATIONS |
| Expected completion date                     | Nov 2015                                                                                                                                                                                  |
| Estimated size (number of pages)             | 250                                                                                                                                                                                       |
| Elsevier VAT number                          | GB 494 6272 12                                                                                                                                                                            |
| Permissions price                            | 0.00 USD                                                                                                                                                                                  |
| VAT/Local Sales Tax                          | 0.00 USD / 0.00 GBP                                                                                                                                                                       |

**ELSEVIER LICENSE  
TERMS AND CONDITIONS**

Oct 21, 2015

---

This is a License Agreement between Richard Stadelmann ("You") and Elsevier ("Elsevier") provided by Copyright Clearance Center ("CCC"). The license consists of your order details, the terms and conditions provided by Elsevier, and the payment terms and conditions.

**All payments must be made in full to CCC. For payment instructions, please see information listed at the bottom of this form.**

|                                              |                                                                                                                                                                                           |
|----------------------------------------------|-------------------------------------------------------------------------------------------------------------------------------------------------------------------------------------------|
| Supplier                                     | Elsevier Limited<br>The Boulevard, Langford Lane<br>Kidlington, Oxford, OX5 1GB, UK                                                                                                       |
| Registered Company Number                    | 1982084                                                                                                                                                                                   |
| Customer name                                | Richard Stadelmann                                                                                                                                                                        |
| Customer address                             | 12124 Fountinabrook Blvd.<br>ORLANDO, FL 32825                                                                                                                                            |
| License number                               | 3733250832259                                                                                                                                                                             |
| License date                                 | Oct 20, 2015                                                                                                                                                                              |
| Licensed content publisher                   | Elsevier                                                                                                                                                                                  |
| Licensed content publication                 | Journal of the European Ceramic Society                                                                                                                                                   |
| Licensed content title                       | Compressive strength degradation in ZrB <sub>2</sub> -based ultra-high temperature ceramic composites                                                                                     |
| Licensed content author                      | J. Ramírez-Rico, M.A. Bautista, J. Martínez-Fernández, M. Singh                                                                                                                           |
| Licensed content date                        | June 2011                                                                                                                                                                                 |
| Licensed content volume number               | 31                                                                                                                                                                                        |
| Licensed content issue number                | 7                                                                                                                                                                                         |
| Number of pages                              | 8                                                                                                                                                                                         |
| Start Page                                   | 1345                                                                                                                                                                                      |
| End Page                                     | 1352                                                                                                                                                                                      |
| Type of Use                                  | reuse in a thesis/dissertation                                                                                                                                                            |
| Intended publisher of new work               | other                                                                                                                                                                                     |
| Portion                                      | figures/tables/illustrations                                                                                                                                                              |
| Number of figures/tables/illustrations       | 1                                                                                                                                                                                         |
| Format                                       | both print and electronic                                                                                                                                                                 |
| Are you the author of this Elsevier article? | No                                                                                                                                                                                        |
| Will you be translating?                     | No                                                                                                                                                                                        |
| Original figure numbers                      | Figure 7                                                                                                                                                                                  |
| Title of your thesis/dissertation            | ZrB <sub>2</sub> -SiC BASED ULTRA HIGH TEMPERATURE CERAMIC COMPOSITES: MECHANICAL PERFORMANCE AND MEASUREMENT AND DESIGN OF THERMAL RESIDUAL STRESSES FOR HYPERSONIC VEHICLE APPLICATIONS |
| Expected completion date                     | Nov 2015                                                                                                                                                                                  |
| Estimated size (number of pages)             | 250                                                                                                                                                                                       |
| Elsevier VAT number                          | GB 494 6272 12                                                                                                                                                                            |
| Permissions price                            | 0.00 USD                                                                                                                                                                                  |
| VAT/Local Sales Tax                          | 0.00 USD / 0.00 GBP                                                                                                                                                                       |

**ELSEVIER LICENSE  
TERMS AND CONDITIONS**

Oct 21, 2015

This is a License Agreement between Richard Stadelmann ("You") and Elsevier ("Elsevier") provided by Copyright Clearance Center ("CCC"). The license consists of your order details, the terms and conditions provided by Elsevier, and the payment terms and conditions.

**All payments must be made in full to CCC. For payment instructions, please see information listed at the bottom of this form.**

|                                              |                                                                                                                                                                                           |
|----------------------------------------------|-------------------------------------------------------------------------------------------------------------------------------------------------------------------------------------------|
| Supplier                                     | Elsevier Limited<br>The Boulevard, Langford Lane<br>Kidlington, Oxford, OX5 1GB, UK                                                                                                       |
| Registered Company Number                    | 1982084                                                                                                                                                                                   |
| Customer name                                | Richard Stadelmann                                                                                                                                                                        |
| Customer address                             | 12124 Fountinabrook Blvd.<br>ORLANDO, FL 32825                                                                                                                                            |
| License number                               | 3733250981176                                                                                                                                                                             |
| License date                                 | Oct 20, 2015                                                                                                                                                                              |
| Licensed content publisher                   | Elsevier                                                                                                                                                                                  |
| Licensed content publication                 | Journal of the European Ceramic Society                                                                                                                                                   |
| Licensed content title                       | Strength of hot pressed ZrB <sub>2</sub> -SiC composite after exposure to high temperatures (1000-1700°C)                                                                                 |
| Licensed content author                      | Manish Patel, J. Janardhan Reddy, V.V. Bhanu Prasad, Vikram Jayaram                                                                                                                       |
| Licensed content date                        | December 2012                                                                                                                                                                             |
| Licensed content volume number               | 32                                                                                                                                                                                        |
| Licensed content issue number                | 16                                                                                                                                                                                        |
| Number of pages                              | 13                                                                                                                                                                                        |
| Start Page                                   | 4455                                                                                                                                                                                      |
| End Page                                     | 4467                                                                                                                                                                                      |
| Type of Use                                  | reuse in a thesis/dissertation                                                                                                                                                            |
| Intended publisher of new work               | other                                                                                                                                                                                     |
| Portion                                      | figures/tables/illustrations                                                                                                                                                              |
| Number of figures/tables/illustrations       | 1                                                                                                                                                                                         |
| Format                                       | both print and electronic                                                                                                                                                                 |
| Are you the author of this Elsevier article? | No                                                                                                                                                                                        |
| Will you be translating?                     | No                                                                                                                                                                                        |
| Original figure numbers                      | Figure 16a                                                                                                                                                                                |
| Title of your thesis/dissertation            | ZrB <sub>2</sub> -SiC BASED ULTRA HIGH TEMPERATURE CERAMIC COMPOSITES: MECHANICAL PERFORMANCE AND MEASUREMENT AND DESIGN OF THERMAL RESIDUAL STRESSES FOR HYPERSONIC VEHICLE APPLICATIONS |
| Expected completion date                     | Nov 2015                                                                                                                                                                                  |
| Estimated size (number of pages)             | 250                                                                                                                                                                                       |
| Elsevier VAT number                          | GB 494 6272 12                                                                                                                                                                            |
| Permissions price                            | 0.00 USD                                                                                                                                                                                  |
| VAT/Local Sales Tax                          | 0.00 USD / 0.00 GBP                                                                                                                                                                       |

**JOHN WILEY AND SONS LICENSE  
TERMS AND CONDITIONS**

Oct 21, 2015

This Agreement between Richard Stadelmann ("You") and John Wiley and Sons ("John Wiley and Sons") consists of your license details and the terms and conditions provided by John Wiley and Sons and Copyright Clearance Center.

|                                       |                                                                                                                                                                                           |
|---------------------------------------|-------------------------------------------------------------------------------------------------------------------------------------------------------------------------------------------|
| License Number                        | 3733251121727                                                                                                                                                                             |
| License date                          | Oct 20, 2015                                                                                                                                                                              |
| Licensed Content Publisher            | John Wiley and Sons                                                                                                                                                                       |
| Licensed Content Publication          | Journal of the American Ceramic Society                                                                                                                                                   |
| Licensed Content Title                | Thermal and Electrical Transport Properties of Spark Plasma-Sintered HfB <sub>2</sub> and ZrB <sub>2</sub> Ceramics                                                                       |
| Licensed Content Author               | Luning Zhang, Dušan A. Pejaković, Jochen Marschall, Matthew Gasch                                                                                                                         |
| Licensed Content Date                 | Mar 15, 2011                                                                                                                                                                              |
| Pages                                 | 9                                                                                                                                                                                         |
| Type of use                           | Dissertation/Thesis                                                                                                                                                                       |
| Requestor type                        | University/Academic                                                                                                                                                                       |
| Format                                | Print and electronic                                                                                                                                                                      |
| Portion                               | Figure/table                                                                                                                                                                              |
| Number of figures/tables              | 2                                                                                                                                                                                         |
| Original Wiley figure/table number(s) | Figure 5A Figure 6A                                                                                                                                                                       |
| Will you be translating?              | No                                                                                                                                                                                        |
| Title of your thesis / dissertation   | ZrB <sub>2</sub> -SiC BASED ULTRA HIGH TEMPERATURE CERAMIC COMPOSITES: MECHANICAL PERFORMANCE AND MEASUREMENT AND DESIGN OF THERMAL RESIDUAL STRESSES FOR HYPERSONIC VEHICLE APPLICATIONS |
| Expected completion date              | Nov 2015                                                                                                                                                                                  |
| Expected size (number of pages)       | 250                                                                                                                                                                                       |
| Requestor Location                    | Richard Stadelmann<br>12124 Fountinabrook Blvd.<br>Apt. 208<br><br>ORLANDO, FL 32825<br>United States<br>Attn: Richard Stadelmann                                                         |
| Billing Type                          | Invoice                                                                                                                                                                                   |
| Billing Address                       | Richard Stadelmann<br>12124 Fountinabrook Blvd.<br>Apt. 208<br><br>ORLANDO, FL 32825<br>United States<br>Attn: Richard Stadelmann                                                         |
| Total                                 | 0.00 USD                                                                                                                                                                                  |

**ELSEVIER LICENSE  
TERMS AND CONDITIONS**

Oct 21, 2015

This is a License Agreement between Richard Stadelmann ("You") and Elsevier ("Elsevier") provided by Copyright Clearance Center ("CCC"). The license consists of your order details, the terms and conditions provided by Elsevier, and the payment terms and conditions.

**All payments must be made in full to CCC. For payment instructions, please see information listed at the bottom of this form.**

|                                              |                                                                                                                                                                                           |
|----------------------------------------------|-------------------------------------------------------------------------------------------------------------------------------------------------------------------------------------------|
| Supplier                                     | Elsevier Limited<br>The Boulevard, Langford Lane<br>Kidlington, Oxford, OX5 1GB, UK                                                                                                       |
| Registered Company Number                    | 1982084                                                                                                                                                                                   |
| Customer name                                | Richard Stadelmann                                                                                                                                                                        |
| Customer address                             | 12124 Fountinabrook Blvd.<br>ORLANDO, FL 32825                                                                                                                                            |
| License number                               | 3733680025275                                                                                                                                                                             |
| License date                                 | Oct 21, 2015                                                                                                                                                                              |
| Licensed content publisher                   | Elsevier                                                                                                                                                                                  |
| Licensed content publication                 | Journal of the European Ceramic Society                                                                                                                                                   |
| Licensed content title                       | Electrical and thermophysical properties of ZrB <sub>2</sub> and HfB <sub>2</sub> based composites                                                                                        |
| Licensed content author                      | Manab Mallik, Ansu J. Kailath, K.K. Ray, R. Mitra                                                                                                                                         |
| Licensed content date                        | August 2012                                                                                                                                                                               |
| Licensed content volume number               | 32                                                                                                                                                                                        |
| Licensed content issue number                | 10                                                                                                                                                                                        |
| Number of pages                              | 11                                                                                                                                                                                        |
| Start Page                                   | 2545                                                                                                                                                                                      |
| End Page                                     | 2555                                                                                                                                                                                      |
| Type of Use                                  | reuse in a thesis/dissertation                                                                                                                                                            |
| Intended publisher of new work               | other                                                                                                                                                                                     |
| Portion                                      | figures/tables/illustrations                                                                                                                                                              |
| Number of figures/tables/illustrations       | 1                                                                                                                                                                                         |
| Format                                       | both print and electronic                                                                                                                                                                 |
| Are you the author of this Elsevier article? | No                                                                                                                                                                                        |
| Will you be translating?                     | No                                                                                                                                                                                        |
| Original figure numbers                      | Figure 5                                                                                                                                                                                  |
| Title of your thesis/dissertation            | ZrB <sub>2</sub> -SiC BASED ULTRA HIGH TEMPERATURE CERAMIC COMPOSITES: MECHANICAL PERFORMANCE AND MEASUREMENT AND DESIGN OF THERMAL RESIDUAL STRESSES FOR HYPERSONIC VEHICLE APPLICATIONS |
| Expected completion date                     | Nov 2015                                                                                                                                                                                  |
| Estimated size (number of pages)             | 250                                                                                                                                                                                       |
| Elsevier VAT number                          | GB 494 6272 12                                                                                                                                                                            |
| Permissions price                            | 0.00 USD                                                                                                                                                                                  |
| VAT/Local Sales Tax                          | 0.00 USD / 0.00 GBP                                                                                                                                                                       |

**ELSEVIER LICENSE  
TERMS AND CONDITIONS**

Oct 21, 2015

This is a License Agreement between Richard Stadelmann ("You") and Elsevier ("Elsevier") provided by Copyright Clearance Center ("CCC"). The license consists of your order details, the terms and conditions provided by Elsevier, and the payment terms and conditions.

**All payments must be made in full to CCC. For payment instructions, please see information listed at the bottom of this form.**

|                                              |                                                                                                                                                                                           |
|----------------------------------------------|-------------------------------------------------------------------------------------------------------------------------------------------------------------------------------------------|
| Supplier                                     | Elsevier Limited<br>The Boulevard, Langford Lane<br>Kidlington, Oxford, OX5 1GB, UK                                                                                                       |
| Registered Company Number                    | 1982084                                                                                                                                                                                   |
| Customer name                                | Richard Stadelmann                                                                                                                                                                        |
| Customer address                             | 12124 Fountinabrook Blvd.<br>ORLANDO, FL 32825                                                                                                                                            |
| License number                               | 3733680314055                                                                                                                                                                             |
| License date                                 | Oct 21, 2015                                                                                                                                                                              |
| Licensed content publisher                   | Elsevier                                                                                                                                                                                  |
| Licensed content publication                 | Journal of the European Ceramic Society                                                                                                                                                   |
| Licensed content title                       | Heat conduction mechanisms in hot pressed ZrB <sub>2</sub> and ZrB <sub>2</sub> -SiC composites                                                                                           |
| Licensed content author                      | Manish Patel, V.V. Bhanu Prasad, Vikram Jayaram                                                                                                                                           |
| Licensed content date                        | September 2013                                                                                                                                                                            |
| Licensed content volume number               | 33                                                                                                                                                                                        |
| Licensed content issue number                | 10                                                                                                                                                                                        |
| Number of pages                              | 10                                                                                                                                                                                        |
| Start Page                                   | 1615                                                                                                                                                                                      |
| End Page                                     | 1624                                                                                                                                                                                      |
| Type of Use                                  | reuse in a thesis/dissertation                                                                                                                                                            |
| Intended publisher of new work               | other                                                                                                                                                                                     |
| Portion                                      | figures/tables/illustrations                                                                                                                                                              |
| Number of figures/tables/illustrations       | 3                                                                                                                                                                                         |
| Format                                       | both print and electronic                                                                                                                                                                 |
| Are you the author of this Elsevier article? | No                                                                                                                                                                                        |
| Will you be translating?                     | No                                                                                                                                                                                        |
| Original figure numbers                      | Figures 3b, 4b, and 5b                                                                                                                                                                    |
| Title of your thesis/dissertation            | ZrB <sub>2</sub> -SiC BASED ULTRA HIGH TEMPERATURE CERAMIC COMPOSITES: MECHANICAL PERFORMANCE AND MEASUREMENT AND DESIGN OF THERMAL RESIDUAL STRESSES FOR HYPERSONIC VEHICLE APPLICATIONS |
| Expected completion date                     | Nov 2015                                                                                                                                                                                  |
| Estimated size (number of pages)             | 250                                                                                                                                                                                       |
| Elsevier VAT number                          | GB 494 6272 12                                                                                                                                                                            |
| Permissions price                            | 0.00 USD                                                                                                                                                                                  |
| VAT/Local Sales Tax                          | 0.00 USD / 0.00 GBP                                                                                                                                                                       |

**ELSEVIER LICENSE  
TERMS AND CONDITIONS**

Oct 21, 2015

---

This is a License Agreement between Richard Stadelmann ("You") and Elsevier ("Elsevier") provided by Copyright Clearance Center ("CCC"). The license consists of your order details, the terms and conditions provided by Elsevier, and the payment terms and conditions.

**All payments must be made in full to CCC. For payment instructions, please see information listed at the bottom of this form.**

|                                              |                                                                                                                                                                                           |
|----------------------------------------------|-------------------------------------------------------------------------------------------------------------------------------------------------------------------------------------------|
| Supplier                                     | Elsevier Limited<br>The Boulevard, Langford Lane<br>Kidlington, Oxford, OX5 1GB, UK                                                                                                       |
| Registered Company Number                    | 1982084                                                                                                                                                                                   |
| Customer name                                | Richard Stadelmann                                                                                                                                                                        |
| Customer address                             | 12124 Fountinabrook Blvd.<br>ORLANDO, FL 32825                                                                                                                                            |
| License number                               | 3733680492942                                                                                                                                                                             |
| License date                                 | Oct 21, 2015                                                                                                                                                                              |
| Licensed content publisher                   | Elsevier                                                                                                                                                                                  |
| Licensed content publication                 | International Journal of Refractory Metals and Hard Materials                                                                                                                             |
| Licensed content title                       | The repeated thermal shock behaviors of a ZrB <sub>2</sub> -SiC composite heated by electric resistance method                                                                            |
| Licensed content author                      | Songhe Meng, Fei Qi, Hongbo Chen, Zhi Wang, Guanghui Bai                                                                                                                                  |
| Licensed content date                        | January 2011                                                                                                                                                                              |
| Licensed content volume number               | 29                                                                                                                                                                                        |
| Licensed content issue number                | 1                                                                                                                                                                                         |
| Number of pages                              | 5                                                                                                                                                                                         |
| Start Page                                   | 44                                                                                                                                                                                        |
| End Page                                     | 48                                                                                                                                                                                        |
| Type of Use                                  | reuse in a thesis/dissertation                                                                                                                                                            |
| Intended publisher of new work               | other                                                                                                                                                                                     |
| Portion                                      | figures/tables/illustrations                                                                                                                                                              |
| Number of figures/tables/illustrations       | 1                                                                                                                                                                                         |
| Format                                       | both print and electronic                                                                                                                                                                 |
| Are you the author of this Elsevier article? | No                                                                                                                                                                                        |
| Will you be translating?                     | No                                                                                                                                                                                        |
| Original figure numbers                      | Figure 6                                                                                                                                                                                  |
| Title of your thesis/dissertation            | ZrB <sub>2</sub> -SiC BASED ULTRA HIGH TEMPERATURE CERAMIC COMPOSITES: MECHANICAL PERFORMANCE AND MEASUREMENT AND DESIGN OF THERMAL RESIDUAL STRESSES FOR HYPERSONIC VEHICLE APPLICATIONS |
| Expected completion date                     | Nov 2015                                                                                                                                                                                  |
| Estimated size (number of pages)             | 250                                                                                                                                                                                       |
| Elsevier VAT number                          | GB 494 6272 12                                                                                                                                                                            |
| Permissions price                            | 0.00 USD                                                                                                                                                                                  |
| VAT/Local Sales Tax                          | 0.00 USD / 0.00 GBP                                                                                                                                                                       |

**ELSEVIER LICENSE  
TERMS AND CONDITIONS**

Oct 21, 2015

This is a License Agreement between Richard Stadelmann ("You") and Elsevier ("Elsevier") provided by Copyright Clearance Center ("CCC"). The license consists of your order details, the terms and conditions provided by Elsevier, and the payment terms and conditions.

**All payments must be made in full to CCC. For payment instructions, please see information listed at the bottom of this form.**

|                                              |                                                                                                                                                                                           |
|----------------------------------------------|-------------------------------------------------------------------------------------------------------------------------------------------------------------------------------------------|
| Supplier                                     | Elsevier Limited<br>The Boulevard, Langford Lane<br>Kidlington, Oxford, OX5 1GB, UK                                                                                                       |
| Registered Company Number                    | 1982084                                                                                                                                                                                   |
| Customer name                                | Richard Stadelmann                                                                                                                                                                        |
| Customer address                             | 12124 Fountinabrook Blvd.<br>ORLANDO, FL 32825                                                                                                                                            |
| License number                               | 3733680492942                                                                                                                                                                             |
| License date                                 | Oct 21, 2015                                                                                                                                                                              |
| Licensed content publisher                   | Elsevier                                                                                                                                                                                  |
| Licensed content publication                 | International Journal of Refractory Metals and Hard Materials                                                                                                                             |
| Licensed content title                       | The repeated thermal shock behaviors of a ZrB <sub>2</sub> -SiC composite heated by electric resistance method                                                                            |
| Licensed content author                      | Songhe Meng, Fei Qi, Hongbo Chen, Zhi Wang, Guanghui Bai                                                                                                                                  |
| Licensed content date                        | January 2011                                                                                                                                                                              |
| Licensed content volume number               | 29                                                                                                                                                                                        |
| Licensed content issue number                | 1                                                                                                                                                                                         |
| Number of pages                              | 5                                                                                                                                                                                         |
| Start Page                                   | 44                                                                                                                                                                                        |
| End Page                                     | 48                                                                                                                                                                                        |
| Type of Use                                  | reuse in a thesis/dissertation                                                                                                                                                            |
| Intended publisher of new work               | other                                                                                                                                                                                     |
| Portion                                      | figures/tables/illustrations                                                                                                                                                              |
| Number of figures/tables/illustrations       | 1                                                                                                                                                                                         |
| Format                                       | both print and electronic                                                                                                                                                                 |
| Are you the author of this Elsevier article? | No                                                                                                                                                                                        |
| Will you be translating?                     | No                                                                                                                                                                                        |
| Original figure numbers                      | Figure 6                                                                                                                                                                                  |
| Title of your thesis/dissertation            | ZrB <sub>2</sub> -SiC BASED ULTRA HIGH TEMPERATURE CERAMIC COMPOSITES: MECHANICAL PERFORMANCE AND MEASUREMENT AND DESIGN OF THERMAL RESIDUAL STRESSES FOR HYPERSONIC VEHICLE APPLICATIONS |
| Expected completion date                     | Nov 2015                                                                                                                                                                                  |
| Estimated size (number of pages)             | 250                                                                                                                                                                                       |
| Elsevier VAT number                          | GB 494 6272 12                                                                                                                                                                            |
| Permissions price                            | 0.00 USD                                                                                                                                                                                  |
| VAT/Local Sales Tax                          | 0.00 USD / 0.00 GBP                                                                                                                                                                       |



**ELSEVIER LICENSE  
TERMS AND CONDITIONS**

Oct 21, 2015

---

---

This is a License Agreement between Richard Stadelmann ("You") and Elsevier ("Elsevier") provided by Copyright Clearance Center ("CCC"). The license consists of your order details, the terms and conditions provided by Elsevier, and the payment terms and conditions.

**All payments must be made in full to CCC. For payment instructions, please see information listed at the bottom of this form.**

|                                              |                                                                                                                                                                                           |
|----------------------------------------------|-------------------------------------------------------------------------------------------------------------------------------------------------------------------------------------------|
| Supplier                                     | Elsevier Limited<br>The Boulevard, Langford Lane<br>Kidlington, Oxford, OX5 1GB, UK                                                                                                       |
| Registered Company Number                    | 1982084                                                                                                                                                                                   |
| Customer name                                | Richard Stadelmann                                                                                                                                                                        |
| Customer address                             | 12124 Fountinabrook Blvd.<br>ORLANDO, FL 32825                                                                                                                                            |
| License number                               | 3733680683734                                                                                                                                                                             |
| License date                                 | Oct 21, 2015                                                                                                                                                                              |
| Licensed content publisher                   | Elsevier                                                                                                                                                                                  |
| Licensed content publication                 | Materials Science and Engineering: A                                                                                                                                                      |
| Licensed content title                       | Ablation behaviors of ultra-high temperature ceramic composites                                                                                                                           |
| Licensed content author                      | Sufang Tang, Jingyi Deng, Shijun Wang, Wenchuan Liu, Ke Yang                                                                                                                              |
| Licensed content date                        | 15 September 2007                                                                                                                                                                         |
| Licensed content volume number               | 465                                                                                                                                                                                       |
| Licensed content issue number                | 1-2                                                                                                                                                                                       |
| Number of pages                              | 7                                                                                                                                                                                         |
| Start Page                                   | 1                                                                                                                                                                                         |
| End Page                                     | 7                                                                                                                                                                                         |
| Type of Use                                  | reuse in a thesis/dissertation                                                                                                                                                            |
| Intended publisher of new work               | other                                                                                                                                                                                     |
| Portion                                      | figures/tables/illustrations                                                                                                                                                              |
| Number of figures/tables/illustrations       | 2                                                                                                                                                                                         |
| Format                                       | both print and electronic                                                                                                                                                                 |
| Are you the author of this Elsevier article? | No                                                                                                                                                                                        |
| Will you be translating?                     | No                                                                                                                                                                                        |
| Original figure numbers                      | Figures 8 and 9                                                                                                                                                                           |
| Title of your thesis/dissertation            | ZrB <sub>2</sub> -SiC BASED ULTRA HIGH TEMPERATURE CERAMIC COMPOSITES: MECHANICAL PERFORMANCE AND MEASUREMENT AND DESIGN OF THERMAL RESIDUAL STRESSES FOR HYPERSONIC VEHICLE APPLICATIONS |
| Expected completion date                     | Nov 2015                                                                                                                                                                                  |
| Estimated size (number of pages)             | 250                                                                                                                                                                                       |
| Elsevier VAT number                          | GB 494 6272 12                                                                                                                                                                            |
| Permissions price                            | 0.00 USD                                                                                                                                                                                  |
| VAT/Local Sales Tax                          | 0.00 USD / 0.00 GBP                                                                                                                                                                       |
| Total                                        | 0.00 USD                                                                                                                                                                                  |

**ELSEVIER LICENSE  
TERMS AND CONDITIONS**

Oct 21, 2015

---

This is a License Agreement between Richard Stadelmann ("You") and Elsevier ("Elsevier") provided by Copyright Clearance Center ("CCC"). The license consists of your order details, the terms and conditions provided by Elsevier, and the payment terms and conditions.

**All payments must be made in full to CCC. For payment instructions, please see information listed at the bottom of this form.**

|                                              |                                                                                                                                                                                           |
|----------------------------------------------|-------------------------------------------------------------------------------------------------------------------------------------------------------------------------------------------|
| Supplier                                     | Elsevier Limited<br>The Boulevard, Langford Lane<br>Kidlington, Oxford, OX5 1GB, UK                                                                                                       |
| Registered Company Number                    | 1982084                                                                                                                                                                                   |
| Customer name                                | Richard Stadelmann                                                                                                                                                                        |
| Customer address                             | 12124 Fountinabrook Blvd.<br>ORLANDO, FL 32825                                                                                                                                            |
| License number                               | 3733680805992                                                                                                                                                                             |
| License date                                 | Oct 21, 2015                                                                                                                                                                              |
| Licensed content publisher                   | Elsevier                                                                                                                                                                                  |
| Licensed content publication                 | Composites Science and Technology                                                                                                                                                         |
| Licensed content title                       | Ablation behavior of ZrB <sub>2</sub> -SiC ultra high temperature ceramics under simulated atmospheric re-entry conditions                                                                |
| Licensed content author                      | Xinghong Zhang, Ping Hu, Jiecai Han, Songhe Meng                                                                                                                                          |
| Licensed content date                        | June 2008                                                                                                                                                                                 |
| Licensed content volume number               | 68                                                                                                                                                                                        |
| Licensed content issue number                | 7-8                                                                                                                                                                                       |
| Number of pages                              | 9                                                                                                                                                                                         |
| Start Page                                   | 1718                                                                                                                                                                                      |
| End Page                                     | 1726                                                                                                                                                                                      |
| Type of Use                                  | reuse in a thesis/dissertation                                                                                                                                                            |
| Intended publisher of new work               | other                                                                                                                                                                                     |
| Portion                                      | figures/tables/illustrations                                                                                                                                                              |
| Number of figures/tables/illustrations       | 1                                                                                                                                                                                         |
| Format                                       | both print and electronic                                                                                                                                                                 |
| Are you the author of this Elsevier article? | No                                                                                                                                                                                        |
| Will you be translating?                     | No                                                                                                                                                                                        |
| Original figure numbers                      | Figure 13                                                                                                                                                                                 |
| Title of your thesis/dissertation            | ZrB <sub>2</sub> -SiC BASED ULTRA HIGH TEMPERATURE CERAMIC COMPOSITES: MECHANICAL PERFORMANCE AND MEASUREMENT AND DESIGN OF THERMAL RESIDUAL STRESSES FOR HYPERSONIC VEHICLE APPLICATIONS |
| Expected completion date                     | Nov 2015                                                                                                                                                                                  |
| Estimated size (number of pages)             | 250                                                                                                                                                                                       |
| Elsevier VAT number                          | GB 494 6272 12                                                                                                                                                                            |
| Permissions price                            | 0.00 USD                                                                                                                                                                                  |
| VAT/Local Sales Tax                          | 0.00 USD / 0.00 GBP                                                                                                                                                                       |

**ELSEVIER LICENSE  
TERMS AND CONDITIONS**

Oct 21, 2015

---

This is a License Agreement between Richard Stadelmann ("You") and Elsevier ("Elsevier") provided by Copyright Clearance Center ("CCC"). The license consists of your order details, the terms and conditions provided by Elsevier, and the payment terms and conditions.

**All payments must be made in full to CCC. For payment instructions, please see information listed at the bottom of this form.**

|                                              |                                                                                                                                                                                           |
|----------------------------------------------|-------------------------------------------------------------------------------------------------------------------------------------------------------------------------------------------|
| Supplier                                     | Elsevier Limited<br>The Boulevard, Langford Lane<br>Kidlington, Oxford, OX5 1GB, UK                                                                                                       |
| Registered Company Number                    | 1982084                                                                                                                                                                                   |
| Customer name                                | Richard Stadelmann                                                                                                                                                                        |
| Customer address                             | 12124 Fountinabrook Blvd.<br>ORLANDO, FL 32825                                                                                                                                            |
| License number                               | 3733680907586                                                                                                                                                                             |
| License date                                 | Oct 21, 2015                                                                                                                                                                              |
| Licensed content publisher                   | Elsevier                                                                                                                                                                                  |
| Licensed content publication                 | Journal of Alloys and Compounds                                                                                                                                                           |
| Licensed content title                       | Ablation behavior of ZrB <sub>2</sub> -SiC sharp leading edges                                                                                                                            |
| Licensed content author                      | Xinxin Jin, Rujie He, Xinghong Zhang, Ping Hu                                                                                                                                             |
| Licensed content date                        | 25 July 2013                                                                                                                                                                              |
| Licensed content volume number               | 566                                                                                                                                                                                       |
| Licensed content issue number                | n/a                                                                                                                                                                                       |
| Number of pages                              | 6                                                                                                                                                                                         |
| Start Page                                   | 125                                                                                                                                                                                       |
| End Page                                     | 130                                                                                                                                                                                       |
| Type of Use                                  | reuse in a thesis/dissertation                                                                                                                                                            |
| Intended publisher of new work               | other                                                                                                                                                                                     |
| Portion                                      | figures/tables/illustrations                                                                                                                                                              |
| Number of figures/tables/illustrations       | 1                                                                                                                                                                                         |
| Format                                       | both print and electronic                                                                                                                                                                 |
| Are you the author of this Elsevier article? | No                                                                                                                                                                                        |
| Will you be translating?                     | No                                                                                                                                                                                        |
| Original figure numbers                      | Figure 2                                                                                                                                                                                  |
| Title of your thesis/dissertation            | ZrB <sub>2</sub> -SiC BASED ULTRA HIGH TEMPERATURE CERAMIC COMPOSITES: MECHANICAL PERFORMANCE AND MEASUREMENT AND DESIGN OF THERMAL RESIDUAL STRESSES FOR HYPERSONIC VEHICLE APPLICATIONS |
| Expected completion date                     | Nov 2015                                                                                                                                                                                  |
| Estimated size (number of pages)             | 250                                                                                                                                                                                       |
| Elsevier VAT number                          | GB 494 6272 12                                                                                                                                                                            |
| Permissions price                            | 0.00 USD                                                                                                                                                                                  |
| VAT/Local Sales Tax                          | 0.00 USD / 0.00 GBP                                                                                                                                                                       |
| Total                                        | 0.00 USD                                                                                                                                                                                  |

**JOHN WILEY AND SONS LICENSE  
TERMS AND CONDITIONS**

Oct 21, 2015

---

This Agreement between Richard Stadelmann ("You") and John Wiley and Sons ("John Wiley and Sons") consists of your license details and the terms and conditions provided by John Wiley and Sons and Copyright Clearance Center.

|                                       |                                                                                                                                                                              |
|---------------------------------------|------------------------------------------------------------------------------------------------------------------------------------------------------------------------------|
| License Number                        | 3733681017764                                                                                                                                                                |
| License date                          | Oct 21, 2015                                                                                                                                                                 |
| Licensed Content Publisher            | John Wiley and Sons                                                                                                                                                          |
| Licensed Content Publication          | Journal of the American Ceramic Society                                                                                                                                      |
| Licensed Content Title                | ZrB2 – SiC Sharp Leading Edges in High Enthalpy Supersonic Flows                                                                                                             |
| Licensed Content Author               | Frédéric Monteverde,Raffaele Savino                                                                                                                                          |
| Licensed Content Date                 | May 8, 2012                                                                                                                                                                  |
| Pages                                 | 8                                                                                                                                                                            |
| Type of use                           | Dissertation/Thesis                                                                                                                                                          |
| Requestor type                        | University/Academic                                                                                                                                                          |
| Format                                | Print and electronic                                                                                                                                                         |
| Portion                               | Figure/table                                                                                                                                                                 |
| Number of figures/tables              | 1                                                                                                                                                                            |
| Original Wiley figure/table number(s) | Figure 1                                                                                                                                                                     |
| Will you be translating?              | No                                                                                                                                                                           |
| Title of your thesis / dissertation   | ZrB2-SiC BASED ULTRA HIGH TEMPERATURE CERAMIC COMPOSITES: MECHANICAL PERFORMANCE AND MEASUREMENT AND DESIGN OF THERMAL RESIDUAL STRESSES FOR HYPERSONIC VEHICLE APPLICATIONS |
| Expected completion date              | Nov 2015                                                                                                                                                                     |
| Expected size (number of pages)       | 250                                                                                                                                                                          |
| Requestor Location                    | Richard Stadelmann<br>12124 Fountinabrook Blvd.<br>Apt. 208<br><br>ORLANDO, FL 32825<br>United States<br>Attn: Richard Stadelmann                                            |
| Billing Type                          | Invoice                                                                                                                                                                      |
| Billing Address                       | Richard Stadelmann<br>12124 Fountinabrook Blvd.<br>Apt. 208<br><br>ORLANDO, FL 32825<br>United States<br>Attn: Richard Stadelmann                                            |
| Total                                 | 0.00 USD                                                                                                                                                                     |



Issy-Les-Moulineaux, 27-10-2015

To the attention of Mr Richard P. Stadelmann

Dear Sir,

As per your request below, we hereby grant you permission to reprint the material detailed in your request at no charge **in your thesis** subject to the following conditions:

1. If any part of the material to be used (for example, figures) has appeared in our publication with credit or acknowledgement to another source, permission must also be sought from that source. If such permissions are not obtained then that materials may not be included in your publication.
2. Any modification of the material is likely to harm the moral right of the authors and therefore should be first submitted and approved by the authors who are the sole owner of the moral right.
3. Suitable and visible acknowledgement to the source must be made, either as a footnote or in a reference list at the end of your publication, as follows:  

*"Reproduced from Authors name. Article title. Journal title year;volume number(issue number):first page-last page. Copyright © year [if applicable: name of learned society, published by] Elsevier Masson SAS. All rights reserved."*
4. Your thesis may be submitted to your institution in either print or electronic form.
5. Reproduction of this material is confined to the purpose for which permission is hereby given.
6. This permission is granted for non-exclusive world **English** rights only. For other languages please reapply separately for each one required. Permission excludes use in an electronic form other than submission. Should you have a specific electronic project in mind please reapply for permission.
7. Should your thesis be published commercially, please reapply for permission.

Yours sincerely,

Regina Lavanya Remigius  
Senior Copyrights Coordinator – Global Rights

**Elsevier**

(A division of Reed Elsevier India Pvt. Ltd.)

---

**From:** Richard Stadelmann [mailto:Richard.Stadelmann@ucf.edu]

**Sent:** Thursday, October 22, 2015 9:15 PM

**To:** PermissionsFrance

**Subject:** Request for reprint permissions in my dissertation

Dear Whom this may concern,

I am completing a doctoral dissertation at the University of Central Florida entitled "ZrB<sub>2</sub>-SiC Based Ultra High Temperature Ceramic Composites: Mechanical Performance and Measurements and Design of Thermal Residual Stresses for Hypersonic Vehicle Applications". I would like your permission to reprint in my dissertation excerpts from the following:

R. Savino, M. De Stefano Fumo, D. Paterna, A. Di Maso, and F. Monteverde, "Arc-jet testing of ultra-high-temperature-ceramics," *Aerospace Science and Technology*, vol. 14, pp. 178-187, 2010.

The excerpts to be reproduced are the following:  
Figure 19

How would I go about requesting preprint permission as the online service mentioned to connect this email. Thank you very much for your time and help with this matter.

Best Regards,

Richard P. Stadelmann  
PhD Candidate  
University of Central Florida  
Department of Mechanical and Aerospace Engineering  
4000 Central Florida Blvd.  
Orlando, FL 32816  
Phone: (239)-410-8704  
Email: [rstadelmann@knights.ucf.edu](mailto:rstadelmann@knights.ucf.edu)

**ELSEVIER LICENSE  
TERMS AND CONDITIONS**

Oct 21, 2015

---

This is a License Agreement between Richard Stadelmann ("You") and Elsevier ("Elsevier") provided by Copyright Clearance Center ("CCC"). The license consists of your order details, the terms and conditions provided by Elsevier, and the payment terms and conditions.

**All payments must be made in full to CCC. For payment instructions, please see information listed at the bottom of this form.**

|                                              |                                                                                                                                                                                           |
|----------------------------------------------|-------------------------------------------------------------------------------------------------------------------------------------------------------------------------------------------|
| Supplier                                     | Elsevier Limited<br>The Boulevard, Langford Lane<br>Kidlington, Oxford, OX5 1GB, UK                                                                                                       |
| Registered Company Number                    | 1982084                                                                                                                                                                                   |
| Customer name                                | Richard Stadelmann                                                                                                                                                                        |
| Customer address                             | 12124 Fountinabrook Blvd.<br>ORLANDO, FL 32825                                                                                                                                            |
| License number                               | 3733681213423                                                                                                                                                                             |
| License date                                 | Oct 21, 2015                                                                                                                                                                              |
| Licensed content publisher                   | Elsevier                                                                                                                                                                                  |
| Licensed content publication                 | Journal of the European Ceramic Society                                                                                                                                                   |
| Licensed content title                       | Plasma wind tunnel testing of ultra-high temperature ZrB <sub>2</sub> -SiC composites under hypersonic re-entry conditions                                                                |
| Licensed content author                      | Frederic Monteverde, Raffaele Savino, Mario De Stefano Fumo, Andrea Di Maso                                                                                                               |
| Licensed content date                        | August 2010                                                                                                                                                                               |
| Licensed content volume number               | 30                                                                                                                                                                                        |
| Licensed content issue number                | 11                                                                                                                                                                                        |
| Number of pages                              | 9                                                                                                                                                                                         |
| Start Page                                   | 2313                                                                                                                                                                                      |
| End Page                                     | 2321                                                                                                                                                                                      |
| Type of Use                                  | reuse in a thesis/dissertation                                                                                                                                                            |
| Intended publisher of new work               | other                                                                                                                                                                                     |
| Portion                                      | figures/tables/illustrations                                                                                                                                                              |
| Number of figures/tables/illustrations       | 1                                                                                                                                                                                         |
| Format                                       | both print and electronic                                                                                                                                                                 |
| Are you the author of this Elsevier article? | No                                                                                                                                                                                        |
| Will you be translating?                     | No                                                                                                                                                                                        |
| Original figure numbers                      | Figure 2                                                                                                                                                                                  |
| Title of your thesis/dissertation            | ZrB <sub>2</sub> -SiC BASED ULTRA HIGH TEMPERATURE CERAMIC COMPOSITES: MECHANICAL PERFORMANCE AND MEASUREMENT AND DESIGN OF THERMAL RESIDUAL STRESSES FOR HYPERSONIC VEHICLE APPLICATIONS |
| Expected completion date                     | Nov 2015                                                                                                                                                                                  |
| Estimated size (number of pages)             | 250                                                                                                                                                                                       |
| Elsevier VAT number                          | GB 494 6272 12                                                                                                                                                                            |
| Permissions price                            | 0.00 USD                                                                                                                                                                                  |
| VAT/Local Sales Tax                          | 0.00 USD / 0.00 GBP                                                                                                                                                                       |

**ELSEVIER LICENSE  
TERMS AND CONDITIONS**

Oct 21, 2015

---

This is a License Agreement between Richard Stadelmann ("You") and Elsevier ("Elsevier") provided by Copyright Clearance Center ("CCC"). The license consists of your order details, the terms and conditions provided by Elsevier, and the payment terms and conditions.

**All payments must be made in full to CCC. For payment instructions, please see information listed at the bottom of this form.**

|                                              |                                                                                                                                                                                           |
|----------------------------------------------|-------------------------------------------------------------------------------------------------------------------------------------------------------------------------------------------|
| Supplier                                     | Elsevier Limited<br>The Boulevard, Langford Lane<br>Kidlington, Oxford, OX5 1GB, UK                                                                                                       |
| Registered Company Number                    | 1982084                                                                                                                                                                                   |
| Customer name                                | Richard Stadelmann                                                                                                                                                                        |
| Customer address                             | 12124 Fountinabrook Blvd.<br>ORLANDO, FL 32825                                                                                                                                            |
| License number                               | 3733681306660                                                                                                                                                                             |
| License date                                 | Oct 21, 2015                                                                                                                                                                              |
| Licensed content publisher                   | Elsevier                                                                                                                                                                                  |
| Licensed content publication                 | Journal of the European Ceramic Society                                                                                                                                                   |
| Licensed content title                       | Physical characterization and arcjet oxidation of hafnium-based ultra high temperature ceramics fabricated by hot pressing and field-assisted sintering                                   |
| Licensed content author                      | Matthew Gasch, Sylvia Johnson                                                                                                                                                             |
| Licensed content date                        | August 2010                                                                                                                                                                               |
| Licensed content volume number               | 30                                                                                                                                                                                        |
| Licensed content issue number                | 11                                                                                                                                                                                        |
| Number of pages                              | 8                                                                                                                                                                                         |
| Start Page                                   | 2337                                                                                                                                                                                      |
| End Page                                     | 2344                                                                                                                                                                                      |
| Type of Use                                  | reuse in a thesis/dissertation                                                                                                                                                            |
| Intended publisher of new work               | other                                                                                                                                                                                     |
| Portion                                      | figures/tables/illustrations                                                                                                                                                              |
| Number of figures/tables/illustrations       | 1                                                                                                                                                                                         |
| Format                                       | both print and electronic                                                                                                                                                                 |
| Are you the author of this Elsevier article? | No                                                                                                                                                                                        |
| Will you be translating?                     | No                                                                                                                                                                                        |
| Original figure numbers                      | Figure 5                                                                                                                                                                                  |
| Title of your thesis/dissertation            | ZrB <sub>2</sub> -SiC BASED ULTRA HIGH TEMPERATURE CERAMIC COMPOSITES: MECHANICAL PERFORMANCE AND MEASUREMENT AND DESIGN OF THERMAL RESIDUAL STRESSES FOR HYPERSONIC VEHICLE APPLICATIONS |
| Expected completion date                     | Nov 2015                                                                                                                                                                                  |
| Estimated size (number of pages)             | 250                                                                                                                                                                                       |
| Elsevier VAT number                          | GB 494 6272 12                                                                                                                                                                            |
| Permissions price                            | 0.00 USD                                                                                                                                                                                  |
| VAT/Local Sales Tax                          | 0.00 USD / 0.00 GBP                                                                                                                                                                       |



## American Physical Society License Details

Oct 26, 2015

This is an Agreement between Richard Stadelmann ("You") and American Physical Society ("Publisher"). It consists of your order details, the terms and conditions provided by American Physical Society, and the payment instructions.

|                                           |                                                                                                                                                                                           |
|-------------------------------------------|-------------------------------------------------------------------------------------------------------------------------------------------------------------------------------------------|
| License Number                            | 3736631198257                                                                                                                                                                             |
| License date                              | Oct 21, 2015                                                                                                                                                                              |
| Licensed Content Publisher                | American Physical Society                                                                                                                                                                 |
| Licensed Content Publication              | Physical Review (1893-1969)                                                                                                                                                               |
| Licensed Content Title                    | Raman Scattering in $\text{SiC}$                                                                                                                                                          |
| Licensed copyright line                   | Copyright © 1968, American Physical Society                                                                                                                                               |
| Licensed Content Author                   | D. W. Feldman et al.                                                                                                                                                                      |
| Licensed Content Date                     | Jun 15, 1968                                                                                                                                                                              |
| Volume number                             | 170                                                                                                                                                                                       |
| I would like to...                        | Thesis/Dissertation                                                                                                                                                                       |
| Requestor type                            | Student                                                                                                                                                                                   |
| Format                                    | Print, Electronic                                                                                                                                                                         |
| Portion                                   | chart/graph/table/figure                                                                                                                                                                  |
| Number of charts/graphs/tables/figures    | 43                                                                                                                                                                                        |
| Portion description                       | Figure 1, Figure 2, Figure 6, and Figure 8                                                                                                                                                |
| Rights for                                | Main product                                                                                                                                                                              |
| Duration of use                           | Life of current edition                                                                                                                                                                   |
| Creation of copies for the disabled       | no                                                                                                                                                                                        |
| With minor editing privileges             | no                                                                                                                                                                                        |
| For distribution to                       | United States                                                                                                                                                                             |
| In the following language(s)              | Original language of publication                                                                                                                                                          |
| With incidental promotional use           | no                                                                                                                                                                                        |
| The lifetime unit quantity of new product | 0 to 499                                                                                                                                                                                  |
| The requesting person/organization is:    | Richard Stadelmann                                                                                                                                                                        |
| Order reference number                    | None                                                                                                                                                                                      |
| Title of your thesis / dissertation       | ZrB <sub>2</sub> -SiC BASED ULTRA HIGH TEMPERATURE CERAMIC COMPOSITES: MECHANICAL PERFORMANCE AND MEASUREMENT AND DESIGN OF THERMAL RESIDUAL STRESSES FOR HYPERSONIC VEHICLE APPLICATIONS |
| Expected completion date                  | Nov 2015                                                                                                                                                                                  |
| Expected size (number of pages)           | 250                                                                                                                                                                                       |
| <b>Total</b>                              | <b>0.00 USD</b>                                                                                                                                                                           |

**JOHN WILEY AND SONS LICENSE  
TERMS AND CONDITIONS**

Oct 21, 2015

---

This Agreement between Richard Stadelmann ("You") and John Wiley and Sons ("John Wiley and Sons") consists of your license details and the terms and conditions provided by John Wiley and Sons and Copyright Clearance Center.

|                                       |                                                                                                                                                                              |
|---------------------------------------|------------------------------------------------------------------------------------------------------------------------------------------------------------------------------|
| License Number                        | 3733701048330                                                                                                                                                                |
| License date                          | Oct 21, 2015                                                                                                                                                                 |
| Licensed Content Publisher            | John Wiley and Sons                                                                                                                                                          |
| Licensed Content Publication          | physica status solidi (a) applications and materials science                                                                                                                 |
| Licensed Content Title                | Raman Investigation of SiC Polytypes                                                                                                                                         |
| Licensed Content Author               | S. Nakashima,H. Harima                                                                                                                                                       |
| Licensed Content Date                 | Nov 16, 2001                                                                                                                                                                 |
| Pages                                 | 26                                                                                                                                                                           |
| Type of use                           | Dissertation/Thesis                                                                                                                                                          |
| Requestor type                        | University/Academic                                                                                                                                                          |
| Format                                | Print and electronic                                                                                                                                                         |
| Portion                               | Figure/table                                                                                                                                                                 |
| Number of figures/tables              | 3                                                                                                                                                                            |
| Original Wiley figure/table number(s) | Figure 2d, Figure 5, and Figure 9                                                                                                                                            |
| Will you be translating?              | No                                                                                                                                                                           |
| Title of your thesis / dissertation   | ZrB2-SiC BASED ULTRA HIGH TEMPERATURE CERAMIC COMPOSITES: MECHANICAL PERFORMANCE AND MEASUREMENT AND DESIGN OF THERMAL RESIDUAL STRESSES FOR HYPERSONIC VEHICLE APPLICATIONS |
| Expected completion date              | Nov 2015                                                                                                                                                                     |
| Expected size (number of pages)       | 250                                                                                                                                                                          |
| Requestor Location                    | Richard Stadelmann<br>12124 Fountinabrook Blvd.<br>Apt. 208<br><br>ORLANDO, FL 32825<br>United States<br>Attn: Richard Stadelmann                                            |
| Billing Type                          | Invoice                                                                                                                                                                      |
| Billing Address                       | Richard Stadelmann<br>12124 Fountinabrook Blvd.<br>Apt. 208<br><br>ORLANDO, FL 32825<br>United States<br>Attn: Richard Stadelmann                                            |
| Total                                 | 0.00 USD                                                                                                                                                                     |

ELSEVIER LICENSE  
TERMS AND CONDITIONS

Oct 21, 2015

This is a License Agreement between Richard Stadelmann ("You") and Elsevier ("Elsevier") provided by Copyright Clearance Center ("CCC"). The license consists of your order details, the terms and conditions provided by Elsevier, and the payment terms and conditions.

**All payments must be made in full to CCC. For payment instructions, please see information listed at the bottom of this form.**

|                                              |                                                                                                                                                                              |
|----------------------------------------------|------------------------------------------------------------------------------------------------------------------------------------------------------------------------------|
| Supplier                                     | Elsevier Limited<br>The Boulevard, Langford Lane<br>Kidlington, Oxford, OX5 1GB, UK                                                                                          |
| Registered Company Number                    | 1982084                                                                                                                                                                      |
| Customer name                                | Richard Stadelmann                                                                                                                                                           |
| Customer address                             | 12124 Fountinabrook Blvd.<br>ORLANDO, FL 32825                                                                                                                               |
| License number                               | 3733701254656                                                                                                                                                                |
| License date                                 | Oct 21, 2015                                                                                                                                                                 |
| Licensed content publisher                   | Elsevier                                                                                                                                                                     |
| Licensed content publication                 | Acta Materialia                                                                                                                                                              |
| Licensed content title                       | Grain size influence on residual stresses in alumina/zirconia composites                                                                                                     |
| Licensed content author                      | V. Sergo, G. Pezzotti, O. Sbaizero, T. Nishida                                                                                                                               |
| Licensed content date                        | 2 March 1998                                                                                                                                                                 |
| Licensed content volume number               | 46                                                                                                                                                                           |
| Licensed content issue number                | 5                                                                                                                                                                            |
| Number of pages                              | 10                                                                                                                                                                           |
| Start Page                                   | 1701                                                                                                                                                                         |
| End Page                                     | 1710                                                                                                                                                                         |
| Type of Use                                  | reuse in a thesis/dissertation                                                                                                                                               |
| Intended publisher of new work               | other                                                                                                                                                                        |
| Portion                                      | figures/tables/illustrations                                                                                                                                                 |
| Number of figures/tables/illustrations       | 1                                                                                                                                                                            |
| Format                                       | both print and electronic                                                                                                                                                    |
| Are you the author of this Elsevier article? | No                                                                                                                                                                           |
| Will you be translating?                     | No                                                                                                                                                                           |
| Original figure numbers                      | Figure 6                                                                                                                                                                     |
| Title of your thesis/dissertation            | ZrB2-SiC BASED ULTRA HIGH TEMPERATURE CERAMIC COMPOSITES: MECHANICAL PERFORMANCE AND MEASUREMENT AND DESIGN OF THERMAL RESIDUAL STRESSES FOR HYPERSONIC VEHICLE APPLICATIONS |
| Expected completion date                     | Nov 2015                                                                                                                                                                     |
| Estimated size (number of pages)             | 250                                                                                                                                                                          |
| Elsevier VAT number                          | GB 494 6272 12                                                                                                                                                               |
| Permissions price                            | 0.00 USD                                                                                                                                                                     |
| VAT/Local Sales Tax                          | 0.00 USD / 0.00 GBP                                                                                                                                                          |

**American Physical Society  
License Details**

Oct 21, 2015

This is an Agreement between Richard Stadelmann ("You") and American Physical Society ("Publisher"). It consists of your order details, the terms and conditions provided by American Physical Society, and the payment instructions.

|                                           |                                                                                                                                                                                           |
|-------------------------------------------|-------------------------------------------------------------------------------------------------------------------------------------------------------------------------------------------|
| License Number                            | 3733701462265                                                                                                                                                                             |
| License date                              | Oct 21, 2015                                                                                                                                                                              |
| Licensed content publisher                | American Physical Society                                                                                                                                                                 |
| Licensed content publication              | Physical Review Letters                                                                                                                                                                   |
| Licensed content title                    | Raman Modes of $\beta$ -SiC Polytype of Silicon Carbide to Ultrahigh Pressures: A Comparison with Silicon and Diamond                                                                     |
| Licensed copyright line                   | Copyright © 1994, American Physical Society                                                                                                                                               |
| Licensed content author                   | Jun Liu and Yogesh K. Vohra                                                                                                                                                               |
| Licensed content date                     | Jun 27, 1994                                                                                                                                                                              |
| Volume number                             | 72                                                                                                                                                                                        |
| Type of Use                               | Thesis/Dissertation                                                                                                                                                                       |
| Requestor type                            | Student                                                                                                                                                                                   |
| Format                                    | Print, Electronic                                                                                                                                                                         |
| Portion                                   | chart/graph/table/figure                                                                                                                                                                  |
| Number of charts/graphs/tables/figures    | 2                                                                                                                                                                                         |
| Portion description                       | Figure 1, and Figure 2                                                                                                                                                                    |
| Rights for                                | Main product                                                                                                                                                                              |
| Duration of use                           | Life of current edition                                                                                                                                                                   |
| Creation of copies for the disabled       | no                                                                                                                                                                                        |
| With minor editing privileges             | no                                                                                                                                                                                        |
| For distribution to                       | Worldwide                                                                                                                                                                                 |
| In the following language(s)              | Original language of publication                                                                                                                                                          |
| With incidental promotional use           | no                                                                                                                                                                                        |
| The lifetime unit quantity of new product | 0 to 499                                                                                                                                                                                  |
| The requesting person/organization is:    | Richard Stadelmann                                                                                                                                                                        |
| Order reference number                    | None                                                                                                                                                                                      |
| Title of your thesis / dissertation       | ZrB <sub>2</sub> -SiC BASED ULTRA HIGH TEMPERATURE CERAMIC COMPOSITES: MECHANICAL PERFORMANCE AND MEASUREMENT AND DESIGN OF THERMAL RESIDUAL STRESSES FOR HYPERSONIC VEHICLE APPLICATIONS |
| Expected completion date                  | Nov 2015                                                                                                                                                                                  |
| Expected size (number of pages)           | 250                                                                                                                                                                                       |
| Total                                     | 0.00 USD                                                                                                                                                                                  |

**JOHN WILEY AND SONS LICENSE  
TERMS AND CONDITIONS**

Oct 21, 2015

This Agreement between Richard Stadelmann ("You") and John Wiley and Sons ("John Wiley and Sons") consists of your license details and the terms and conditions provided by John Wiley and Sons and Copyright Clearance Center.

|                                       |                                                                                                                                                                              |
|---------------------------------------|------------------------------------------------------------------------------------------------------------------------------------------------------------------------------|
| License Number                        | 3733710388457                                                                                                                                                                |
| License date                          | Oct 21, 2015                                                                                                                                                                 |
| Licensed Content Publisher            | John Wiley and Sons                                                                                                                                                          |
| Licensed Content Publication          | Journal of the American Ceramic Society                                                                                                                                      |
| Licensed Content Title                | Piezo-Spectroscopic Coefficients of Tetragonal-Prime Yttria-Stabilized Zirconia                                                                                              |
| Licensed Content Author               | Andi M. Limarga,David R. Clarke                                                                                                                                              |
| Licensed Content Date                 | Mar 30, 2007                                                                                                                                                                 |
| Pages                                 | 4                                                                                                                                                                            |
| Type of use                           | Dissertation/Thesis                                                                                                                                                          |
| Requestor type                        | University/Academic                                                                                                                                                          |
| Format                                | Print and electronic                                                                                                                                                         |
| Portion                               | Figure/table                                                                                                                                                                 |
| Number of figures/tables              | 3                                                                                                                                                                            |
| Original Wiley figure/table number(s) | Figure 2, Figure 3, and Figure 5                                                                                                                                             |
| Will you be translating?              | No                                                                                                                                                                           |
| Title of your thesis / dissertation   | ZrB2-SiC BASED ULTRA HIGH TEMPERATURE CERAMIC COMPOSITES: MECHANICAL PERFORMANCE AND MEASUREMENT AND DESIGN OF THERMAL RESIDUAL STRESSES FOR HYPERSONIC VEHICLE APPLICATIONS |
| Expected completion date              | Nov 2015                                                                                                                                                                     |
| Expected size (number of pages)       | 250                                                                                                                                                                          |
| Requestor Location                    | Richard Stadelmann<br>12124 Fountinabrook Blvd.<br>Apt. 208<br><br>ORLANDO, FL 32825<br>United States<br>Attn: Richard Stadelmann                                            |
| Billing Type                          | Invoice                                                                                                                                                                      |
| Billing Address                       | Richard Stadelmann<br>12124 Fountinabrook Blvd.<br>Apt. 208<br><br>ORLANDO, FL 32825<br>United States<br>Attn: Richard Stadelmann                                            |
| Total                                 | 0.00 USD                                                                                                                                                                     |

**ELSEVIER LICENSE  
TERMS AND CONDITIONS**

Oct 21, 2015

This is a License Agreement between Richard Stadelmann ("You") and Elsevier ("Elsevier") provided by Copyright Clearance Center ("CCC"). The license consists of your order details, the terms and conditions provided by Elsevier, and the payment terms and conditions.

**All payments must be made in full to CCC. For payment instructions, please see information listed at the bottom of this form.**

|                                              |                                                                                                                                                                                           |
|----------------------------------------------|-------------------------------------------------------------------------------------------------------------------------------------------------------------------------------------------|
| Supplier                                     | Elsevier Limited<br>The Boulevard, Langford Lane<br>Kidlington, Oxford, OX5 1GB, UK                                                                                                       |
| Registered Company Number                    | 1982084                                                                                                                                                                                   |
| Customer name                                | Richard Stadelmann                                                                                                                                                                        |
| Customer address                             | 12124 Fountinabrook Blvd.<br>ORLANDO, FL 32825                                                                                                                                            |
| License number                               | 3733710530809                                                                                                                                                                             |
| License date                                 | Oct 21, 2015                                                                                                                                                                              |
| Licensed content publisher                   | Elsevier                                                                                                                                                                                  |
| Licensed content publication                 | Journal of the European Ceramic Society                                                                                                                                                   |
| Licensed content title                       | Stress measurements in ZrB <sub>2</sub> -SiC composites using Raman spectroscopy and neutron diffraction                                                                                  |
| Licensed content author                      | Jeremy Watts, Greg Hilmis, William G. Fahrenholtz, Don Brown, Bjorn Clausen                                                                                                               |
| Licensed content date                        | August 2010                                                                                                                                                                               |
| Licensed content volume number               | 30                                                                                                                                                                                        |
| Licensed content issue number                | 11                                                                                                                                                                                        |
| Number of pages                              | 7                                                                                                                                                                                         |
| Start Page                                   | 2165                                                                                                                                                                                      |
| End Page                                     | 2171                                                                                                                                                                                      |
| Type of Use                                  | reuse in a thesis/dissertation                                                                                                                                                            |
| Intended publisher of new work               | other                                                                                                                                                                                     |
| Portion                                      | figures/tables/illustrations                                                                                                                                                              |
| Number of figures/tables/illustrations       | 1                                                                                                                                                                                         |
| Format                                       | both print and electronic                                                                                                                                                                 |
| Are you the author of this Elsevier article? | No                                                                                                                                                                                        |
| Will you be translating?                     | No                                                                                                                                                                                        |
| Original figure numbers                      | Figure 2                                                                                                                                                                                  |
| Title of your thesis/dissertation            | ZrB <sub>2</sub> -SiC BASED ULTRA HIGH TEMPERATURE CERAMIC COMPOSITES: MECHANICAL PERFORMANCE AND MEASUREMENT AND DESIGN OF THERMAL RESIDUAL STRESSES FOR HYPERSONIC VEHICLE APPLICATIONS |
| Expected completion date                     | Nov 2015                                                                                                                                                                                  |
| Estimated size (number of pages)             | 250                                                                                                                                                                                       |
| Elsevier VAT number                          | GB 494 6272 12                                                                                                                                                                            |
| Permissions price                            | 0.00 USD                                                                                                                                                                                  |
| VAT/Local Sales Tax                          | 0.00 USD / 0.00 GBP                                                                                                                                                                       |

**ELSEVIER LICENSE  
TERMS AND CONDITIONS**

Oct 21, 2015

---

This is a License Agreement between Richard Stadelmann ("You") and Elsevier ("Elsevier") provided by Copyright Clearance Center ("CCC"). The license consists of your order details, the terms and conditions provided by Elsevier, and the payment terms and conditions.

**All payments must be made in full to CCC. For payment instructions, please see information listed at the bottom of this form.**

|                                              |                                                                                                                                                                                           |
|----------------------------------------------|-------------------------------------------------------------------------------------------------------------------------------------------------------------------------------------------|
| Supplier                                     | Elsevier Limited<br>The Boulevard, Langford Lane<br>Kidlington, Oxford, OX5 1GB, UK                                                                                                       |
| Registered Company Number                    | 1982084                                                                                                                                                                                   |
| Customer name                                | Richard Stadelmann                                                                                                                                                                        |
| Customer address                             | 12124 Fountinabrook Blvd.<br>ORLANDO, FL 32825                                                                                                                                            |
| License number                               | 3733710726879                                                                                                                                                                             |
| License date                                 | Oct 21, 2015                                                                                                                                                                              |
| Licensed content publisher                   | Elsevier                                                                                                                                                                                  |
| Licensed content publication                 | Journal of the European Ceramic Society                                                                                                                                                   |
| Licensed content title                       | Strengthening contribution arising from residual stresses in Al <sub>2</sub> O <sub>3</sub> /ZrO <sub>2</sub> composites: a piezo-Spectroscopy investigation                              |
| Licensed content author                      | Giuseppe Pezzotti, Valter Sergo, Orfeo Sbaizero, Naoki Muraki, Sergio Meriani, Toshihiko Nishida                                                                                          |
| Licensed content date                        | February 1999                                                                                                                                                                             |
| Licensed content volume number               | 19                                                                                                                                                                                        |
| Licensed content issue number                | 2                                                                                                                                                                                         |
| Number of pages                              | 7                                                                                                                                                                                         |
| Start Page                                   | 247                                                                                                                                                                                       |
| End Page                                     | 253                                                                                                                                                                                       |
| Type of Use                                  | reuse in a thesis/dissertation                                                                                                                                                            |
| Intended publisher of new work               | other                                                                                                                                                                                     |
| Portion                                      | figures/tables/illustrations                                                                                                                                                              |
| Number of figures/tables/illustrations       | 2                                                                                                                                                                                         |
| Format                                       | both print and electronic                                                                                                                                                                 |
| Are you the author of this Elsevier article? | No                                                                                                                                                                                        |
| Will you be translating?                     | No                                                                                                                                                                                        |
| Original figure numbers                      | Figures 4 and 5                                                                                                                                                                           |
| Title of your thesis/dissertation            | ZrB <sub>2</sub> -SiC BASED ULTRA HIGH TEMPERATURE CERAMIC COMPOSITES: MECHANICAL PERFORMANCE AND MEASUREMENT AND DESIGN OF THERMAL RESIDUAL STRESSES FOR HYPERSONIC VEHICLE APPLICATIONS |
| Expected completion date                     | Nov 2015                                                                                                                                                                                  |
| Estimated size (number of pages)             | 250                                                                                                                                                                                       |
| Elsevier VAT number                          | GB 494 6272 12                                                                                                                                                                            |
| Permissions price                            | 0.00 USD                                                                                                                                                                                  |
| VAT/Local Sales Tax                          | 0.00 USD / 0.00 GBP                                                                                                                                                                       |

# JOHN WILEY AND SONS LICENSE TERMS AND CONDITIONS

Oct 25, 2015

This Agreement between Richard Stadelmann ("You") and John Wiley and Sons ("John Wiley and Sons") consists of your license details and the terms and conditions provided by John Wiley and Sons and Copyright Clearance Center.

|                                       |                                                                                                                                                                              |
|---------------------------------------|------------------------------------------------------------------------------------------------------------------------------------------------------------------------------|
| License Number                        | 3735990583011                                                                                                                                                                |
| License date                          | Oct 25, 2015                                                                                                                                                                 |
| Licensed Content Publisher            | John Wiley and Sons                                                                                                                                                          |
| Licensed Content Publication          | Journal of the American Ceramic Society                                                                                                                                      |
| Licensed Content Title                | Toughening of a Particulate-Reinforced Ceramic-Matrix Composite by Thermal Residual Stress                                                                                   |
| Licensed Content Author               | Minoru Taya,S. Hayashi,Albert S. Kobayashi,H. S. Yoon                                                                                                                        |
| Licensed Content Date                 | Mar 8, 2005                                                                                                                                                                  |
| Pages                                 | 10                                                                                                                                                                           |
| Type of Use                           | Dissertation/Thesis                                                                                                                                                          |
| Requestor type                        | University/Academic                                                                                                                                                          |
| Format                                | Print and electronic                                                                                                                                                         |
| Portion                               | Figure/table                                                                                                                                                                 |
| Number of figures/tables              | 3                                                                                                                                                                            |
| Original Wiley figure/table number(s) | Figure 8, Figure 9, and Figure 12                                                                                                                                            |
| Will you be translating?              | No                                                                                                                                                                           |
| Title of your thesis / dissertation   | ZrB2-SiC BASED ULTRA HIGH TEMPERATURE CERAMIC COMPOSITES: MECHANICAL PERFORMANCE AND MEASUREMENT AND DESIGN OF THERMAL RESIDUAL STRESSES FOR HYPERSONIC VEHICLE APPLICATIONS |
| Expected completion date              | Nov 2015                                                                                                                                                                     |
| Expected size (number of pages)       | 250                                                                                                                                                                          |
| Requestor Location                    | Richard Stadelmann<br>12124 Fountinabrook Blvd.<br>Apt. 208<br>None<br>ORLANDO, FL 32825<br>United States<br>Attn: Richard Stadelmann                                        |
| Billing Type                          | Invoice                                                                                                                                                                      |
| Billing Address                       | Richard Stadelmann<br>12124 Fountinabrook Blvd.<br>Apt. 208<br>None<br>ORLANDO, FL 32825<br>United States<br>Attn: Richard Stadelmann                                        |
| Total                                 | <b>0.00 USD</b>                                                                                                                                                              |



## LIST OF REFERENCES

- [1] J. D. Anderson, Jr., *Hypersonic and high temperature gas dynamics*. Reston, VA: American Institute of Aeronautics and Astronautics. 2nd ed., 2006.
- [2] W. H. Mason, "Some Hypersonic Aerodynamics," *Configuration Aerodynamics Class-Presentation*.
- [3] J. D. Anderson, Jr., *Modern compressible flow : with historical perspective*: New York : McGraw-Hill, c1990. 2nd ed., 1990.
- [4] J. E. A. John, *Gas dynamics*: Boston, Allyn and Bacon, 1969.
- [5] J. D. Anderson, Jr., *Fundamentals of aerodynamics*, 2nd ed. ed. New York: McGraw-Hill, 1991.
- [6] R. W. Fox and A. T. McDonald, *Introduction to fluid mechanics*: New York : Wiley, c1985. 3rd ed., 1985.
- [7] P. W. Huber, C. Langley Research, A. United States National, and A. Space, *Hypersonic shock-heated flow parameters for velocities to 46,000 feet per second and altitudes to 323,000 feet*. Washington, D.C: National Aeronautics and Space Administration, 1963.
- [8] W. E. Moeckel, "Oblique-Shock Relations at Hypersonic Speeds for Air in Chemical Equilibrium," *NACA TN 3895*, 1957.
- [9] T. R. A. Bussing and S. Eberhardt, "Chemistry associated with hypersonic vehicles," *Journal of Thermophysics and Heat Transfer*, vol. 3, pp. 245-253, 1989.
- [10] P. V. Marrone, *Inviscid nonequilibrium flow behind bow and normal shock waves, Part I. general analysis and numerical examples* vol. Rept. QM-1626-A-12(1). Buffalo: Cornell Aeronautical Laboratory. (now CALSPAN), 1963.
- [11] T. A. Parthasarathy, M. D. Petry, G. Jefferson, M. K. Cinibulk, T. Mathur, and M. R. Gruber, "Development of a Test to Evaluate Aerothermal Response of Materials to Hypersonic Flow Using a Scramjet Wind Tunnel," *International Journal of Applied Ceramic Technology*, vol. 8, pp. 832-847, 2011.
- [12] J. F. Justin, A. Jankowaik "Ultra High Temperature Ceramics: Densification, Properties and Thermal Stability," *Journal of Aerospace Lab*, 2011.
- [13] M. M. Opeka, I. G. Talmy, E. J. Wuchina, J. A. Zaykoski, and S. J. Causey, "Mechanical, Thermal, and Oxidation Properties of Refractory Hafnium and zirconium Compounds," *Journal of the European Ceramic Society*, vol. 19, pp. 2405-2414, 1999.

- [14] P. Hu and Z. Wang, "Flexural strength and fracture behavior of ZrB<sub>2</sub>-SiC ultra-high temperature ceramic composites at 1800°C," *Journal of the European Ceramic Society*, vol. 30, pp. 1021-1026, 2010.
- [15] P. Greulich-Weber. (2010). *Silicon Carbide: Basics*.
- [16] J. W. Lawson, C. W. Bauschlicher, M. S. Daw, and W. Y. Ching, "Ab Initio Computations of Electronic, Mechanical, and Thermal Properties of ZrB<sub>2</sub> and HfB<sub>2</sub>," *Journal of the American Ceramic Society*, vol. 94, pp. 3494-3499, 2011.
- [17] I. R. Shein and A. L. Ivanovskii, "Band structure of ZrB<sub>2</sub>, VB<sub>2</sub>, NbB<sub>2</sub>, and TaB<sub>2</sub> hexagonal diborides: Comparison with superconducting MgB<sub>2</sub>," *Physics of the Solid State*, vol. 44, pp. 1833-1839, 2002.
- [18] T. Oguchi, "Cohesion in AlB<sub>2</sub>-Type Diborides: A First-Principles Study," *Journal of the Physical Society of Japan*, vol. 71, pp. 1495-1500, 2002.
- [19] P. Vajeeston, P. Ravindran, C. Ravi, and R. Asokamani, "Electronic structure, bonding, and ground-state properties of AlB<sub>2</sub>-type transition-metal diborides," *Phys. Rev. B*, vol. 63, p. 045115, 2001.
- [20] X. Zhang, X. Luo, J. Han, J. Li, and W. Han, "Electronic structure, elasticity and hardness of diborides of zirconium and hafnium: First principles calculations," *Computational Materials Science*, vol. 44, pp. 411-421, 2008.
- [21] E. Deligoz, K. Colakoglu, and Y. O. Ciftci, "Phonon dispersion and thermodynamical properties in ZrB<sub>2</sub>, NbB<sub>2</sub>, and MoB<sub>2</sub>," *Solid State Communications*, vol. 150, pp. 405-410, 2010.
- [22] S. Nakashima and H. Harima, "Raman Investigation of SiC Polytypes," *phys. stat. sol.*, vol. 162, 1997.
- [23] "The electronic structure and spectroscopic properties of 3C, 2H, 4H, 6H, 15R and 21R polymorphs of SiC," *Materials Science and Engineering A*, vol. 422, p. 147, 2006.
- [24] C. H. Park, B.-H. Cheong, K.-H. Lee, and K. J. Chang, "Structural and electronic properties of cubic, 2H, 4H, and 6H SiC," *Physical Review B*, vol. 49, pp. 4485-4493, 1994.
- [25] P. Käckell, B. Wenzien, and F. Bechstedt, "Influence of atomic relaxations on the structural properties of SiC polytypes from *ab initio* calculations," *Physical Review B*, vol. 50, pp. 17037-17046, 1994.
- [26] O. Madelung, U. Rössler, and M. Schulz, "Silicon carbide (SiC), crystal structure, unit cells, chemical bond, high pressure phases," in *Group IV Elements, IV-IV and III-V Compounds. Part b - Electronic, Transport, Optical and Other Properties*. vol. 41A1b, ed: Springer Berlin Heidelberg, 2002, pp. 1-5.

- [27] Z. Xie, A. C. Terracciano, D. A. Cullen, R. G. Blair, and N. Orlovskaya, "High Temperature Ir Segregation in Ir-B Ceramics: Effect of Oxygen Presence on Stability of IrB<sub>2</sub> and Other Ir-B Phases," *Advances in Applied Ceramics*, vol. 0, p. 1743676115Y.0000000002.
- [28] Z. Xie, R. G. Blair, N. Orlovskaya, D. A. Cullen, S. H. Lapidus, D. Kata, *et al.*, "In search of the elusive IrB<sub>2</sub>: Can mechanochemistry help?," *Journal of Solid State Chemistry*, vol. 233, pp. 108-119, 2016.
- [29] R. Loehman, Corral, E., Dumm, H.P., Kotula, P., Tandon, R., "Ultra-high temperature ceramics for hypersonic vehicle applications," Sandia National Laboratories 2006.
- [30] E. V. Clougherty, Kaufman, L., "Investigation of Boride Compounds for Very High Temperature Applications," ManLabs, Inc., Cambridge, MA, 1963.
- [31] L. Zou, N. Wali, J.-M. Yang, and N. P. Bansal, "Microstructural development of a Cf/ZrC composite manufactured by reactive melt infiltration," *Journal of the European Ceramic Society*, vol. 30, pp. 1527-1535, 2010.
- [32] G. Honstein, C. Chatillon, and F. Baillet, "Thermodynamic approach to the vaporization and growth phenomena of SiC ceramics. I. SiC and SiC-SiO<sub>2</sub> mixtures under neutral conditions," *Journal of the European Ceramic Society*, vol. 32, pp. 1117-1135, 2012.
- [33] Q. Lonné, N. Glandut, and P. Lefort, "Surface densification of porous ZrB<sub>2</sub>-39mol.% SiC ceramic composites by a laser process," *Journal of the European Ceramic Society*, vol. 32, pp. 955-963, 2012.
- [34] D. Zivkovic and L. Stuparevic, "Calculation of the thermodynamic properties in the Ir-B system based on the known phase diagram," *RMZ - Materials and geoenvironment*, vol. 52, pp. 463-468, 2005.
- [35] H. Ipsier and P. Rogl, "Constitution diagrams of the binary systems Pd-B and Ir-B," *Journal of the Less Common Metals*, vol. 82, p. 363, 1981.
- [36] Z. Xie, *Rhenium, osmium and iridium diborides by mechanochemistry : synthesis, structure, thermal stability and mechanical properties*: University of Central Florida, Orlando, FL, 2014.
- [37] J. J. Gilman, "Mechanochemistry," *Science*, vol. 274, pp. 65-65, 1996.
- [38] M. C. Lea, "The Father of Mechanochemistry Laszlo Takacs," *Bull. Hist. Chem*, vol. 82, 2003.
- [39] S. L. James, C. J. Adams, C. Bolm, D. Braga, P. Collier, T. Friscic, *et al.*, "Mechanochemistry: opportunities for new and cleaner synthesis," *Chemical Society Reviews*, vol. 41, pp. 413-447, 2012.

- [40] P. Balaz, *Mechanochemistry in Nanoscience and Minerals Engineering*. Berlin Heidelberg: Springer-Verlag, 2008.
- [41] C. Suryanarayana, "Mechanical alloying and milling," *Progress in Materials Science*, vol. 46, pp. 1-184, 2001.
- [42] T. Sritharan, F. Y. C. Boey, and A. Srinivas, "Synthesis of complex ceramics by mechanochemical activation," *Journal of Materials Processing Technology*, vol. 192–193, pp. 255-258, 2007.
- [43] Z. Ž. Lazarević, N. Ž. Romčević, J. D. Bobić, M. J. Romčević, Z. Dohčević-Mitrović, and B. D. Stojanović, "Study on bi-layered ceramics powders prepared by the mechanochemical synthesis," *Journal of Alloys and Compounds*, vol. 486, pp. 848-852, 2009.
- [44] H.-J. Kim, H.-J. Choi, and J.-G. Lee, "Mechanochemical Synthesis and Pressureless Sintering of TiB<sub>2</sub>–AlN Composites," *Journal of the American Ceramic Society*, vol. 85, pp. 1022-1024, 2002.
- [45] A. L. Black, J. M. Lenhardt, and S. L. Craig, "From molecular mechanochemistry to stress-responsive materials," *Journal of Materials Chemistry*, vol. 21, pp. 1655-1663, 2011.
- [46] D. Restrepo, *Mechanochemistry for solid-state syntheses and catalysis*: University of Central Florida, Orland, FL, 2013.
- [47] M. Petruschke, "Tribochemistry. von G. HEINICKE. Berlin: Akademie-Verlag 1984. Bestellnummer: 7631993(6746). 495 S., 329 Bilder, 106 Tabellen, 98,- M," *Acta Polymerica*, vol. 36, pp. 400-401, 1985.
- [48] N. Orlovskaya, Z. Xie, M. Klimov, H. Heinrich, D. Restrepo, R. Blair, *et al.*, "Mechanochemical synthesis of ReB<sub>2</sub> powder," *Journal of Materials Research*, vol. 26, pp. 2772-2779, 2011.
- [49] Z. Xie, R. G. Blair, N. Orlovskaya, D. A. Cullen, and E. Andrew Payzant, "Thermal stability of hexagonal OsB<sub>2</sub>," *Journal of Solid State Chemistry*, vol. 219, pp. 210-219, 2014.
- [50] Z. Xie, M. Graule, N. Orlovskaya, E. Andrew Payzant, D. A. Cullen, and R. G. Blair, "Novel high pressure hexagonal OsB<sub>2</sub> by mechanochemistry," *Journal of Solid State Chemistry*, vol. 215, pp. 16-21, 2014.
- [51] Z. Xie, M. Lugovy, N. Orlovskaya, T. Graule, J. Kuebler, M. Mueller, *et al.*, "Hexagonal OsB<sub>2</sub>: Sintering, microstructure and mechanical properties," *Journal of Alloys and Compounds*, vol. 634, pp. 168-178, 2015.

- [52] Z. L. Xie, R. G. Blair, N. Orlovskaya, and E. A. Payzant, "Hexagonal OsB<sub>2</sub> reduction upon heating in H<sub>2</sub> containing environment," *Advances in Applied Ceramics*, vol. 114, pp. 114-120, 2015.
- [53] N. Orlovskaya, Z. Xie, and R. G. Blair, "MECHANOCHEMICAL SYNTHESIS OF HEXAGONAL OsB<sub>2</sub>," ed: Google Patents, 2014.
- [54] Z. Xie, V. DeLucca, R. A. Haber, D. T. Restrepo, J. Todd, R. G. Blair, *et al.*, "Synthesis and of AlMgB<sub>14</sub>," *Journal of American Ceramic Society*, *In preparation for submission*, 2015.
- [55] W.-W. Wu, G.-J. Zhang, Y.-M. Kan, and Y. Sakka, "Synthesis, microstructure and mechanical properties of reactively sintered ZrB<sub>2</sub>-SiC-ZrN composites," *Ceramics International*, vol. 39, pp. 7273-7277, 2013.
- [56] S.-Q. Guo, Y. Kagawa, and T. Nishimura, "Mechanical behavior of two-step hot-pressed ZrB<sub>2</sub>-based composites with ZrSi<sub>2</sub>," *Journal of the European Ceramic Society*, vol. 29, pp. 787-794, 2009.
- [57] L. A. Chevykalova, I. Y. Kelina, I. L. Mikhal'chik, A. V. Arakcheev, L. A. Plyasunkova, A. A. Kasimovskii, *et al.*, "Preparation of Ultra-High Temperature Ceramic Material Based on Zirconium Boride by SPS Method," *Refractories and Industrial Ceramics*, vol. 54, pp. 455-462, 2014.
- [58] Y. Zhao, L.-J. Wang, G.-J. Zhang, W. Jiang, and L.-D. Chen, "Preparation and Microstructure of a ZrB<sub>2</sub>-SiC Composite Fabricated by the Spark Plasma Sintering-Reactive Synthesis (SPS-RS) Method," *Journal of the American Ceramic Society*, vol. 90, pp. 4040-4042, 2007.
- [59] R. Licheri, R. Orrù, C. Musa, and G. Cao, "Combination of SHS and SPS Techniques for fabrication of fully dense ZrB<sub>2</sub>-ZrC-SiC composites," *Materials Letters*, vol. 62, pp. 432-435, 2008.
- [60] Z. Yuan, Z. Jin, R. Kang, and Q. Wen, "Tribochemical polishing CVD diamond film with FeNiCr alloy polishing plate prepared by MA-HPS technique," *Diamond and Related Materials*, vol. 21, pp. 50-57, 2012.
- [61] X. Dong, F. Lü, L. Yang, Y. Zhang, and X. Wang, "Influence of spark plasma sintering temperature on electrochemical performance of La<sub>0.80</sub>Mg<sub>0.20</sub>Ni<sub>3.75</sub> alloy," *Materials Chemistry and Physics*, vol. 112, pp. 596-602, 2008.
- [62] G.-J. Zhang, Z.-Y. Deng, N. Kondo, J.-F. Yang, and T. Ohji, "Reactive Hot Pressing of ZrB<sub>2</sub>-SiC Composites," *Journal of the American Ceramic Society*, vol. 83, pp. 2330-2332, 2000.

- [63] W.-W. Wu, G.-J. Zhang, Y.-M. Kan, and P.-L. Wang, "Reactive Hot Pressing of ZrB<sub>2</sub>-SiC-ZrC Ultra High-Temperature Ceramics at 1800°C," *Journal of the American Ceramic Society*, vol. 89, pp. 2967-2969, 2006.
- [64] R. Orrù and G. Cao, "Comparison of Reactive and Non-Reactive Spark Plasma Sintering Routes for the Fabrication of Monolithic and Composite Ultra High Temperature Ceramics (UHTC) Materials," *Materials*, vol. 6, pp. 1566-1583, 2013.
- [65] S. Ran, O. Van der Biest, and J. Vleugels, "ZrB<sub>2</sub>-SiC composites prepared by reactive pulsed electric current sintering," *Journal of the European Ceramic Society*, vol. 30, pp. 2633-2642, 2010.
- [66] H. Wang, S.-H. Lee, and L. Feng, "HfB<sub>2</sub>-SiC composite prepared by reactive spark plasma sintering," *Ceramics International*, vol. 40, pp. 11009-11013, 2014.
- [67] C. Tallon, D. Chavara, A. Gillen, D. Riley, L. Edwards, S. Moricca, *et al.*, "Colloidal Processing of Zirconium Diboride Ultra-High Temperature Ceramics," *Journal of the American Ceramic Society*, vol. 96, pp. 2374-2381, 2013.
- [68] G. Liu, J. Li, and K. Chen, "Combustion synthesis of refractory and hard materials: A review," *International Journal of Refractory Metals and Hard Materials*, vol. 39, pp. 90-102, 2013.
- [69] W.-W. Wu, G.-J. Zhang, Y.-M. Kan, and P.-L. Wang, "Combustion synthesis of ZrB<sub>2</sub>-SiC composite powders ignited in air," *Materials Letters*, vol. 63, pp. 1422-1424, 2009.
- [70] C.-N. Sun, M. C. Gupta, and K. M. B. Taminger, "Electron Beam Sintering of Zirconium Diboride," *Journal of the American Ceramic Society*, vol. 93, pp. 2484-2486, 2010.
- [71] R. He, R. Zhang, X. Zhu, K. Wei, Z. Qu, Y. Pei, *et al.*, "Improved Green Strength and Green Machinability of ZrB<sub>2</sub>-SiC Through Gelcasting Based on a Double Gel Network," *Journal of the American Ceramic Society*, vol. 97, pp. 2401-2404, 2014.
- [72] D. S. King, G. E. Hilmas, and W. G. Fahrenholtz, "Plasma arc welding of ZrB<sub>2</sub>-20vol% ZrC ceramics," *Journal of the European Ceramic Society*, vol. 34, pp. 3549-3557, 2014.
- [73] Z. Lü, D. Jiang, J. Zhang, and Q. Lin, "Processing and properties of ZrB<sub>2</sub>-SiC composites obtained by aqueous tape casting and hot pressing," *Ceramics International*, vol. 37, pp. 293-301, 2011.
- [74] J. Q. Hu, Q. Y. Lu, K. B. Tang, B. Deng, R. R. Jiang, Y. T. Qian, *et al.*, "Synthesis and Characterization of SiC Nanowires through a Reduction-Carburization Route," *The Journal of Physical Chemistry B*, vol. 104, pp. 5251-5254, 2000.
- [75] L. Zhang, W. Yang, H. Jin, Z. Zheng, Z. Xie, H. Miao, *et al.*, "Ultraviolet photoluminescence from 3C-SiC nanorods," *Applied Physics Letters*, vol. 89, p. 143101, 2006.

- [76] S. C. Zhang, G. E. Hilmas, and W. G. Fahrenholtz, "Pressureless Sintering of ZrB<sub>2</sub>-SiC Ceramics," *Journal of the American Ceramic Society*, vol. 91, pp. 26-32, 2008.
- [77] E. Padovano, C. Badini, S. Biamino, M. Pavese, W. S. Yang, and P. Fino, "Pressureless sintering of ZrB<sub>2</sub>-SiC composite laminates using boron and carbon as sintering aids," *Advances in Applied Ceramics*, vol. 112, pp. 478-486, 2013.
- [78] A. K. Khanra, L. C. Pathak, and M. M. Godkhindi, "Carbothermal synthesis of zirconium diboride (ZrB<sub>2</sub>) whiskers," *Advances in Applied Ceramics*, vol. 106, pp. 155-160, 2007.
- [79] H.-Y. Qiu, W.-M. Guo, J. Zou, and G.-J. Zhang, "ZrB<sub>2</sub> powders prepared by boro/carbothermal reduction of ZrO<sub>2</sub>: The effects of carbon source and reaction atmosphere," *Powder Technology*, vol. 217, pp. 462-466, 2012.
- [80] I. Akin, M. Hotta, F. C. Sahin, O. Yucel, G. Goller, and T. Goto, "Microstructure and densification of ZrB<sub>2</sub>-SiC composites prepared by spark plasma sintering," *Journal of the European Ceramic Society*, vol. 29, pp. 2379-2385, 2009.
- [81] L. S. Walker, W. R. Pinc, and E. L. Corral, "Powder Processing Effects on the Rapid Low-Temperature Densification of ZrB<sub>2</sub>-SiC Ultra-High Temperature Ceramic Composites Using Spark Plasma Sintering," *Journal of the American Ceramic Society*, vol. 95, pp. 194-203, 2012.
- [82] H. Yuan, J. Li, Q. Shen, and L. Zhang, "In situ synthesis and sintering of ZrB<sub>2</sub> porous ceramics by the spark plasma sintering-reactive synthesis (SPS-RS) method," *International Journal of Refractory Metals and Hard Materials*, vol. 34, pp. 3-7, 2012.
- [83] N. Gupta, A. Mukhopadhyay, K. Pavani, and B. Basu, "Spark plasma sintering of novel ZrB<sub>2</sub>-SiC-TiSi<sub>2</sub> composites with better mechanical properties," *Materials Science and Engineering: A*, vol. 534, pp. 111-118, 2012.
- [84] A. Snyder, Z. Bo, S. Hodson, T. Fisher, and L. Stanciu, "The effect of heating rate and composition on the properties of spark plasma sintered zirconium diboride based composites," *Materials Science and Engineering: A*, vol. 538, pp. 98-102, 2012.
- [85] X. Zhang, L. Xu, S. Du, C. Liu, J. Han, and W. Han, "Spark plasma sintering and hot pressing of ZrB<sub>2</sub>-SiC<sub>W</sub> ultra-high temperature ceramics," *Journal of Alloys and Compounds*, vol. 466, pp. 241-245, 2008.
- [86] W. G. Fahrenholtz, G. E. Hilmas, A. L. Chamberlain, and J. W. Zimmermann, "Processing and characterization of ZrB<sub>2</sub>-based ultra-high temperature monolithic and fibrous monolithic ceramics," *Journal of Materials Science*, vol. 39, pp. 5951-5957, 2004.
- [87] H. C. Starck, "Alpha SiC Grade UF-10."
- [88] G. A. Slack, "Thermal conductivity of pure and impure silicon, silicon carbide, and diamond," *Journal of Applied Physics*, vol. 35, pp. 3460-3466, 1964.

- [89] W. G. Fahrenholtz, G. E. Hilmas, I. G. Talmy, and J. A. Zaykoski, "Refractory Diborides of Zirconium and Hafnium," *Journal of the American Ceramic Society*, vol. 90, pp. 1347-1364, 2007.
- [90] D. E. Wiley, W. R. Manning, and J. O. Hunter, "Elastic properties of polycrystalline TiB<sub>2</sub>, ZrB<sub>2</sub>, and HfB<sub>2</sub> from room temperature to 1300 °K," *Journal of The Less-Common Metals*, vol. 18, pp. 149-157, 1969.
- [91] S. Hayun, V. Paris, R. Mitrani, S. Kalabukhov, M. P. Dariel, E. Zaretsky, *et al.*, "Microstructure and mechanical properties of silicon carbide processed by Spark Plasma Sintering (SPS)," *Ceramics International*, vol. 38, pp. 6335-6340, 2012.
- [92] L. Yin, E. Y. J. Vancoille, K. Ramesh, and H. Huang, "Surface characterization of 6H-SiC (0001) substrates in indentation and abrasive machining," *International Journal of Machine Tools and Manufacture*, p. 607, 2004.
- [93] A. Rezaie, W. G. Fahrenholtz, and G. E. Hilmas, "Effect of hot pressing time and temperature on the microstructure and mechanical properties of ZrB<sub>2</sub>-SiC," *Journal of Materials Science*, vol. 42, pp. 2735-2744, 2007.
- [94] Y.-Y. Wang, K. Liu, C.-L. Zhou, C.-H. Wang, R.-x. Liu, and Y.-N. Luan, "Electrical and Mechanical Properties of ZrB<sub>2</sub>-Based Composite Ceramic," ed: Trans Tech Publications, Zürich, 2012, p. 744.
- [95] Z. Li and R. C. Bradt, "Thermal expansion and thermal expansion anisotropy of SiC polytypes," *Waermedehnung und Anisotropie der Waermedehnung von SiC Polytypen*, p. 445, 1988.
- [96] F. Monteverde, S. Guicciardi, and A. Bellosi, "Advances in microstructure and mechanical properties of zirconium diboride based ceramics," *Materials Science and Engineering: A*, vol. 346, pp. 310-319, 2003.
- [97] A. L. Chamberlain, W. G. Fahrenholtz, G. E. Hilmas, and D. T. Ellerby, "High-Strength Zirconium Diboride-Based Ceramics," *Journal of the American Ceramic Society*, vol. 87, pp. 1170-1172, 2004.
- [98] S. C. Zhang, G. E. Hilmas, and W. G. Fahrenholtz, "Mechanical properties of sintered ZrB<sub>2</sub>-SiC ceramics," *Journal of the European Ceramic Society*, vol. 31, pp. 893-901, 2011.
- [99] S. Chakraborty, D. Debnath, A. Mallick, and P. Das, "Mechanical and Thermal Properties of Hot-Pressed ZrB<sub>2</sub>-SiC Composites," *Metallurgical and Materials Transactions A*, vol. 45, pp. 6277-6284, 2014.
- [100] Q. Liu, W. Han, X. Zhang, S. Wang, and J. Han, "Microstructure and mechanical properties of ZrB<sub>2</sub>-SiC composites," *Materials Letters*, vol. 63, pp. 1323-1325, 2009.



- [101] J. Watts, G. Hilmas, and W. G. Fahrenholtz, "Mechanical Characterization of Annealed ZrB<sub>2</sub>-SiC Composites," *Journal of the American Ceramic Society*, vol. 96, pp. 845-851, 2013.
- [102] TAMARI, N., TANAKA, T., TANAKA, K., *et al.*, *Effect of spark plasma sintering on densification and mechanical properties of silicon carbide* vol. 103. Tokyo, JAPON: Nippon seramikkusu kyokai, 1995.
- [103] M. S. Asl, M. G. Kakroudi, and S. Noori, "Hardness and toughness of hot pressed ZrB<sub>2</sub>-SiC composites consolidated under relatively low pressure," *Journal of Alloys and Compounds*, vol. 619, pp. 481-487, 2015.
- [104] E. W. Neuman, G. E. Hilmas, and W. G. Fahrenholtz, "Strength of Zirconium Diboride to 2300°C," *Journal of the American Ceramic Society*, vol. 96, pp. 47-50, 2013.
- [105] J. Zou, G.-J. Zhang, C.-F. Hu, T. Nishimura, Y. Sakka, H. Tanaka, *et al.*, "High-temperature bending strength, internal friction and stiffness of ZrB<sub>2</sub>-20vol% SiC ceramics," *Journal of the European Ceramic Society*, vol. 32, pp. 2519-2527, 2012.
- [106] E. W. Neuman, G. E. Hilmas, and W. G. Fahrenholtz, "Mechanical behavior of zirconium diboride-silicon carbide ceramics at elevated temperature in air," *Journal of the European Ceramic Society*, vol. 33, pp. 2889-2899, 2013.
- [107] M. Patel, J. J. Reddy, V. V. Bhanu Prasad, and V. Jayaram, "Strength of hot pressed ZrB<sub>2</sub>-SiC composite after exposure to high temperatures (1000-1700°C)," *Journal of the European Ceramic Society*, vol. 32, pp. 4455-4467, 2012.
- [108] R. Zhang, X. Cheng, D. Fang, L. Ke, and Y. Wang, "Ultra-high-temperature tensile properties and fracture behavior of ZrB<sub>2</sub>-based ceramics in air above 1500°C," *Materials & Design*, vol. 52, pp. 17-22, 2013.
- [109] J. Ramírez-Rico, M. A. Bautista, J. Martínez-Fernández, and M. Singh, "Compressive strength degradation in ZrB<sub>2</sub>-based ultra-high temperature ceramic composites," *Journal of the European Ceramic Society*, vol. 31, pp. 1345-1352, 2011.
- [110] J. Watts, G. Hilmas, W. G. Fahrenholtz, and R. Cutler, "Mechanical Characterization of ZrB<sub>2</sub>-SiC Composites with Varying SiC Particle Sizes," *Journal of the American Ceramic Society*, vol. 94, pp. 4410-4418, 2011.
- [111] S. Zhu, W. G. Fahrenholtz, and G. E. Hilmas, "Influence of silicon carbide particle size on the microstructure and mechanical properties of zirconium diboride-silicon carbide ceramics," *Journal of the European Ceramic Society*, vol. 27, pp. 2077-2083, 2007.
- [112] S. Kim, J.-M. Chae, S.-M. Lee, Y.-S. Oh, H.-T. Kim, and B.-K. Jang, "Change in microstructures and physical properties of ZrB<sub>2</sub>-SiC ceramics hot-pressed with a variety of SiC sources," *Ceramics International*, vol. 40, pp. 34770-3483, 2014.

- [113] J. K. Sonber, T. S. R. C. Murthy, C. Subramanian, N. Krishnamurthy, R. C. Hubli, and A. K. Suri, "Effect of  $\text{CrSi}_2$  and  $\text{HfB}_2$  addition on densification and properties of  $\text{ZrB}_2$ ," *International Journal of Refractory Metals and Hard Materials*, vol. 31, pp. 125-131, 2012.
- [114] W.-B. Tian, Y.-M. Kan, G.-J. Zhang, and P.-L. Wang, "Effect of carbon nanotubes on the properties of  $\text{ZrB}_2$ -SiC ceramics," *Materials Science and Engineering: A*, vol. 487, pp. 568-573, 2008.
- [115] Y. Zhao, L.-J. Wang, G.-J. Zhang, W. Jiang, and L.-D. Chen, "Effect of holding time and pressure on properties of  $\text{ZrB}_2$ -SiC composite fabricated by the spark plasma sintering reactive synthesis method," *International Journal of Refractory Metals and Hard Materials*, vol. 27, pp. 177-180, 2009.
- [116] M. W. Bird, R. P. Aune, F. Yu, P. F. Becher, and K. W. White, "Creep behavior of a zirconium diboride-silicon carbide composite," *Journal of the European Ceramic Society*, vol. 33, pp. 2407-2420, 2013.
- [117] W.-M. Guo, Z.-G. Yang, J. Vleugels, and G.-J. Zhang, "Effect of pressure loading cycle on spark plasma sintered  $\text{ZrB}_2$ -SiC- $\text{Yb}_2\text{O}_3$  ceramics," *Ceramics International*, vol. 38, pp. 5293-5297, 2012.
- [118] S. Gangireddy, J. W. Halloran, and Z. N. Wing, "Flexural creep of zirconium diboride-silicon carbide up to 2200°C in minutes with non-contact electromagnetic testing," *Journal of the European Ceramic Society*, vol. 33, pp. 2901-2908, 2013.
- [119] M. W. Bird, R. P. Aune, A. F. Thomas, P. F. Becher, and K. W. White, "Temperature-dependent mechanical and long crack behavior of zirconium diboride-silicon carbide composite," *Journal of the European Ceramic Society*, vol. 32, pp. 3453-3462, 2012.
- [120] M. Mallik, K. K. Ray, and R. Mitra, "Effect of  $\text{Si}_3\text{N}_4$  Addition on Compressive Creep Behavior of Hot-Pressed  $\text{ZrB}_2$ -SiC Composites," *Journal of the American Ceramic Society*, vol. 97, pp. 2957-2964, 2014.
- [121] J. W. Zimmermann, G. E. Hilmas, and W. G. Fahrenholtz, "Thermal Shock Resistance and Fracture Behavior of  $\text{ZrB}_2$ -Based Fibrous Monolith Ceramics," *Journal of the American Ceramic Society*, vol. 92, pp. 161-166, 2009.
- [122] S. Meng, F. Qi, H. Chen, Z. Wang, and G. Bai, "The repeated thermal shock behaviors of a  $\text{ZrB}_2$ -SiC composite heated by electric resistance method," *International Journal of Refractory Metals and Hard Materials*, vol. 29, pp. 44-48, 2011.
- [123] J. K. Kurihara, T. Tomimatsu, Y. F. Liu, S. Q. Guo, and Y. Kagawa, "Mode I fracture toughness of SiC particle-dispersed  $\text{ZrB}_2$  matrix composite measured using DCDC specimen," *Ceramics International*, vol. 36, pp. 381-384, 2010.

- [124] N. Orlovskaya, R. Stadelmann, M. Lugovy, V. Subbotin, G. Subhash, M. Neubert, *et al.*, "Mechanical properties of ZrB<sub>2</sub>-SiC ceramic composites: room temperature instantaneous behaviour," *Advances in Applied Ceramics*, vol. 112, pp. 9-16, 2013.
- [125] M. Mallik, K. K. Ray, and R. Mitra, "Oxidation behavior of hot pressed ZrB<sub>2</sub>-SiC and HfB<sub>2</sub>-SiC composites," *Journal of the European Ceramic Society*, vol. 31, pp. 199-215, 2011.
- [126] C. Tian, D. Gao, Y. Zhang, C. Xu, Y. Song, and X. Shi, "Oxidation behaviour of zirconium diboride-silicon carbide ceramic composites under low oxygen partial pressure," *Corrosion Science*, vol. 53, pp. 3742-3746, 2011.
- [127] P. Hu, W. Guolin, and Z. Wang, "Oxidation mechanism and resistance of ZrB<sub>2</sub>-SiC composites," *Corrosion Science*, vol. 51, pp. 2724-2732, 2009.
- [128] W.-M. Guo and G.-J. Zhang, "Oxidation resistance and strength retention of ZrB<sub>2</sub>-SiC ceramics," *Journal of the European Ceramic Society*, vol. 30, pp. 2387-2395, 2010.
- [129] M. M. Opeka, I. G. Talmy, and J. A. Zaykoski, "Oxidation-based materials selection for 2000°C + hypersonic aerosurfaces: Theoretical considerations and historical experience," *Journal of Materials Science*, vol. 39, pp. 5887-5904, 2004.
- [130] J. Han, P. Hu, X. Zhang, S. Meng, and W. Han, "Oxidation-resistant ZrB<sub>2</sub>-SiC composites at 2200°C," *Composites Science and Technology*, vol. 68, pp. 799-806, 2008.
- [131] T. A. Parthasarathy, R. A. Rapp, M. Opeka, and R. J. Kerans, "A model for the oxidation of ZrB<sub>2</sub>, HfB<sub>2</sub>, and TiB<sub>2</sub>," *Acta Materialia*, vol. 55, pp. 5999-6010, 2007.
- [132] S. C. Singhal, "Oxidation kinetics of hot-pressed silicon carbide," *Journal of Materials Science*, vol. 11, pp. 1246-1253, 1976.
- [133] E. Gulbransen and S. Jansson, "The high-temperature oxidation, reduction, and volatilization reactions of silicon and silicon carbide," *Oxidation of Metals*, vol. 4, pp. 181-201, 1972.
- [134] W.-B. Han, P. Hu, X.-H. Zhang, J.-C. Han, and S.-H. Meng, "High-Temperature Oxidation at 1900°C of ZrB<sub>2</sub>-xSiC Ultrahigh-Temperature Ceramic Composites," *Journal of the American Ceramic Society*, vol. 91, pp. 3328-3334, 2008.
- [135] H. Yuan, J. Li, Q. Shen, and L. Zhang, "Preparation and thermal conductivity characterization of ZrB<sub>2</sub> porous ceramics fabricated by spark plasma sintering," *International Journal of Refractory Metals and Hard Materials*, vol. 36, pp. 225-231, 2013.
- [136] L. Zhang, D. A. Pejaković, J. Marschall, and M. Gasch, "Thermal and Electrical Transport Properties of Spark Plasma-Sintered HfB<sub>2</sub> and ZrB<sub>2</sub> Ceramics," *Journal of the American Ceramic Society*, vol. 94, pp. 2562-2570, 2011.

- [137] E. Zapata-Solvas, D. D. Jayaseelan, P. M. Brown, and W. E. Lee, "Thermal properties of  $\text{La}_2\text{O}_3$ -doped  $\text{ZrB}_2$ - and  $\text{HfB}_2$ -based ultra-high temperature ceramics," *Journal of the European Ceramic Society*, vol. 33, pp. 3467-3472, 2013.
- [138] M. Mallik, A. J. Kailath, K. K. Ray, and R. Mitra, "Electrical and thermophysical properties of  $\text{ZrB}_2$  and  $\text{HfB}_2$  based composites," *Journal of the European Ceramic Society*, vol. 32, pp. 2545-2555, 2012.
- [139] M. Patel, V. V. B. Prasad, and V. Jayaram, "Heat conduction mechanisms in hot pressed  $\text{ZrB}_2$  and  $\text{ZrB}_2\text{SiC}$  composites," *Journal of the European Ceramic Society*, vol. 33, pp. 1615-1624, 2013.
- [140] S. Meng, H. Chen, J. Hu, and Z. Wang, "Radiative properties characterization of  $\text{ZrB}_2$ - $\text{SiC}$ -based ultrahigh temperature ceramic at high temperature," *Materials & Design*, vol. 32, pp. 377-381, 2011.
- [141] L. Liu, H. Li, X. Shi, W. Feng, Y. Wang, and D. Yao, "Effects of  $\text{SiC}$  addition on the ablation properties of  $\text{C/C}$  composites in different heat fluxes under oxyacetylene torch," *Vacuum*, vol. 90, pp. 97-99, 2013.
- [142] J. W. Zimmermann, G. E. Hilmas, and W. G. Fahrenholtz, "Thermal shock resistance of  $\text{ZrB}_2$  and  $\text{ZrB}_2$ -30%  $\text{SiC}$ ," *Materials Chemistry and Physics*, vol. 112, pp. 140-145, 2008.
- [143] C.-A. Wang and M.-F. Wang, "Thermal shock behavior of  $\text{ZrB}_2$ - $\text{SiC}$  ceramics with different quenching media," *Frontiers of Materials Science*, vol. 7, pp. 184-189, 2013.
- [144] Z. Wang, C. Hong, X. Zhang, X. Sun, and J. Han, "Microstructure and thermal shock behavior of  $\text{ZrB}_2$ - $\text{SiC}$ -graphite composite," *Materials Chemistry and Physics*, vol. 113, pp. 338-341, 2009.
- [145] W. Li, F. Yang, and D. Fang, "Thermal shock modeling of Ultra-High Temperature Ceramics under active cooling," *Computers & Mathematics with Applications*, vol. 58, pp. 2373-2378, 2009.
- [146] D. Li, W. Li, W. Zhang, and D. Fang, "Thermal shock resistance of ultra-high temperature ceramics including the effects of thermal environment and external constraints," *Materials & Design*, vol. 37, pp. 211-214, 2012.
- [147] X. Jin, R. He, X. Zhang, and P. Hu, "Ablation behavior of  $\text{ZrB}_2$ - $\text{SiC}$  sharp leading edges," *Journal of Alloys and Compounds*, vol. 566, pp. 125-130, 2013.
- [148] H. Jin, S. Meng, Q. Yang, and Y. Zhu, "Thermal shock resistance of a  $\text{ZrB}_2$ - $\text{SiC}$ -graphite composite in low oxygen partial pressure environment," *Ceramics International*, vol. 39, pp. 5591-5596, 2013.

- [149] L. Weng, W.-b. Han, and C.-q. Hong, "Fabrication and plasma arc thermal shock resistance of HfB<sub>2</sub>-based ultra high temperature ceramics," *Journal of Central South University*, vol. 19, pp. 887-891, 2012.
- [150] W.-g. Li, T.-b. Cheng, R.-b. Zhang, and D.-n. Fang, "Properties and appropriate conditions of stress reduction factor and thermal shock resistance parameters for ceramics," *Applied Mathematics and Mechanics*, vol. 33, pp. 1351-1360, 2012.
- [151] W. Li, D. Li, T. Cheng, and D. Fang, "Temperature-damage-dependent thermal shock resistance model for ultra-high temperature ceramics," *Engineering Fracture Mechanics*, vol. 82, pp. 9-16, 2012.
- [152] W. Zhi, Q. Qiang, W. Zhanjun, and S. Guodong, "The thermal shock resistance of the ZrB<sub>2</sub>-SiC-ZrC ceramic," *Materials & Design*, vol. 32, pp. 3499-3503, 2011.
- [153] D. Chen, W. Li, X. Zhang, P. Hu, J. Han, C. Hong, *et al.*, "Microstructural feature and thermal shock behavior of hot-pressed ZrB<sub>2</sub>-SiC-ZrO<sub>2</sub> composite," *Materials Chemistry and Physics*, vol. 116, pp. 348-352, 2009.
- [154] F. Qi, S. Meng, and H. Guo, "Repeated thermal shock behavior of the ZrB<sub>2</sub>-SiC-ZrC ultrahigh-temperature ceramic," *Materials & Design*, vol. 35, pp. 133-137, 2012.
- [155] J. Xie, K. Li, H. Li, Q. Fu, and L. Guo, "Ablation behavior and mechanism of C/C-ZrC-SiC composites under an oxyacetylene torch at 3000°C," *Ceramics International*, vol. 39, pp. 4171-4178, 2013.
- [156] H. Li, L. Zhang, L. Cheng, and Y. Wang, "Ablation Resistance of Different Coating Structures for C/ZrB<sub>2</sub>-SiC Composites Under Oxyacetylene Torch Flame," *International Journal of Applied Ceramic Technology*, vol. 6, pp. 145-150, 2009.
- [157] L. Wei, X. Yang, W. Song, M. Yan, and C. Zhao-hui, "Ablation behavior of three-dimensional braided C/SiC composites by oxyacetylene torch under different environments," *Ceramics International*, vol. 39, pp. 463-468, 2013.
- [158] X. Fang, F. Liu, H. Su, B. Liu, and X. Feng, "Ablation of C/SiC, C/SiC-ZrO<sub>2</sub> and C/SiC-ZrB<sub>2</sub> composites in dry air and air mixed with water vapor," *Ceramics International*, vol. 40, pp. 2985-2991, 2014.
- [159] S. Tang, J. Deng, S. Wang, W. Liu, and K. Yang, "Ablation behaviors of ultra-high temperature ceramic composites," *Materials Science and Engineering: A*, vol. 465, pp. 1-7, 2007.
- [160] N. Li, P. Hu, X. Zhang, Y. Liu, and W. Han, "Effects of oxygen partial pressure and atomic oxygen on the microstructure of oxide scale of ZrB<sub>2</sub>-SiC composites at 1500°C," *Corrosion Science*, vol. 73, pp. 44-53, 2013.

- [161] Y. Cui, A. Li, B. Li, X. Ma, R. Bai, W. Zhang, *et al.*, "Microstructure and ablation mechanism of C/C–SiC composites," *Journal of the European Ceramic Society*.
- [162] Z. Yan, Z. Ma, S. Zhu, L. Liu, and Q. Xu, "Reflectivity and laser ablation of ZrB<sub>2</sub>/Cu ultra high temperature ceramic," 2013, pp. 87960T-87960T-7.
- [163] W. Tan, M. Adducci, and R. Trice, "Evaluation of Rare-Earth Modified ZrB<sub>2</sub>–SiC Ablation Resistance Using an Oxyacetylene Torch," *Journal of the American Ceramic Society*, vol. 97, pp. 2639-2645, 2014.
- [164] L. Liu, H. Li, W. Feng, X. Shi, H. Wu, and J. Zhu, "Effect of surface ablation products on the ablation resistance of C/C–SiC composites under oxyacetylene torch," *Corrosion Science*, vol. 67, pp. 60-66, 2013.
- [165] S. Tang, J. Deng, S. Wang, and W. Liu, "Comparison of thermal and ablation behaviors of C/SiC composites and C/ZrB<sub>2</sub>–SiC composites," *Corrosion Science*, vol. 51, pp. 54-61, 2009.
- [166] X. Zhang, P. Hu, J. Han, and S. Meng, "Ablation behavior of ZrB<sub>2</sub>–SiC ultra high temperature ceramics under simulated atmospheric re-entry conditions," *Composites Science and Technology*, vol. 68, pp. 1718-1726, 2008.
- [167] X. Zhang, R. Liu, X. Xiong, and Z. Chen, "Mechanical properties and ablation behavior of ZrB<sub>2</sub>–SiC ceramics fabricated by spark plasma sintering," *International Journal of Refractory Metals and Hard Materials*, vol. 48, pp. 120-125, 2015.
- [168] F. Monteverde and R. Savino, "ZrB<sub>2</sub>–SiC Sharp Leading Edges in High Enthalpy Supersonic Flows," *Journal of the American Ceramic Society*, vol. 95, pp. 2282-2289, 2012.
- [169] P. Hu, K. Gui, Y. Yang, S. Dong, and X. Zhang, "Effect of SiC Content on the Ablation and Oxidation Behavior of ZrB<sub>2</sub>-Based Ultra High Temperature Ceramic Composites," *Materials*, vol. 6, pp. 1730-1744, 2013.
- [170] R. Savino, M. De Stefano Fumo, D. Paterna, A. Di Maso, and F. Monteverde, "Arc-jet testing of ultra-high-temperature-ceramics," *Aerospace Science and Technology*, vol. 14, pp. 178-187, 2010.
- [171] A. G. Esser, "Flow field characterisation of DLR's arc-heated facilities L2K and L3K," *ESA SP*, vol. 426, pp. 545-551, 1998.
- [172] F. Monteverde, R. Savino, M. D. S. Fumo, and A. Di Maso, "Plasma wind tunnel testing of ultra-high temperature ZrB<sub>2</sub>–SiC composites under hypersonic re-entry conditions," *Journal of the European Ceramic Society*, vol. 30, pp. 2313-2321, 2010.

- [173] F. Monteverde and R. Savino, "Stability of ultra-high-temperature ZrB<sub>2</sub>-SiC ceramics under simulated atmospheric re-entry conditions," *Journal of the European Ceramic Society*, vol. 27, pp. 4797-4805, 2007.
- [174] P. J. Ritt, P. A. Williams, S. C. Splinter, and J. H. Perepezko, "Arc jet testing and evaluation of Mo-Si-B coated Mo and SiC-ZrB<sub>2</sub> ceramics," *Journal of the European Ceramic Society*, vol. 34, pp. 3521-3533, 2014.
- [175] R. Savino, M. De Stefano Fumo, L. Silvestroni, and D. Sciti, "Arc-jet testing on HfB<sub>2</sub> and HfC-based ultra-high temperature ceramic materials," *Journal of the European Ceramic Society*, vol. 28, pp. 1899-1907, 2008.
- [176] M. Gasch and S. Johnson, "Physical characterization and arcjet oxidation of hafnium-based ultra high temperature ceramics fabricated by hot pressing and field-assisted sintering," *Journal of the European Ceramic Society*, vol. 30, pp. 2337-2344, 2010.
- [177] L. Scatteia, G. Tomassetti, G. Rufolo, F. De Filippis, and G. Marino, "Advanced Ceramic Materials for Sharp Hot Structures: Material Development and On-Ground Arc-Jet Qualification Testing on Scaled Demonstrators," *AIP Conference Proceedings*, vol. 746, pp. 129-140, 2005.
- [178] D. M. Smith and W. Kirsten, "Flow Calibration of the AEDC H2 Mach 3.4 Arc Jet Nozzle," in *14th AIAA/AHI Space Planes and Hypersonic Systems and Technologies Conference*, ed: American Institute of Aeronautics and Astronautics, 2006.
- [179] D. M. Smith, "Calibration of the AEDC H2 Mach 4.2 Arc Jet Nozzle for Characterization of High-Temperature Materials," in *17th AIAA International Space Planes and Hypersonic Systems and Technologies Conference*, ed: American Institute of Aeronautics and Astronautics, 2011.
- [180] J. Watts, G. Hilmas, W. G. Fahrenholtz, D. Brown, and B. Clausen, "Measurement of thermal residual stresses in ZrB<sub>2</sub>-SiC composites," *Journal of the European Ceramic Society*, vol. 31, pp. 1811-1820, 2011.
- [181] J. Watts, G. Hilmas, W. G. Fahrenholtz, D. Brown, and B. Clausen, "Stress measurements in ZrB<sub>2</sub>-SiC composites using Raman spectroscopy and neutron diffraction," *Journal of the European Ceramic Society*, vol. 30, pp. 2165-2171, 2010.
- [182] K. N. John Ferraro, Chris W. Brown, *Introductory Raman Spectroscopy*: Academic Press, 2003.
- [183] E. Smith, G. Dent, and G. Dent, *Modern Raman spectroscopy : a practical approach*. Chichester ; Hoboken, NJ: J. Wiley, 2005.
- [184] H. J. Bowley, D. J. Gardiner, and P. R. Graves, *Practical Raman spectroscopy*. Berlin ; New York: Springer-Verlag, 1989.

- [185] B. J. Bulkin and J. G. Grasselli, *Analytical Raman spectroscopy*. New York: Wiley, 1991.
- [186] J. Loader, *Basic laser Raman spectroscopy*. [London] [Philadelphia: Heyden Sadtler Research Laboratories, 1970.
- [187] K. Nakamoto, K. Nakamoto, and D. P. Strommen, *Laboratory Raman spectroscopy*. New York: Wiley, 1984.
- [188] M. C. Tobin, *Laser Raman spectroscopy*. New York: Wiley-Interscience, 1971.
- [189] D. W. Feldman, J. H. Parker, W. J. Choyke, and L. Patrick, "Phonon Dispersion Curves by Raman Scattering in SiC, Polytypes 3C, 4H, 6H, 15R, and 21R," *Physical Review*, vol. 173, pp. 787-793, 1968.
- [190] S. Nakashima and H. Harima, "Raman Investigation of SiC Polytypes," *physica status solidi (a)*, vol. 162, pp. 39-64, 1997.
- [191] D. W. Feldman, J. H. Parker, W. J. Choyke, and L. Patrick, "Raman Scattering in 6H-SiC," *Physical Review*, vol. 170, pp. 698-704, 1968.
- [192] P. J. Colwell and M. V. Klein, "Raman Scattering from Electronic Excitations in n-Type Silicon Carbide," *Physical Review B*, vol. 6, pp. 498-515, 1972.
- [193] L. Patrick, "Infrared Absorption in SiC Polytypes," *Physical Review*, vol. 167, pp. 809-813, 1968.
- [194] R. Loudon, "The Raman effect in crystals," *Advances in Physics*, vol. 13, pp. 423-482, 1964.
- [195] T. C. Damen, S. P. S. Porto, and B. Tell, "Raman Effect in Zinc Oxide," *Physical Review*, vol. 142, pp. 570-574, 1966.
- [196] S. Nakashima, K. Kisoda, and J. P. Gauthier, "Raman determination of structures of long-period SiC polytypes," *Journal of Applied Physics*, vol. 75, pp. 5354-5360, 1994.
- [197] S.-i. Nakashima, A. Wada, and Z. Inoue, "Raman Scattering from Anisotropic Phonon Modes in SiC Polytypes," *Journal of the Physical Society of Japan*, vol. 56, pp. 3375-3380, 1987/09/15 1987.
- [198] P. J. Withers and H. K. H. D. Bhadeshia, "Overview - Residual stress part 2 - Nature and origins," *Materials Science and Technology*, vol. 17, pp. 366-375, 2001.
- [199] K. Chawla, *Ceramic Matrix Composites*. Massachusetts: Kluwer Academic Publishers, 2003.
- [200] M. E. Fitzpatrick and A. Lodini, *Analysis of residual stress by diffraction using neutron and synchrotron radiation*. London ; New York: Taylor & Francis, 2003.



- [201] V. Sergo, G. Pezzotti, O. Sbaizero, and T. Nishida, "Grain size influence on residual stresses in alumina/zirconia composites," *Acta Materialia*, vol. 46, pp. 1701-1710, 1998.
- [202] W. Kreher, W. Pompe, *Internal Stresses In Heterogeneous Solids*. Berlin: Akademie Verlag, 1989.
- [203] M. W. Barsoum, *Fundamentals of ceramics / Michel W. Barsoum*: Bristol, UK ; Philadelphia, PA : Institute of Physics Pub., 2003.[Rev. ed.]. 2003.
- [204] P. J. Withers and H. K. H. D. Bhadeshia, "Overview - Residual stress part 1 - Measurement techniques," *Materials Science and Technology*, vol. 12, pp. 355-365, 2001.
- [205] M. Ortiz and S. Suresh, "Statistical Properties of Residual Stresses and Intergranular Fracture in Ceramic Materials," *Journal of Applied Mechanics*, vol. 60, pp. 77-84, 1993.
- [206] D. R. Clarke. *Piez spectroscopy*. Available: <http://clarke.seas.harvard.edu/#>
- [207] V. Sergo, G. Pezzotti, G. Katagiri, N. Muraki, and T. Nishida, "Stress Dependence of the Raman Spectrum of  $\beta$ -Silicon Nitride," *Journal of the American Ceramic Society*, vol. 79, pp. 781-784, 1996.
- [208] D. R. Clarke and D. J. Gardiner, "Recent advances in piezospectroscopy," *International Journal of Materials Research*, vol. 98, pp. 756-762, 2007.
- [209] Q. Ma and D. R. Clarke, "Stress Measurement in Single-Crystal and Polycrystalline Ceramics Using Their Optical Fluorescence," *Journal of the American Ceramic Society*, vol. 76, pp. 1433-1440, 1993.
- [210] A. M. Limarga and D. R. Clarke, "Piezo-Spectroscopic Coefficients of Tetragonal-Prime Yttria-Stabilized Zirconia," *Journal of the American Ceramic Society*, vol. 90, pp. 1272-1275, 2007.
- [211] B. Dietrich and K. F. Dombrowski, "Experimental challenges of stress measurements with resonant micro-Raman spectroscopy," *Journal of Raman Spectroscopy*, vol. 30, pp. 893-897, 1999.
- [212] K. Pinardi, S. C. Jain, M. Willander, A. Atkinson, H. E. Maes, and R. Van Overstraeten, "A method to interpret micro-Raman experiments made to measure nonuniform stresses: Application to local oxidation of silicon structures," *Journal of Applied Physics*, vol. 84, pp. 2507-2512, 1998.
- [213] A. Atkinson and S. C. Jain, "Spatially resolved stress analysis using Raman spectroscopy," *Journal of Raman Spectroscopy*, vol. 30, pp. 885-891, 1999.
- [214] V. Sergo, D. M. Lipkin, G. D. Portu, and D. R. Clarke, "Edge Stresses in Alumina/Zirconia Laminates," *Journal of the American Ceramic Society*, vol. 80, pp. 1633-1638, 1997.

- [215] I. D. Wolf, "Micro-Raman spectroscopy to study local mechanical stress in silicon integrated circuits," *Semiconductor Science and Technology*, vol. 11, p. 139, 1996.
- [216] H. Harima, "Raman scattering characterization on SiC," *Microelectronic Engineering*, vol. 83, pp. 126-129, 2006.
- [217] S. G. Sridhara, T. J. Eperjesi, R. P. Devaty, and W. J. Choyke, "Penetration depths in the ultraviolet for 4H, 6H and 3C silicon carbide at seven common laser pumping wavelengths," *Materials Science and Engineering: B*, vol. 61-62, pp. 229-233, 7/30/ 1999.
- [218] N. J. Everall, "Modeling and Measuring the Effect of Refraction on the Depth Resolution of Confocal Raman Microscopy," *Applied Spectroscopy*, vol. 54, pp. 773-782, 2000.
- [219] J. Liu and Y. K. Vohra, "Raman Modes of 6H Polytype of Silicon Carbide to Ultrahigh Pressures: A Comparison with Silicon and Diamond," *Physical Review Letters*, vol. 72, pp. 4105-4108, 1994.
- [220] J. F. DiGregorio and T. E. Furtak, "Analysis of Residual Stress in 6H-SiC Particles within Al<sub>2</sub>O<sub>3</sub>/SiC Composites through Raman Spectroscopy," *Journal of the American Ceramic Society*, vol. 75, pp. 1854-1857, 1992.
- [221] K. Grodecki, A. Wyszomolek, R. Stepniewski, J. M. Baranowski, W. Hofman, E. Tymicki, *et al.*, "Raman Piezospectroscopy of Phonons in Bulk 6H-SiC," *ACTA PHYSICA POLONICA A*, vol. 116, pp. 947-949, 2009.
- [222] G. Gouadec, P. Colomban, and N. P. Bansal, "Raman Study of Hi-Nicalon-Fiber-Reinforced Celsian Composites: II, Residual Stress in Fibers," *Journal of the American Ceramic Society*, vol. 84, pp. 1136-1142, 2001.
- [223] M. Mu, S. Osswald, Y. Gogotsi, and K. I. Winey, "An in situ Raman spectroscopy study of stress transfer between carbon nanotubes and polymer," *Nanotechnology*, vol. 20, p. 335703, 2009.
- [224] G. Lucazeau and L. Abello, "Micro-Raman analysis of residual stresses and phase transformations in crystalline silicon under microindentation," *Journal of Materials Research*, vol. 12, pp. 2262-2273, 1997.
- [225] Y. Gogotsi, C. Baek, and F. Kirscht, "Raman microspectroscopy study of processing-induced phase transformations and residual stress in silicon," *Semiconductor Science and Technology*, vol. 14, p. 936, 1999.
- [226] N. Orlovskaya, J. Kuebler, V. Subbotin, and M. Lugovy, "Design of Si<sub>3</sub>N<sub>4</sub>-based ceramic laminates by the residual stresses," *Journal of Materials Science*, vol. 40, pp. 5443-5450, 2005.

- [227] G. Pezzotti, "In situ study of fracture mechanisms in advanced ceramics using fluorescence and Raman microprobe spectroscopy," *Journal of Raman Spectroscopy*, vol. 30, pp. 867-875, 1999.
- [228] N. Orlovskaya, D. Steinmetz, S. Yarmolenko, D. Pai, J. Sankar, and J. Goodenough, "Detection of temperature- and stress-induced modifications of LaCoO<sub>3</sub> by micro-Raman spectroscopy," *Physical Review B*, vol. 72, p. 014122, 2005.
- [229] N. Orlovskaya, M. Lugovy, C. Carpenter, S. Pathak, D. Steinmetz, E. Lara-Curzio, *et al.*, "On thermal and vibrational properties of LaGaO<sub>3</sub> single crystals," *Acta Materialia*, vol. 57, pp. 2984-2992, 2009.
- [230] S. Lukich, C. Carpenter, and N. Orlovskaya, "Temperature and stress induced changes of the vibrational response of cubic and rhombohedral 10mol%Sc<sub>2</sub>O<sub>3</sub>-1mol%CeO<sub>2</sub>-ZrO<sub>2</sub> ceramics," *Journal of Power Sources*, vol. 195, pp. 2301-2309, 2010.
- [231] M. Li, Z. Feng, G. Xiong, P. Ying, Q. Xin, and C. Li, "Phase Transformation in the Surface Region of Zirconia Detected by UV Raman Spectroscopy," *The Journal of Physical Chemistry B*, vol. 105, pp. 8107-8111, 2001.
- [232] P. Puech, F. Demangeot, J. Frandon, C. Piquier, M. Kuball, V. Domnich, *et al.*, "GaN nanoindentation: A micro-Raman spectroscopy study of local strain fields," *Journal of Applied Physics*, vol. 96, pp. 2853-2856, 2004.
- [233] S. Maschio, E. Lucchuni, and V. Sergo, "Piezospectroscopic Analysis of the Residual Stresses in the Strontium Hexaluminate/Zirconia (SrAl<sub>12</sub>O<sub>19</sub>/ZrO<sub>2</sub>) System," *Journal of the American Ceramic Society*, vol. 82, pp. 3145-3149, 1999.
- [234] N. Muraki, G. Katagiri, V. Sergo, G. Pezzotti, and T. Nishida, "Mapping of residual stresses around an indentation in β-Si<sub>3</sub>N<sub>4</sub> using Raman spectroscopy," *Journal of Materials Science*, vol. 32, pp. 5419-5423, 1997.
- [235] V. J. Tekippe and A. K. Ramdas, "A piezospectroscopic study of the Raman spectrum of α - quartz," *Physics Letters A*, vol. 35, pp. 143-144, 1971.
- [236] H. Tomaszewski, J. Strzeszewski, L. Adamowicz, and V. Sergo, "Indirect Determination of the Piezospectroscopic Coefficients of Ceria-Stabilized Tetragonal Zirconia Polycrystals," *Journal of the American Ceramic Society*, vol. 85, pp. 2855-2857, 2002.
- [237] Q. Ma and D. R. Clarke, "Piezospectroscopic Determination of Residual Stresses in Polycrystalline Alumina," *Journal of the American Ceramic Society*, vol. 77, pp. 298-302, 1994.
- [238] C. Baudín de la Lastra, S. Bueno, L. Micele, and G. d. Portu, "Piezo-spectroscopic characterization of alumina-aluminium titanate laminates," 2006.

- [239] V. Sergo, V. Lughi, G. Pezzotti, E. Lucchini, S. Meriani, N. Muraki, *et al.*, "The effect of wear on the tetragonal-to-monoclinic transformation and the residual stress distribution in zirconia-toughened alumina cutting tools," *Wear*, vol. 214, pp. 264-270, 1998.
- [240] M. Taya, S. Hayashi, A. S. Kobayashi, and H. S. Yoon, "Toughening of a Particulate-Reinforced Ceramic-Matrix Composite by Thermal Residual Stress," *Journal of the American Ceramic Society*, vol. 73, pp. 1382-1391, 1990.
- [241] K. T. Faber and A. G. Evans, "Crack deflection processes—I. Theory," *Acta Metallurgica*, vol. 31, pp. 565-576, 1983.
- [242] G. C. Wei and P. F. Becher, "Improvements in Mechanical Properties in SiC by the Addition of TiC Particles," *Journal of the American Ceramic Society*, vol. 67, pp. 571-574, 1984.
- [243] M. A. Janney, "Mechanical properties and oxidation behavior of a hot-pressed SiC-15-vol%-TiB<sub>2</sub> composite," *Am. Ceram. Soc. Bull.*, vol. 66, pp. 322-324, 1987.
- [244] P. L. Swanson, C. J. Fairbanks, B. R. Lawn, Y.-W. Mai, and B. J. Hockey, "Crack-Interface Grain Bridging as a Fracture Resistance I, Mechanism in Ceramics: I, Experimental Study on Alumina," *Journal of the American Ceramic Society*, vol. 70, pp. 279-289, 1987.
- [245] B. Budiansky, J. C. Amazigo, and A. G. Evans, "Small-scale crack bridging and the fracture toughness of particulate-reinforced ceramics," *Journal of the Mechanics and Physics of Solids*, vol. 36, pp. 167-187, 1988.
- [246] A. V. Virkar and D. L. Johnson, "Fracture Behavior of ZrO<sub>2</sub>-Zr Composites," *Journal of the American Ceramic Society*, vol. 60, pp. 514-519, 1977.
- [247] R. A. Cutler and A. V. Virkar, "The effect of binder thickness and residual stresses on the fracture toughness of cemented carbides," *Journal of Materials Science*, vol. 20, pp. 3557-3573, 1985.
- [248] A. G. Evans, A. H. Heuer, and D. L. Porter, "The fracture toughness of ceramics," *Pro. Int. Conf. Fract.*, vol. 4th, pp. 529-56, 1977.
- [249] G. Pezzotti, V. Sergo, O. Sbaizero, N. Muraki, S. Meriani, and T. Nishida, "Strengthening contribution arising from residual stresses in Al<sub>2</sub>O<sub>3</sub>/ZrO<sub>2</sub> composites: a piezo-Spectroscopy investigation," *Journal of the European Ceramic Society*, vol. 19, pp. 247-253, 1999.
- [250] J. D. Eshelby, "The Determination of the Elastic Field of an Ellipsoidal Inclusion, and Related Problems," *Proceedings of the Royal Society of London. Series A, Mathematical and Physical Sciences*, vol. 241, pp. 376-396, 1957.

- [251] M. Shafiul Ferdous, C. Makabe, M. S. Rana, and T. Miyazaki, "Improving the fatigue strength of a multiple hole specimen by applying additional holes or notches," *Engineering Failure Analysis*, vol. 18, pp. 75-87, 2011.
- [252] S. Pathak, D. Steinmetz, J. Kuebler, E. Andrew Payzant, and N. Orlovskaya, "Mechanical behavior of  $\text{La}_{0.8}\text{Sr}_{0.2}\text{Ga}_{0.8}\text{Mg}_{0.2}\text{O}_3$  perovskites," *Ceramics International*, vol. 35, pp. 1235-1241, 2009.
- [253] N. Orlovskaya, M. Lugovy, S. Pathak, D. Steinmetz, J. Lloyd, L. Fegely, *et al.*, "Thermal and mechanical properties of  $\text{LaCoO}_3$  and  $\text{La}_{0.8}\text{Ca}_{0.2}\text{CoO}_3$  perovskites," *Journal of Power Sources*, vol. 182, pp. 230-239, 2008.
- [254] N. Fist, J. Dinan, R. Stadelmann, and N. Orlovskaya, "*In situ* three point bending device for measurements of vibrational response of ceramics under stress by microRaman spectroscopy," *Advances in Applied Ceramics*, vol. 111, pp. 433-439, 2012.
- [255] K. P. J. Williams, I. C. Wilcock, I. P. Hayward, and A. Whitley, *Spectroscopy (Eugene, Or.)*, vol. 11, 1996.
- [256] R. Stadelmann, B. Hughes, N. Orlovskaya, "A guideline of mapping parameters for Raman mapping of  $\text{ZrB}_2$ -SiC ceramic composites," *Accepted to Advances in Applied Ceramics*, 2015.
- [257] M. Radovic, E. Lara-Curzio, and L. Riester, "Comparison of different experimental techniques for determination of elastic properties of solids," *Materials Science and Engineering A*, vol. 368, pp. 56-70, 2004.
- [258] A. Migliori and J. L. Sarrao, *Resonant ultrasound spectroscopy : applications to physics, materials measurements, and non-destructive evaluation*: New York : J. Wiley, 1997., 1997.
- [259] J. Kübler, "Fracture Toughness of Ceramics Using the SEVNB Method: First Results of a Joint VAMAS/ESIS Round Robin," in *23rd Annual Conference on Composites, Advanced Ceramics, Materials, and Structures: A: Ceramic Engineering and Science Proceedings*, ed: John Wiley & Sons, Inc., 2008, pp. 494-502.
- [260] R. Stadelmann, B. Hughes, N. Orlovskaya, S. Grasso, and M. J. Reece, "2D Raman mapping and thermal residual stresses in SiC grains of  $\text{ZrB}_2$ -SiC ceramic composites," *Ceramics International*, vol. 41, pp. 13630-13637, 2015.
- [261] M. Donohue, C. Carpenter, and N. Orlovskaya, "Vibrational Properties of  $\text{Zr}(\text{Hf})\text{B}_2$ -SiC UHTC Composites by Micro-Raman Spectroscopy," in *Boron Rich Solids*, N. Orlovskaya and M. Lugovy, Eds., ed: Springer Netherlands, 2011, pp. 287-302.

- [262] M. Lugovy, N. Orlovskaya, V. Slyunyayev, E. Mitrentsis, C.G. Aneziris, T. Graule, *et al.*, "Temperature dependence of elastic properties of ZrB<sub>2</sub>-SiC composites," *Ceramics International*, 2015.
- [263] S.-Q. Guo, "Densification of ZrB<sub>2</sub>-based composites and their mechanical and physical properties: A review," *Journal of the European Ceramic Society*, vol. 29, pp. 995-1011, 2009.
- [264] R. S. Figliola and D. E. Beasley, *Theory and design for mechanical measurements*, 2nd ed. ed. New York: Wiley, 1995.
- [265] R. Stadelmann, *Mechanical properties and thermal residual stresses of ZrB<sub>2</sub>-SiC ceramic composites for hypersonic vehicle applications*: University of Central Florida, Orlando, FL, 2013.